
Structural and Functional Characterization of
CRM1-Nup214 Interactions
Reveals Multiple FG-binding Sites Involved in
Nucleocytoplasmic Transport

Dissertation
for the award of the degree
"Doctor rerum naturalium"
of the Georg-August-Universität, Göttingen

within the doctoral program "Biomolecules: Structure - Function - Dynamics"
of the Georg-August University School of Science (GAUSS)

submitted by
Sarah A. Port

from Dachau
Göttingen 2015

Thesis Committee/ Examination Board:

Prof. Dr. Ralph H. Kehlenbach (referee)

Department of Molecular Biology
Georg-August-Universität, Göttingen

Dr. Achim Dickmanns (2nd referee)

Department for Molecular Structural Biology
Georg-August-Universität, Göttingen

Prof. Dr. Heinz Neumann

Department for Molecular Structural Biology
Applied Synthetic Biology
Georg-August-Universität, Göttingen

Further Members of the Examination Board:

Prof. Dr. Heike Krebber

Institute for Microbiology and Genetics
Department Molecular Genetics
Georg-August-Universität, Göttingen

Prof. Dr. Holger Stark

Molecular Electron Cryomicroscopy
Max-Planck-Institute for Biophysical Chemistry
& Georg-August-Universität, Göttingen

Prof. Dr. Henning Urlaub

Bioanalytical Mass Spectrometry
Max-Planck-Institute for Biophysical Chemistry
& Georg-August-Universität, Göttingen

Date of the oral examination: April 27th, 2015

Statutory declaration:

I hereby declare that I have written this PhD thesis independently with no other sources and aids than clearly stated.

This thesis was not submitted in the same or in a substantially similar version to any other authority to achieve an academic grading and was not published elsewhere.

Sarah A. Port

Contents

Abstract	7
1. Introduction	8
1.1. The nuclear pore complex (NPC)	8
1.1.1. The architecture of the NPC	8
1.1.2. The composition of the NPC	8
1.1.3. The nucleoporin 214 (Nup214)	10
1.2. Nuclear transport	12
1.2.1. Models of nuclear transport	12
1.2.2. Nuclear transport receptors	14
1.2.3. The nuclear export receptor CRM1	15
1.3. Interaction of transport receptors with the NPC	17
1.3.1. Karyopherins interact with FG-repeat domains on nucleoporins	17
1.3.2. Available structures of transport factors with FG-repeats	17
1.4. Aim of this Work	20
2. Material and Methods	21
2.1. Material	21
2.1.1. Software	21
2.1.2. Technical Equipment	21
2.1.3. Consumables	22
2.1.4. Kits	23
2.1.5. Chemicals, Reagents, Enzymes	23
2.1.6. Buffers, Stock solutions, Media	25
2.1.7. Cell lines	26
2.1.8. <i>E. coli</i> strains	27
2.1.9. Antibodies	27
2.1.10. Oligonucleotides	28
2.1.11. Synthesized Genes	33
2.1.12. Vectors	34
2.1.13. Plasmids	36
2.2. Molecular Biology Methods	42
2.2.1. RbCl chemically competent cells	42
2.2.2. Agarose gel electrophoresis	42
2.2.3. Quantification of dsDNA	42
2.2.4. Polymerase chain reaction (PCR)	43
2.2.5. Site-directed mutagenesis	43
2.2.6. Restriction enzyme digest	43
2.2.7. Ligation of DNA fragments	44
2.2.8. Transformation of <i>E. coli</i> strains with plasmid DNA	44
2.2.9. Purification of plasmid DNA	44
2.2.10. DNA sequencing	45
2.3. Biochemical Methods	46
2.3.1. SDS-PAGE	46
2.3.2. Coomassie staining of SDS-PAGE gels	46
2.3.3. Silver staining of SDS-PAGE gels	46
2.3.4. Western blotting	47
2.3.5. Chemically synthesized peptides	48
2.3.6. Protein purification	48

2.3.7.	Loading of Ran with GTP/GDP	50
2.3.8.	<i>In vitro</i> binding assays	51
2.3.9.	RanGAP assay	52
2.3.10.	Complex formation tests	52
2.3.11.	Purification of Antibodies	52
2.4.	Cell Biology Methods	53
2.4.1.	Cultivation of mammalian cells	53
2.4.2.	Transfection of DNA in mammalian cells	53
2.4.3.	<i>In vitro</i> export assays	53
2.4.4.	Detection of proteins by indirect immunofluorescence	54
2.4.5.	Quantification of GFP-SPN1 distribution	54
2.5.	Structural Biology Methods	55
2.5.1.	Preparative purification of protein complexes	55
2.5.2.	Cross-linking of protein complexes	55
2.5.3.	Mass spectrometry	55
2.5.4.	Electron microscopy	55
2.5.5.	Crystallography	56
3.	Results	57
3.1.	Development of a bead-based flow cytometry assay for protein-protein interactions (Halo assay)	57
3.1.1.	Optimization of assay conditions	57
3.1.2.	Biochemical verification of the novel CRM1-binding assay	58
3.1.3.	Comparison of CRM1-binding to different Nup214 fragments reveals a detection range of 3 orders of magnitude	61
3.1.4.	Application of the Halo assay to analyze CRM1-cargo interactions	62
3.2.	Biochemical characterization of CRM1-Nup214 binding	63
3.2.1.	CRM1 is the karyopherin with the highest avidity for Nup214	63
3.2.2.	Nup214 promotes the formation of CRM1 export complexes in a RanGTP-dependent manner	63
3.2.3.	Binding of Nup214 fragments to the export complex is independent of their stabilization effect in RanGAP assays	66
3.2.4.	The Ran C-terminus destabilizes the CRM1-RanGTP-Nup214 complex	70
3.3.	Structural characterization of CRM1-RanGTP-SPN1-Nup214 complexes	72
3.3.1.	Electron microscopy	72
3.3.2.	Cross-linking mass spectrometry	75
3.3.3.	Crystallography	84
3.4.	Functional characterization of CRM1-Nup214 interactions	91
3.4.1.	Analysis of prominent features of Nup214 revealed several FG-repeats important for CRM1-binding	91
3.4.2.	Analysis of the structure-derived Nup214 mutants confirms the importance of the identified phenylalanines in CRM1-binding	94
3.4.3.	Importance of the identified binding residues in cellular context	96
3.4.4.	Characterization of structure-derived CRM1 mutants	98
3.5.	Analysis of RanBP3-CRM1 interactions	105
3.5.1.	The stabilization of export complexes by RanBP3 is concentration-dependent	105
3.5.2.	RanBP3 and Nup214 compete for binding to CRM1 export complexes	106
3.5.3.	RanBP3 and Nup214 can bind free CRM1 simultaneously, but not the CRM1 export complex	107

4. Discussion	108
4.1. The Halo assay is a novel, semi-quantitative assay for the analysis of protein-protein interactions	108
4.2. Structural analysis of a CRM1 export complex bound to long segments of FG-repeats from Nup214	108
4.3. CRM1 conformation and function is highly sensitive towards manipulation	109
4.4. Integrative structural and functional analysis reveals that Nup214 stabilizes CRM1 export complexes by acting as a molecular clamp	110
4.4.1. Integration of electron microscopy, cross-linking mass spectrometry and crystallography data suggests flexible regions of Nup214 between anchored phenylalanine residues in binding pockets of CRM1	110
4.4.2. Nup214 couples the N- and C-terminal arch of CRM1	113
4.5. Interaction of FG-nucleoporins and karyopherins might rely on overlapping as well as specific binding sites	115
4.5.1. Comparison of binding sites from Nup214 and RanBP3 on CRM1	115
4.5.2. Implications for the interaction of CRM1 with other nucleoporins	118
4.6. Regulation of nuclear transport by nucleoporin-karyopherin interactions	119
4.7. Outlook	120
References	121
List of Figures	133
List of Tables	135
Appendices	136
A. Synthesized genes	136
B. Halo assay - analysis with fluorescence microscopy	141
C. Cross-linking mass spectrometry data	142
C.1. Cross-linking of the GST-Nup214(1968-2033) complex with BS ³ and BS ² G	142
C.2. Cross-linking of His-Nup214(1916-2033)-His complexes with BS ³	143
C.3. Cross-linking of the MBP-Nup214(1916-2033)-His complex with BS ³ and EDC	161
D. Protein alignments	166
D.1. Alignment of <i>H. sapiens</i> CRM1 and <i>S. cerevisiae</i> Xpo1p	166
D.2. Alignment of <i>H. sapiens</i> Nup214 and <i>S. cerevisiae</i> Nup159	167
D.3. Alignment of <i>H. sapiens</i> RanBP3 and <i>S. cerevisiae</i> Yrb2p	169
E. Interactions of Nup214 to CRM1 in the crystal structure of the Nup214 complex .	170
F. Comparison of the CRM1-RanGTP-SPN1 architecture in the crystal structure of the Nup214 complex and the export complex	172
G. Nup214 fragments and mutants	173
H. CRM1 mutants	174
I. Comparison of CRM1 from the Nup214 complex crystal structure to Xpo1p from the Yrb2 complex	179
J. Abbreviations	180
K. Amino acid codes	181
Curriculum vitae	182
Publications	183

Abstract

Transport into and out of the nucleus occurs through nuclear pore complexes (NPCs) that are embedded in the nuclear envelope. NPCs are massive macromolecular complexes of around 125 kDa in vertebrates. Around 30 different nucleoporins (Nups) build the NPC, a third of which contain phenylalanine glycine (FG)-repeats (FG-Nups). The FG-repeats form the permeability barrier of the NPC, thereby restricting diffusion for most molecules larger than 20-40 kDa. In order for larger molecules to translocate through the NPCs, they have to be actively transported in complexes with transport receptors. Transport receptors were shown to interact with FG-repeats of nucleoporins, consequently overcoming the permeability barrier of the NPCs. The most prominent transport receptor for nuclear import is importin β , whereas CRM1 is the major nuclear export receptor. With the exception of some crystal structures of importin β with short, mostly chemically synthesized, FG-repeat containing peptides, structural information on how transport receptors interact with FG-Nups to mediate translocation through the NPC has not been available so far.

In this work, the interactions of CRM1 export complexes with Nup214 were analyzed by structural and biochemical methods.

A complex containing CRM1, RanGTP, SPN1 and a Nup214(1916-2033) fragment was analyzed by cross-linking mass spectrometry and X-ray crystallography. The crystal structure revealed three FG-sites on the Nup214 fragment that bound to CRM1 by winding along the outer ring from HEAT-repeat 14, across the interacting region of the N- and C- termini, through to HEAT-repeat 4. Seven phenylalanine residues could be identified in Nup214 that bound to hydrophobic pockets on CRM1. Moreover, the residues between the bound phenylalanine residues seemed to be flexible or bound rather loosely to the CRM1 surface.

Structure-derived Nup214 and CRM1 mutants were analyzed for their binding properties. Analysis of CRM1 mutants revealed that mutagenesis in several regions of CRM1 can affect its cooperative binding to RanGTP and NES. More than 90% of the CRM1 mutants designed to decrease binding to Nup214, also showed altered binding to RanGTP and an NES peptide. Two CRM1 mutants displayed decreased binding to Nup214 but remained unaltered with respect to RanGTP and NES binding, verifying that the hydrophobic pockets on CRM1 binding to Nup214 residues F1938 and F1982 in the crystal structure are indeed involved in the interaction. Correspondingly, mutagenesis of the Nup214 phenylalanine residues bound in the structure clearly reduced binding to CRM1.

The obtained crystal structure of the Nup214 complex is the first structure of a karyopherin with long fragments of a FG-nucleoporin. The crystal structure combined with data from binding- and transport assays suggests that binding sites of FG-nucleoporins on CRM1 partially, but not completely, overlap. Furthermore, Nup214 stabilizes CRM1 export complexes by acting as a molecular clamp.

1 Introduction

1.1 The nuclear pore complex (NPC)

1.1.1 The architecture of the NPC

The nucleus is the major cellular feature that distinguishes prokaryotes from higher organisms. The spatial separation of transcriptional and translational events in the eukaryotic cell leads to the need for effective transport of RNA and proteins between the nucleus and the cytoplasm. Crossing of the nuclear membrane occurs through so-called nuclear pore complexes (NPC) which serve as the only gateway for nucleocytoplasmic transport. NPCs function as a diffusion barrier. Therefore, in general, only small metabolites can diffuse freely between cytoplasm and nucleus, most macromolecules larger than 20-40 kDa have to be actively transported. Exceptions include for example histones, which are actively transported even though they are only around 20 kDa in size [1, 2, 3]. On the other hand, large molecules were also shown to diffuse passively into the nucleus [4].

The NPC is one of the largest macromolecular complexes of the cell. Its size ranges from around 60 MDa in yeast to around 125 MDa in vertebrates [5]. Early electron tomography studies already revealed an eight-fold symmetry of the NPCs [6] which was confirmed and refined in several studies ever since [7, 8, 9, 10]. NPCs can be divided into several structural subunits. The main channel of the NPC consists of a central framework, which is embedded in the nuclear envelope. The central channel is bordered by a cytoplasmic and a nuclear ring. Eight flexible cytoplasmic filaments protrude from the cytoplasmic ring into the cytoplasm. The nuclear basket, a structure comprised of eight filaments joined with a distal ring, is attached to the NPC on the nuclear side. This characteristic architecture of the nuclear pore complex is conserved in yeast, plants and vertebrates [11, 12, 13, 14], however the dimensions of the NPCs differ across species. NPCs from *Dictyostelium discoideum* and human were analyzed by high-resolution cryoelectron tomography [10, 15]. The NPCs from *Dictyostelium discoideum* transport-active nuclei were found to be 100 nm in length with an outer diameter luminal spoke ring of 125 nm. The inner diameter of the spoke ring was only around 60 nm although its size is thought to be flexible in presence or absence of transport cargoes. The distal nuclear ring on the far-nuclear side of the nuclear basket was 40 nm in diameter [10]. In contrast, the tomographic structure of the human NPC revealed an inner diameter of the nuclear and cytoplasmic ring of 84 nm and an inner diameter of 41 nm for the spoke ring [15].

1.1.2 The composition of the NPC

Comprehensive proteomic studies in yeast and vertebrates revealed that the massive macromolecular structure of the NPC is built of only around 30 different proteins, named nucleoporins (Nups) [11, 14] (figure 1). Although the definite composition is still under debate due to inconsistent results, attributed to different isolation methods and technical limitations [11, 14, 16, 17, 18], nucleoporins are thought to be present in multiples of eight, resulting in a

total amount of around 600 individual nucleoporins per NPC.

Nucleoporins can be classified according to their positions within the NPC. The central channel was proposed to consist of a series of concentric cylinders. The outer layer of the channel is built by coat nucleoporins, followed by a layer of adapter nucleoporins. The inner surface of the channel is layered by so-termed channel nucleoporins [19]. In addition, nuclear basket nucleoporins can be found on the nuclear side and cytoplasmic filament nucleoporins on the cytoplasmic face of the NPC. Surprisingly, integrative approaches of structural studies combined with homology modeling have revealed that most nucleoporins consist of only four structural elements (reviewed in [5]). These elements are α -helical repeats, β -propellers, coiled-coil domains implicated in protein-protein interaction and intrinsically unstructured phenylalanine-glycine (FG) repeats [20]. The structural features of nucleoporins are reviewed in [18]. Nucleoporins containing FG-repeats are called FG-nucleoporins. About one third of nucleoporins belong to this class [21]. FG-repeats were shown to form the permeability barrier of the NPC and facilitate nuclear transport by interaction with transport receptors [21, 22, 23, 24]. With respect to the formation of the permeability barrier, Nup98 was found to be essential [25].

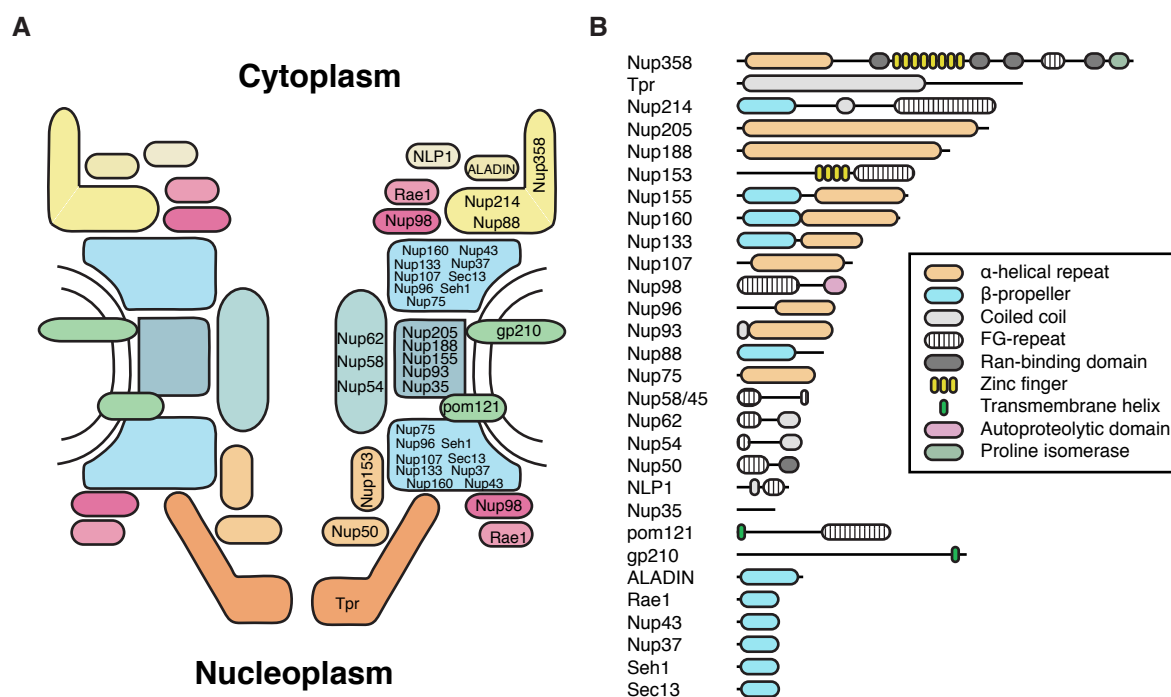


Figure 1: Nucleoporins sorted by (A) their position in the nuclear pore complex and (B) size (modified from [5]).

Immunogold electron microscopy studies mapped the position and mobility of the individual nucleoporins on the NPC, thereby determining that at least 18 of the nucleoporins are located symmetrically on the nuclear and cytoplasmic sides of the NPC (reviewed in [14, 26, 27]). In yeast, Nup42 and Nup159 were found to be exclusively cytoplasmic, whereas Nup1, Nup2 and Nup60 were localized on the nuclear face of the NPC [28, 29]. In vertebrates, the fiber-like nucleoporin Tpr is located exclusively on the nuclear side of the NPC and forms the filaments of the nuclear basket [30]. On the cytoplasmic side, the cytoplasmic ring is formed by the

asymmetrically located nucleoporins Nup358, Nup214 and Nup88. Aside from these fixed structural features of the NPC, studies also revealed a mobile portion of nucleoporins. Nup98, for example, was shown to be part of the nuclear basket and also found on the cytoplasmic side of the NPC [31]. Furthermore, Nup98 is thought to shuttle between the NPC and "GLFG nuclear bodies" [32]. Similarly, the N-terminus of Nup153 was mapped to the nuclear ring and its Zinc-finger domain to the distal ring of the nuclear basket whereas the C-terminal FG-repeats of Nup153 were found throughout the NPC and even close to the cytoplasmic face [33]. This could be explained by a study that found FG-repeat domains to be natively unfolded [34]. Systematic deletion of the FG-repeat domains of 11 *Saccharomyces cerevisiae* nucleoporins revealed that up to half of the total FG-repeat mass can be deleted without significant defects in protein import or the permeability barrier [29].

An extensive list of nucleoporin knock-downs and their effect on the NPC can be found in [32].

Distinct subcomplexes of the NPC have been revealed by mass spectrometry of isolated nucleoporins [35, 36]. The Nup88-Nup214 complex was identified on the cytoplasmic side [37]. The Nup107-Nup160 complex, which is also termed Y-complex [38] due to its characteristic Y-shaped structure, can be found at the central spoke ring. It consists of Nup160, Nup133, Nup107, Nup96, Nup85 and Sec13. It is the major building block of the NPC and is present in eight copies on each side of the central ring [11, 39, 40, 41, 42, 43, 44]. Recently, the crystal structure of the reconstituted yeast Y-complex was solved at a 7.4 Å resolution [45].

The overall composition of the NPC seems to be similar in yeast and vertebrates [9, 13, 46, 47] and also the structure and function of two thirds of yeast and vertebrate nucleoporins are at least partially conserved [48]. As the protein sequence homologies between yeast and vertebrates are sometimes quite low, for example for Nup133 [40], relations of yeast and vertebrate nucleoporins are mainly based on similar functions, NPC localization and interactions to other nucleoporins [48]. Furthermore, as the vertebrate NPC has twice the molecular weight compared to the yeast NPC, the vertebrate NPC probably has also some additional structural features [48].

The major physiological and best-characterized role of the NPC is the mediation of transport between the nucleus and the cytoplasm. Moreover, NPCs were also shown to function in gene expression regulation, chromosome positioning during mitosis, apoptosis and in the secretory pathway (reviewed in [32]).

1.1.3 The nucleoporin 214 (Nup214)

The nucleoporin 214 (Nup214), also named CAN, is the third largest human nucleoporin and the one with the largest FG-repeat domain. It is asymmetrically located on the cytoplasmic face of the NPC in a complex with Nup88 [37, 49]. Depletion of Nup214 or the adjoining Nup358 led to NPCs without cytoplasmic filaments that nevertheless seemed to be largely structurally and functionally intact [50].

Nup214 is quite poorly conserved between species. The yeast homologue Nup159 is about 50 kDa smaller with a different secondary structure prediction. Nup159 has an N-terminal beta-propeller domain followed by a 200 residue region enriched in FG repeats which was shown to be important for CRM1 binding [35], and a C-terminal coiled-coil domain for interaction with Nup82. The N-terminus of Nup214 is a well structured seven-bladed-beta-propeller domain [51, 52, 53] (figure 2) that was shown to interact with the DEAD box helicase Ddx19 [23, 51, 53, 54, 55, 56], suggesting a role in the export of mRNA. Interaction of Nup214 with Nup88 is mediated via predicted coiled-coil domains [54, 57]. The C-terminus is comprised of a large number of FG-repeats, suggesting that is largely unstructured. The FG-repeat region is important for the interaction of Nup214 with CRM1 [54, 58]. An alignment of Nup214 and Nup159 can be found in the appendix (figure S6).

Recently, a conserved FG-repeat motive in Nup214 has been characterized for its importance in CRM1-binding [59]. This study revealed that several regions in Nup214 are important for binding to CRM1 which could explain why Nup214 is the nucleoporin with the highest avidity to CRM1. Binding of CRM1 to Nup214 is increased in the presence of RanGTP [24]. Furthermore, Nup214 was shown to stabilize export complexes consisting of CRM1, RanGTP and a cargo [60]. The high affinity, RanGTP-dependent interaction as well as the stabilization of export complexes indicate a role of Nup214 in nuclear export.

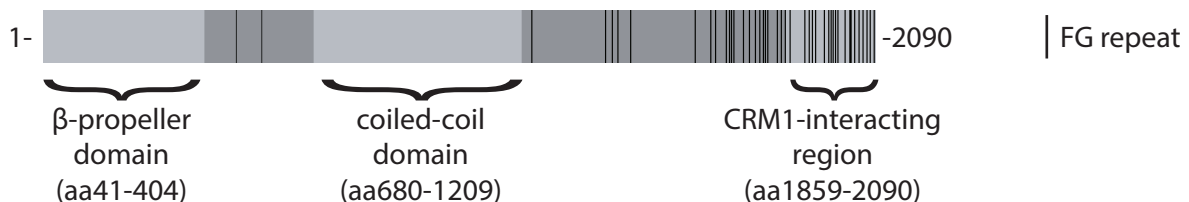


Figure 2: Secondary structure of Nup214. Nup214 has an N-terminal beta-propeller domain (aa 41-404) and a coiled-coil domain (aa680-1209). The C-terminal region (aa1859-2090) was shown to interact with CRM1 and contains a large number of FG-repeats, suggesting that it is natively unfolded.

Early studies suggested an interaction of Nup214 with the import receptors importin β [61], transportin [62] and importin 5 [63], but only its role in nuclear export has been investigated further. Nup214 was shown to bind the export receptor CRM1 [24, 54, 64, 65] and to function in the nuclear export of some, but not all CRM1-dependent cargoes. CRM1 cargoes that show Nup214-dependent nuclear export include NMD3 which is the adapter for export of 60 S ribosomal subunits [66], the nuclear factor of activated T-cells (NFAT) and HIV-1 Rev [60]. In addition, Nup214 or its yeast homologue Nup159 were shown to bind several other transport factors including Dbp5 [55], TAP [23, 67], scMex67p [23] and scGle1 [65].

Even though Nup214 does not affect the export of all CRM1 cargoes, it was shown to be an essential protein in mice, as *Nup214* $-/-$ embryonic stem cells are not viable and embryos die early in development *in utero* [68]. Nup214 depletion was shown to lead to cell cycle arrest and reduced cell growth *in vivo* and *in vitro* [68, 60].

Nup214 is one of four nucleoporins that have been observed as oncogenic fusion proteins after chromosomal translocations [69] and in fact was first identified as a fusion protein in leukemogenesis [49, 70]. Fusions of Nup214 with the histone chaperone SET [71], the chromatin-binding protein DEK [72], the tyrosine kinase ABL [73], the membrane transporter XKR3 [74] and SQSTM1, which functions as an activator of NF κ B signaling [75] have been identified in different kinds of leukemia. Nup214 fusions are used as a diagnostic and therapeutic markers and are commonly associated with poor prognosis. The role of Nup214 in acute leukemias has recently been reviewed [76, 77].

1.2 Nuclear transport

1.2.1 Models of nuclear transport

Transport kinetic studies estimated that there are around 1000 translocation events, translocating around 80 MDa through a single NPC per second (reviewed in [78]). Even though much progress has been made in revealing the structure of the NPC components and subcomplexes as well as the overall structure, it still remains unclear how the nucleoporins function within the NPC to mediate nucleocytoplasmic transport [14, 79, 80]. Therefore, different models of nucleocytoplasmic transport have been proposed in the course of the years, the most prominent being the virtual gating model [14, 27], the selective phase model or FG-hydrogel model [81], and the oily-spaghetti model [82], which have been extensively reviewed in [33, 78, 83, 84]. Models vary mainly in their description of the permeability barrier of the NPC. In the virtual gating model [14, 27], the permeability barrier is explained by thermodynamic considerations. The entropy loss that a molecule undergoes when entering the nuclear pore has to be compensated by a change in enthalpy when it interacts with the molecules within the pore. Molecules that bind to the FG-Nups lining the channel experience a high change in enthalpy and can therefore translocate through the pore, whereas molecules that do not bind to FG-Nups are repulsed due to unfavorable energy changes. In the selective phase model [81], the interacting FG-repeats from nucleoporins form a three-dimensional sieve. The mesh of the sieve results in size-dependent retention of proteins. Transport receptors can translocate through the nuclear pore by interaction with the FG-repeats which leads to a temporary and localized opening of the mesh.

Even though the molecular mechanisms of translocation are still unclear, it is well understood that nucleocytoplasmic transport occurs with the help of soluble nuclear transport receptors (NTRs) [85, 86]. The major transport receptors are members of the importin β superfamily, also called karyopherins. There are at least 20 karyopherins in human and 14 in yeast [87, 88], which can roughly be divided into importins or import receptors that mediate nuclear import and exportins or export receptors that mediate nuclear export. So far, only importin 13, exportin 4 and Msn5 are known to have a bi-directional function in import and export [89, 90, 91]. By definition, karyopherins can interact with the GTP-binding nuclear protein Ran [92, 93] as well as their cargoes [94, 95]. The different karyopherins share similar molecular parameters, for example a molecular weight between 95 and 145 kDa, an acidic isoelectric point, and similar structural features [78, 87, 96, 97].

In order to be recognized by transport receptors, most proteins that need to be imported or exported contain a nuclear localization signal (NLS) or a nuclear export signal (NES), respectively [78, 88, 97]. Import receptors bind to the NLS of import cargoes and import them through the nuclear pore complex into the nucleus. For nuclear export, the major export receptor CRM1 recognizes the NES of export cargoes.

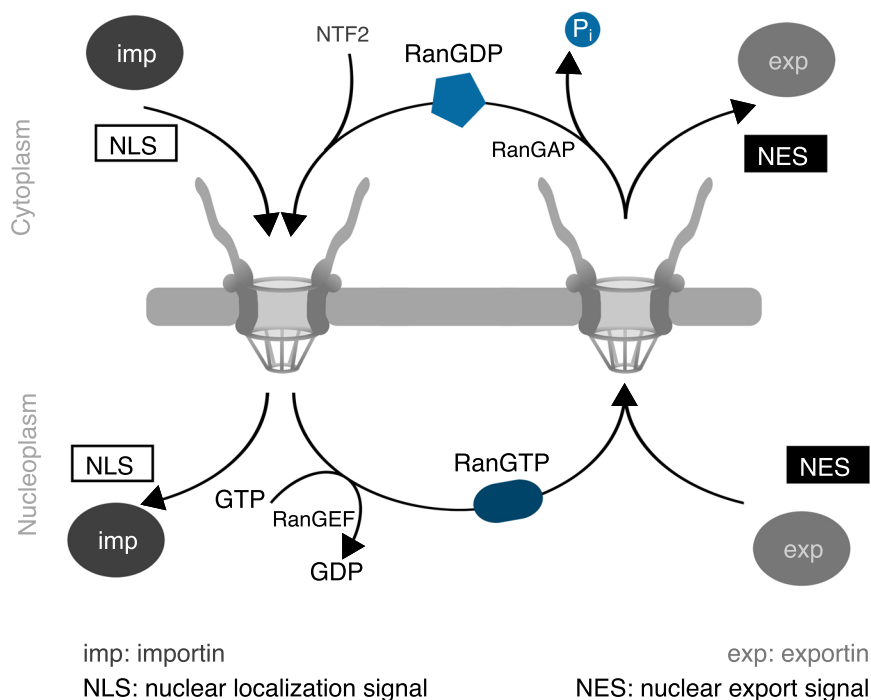


Figure 3: The Ran cycle in nucleocytoplasmic transport. Upon nuclear import of RanGDP by NTF2, RanGDP is converted to RanGTP by RanGEF. RanGTP and an NES-containing cargo bind cooperatively to export receptors. The export complex translocates to the cytoplasm where it dissociates upon hydrolysis of RanGTP by RanGAP.

Karyopherin-mediated nucleocytoplasmic transport is coupled to a gradient of Ran in its GTP or GDP-bound state [93, 98] (figure 3). The ratio of nuclear to cytoplasmic RanGTP was estimated to be between 200 to 1000 in *in silico* simulations [99] and experimental studies [100, 101]. RanGTP is constantly depleted from the nucleus in export receptor-cargo complexes. The Ran efflux rate from the nucleus was shown to exceed 520 molecules per second per nucleus [99] implicating the need for a tight regulation of the Ran-gradient. The RanGTP-gradient is established by RanGAP1 in the cytoplasm [102, 103, 104], the Ran guanine nucleotide exchange factor (RanGEF/ RCC1) in the nucleus [105, 106] and the RanGDP import receptor NTF2 (reviewed by [78]). NTF2 was first identified as a stimulating factor of NLS-mediated import [107, 108, 109, 110]. Later, NTF2 was shown to bind to the Switch II region of Ran, a region that has different conformations in its GTP or GDP bound state. NTF2 can therefore discriminate between GDP- and GTP-loaded Ran, leading to exclusive import of RanGDP [111]. In the nucleus, RanGDP is converted to RanGTP by RanGEF. RanGEF was found to associate to chromatin with one copy of RanGEF binding to histones H2A and H2B of one nucleosome [106, 112, 113]. RanGEF does not discriminate between GTP and GDP,

but only stimulates nucleotide exchange by five orders of magnitude [106]. Conversion from RanGDP to RanGTP is therefore achieved by the high GTP to GDP ratio in the nucleus.

Importins recognize their cargoes via the NLS in the cytoplasm and translocate through the NPC into the nucleus [92, 93]. In the nucleus, binding of RanGTP to importins leads to import cargo release [92, 93] whereas RanGTP binding to exportins leads to cooperative binding of export cargoes, which are recognized via a nuclear export signal (NES) [94]. Subsequently, the trimeric exportin-RanGTP-cargo export complex is transported through the NPC into the cytoplasm, where it dissociates upon RanGAP1 (GTPase-activating protein) and RanBP1/RanBP2-mediated hydrolysis of RanGTP to RanGDP [24].

1.2.2 Nuclear transport receptors

Transport receptors have been extensively studied by X-ray crystallography. The structures of human and yeast importin β [114, 115], transportin [116], and the exportins CRM1 [117] and Cse1p [118] indicate that karyopherins consist of tandem "Huntingtin, elongation factor 3 (EF3), protein phosphatase 2A (PP2A), and the P3 kinase TOR1" (HEAT) repeats [119, 120]. HEAT repeats have a length of around 40-60 amino acids and consist of two anti-parallel helices that are connected by a short linker [119, 120].

The best studied import receptor is importin β , which was crystallized with several cargoes, adaptors, RanGTP and FG repeat-containing peptides [114, 121, 122, 123, 124, 125]. On the other hand, CRM1 is the most studied export receptor and will be described in further detail in section 1.2.3.

Even though the structure of karyopherins is similar, there are distinct differences between import and export complexes. Import receptors bind either their cargo or RanGTP at the inner surface of their superhelical structure [115, 121, 126] whereas export receptors bind RanGTP at the inner surface and their cargo via the NES-binding cleft embedded on the outer surface [116, 118, 127] (figure 4).

The so-called classical NLS with one or two clusters of basic amino acids was first characterized in the SV40 Large T antigen and in nucleoplasmin [85].

In general, export receptors recognize their cargo by an NES (reviewed in [78, 97]). The leucine-rich NES was initially discovered in the HIV-1 Rev protein, a viral adapter that promotes export of unspliced and partially spliced viral mRNA [128] and PKI, an inhibitor of the catalytic subunit of the cAMP-dependent protein kinase [129], and defined as a conserved motif with three to four hydrophobic amino acids. Hydrophobic NESs are conserved in all eukaryotes and are recognized by the also highly conserved major export factor CRM1 [94, 130].

In addition to direct interaction of the NTRs with a NLS or NES containing cargo, nuclear transport can also be mediated via adapter proteins, the most prominent being importin α which serves as an adapter for importin β [131, 132, 133]. The crystal structure of importin α [134]/Kap60p [135] revealed that it consists of armadillo (ARM) repeats. ARM repeats were first observed in the *Drosophila* ARM protein [136] and now used to describe a structure of three

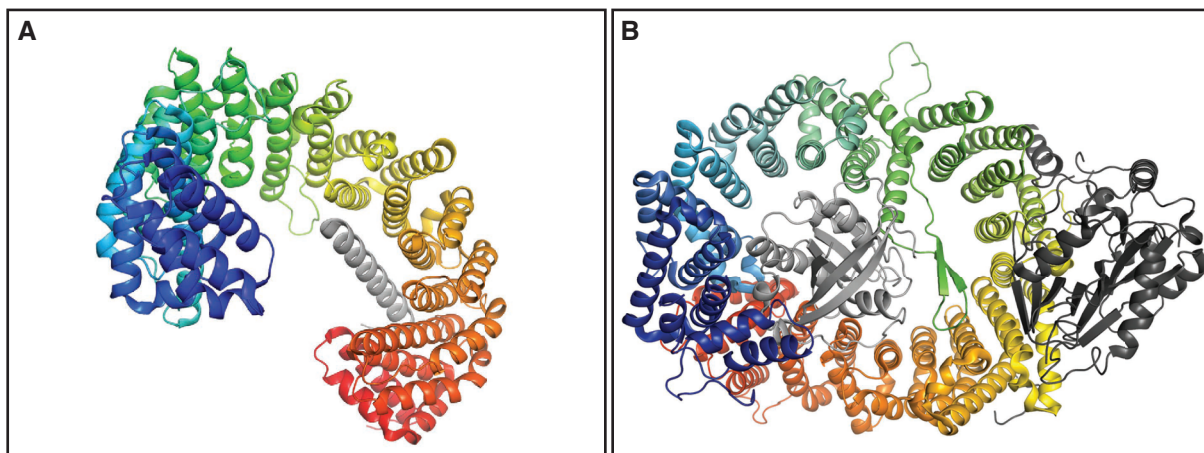


Figure 4: Comparison of import and export complexes. (A) Complex of importin β (colored) bound to the IBB domain of SPN1 (gray) (PDB ID: 2QNA, [126]). (B) Complex of CRM1 (colored) bound to RanGTP (light gray) and SPN1 (dark gray) (PDB ID: 3GJX, [127]).

helices that consist of about 40 amino acids. The ARM repeats of importin α form a super-helical structure [134, 137, 138] which creates a shallow concave binding groove and serves as a binding pocket for the NLS [134, 137]. The extensive contacts between the importin α ARM repeats and the NLS are mediated through hydrophobic and charge-based interactions [134, 137, 138, 139]. It was also discovered that the binding of importin α to its cargo can be disturbed upon phosphorylation of an amino acid close to the NLS [140].

1.2.3 The nuclear export receptor CRM1

The major nuclear export receptor is chromosome region maintenance 1 (CRM1). CRM1 is essential in all organisms tested so far and highly conserved in eukaryotes [141]. CRM1 mediates the export of a large variety of cargoes, most of them via a leucine-rich NES [94, 130, 142, 143, 144, 145]. CRM1 cargoes include eukaryotic translation initiation and termination factors [146], the import adaptor snurportin1 (SPN1) [131] or ribonuclear particles (RNPs) [147, 148].

Initially, CRM1 was identified in cold-sensitive *Schizosaccharomyces pombe* strains with deformed chromosomes [149]. The first indication of its role in nuclear transport was its interaction with the nucleoporin 214 (Nup214) [54, 58].

The most prominent inhibitor of CRM1 is leptomycin B (LMB) which was isolated from *Streptomyces sp.* [150, 151, 152] and covalently modifies cysteine 528 of human CRM1 within the NES cleft thereby inhibiting cargo binding [153, 154]. Later on, a group of inhibitors called Ratjadones were also shown to work via the same mechanism [155]. Crystal structures of CRM1 bound to LMB, Anguinomycin A or Ratjadone A later confirmed their mechanism of inhibition [156].

Early on, CRM1 was implicated in the replication cycle of the human immunodeficiency virus (HIV) as it interacts with the HIV-1 protein Rev. Recently, CRM1 also

gained importance as a target in cancer therapy, as it was shown to interact with several (proto-) oncogenes like p53, Rb, BRCA1, p21/CIP, p27/KIP1 and cyclin D1 [157, 158, 159, 160, 161], implicating a role in breast cancer, pancreatic cancer, leukemia and lymphoma [157, 162, 163, 164, 165, 166, 167, 168, 169]. Medical research focuses on inhibitors that target the NES binding cleft on CRM1 (reviewed in [170]).

CRM1 has been extensively studied by crystallography, yielding more than 30 crystal structures of CRM1, either alone or bound to other factors, in the Protein Data Bank (PDB). CRM1 consists of 21 HEAT repeats that form a superhelical structure. The N-terminal CRIME (CRM1-importin β etc.) domain [54, 171] is the most conserved region between the karyopherins and is necessary for the binding of RanGTP [116, 121]. CRM1 was captured in several different states of its transport cycle. There are structures of free CRM1 [172, 173], CRM1 bound to the cargo SPN1 [174], CRM1 bound to RanGTP [175], CRM1 bound to RanGTP and the export complex assembly factor RanBP3 [176], the CRM1-RanGTP-SPN1 export complex [127] and CRM1 bound to RanGTP and the export complex dissociation factor RanBP1 [156, 177]. An extensive list of all crystal structures containing CRM1 can be found in [170]. Furthermore, CRM1 has also been studied by electron microscopy, small angle X-ray scattering and molecular dynamics simulations [172, 173, 178, 179].

All available structural information leads to the conclusion that CRM1 is a highly dynamic protein that undergoes major conformational changes throughout its transport cycle. The structural features most involved in these conformational changes are the acidic loop within HEAT repeat 9, the NES binding cleft located between the A-helices of HEAT repeats 11 and 12, and the HEAT repeat 21 at the C-terminus.

The acidic loop, also termed HEAT9 loop, is a 26 residue-loop that protrudes from the two helices of HEAT repeat 9 and forms a β -hairpin. Structure of CRM1 bound to a cargo show the acidic loop spanning across the ring of the CRM1 molecule and interacting on the opposite side of the toroid with the HEAT repeats 14 and 15. The acidic loop thereby acts as a diagonal brace, stabilizing the binding of RanGTP as well as keeping the NES binding cleft in an open conformation [127]. On the other hand, crystal structures of free CRM1 or CRM1 bound to RanGTP and export complex dissociation factor RanBP1 have the acidic loop folded backwards onto the inner surface of HEAT repeats 11 and 12, coinciding with a closed conformation of the NES binding cleft [172, 177].

HEAT repeat 21 is at the C-terminus of the CRM1 molecule. In all CRM1 crystal structures, the helix B of HEAT21 is either positioned in a stack with the other HEAT repeats (see e.g. [127]) or folded away from the stack, spanning across the ring of the CRM1 molecule and interacting with the inner surface of the CRM1 molecule at the rear side of the NES binding cleft (see e.g. [172, 174]).

Unbound CRM1 seems to be flexible to adapt several conformations, with a preference for an acidic loop that is folded backwards and a ring-spanning HEAT21 helix [172].

Although the dynamics of CRM1 have been extensively studied with crystallography, there are no crystal structures available with CRM1 bound to any nucleoporin.

1.3 Interaction of transport receptors with the NPC

1.3.1 Karyopherins interact with FG-repeat domains on nucleoporins

All current transport models are based on transient interactions of karyopherins with FG-repeat domains of nucleoporins. Nucleoporins contain multiple FG-repeats which are clustered into a single FG-repeat domain in most of the nucleoporins. Nevertheless, it has been shown for the yeast nucleoporin Nup116p that it could in principle bind two transport factors, the mRNA export factor Mex67p and importin β homologue Kap95p, with distinct regions at the same time [180, 181]. Of the 33 Nup116 FG-repeats, Mex67p associates with the first 12 repeats, whereas Kap95p interacts with the last 12 repeats [181]. Correlating to the large number of FG-repeats in the nucleoporins, it is not surprising that transport receptors might contain multiple nucleoporin binding sites [182]. For importin β it has been shown that it can bind to nucleoporins with the N-terminal region (between HEAT repeats 4 - 9) [183, 184, 185] as well as with a later identified region in the C-terminal part [84]. Furthermore, available structures confirm that also TAP [186], exportin-t [187] and nuclear transport factor 2 (NTF2) [188] contain at least two phenylalanine binding sites and Mtr2p even was shown to have three nucleoporin binding regions [180]. Computational models suggest that transport receptors bind multiple FGs at the same time [189, 190]. Interaction of importin β with the NPC seems to involve Nup358 [191, 192, 193], the Nup62 complex [194] and Nup153 [195, 196]. An extensive list of observed interactions between karyopherins and nucleoporins can be found in [21].

It has been suggested that weak interactions of transport receptors with the nucleoporins are used to concentrate the transport receptors and other transport factors as well as cargoes independently at the periphery of the NPC and therefore promote cargo-receptor complex formation. This has been shown for the cargo-free Xpo-t binding to Nup214 [187] and the yeast Kap60p binding to Nup2p [197]. Also the import adapter Snurportin 1 (SPN1) associates with U snRNPs directly at Nup214 [198]. Similarly, importin α/β cargoes DBC-1 and DMAP-1 bind independent of transport receptors at Nup358 [199]. The binding of RanGAP to Nup358 was shown to be important for nuclear import [200, 201].

1.3.2 Available structures of transport factors with FG-repeats

The interaction of transport receptors and adapters with nucleoporins has been the subject of many studies. Structural approaches to elucidate the interaction on a molecular level are complicated by the fact that FG-repeat containing regions are natively unfolded [34]. All available structures in the PDB of transport receptors or adapters in complex with nucleoporin fragments or nucleoporin-derived peptides are summarized in table 1.

Of the 14 structures, 5 structures show an interaction that is not FG-mediated. This is the case for structures containing human and yeast importin α bound either to an Nup2p N-terminal fragment or to Nup50 as well as a structure of Kap121p bound to Nup53p [135, 197, 202, 203]. Four of the structures show an overlap of the nucleoporin interaction surface with the NLS

binding site, which could lead to a destabilization of NLS binding by nucleoporins (PDB IDs: 1UNO, 2C1T, 2C1M, 3W3Y), two of them show an interaction of the nucleoporin at the C-terminus of the transport factor (PDB IDs: 3TJ3, 3W3Y).

Interactions of transport factors with FG-repeats have been characterized in complexes containing fragments of importin β , NTF2, p15-TAP, the UBA domains of TAP and Mex67 as well as for Xpo1p. Two structures are available that show the interaction of synthetic FXFG peptides with the UBA domains of Tap (PDB ID: 1OAI) [204] and Mex67 (PDB ID: 2KHH) [205]. First indications of the binding mode between transport receptors and FG-containing nucleoporins came from a crystal structure of an N-terminal fragment of importin β bound to a synthetic peptide containing five FxFG nucleoporin repeats from Nsp1p (PDB ID: 1F59) [122]. Even though a 112-residue fragment of Nsp1p had been used for crystallization, only two short regions of 8 and 13 residues could be observed in the structure. Of those only 4 and 10 residues, respectively, could actually be assigned. Both fragments each contain two phenylalanine residues. The structure revealed two FG binding sites on the outer convex surface of importin β . Binding of phenylalanine residues occurs in hydrophobic pockets which are formed between HEAT repeats 5 and 6 as well as 6 and 7 of importin β . These interaction sites could be verified by another crystal structure of the same fragments (PDB ID: 1O6O) [206] as well as by structures containing the same importin β fragment with a synthetic GLFG peptide (PDB ID: 1O6P) [206] and yeast importin β in complex with a 39 residue fragment of yeast Nup1p (PDB ID: 2BPT) [207]. Moreover, the latter structure also contained an additional binding site of a third phenylalanine residue between HEAT repeats 7 and 8 of yeast importin β .

The export factor TAP-p15 does not contain HEAT- or ARM-repeats, but nevertheless was shown to bind the FG-containing nucleoporins Nup214 as well as Nup98 [208]. A TAP-p15 fragment was crystallized with a Nup214-derived peptide containing one FG repeat (PDB ID: 1JN5) [209]. The binding of the phenylalanine residue of the Nup214-peptide to a hydrophobic pocket on TAP was comparable to the binding the Nsp1p fragment to importin β [122]. Two FG-binding sites were also identified in a structure of a NTF2-dimer, each binding a phenylalanine residue from a synthetic FXFG peptide (PDB ID: 1GYB) [210]. Only recently, a structure of the yeast homologue of CRM1, Xpo1p, has been published in complex with the RanBP3 homologue Yrb2p. The structure revealed two FG-binding regions on Xpo1p, each binding three phenylalanine residues of Yrb2p (PDB ID: 3WYF) [176].

The available crystal structures of transport receptors with FG-repeat containing fragments indicate that there are multiple possible interaction sites between phenylalanine side chains from individual nucleoporins and hydrophobic pockets on the respective transport receptors. However, no structures of transport receptors with a larger FG-repeat containing fragment are available so far. Deciphering the molecular interactions of transport receptors and nucleoporins could help to understand how transport complexes translocate through the nuclear pore - if they immerse into the sieve-like structure as suggested in the selective phase model or if they transit from one to the next FG-Nup through the channel as suggested in the virtual gating model.

Table 1: Overview of structures of transport factors with FG-repeats.

PBD ID	Proteins	Resolution [Å]	Reference
1F59	<i>Hs</i> importin β (1-442) bound to <i>Sc</i> FXFG repeats	2.80	[122]
1O6P	<i>Hs</i> importin β (1-442) bound to a synthetic GLFG peptide	2.80	[206]
1O6O	<i>Hs</i> importin β (1-442) bound to <i>Sc</i> Nsp1p	2.80	[206]
2BPT	<i>Sc</i> importin β bound to <i>Sc</i> Nup1p	1.99	[207]
1GYB	<i>Sc</i> NTF2(N77Y mutant) bound to synthetic FXFG peptide	1.90	[210]
3W3Y	<i>Sc</i> Kap121p bound to <i>Sc</i> Nup53p	2.80	[203]
2KHH	<i>Sc</i> Mex67 UBA domain bound to synthetic FXFG peptide	NMR	[205]
1JN5	<i>Hs</i> p15 and <i>Hs</i> TAP bound to <i>Hs</i> Nup214 peptide with 1 FG repeat (aa1810-1815)	1.90	[209]
1OAI	<i>Hs</i> Tap UBA domain bound to synthetic FXFG peptide	1.00	[204]
3WYF	<i>Sc</i> Xpo1p - <i>Sc</i> Yrb2p - <i>Sc</i> Gsp1p-GTP complex	2.22	[176]
1UN0	<i>Sc</i> importin α bound to Nup2p N-terminal fragment	2.60	[197]
2C1T	<i>Sc</i> importin α bound to <i>Sc</i> Nup2	2.60	[135]
2C1M	<i>Mm</i> importin α bound to <i>Mm</i> Nup50	2.20	[135]
3TJ3	<i>Hs</i> importin α bound to <i>Hs</i> Nup50 N-terminal fragment	2.70	[202]

Sc: *S. cerevisiae*, *Hs*: *H. sapiens*, *Mm*: *M. musculus*

1.4 Aim of this Work

To understand nucleocytoplasmic transport at a molecular level, it is necessary not only to determine the NPC structure at an atomic resolution [5], but also to capture the molecular interaction of transport complexes with components of the NPC. Available crystal structures of karyopherins bound to FG-containing peptides only show binding of individual phenylalanines. There is no structure available that shows binding of a larger fragment of FG-Nups to a transport receptor.

The interaction of the major export receptor CRM1 with the cytoplasmic Nup214 was chosen as an example to address this issue. Nup214 is the third largest nucleoporin in humans and contains the largest FG-repeat domain of all FG-nucleoporins. The CRM1-interacting region was initially mapped to the C-terminus of Nup214 [54, 58] and later refined to several regions within the C-terminus [59]. On the other hand, the nucleoporin-interacting region on CRM1 is totally unclear. Due to its characteristic structure, the identification of the Nup214-binding sites on CRM1 with common biochemical approaches like the analysis of truncated fragments would likely be inconclusive as truncations might not only affect binding to Nups, but also the cooperative binding of RanGTP and NES-cargo. The Nup214-binding sites on CRM1 should therefore be identified by structural approaches. Although crystal structures of importins with FG-repeat containing peptides in conjunction with the high structural conservation between importin β and CRM1 within the N-terminal HEAT-repeats suggests that FG-repeats might bind to a similar region on the outer surface of CRM1, there is no experimental evidence for this assumption.

The aim of this work was therefore to identify the interacting regions of Nup214 and CRM1 with structural approaches using electron microscopy, cross-linking mass spectrometry and X-ray crystallography. Furthermore, identified interaction sites should be verified and characterized by biochemical and cellular assays. The gained insight in the interaction principles of nucleoporins and karyopherins would help to elucidate the molecular mechanism of nucleocytoplasmic transport.

2 Material and Methods

2.1 Material

2.1.1 Software

Table 2: Software.

Software	Company
Adobe Illustrator CS6	Adobe
Adobe Photoshop CS6	Adobe
AxioVision (LE) Rel. 4.5	Carl Zeiss
BibDesk 1.6.2	Copyright Michael O. McCracken
Chimera 1.8	UCSF/NIH
Image Reader LAS-3000	Fujifilm
ImageJ	NIH
ImageStudio, ImageStudio Lite 4.0.21	LI-COR
MacPyMOL	Schrödinger LLC
NanoDrop 2000 Software	ThermoScientific
SerialCloner 2.6.1	SerialBasics
TeXShop 3.18	GPL public license

2.1.2 Technical Equipment

Table 3: Technical equipment.

Equipment	Company
ÄKTA column HiLoad 26/60 Superdex 200 prep grade	GE Healthcare
ÄKTA column HiLoad 26/60 Superdex 75 prep grade	GE Healthcare
ÄKTA column HiPrep 26/10 Desalting (Sephadex G-25)	GE Healthcare
ÄKTA column MonoQ	GE Healthcare
ÄKTA column Superdex 200 10/300 GL	GE Healthcare
ÄKTA column Superdex 75 10/300 GL	GE Healthcare
ÄKTApurifier	Amersham Biosciences
Autoclave Sterilizer DX-200	System
BioPhotometer	Eppendorf
CASY 1	Schärfe System
Cell culture hood Herasafe™ KS	ThermoScientific
Cell culture incubator Heracell™ 150i	ThermoScientific
Centrifuge 5415R	Eppendorf
Centrifuge 5424	Eppendorf
Centrifuge Allegra® X-15R with rotor SX4750	Beckman Coulter
Centrifuge Avanti™ J-30I with rotor JA30.50Ti	Beckman Coulter
Centrifuge J6-MI with rotor TY-JS 4.2	Beckman Coulter
Confocal microscope LSM 510 meta	Zeiss
Developer machine CURIX60	Agfa
Documentation system GelSTICK "touch"	INTAS Science Imaging Instruments
Documentation system LAS-3000	Fujifilm
Dual Gel Caster for Mini Vertical Units	Hoefler

Equipment	Company
EmulsiFlex-C3	Avestin
FACSCanto™ II	BD Biosciences
Fluorescence microscope Axioskop 2	Zeiss
Incubator Heraeus function line	Heraeus
Incubator Shaker INNOVA 4430	New Brunswick Scientific
Mini Trans-Blot® Cell	Bio-Rad
Odyssey® Sa Infrared Imaging System	LI-COR
SE250 Mighty Small II Mini Vertical Electrophoresis Unit	Hofer
Spectrophotometer NanoDrop 2000c	ThermoScientific
Thermocycler FlexCycler ²	Analytik Jena AG
Thermocycler PTC-200 DNA Engine	MJ Research
Thermocycler Tprofessional	Biometra
Thermomixer comfort	Eppendorf
Thermomixer compact	Eppendorf
Ultracentrifuge Optima™ MAX-XP with rotors TLA100.3, TLA120.1	Beckman Coulter
UV cross linker with Ultratech 400 W halogen metal vapor lamp and a B270 glass screen	Osram/ Schott
Vortexer MS2 Minishaker	IKA
Waterbath with Bath Circulator LAUDA A100	Thermal Exchange
Western blot incubation boxes	LI-COR
XCell SureLock® Mini-Cell	life technologies

2.1.3 Consumables

Table 4: Consumables.

Consumable	Company
5ml Polystyrene Round-Bottom Tubes	BD Biosciences
Amersham Hybond ECL Nitrocellulose Blotting Membrane	GE Healthcare
Amersham Hyperfilm™ ECL	GE Healthcare
Amersham Protran 0.45 µm NC Nitrocellulose Blotting Membrane	GE Healthcare
Amicon® Ultra Centrifugal Filters, Ultracel®	Millipore
Cell culture consumables	Sarstedt, Nalge Nunc International, greiner bio-one
Cell culture plastic ware	Sarstedt, greiner bio-one
Diagnostic Microscope Slides, 10 wells	Erie Scientific Company
DNA Pick-Tips	Süd-Laborbedarf GmbH
Medix XBU medical x-ray film	FOMA Bohemia
Microscope cover slips (12 mm Ø)	Marienfeld
Microscope slides (76x26 mm)	Glaswarenfabrik Karl Hecht GmbH & Co KG
Minisart RC 15, single use syringe filters (0.45 µm, 0.20 µm)	sartorius stedim biotech
Minisart single use filter units (0.45 µm)	sartorius stedim biotech
Novex® 10-20% Tricine Protein Gels	life technologies
NuPAGE® Novex® 4-12% Bis-Tris Protein Gels	life technologies
Parafilm "M"	Bemis Company, Inc.
pH indicator strips	Machery-Nagel
Reaction tubes	Sarstedt, greiner bio-one

Consumable	Company
Spin-XR, PES membrane	Corning
Syringes and needles	Braun, servoprax
VIVASPIN, PES membrane	sartorius stedim biotech

2.1.4 Kits

Table 5: Kits.

Kit	Company
CloneJET PCR Cloning Kit	ThermoScientific
NucleoBond™ Xtra Midi	Macherey-Nagel
NucleoSpin® Gel and PCR Clean-up	Macherey-Nagel
NucleoSpin® Plasmid	Macherey-Nagel
Pierce® BCA Protein Assay Kit	ThermoScientific
Pierce® Silver Stain Kit	ThermoScientific
SilverQuest™ Staining Kit	invitrogen

2.1.5 Chemicals, Reagents, Enzymes

All standard chemicals and solvents used for this work were obtained from AppliChem GmbH (Darmstadt), Carl Roth GmbH + Co. KG (Karlsruhe), Serva Electrophoresis GmbH (Heidelberg), Sigma-Aldrich (Taufkirchen) or Merck (Darmstadt).

Table 6: Chemicals and Reagents.

Reagent	Company
β-Mercaptoethanol	Roth
Acrylamide 4K Solution (30%)	AppliChem
Adenosine 5'-triphosphate disodium salt hydrate (A3377)	Sigma-Aldrich
Advanced protein assay reagent 5x	Cytoskeleton Inc.
Amersham Cy3™ Mono-Reactive Dye Pack	GE Healthcare
Amylose Resin High Flow	New England BioLabs
Bio-Rad Protein Assay dye reagent concentrate	Bio-Rad Laboratories GmbH
Bovine Serum Albumin (BSA) (20 mg/ml)	ThermoScientific
BSA, fraction V	AppliChem
Crosslinker BS ³	ThermoScientific
Crosslinker DTSSP	ThermoScientific
Crosslinker EDC	Pierce
Cyanogen bromide-activated Sepharose 4B	Sigma-Aldrich
Dako Fluorescent Mounting Medium	Dako
dNTP Set, 100 mM Solutions	ThermoScientific
FBS Superior	Biochrom
FluorSave Reagent	Millipore
Formaldehyde solution min. 37%	Millipore
Gelatin from cold water fish	Sigma-Aldrich
GeneRuler 100bp DNA Ladder	ThermoScientific
GeneRuler 1kb DNA Ladder	ThermoScientific

Reagent	Company
Gibco® DMEM (1x)	life technologies
Gibco® Opti-MEM® (1x)	life technologies
Gibco® Penicillin Streptomycin (Pen Strep)	life technologies
Glutathione Sepharose 4 Fast Flow	GE Healthcare
Glutathione Sepharose High Performance	GE Healthcare
Guanosine 5'-diphosphate sodium salt (G7127)	Sigma-Aldrich
Guanosine 5'-triphosphate sodium salt hydrate (51120)	Sigma-Aldrich
HistoGel	Linaris Biologische Produkte GmbH
Immobilon™ Western Chemiluminescent HRP Substrate	Millipore
IPTG	ThermoScientific
L-Glutamine 200 mM	Gibco (life technologies)
Lectin from <i>Triticum vulgare</i>	Sigma-Aldrich
Lectin from <i>Triticum vulgare</i> -Agarose	Sigma-Aldrich
Leptomycin B	Enzo Life Sciences
Lipofectamine® 2000	life technologies
NeutrAvidin® Agarose	ThermoScientific
NeutrAvidin DyeLight800	ThermoScientific
Ni-NTA Agarose	Qiagen
Novex® Tricine SDS Running Buffer (10X)	life technologies
NuPAGE® MES SDS Running Buffer (20x)	life technologies
NuPAGE® MOPS SDS Running Buffer (20x)	life technologies
NuPAGE® LDS Sample Buffer (4x)	life technologies
Oligofectamine™ Reagent	life technologies
Oligonucleotides	Sigma-Aldrich
ortho-Phosphoric acid 85% p.A.	AppliChem
PageRuler Plus Prestained Protein Ladder	ThermoScientific
PageRuler Prestained Protein Ladder	ThermoScientific
PageRuler Unstained Protein Ladder	ThermoScientific
Poly-L-lysine solution 0.1% (w/v)	Sigma-Aldrich
Protein A-Agarose	Roche
SERVA DNA Stain Clear G	SERVA
Spectra Multicolor Low Range Protein Ladder	ThermoScientific
Streptavidin HRP	BD Pharmingen
TALON® Metal Affinity Resin	Takara Bio Company
Trichostatin A (T8552)	Sigma-Aldrich

Table 7: Enzymes.

Enzyme	Company
Creatine phosphokinase, Rabbit Skeletal Muscle	CALBIOCHEM
DNAseI	AppliChem
Pfu Ultra II polymerase	Agilent
Phusion High-Fidelity DNA Polymerase	ThermoScientific
Restriction enzymes	ThermoScientific
T4 DNA ligase	ThermoScientific
Gibco® Trypsin/ EDTA 0.25% (1x)	life technologies

2.1.6 Buffers, Stock solutions, Media

Table 8: Buffers and Solutions.

Buffer	Composition
Coomassie destaining solution	10% acetic acid
Coomassie fixing solution	40% ethanol, 10% acetic acid
Coomassie staining	5% aluminum sulfate-(14-18)-hydrate, 10% ethanol, 2% ortho-phosphoric acid, 0.02% CBB-G250
CRM1 desalting buffer	50 mM HEPES pH 7.5, 50 mM NaCl, 2 mM Mg(OAc) ₂ , 2 mM DTT
CRM1 high salt buffer	50 mM HEPES pH 7.5, 500 mM NaCl, 2 mM Mg(OAc) ₂ , 2 mM DTT
CRM1 prep buffer	50 mM HEPES pH 7.5, 500 mM NaCl, 2 mM MgCl ₂ , 20 mM β-mercaptoethanol, 100 μM PMSF, 1 μg/ml of each AP and LP
DNA loading buffer (6x)	0.2% bromophenol blue, 0.2% xylene cyanole, 60% glycerol, 60 mM EDTA
Export complex buffer	20 mM Tris pH 7.4, 50 mM NaCl, 1 mM Mg(OAc) ₂ , 2 mM DTT
EM buffer	20 mM HEPES pH 7.4, 50 mM NaCl, 1 mM Mg(OAc) ₂ , 1 mM DTT
GST prep buffer	50 mM Tris pH 6.8, 300 mM NaCl, 1 mM MgCl ₂ , 0.25 mM EDTA, 1 mM DTT, 1 μg/ml of each AP and LP
Halo mix (4x)	500 mM NaCl, 40 mg/ml BSA, 1 mM DTT, 2% 1,6-hexanediol
HBS (2x) buffer	50 mM HEPES, 250 mM NaCl, 1.5 mM Na ₂ HPO ₄ , pH 6.98
His prep buffer	50 mM Tris pH 6.8, 200 mM NaCl, 1 mM MgCl ₂ , 10% glycerol, 4 mM β-mercaptoethanol, 100 μM PMSF, 1 μg/ml of each AP and LP
Laemmli running buffer (10x)	250 mM Tris, 1.92 M glycine, 0.5% SDS
Nup214 complex buffer	20 mM Tris pH7.4, 50 mM NaCl, 1 mM Mg(OAc) ₂ , 2% sucrose, 1 mM DTT
PBS (10x)	1.37 M NaCl, 27 mM KCl, 100 mM Na ₂ HPO ₄ , 18 mM KH ₂ PO ₄ , pH 7.5
PBST	1x PBS + 0.1% Tween-20
PonceauS staining solution	0.5% PonceauS in 1% acetic acid
Pulldown buffer	50 mM Tris pH 7.4, 200 mM NaCl, 1 mM MgCl ₂ , 5% glycerol, 1 mM DTT
Ran prep buffer	50 mM HEPES pH 8.0, 500 mM NaCl, 5 mM MgCl ₂ , 100 μM PMSF, 1 μg/ml of each AP and LP
SDS sample buffer (4x)	125 mM Tris pH 6.8, 4% SDS, 0.02% Bromophenol blue, 10% glycerol
Silver staining - fixing solution	50% methanol, 10% acetic acid, 100 mM ammonium acetate
Silver staining - sensitizing solution	0.005% sodium thiosulfate
Silver staining - staining solution	0.1% silver nitrate
Silver staining - developing solution	0.037% formaldehyde, 2% sodium carbonate
Silver staining - stopping solution	50 mM EDTA
TAE buffer (50x)	2 M Tris, 0.05 M EDTA, 5.71% acetic acid
TFB-I	30 mM potassium acetate, 10 mM CaCl ₂ , 50 mM MnCl ₂ , 100 mM RbCl, 15% glycerol
TFB-II	100 mM MOPS, 75 mM CaCl ₂ , 10 mM RbCl, 15% glycerol
Transport buffer (10x)	200 mM HEPES, 1.1 M KOAc, 20 mM Mg(OAc) ₂ , 10 mM EGTA, pH 7.3
Western blot transfer buffer (10x)	250 mM Tris, 1.93 M glycine, 0.2% SDS

Table 9: Stock solutions.

Stock solution	Composition
1,4-Dithiothreitol (DTT)	1 M in H ₂ O
Ammonium persulfate (APS)	10% APS (Sigma) in H ₂ O
Ampicillin	100 mg/ml in H ₂ O
Aprotinin	1 mg/ml in 20 mM HEPES pH 7.4
Adenosine triphosphate (ATP)	100 mM ATP in 100 mM Mg(OAc) ₂ , 20 mM HEPES (pH 7.4)
Chloramphenicol	30 mg/ml
Creatine phosphokinase	2000 U/ml in 50% glycerol, 20 mM HEPES pH 7.4
Creatine Phosphate	80 mg/ml in H ₂ O
Dexamethasone	2.5 mM in EtOH
digitonin	10% (w/v) in DMSO
Hoechst 33258	10 mg/ml
Ionomycin	1 mM in DMSO
Isopropyl β-D-1-thiogalactopyranoside (IPTG)	1 M in H ₂ O
Kanamycin	60 mg/ml in H ₂ O
Leupeptin/Pepstatin	1 mg/ml each, in DMSO
Phenylmethylsulfonyl fluoride (PMSF)	100 mM in 2-propanol
Trichostatin A (TSA)	1 mM in EtOH
Lectin (WGA)	2 mg/ml

Table 10: Bacterial media.

Medium	Composition
2YT	1.6% (w/v) tryptone, 1% (w/v) yeast extract, 0.5% (w/v) NaCl, pH 7.0
LB	1% (w/v) bacto-tryptone, 0.5% (w/v) yeast extract, 1% (w/v) NaCl, pH 7.0
LB agar plates	LB supplemented with 1.5% (w/v) bacto-agar
MBP rich medium	1% (w/v) tryptone, 0.5% (w/v) yeast extract, 0.5% (w/v) NaCl, 0.2% (w/v) glucose
SOC	2% (w/v) tryptone, 0.5% (w/v) yeast extract, 10 mM NaCl, 2.5 mM KCl, 10 mM MgCl ₂ , 10 mM MgSO ₄ , 0.36% (w/v) glucose, pH 7.0

2.1.7 Cell lines

Table 11: Cell lines.

Cell line	Specification	Origin
HeLa P4	adherent human cervix carcinoma cells that express CD4	[211]
HeLa NFAT spinner	HeLa cells that are stably transfected with a vector coding for the fusion protein GFP-NFAT (nuclear factor of activated T-cells)	[145]

2.1.8 *E. coli* strains

Table 12: *E. coli* strains.

<i>E. coli</i> strain	Specification & Genotype
DH5 α	F- Φ 80lacZ Δ M15 Δ (lacZYA-argF) U169 recA1 endA1 hsdR17 (rK-, mK+) phoA supE44 λ - thi-1 gyrA96 relA1
XL10-Gold	endA1 glnV44 recA1 thi-1 gyrA96 relA1 lac Hte Δ (mcrA)183 Δ (mcrCB-hsdSMR-mrr)173 tetR F'[proAB lacIqZ Δ M15 Tn10(TetR Amy CmR)]
JM109	endA1 glnV44 thi-1 relA1 gyrA96 recA1 mcrB+ Δ (lac-proAB) e14- [F' traD36 proAB+ lacIq lacZ Δ M15] hsdR17(rK- mK+)
BL21 (DE3) codon+	F- ompT hsdS(rB- mB-) dcm+ TetR gal λ (DE3) endA Hte [argU proL CamR]
LEMO21 (DE3)	fhuA2 [lon] ompT gal (λ DE3) [dcm] Δ hsdS/ pLemo(CamR)
TG1	F' [traD36 proAB+ lacIq lacZ Δ M15]supE thi-1 Δ (lac-proAB) Δ (mcrB-hsdSM)5, (rK- mK-)
M15	F-, Φ 80 Δ lacM15, thi, lac-, mtl-, recA+, KmR Phenotype: Nal[s] Str[s] Rif[s] Thi[-] lac[-] Ara[+] Gal[+] Mtl[-] F[-] RecA[+] Uvr[+] Lon[+]
SG13009	Phenotype: Nal[s] Str[s] Rif[s] Thi[-] lac[-] Ara[-] Gal[+] Mtl[-] F[-] RecA[+] Uvr[+] Lon[+]

2.1.9 Antibodies

Table 13: Primary antibodies.

Name	Species	Origin	Application	Dilution	Number
α -CRM1	goat	[59]	IF/ WB	1:1000	Ab004
α -GST	goat	Amersham	IF/ WB	1:1000/ 1:2000	Ab127
α -HA	rabbit	Sigma	IF	1:500	Ab134
α -HA	mouse	Convance	IF/ WB	1:1000	Ab186
α -His	mouse	Qiagen	WB	1:1000	Ab140
α -Nup214	rabbit	Covalab	WB	1:1000	Ab204
α -Nup214	rabbit	Covalab	WB	1:1000	Ab205
α -Nup214	rabbit	Genosphere Biotechnologies	WB	1:5000	Ab206
α -Nup214	rabbit	Genosphere Biotechnologies	IF/ WB	1:1000/ 1:5000	Ab207
α -Nup214 "D"	rabbit	against CASSSFGEQKPTGT	IF/ WB	1:200	Ab038
α -Nup214 "F"	rabbit	R. Kehlenbach	IF/ WB	1:200/ 1:500	Ab039
α -Ran	mouse	BD	1:2000	1:5000	Ab051
α -RanBP3	mouse	BD	IF/ WB	1:2000/ 1:2500	Ab059
α -Rev #7	mouse	J. Hauber, Hamburg	IF/ WB	1:1000	Ab176
α -SPN1	rabbit	ProteinTech	WB	1:1000	Ab065

Table 14: Secondary antibodies.

Name	Species	Origin	Application	Dilution
α -mouse HRP	goat	Jackson ImmunoResearch	WB	1:10000
α -rabbit HRP	goat	Jackson ImmunoResearch	WB	1:10000
α -goat HRP	donkey	Jackson ImmunoResearch	WB	1:10000
α -mouse 680	donkey	LI-COR	WB	1:10000
α -mouse 800	donkey	LI-COR	WB	1:10000
α -rabbit 680	donkey	LI-COR	WB	1:10000
α -rabbit 800	donkey	LI-COR	WB	1:10000
α -goat 680	donkey	LI-COR	WB	1:10000
α -goat 800	donkey	LI-COR	WB	1:10000
α -goat 488	donkey	Molecular Probes	IF	1:1000
α -goat 594	donkey	Molecular Probes	IF	1:1000
α -mouse 488	donkey	Molecular Probes	IF	1:1000
α -mouse 594	donkey	Molecular Probes	IF	1:1000
α -mouse 647	donkey	Molecular Probes	IF	1:1000
α -rabbit 488	donkey	Molecular Probes	IF	1:1000
α -rabbit 594	donkey	Molecular Probes	IF	1:1000
α -rabbit 647	donkey	Molecular Probes	IF	1:1000

2.1.10 Oligonucleotides

All oligonucleotides were obtained from Sigma-Aldrich either lyophilized or as a 100 μ M solution at a synthesis scale of 0.025 μ mol and the purification grade "desalted".

Oligonucleotides for cloning

Recognition sites for restriction enzymes were inserted at the 5' end of the oligonucleotides according to the respective cloning strategy. A 3-6 bp tail at the 5' end was added to ensure cleavage efficiency of the respective restriction enzymes as specified by the manufacturer (ThermoScientific). Commonly, primers for cloning were designed to have an initial melting temperature of 57-59 °C.

Table 15: Oligonucleotides for cloning. Capital letters highlight the recognition sites for restriction enzymes.

Number	Name	Sequence (5' → 3')
G117	Nup214 F NcoI	aaCCATGGgtggaatagctttggccagc
G118	Nup214 R KpnI	gaGGTACcttatcagctcgccagccacc
G864	Nup214 1990 Sall R	tttGTCGACttaccctccaaccaggggat
G865	Nup214 a1 1968 EcoRI F	tttGAATTCtagtggtagtggtgcagcac
G866	Nup214 a1 1990 Sall R	tttGTCGACtaaccacctgaaccgggagaac
G867	Nup214 a1 2033 Sall R	tttGTCGACtagtggtattactgctgctacaaa
G897	Nup214 1859 a1 EcoR F	tttGAATTCggtattgttttggtcagcagagc
G898	Nup214 2090a1 Sall R	tttGTCGACggctacgccaaccaccaaagc
G904	Nup214_wt_2033_r(XhoI)	aaaCTCGAGtgtggtgtgctgctgctc
G905	Nup214_wt_1961_f(NcoI)	aaaCCATGGgcttttctctccaacaaaacag
G952	Nup214_wt_1961_f(EcoRI)	tttGAATTCtttctctgccaacaaaacaggt
G953	Nup214_a1_1961_f(EcoRI)	tttGAATTCtttagctgcccgaataaaaaccgg

Number	Name	Sequence (5' → 3')
G954	GST-214 1991 Na EcoRI F	tttGAATTCtagttccggcaagcggtagc
G955	GST-214 2090 N Sall R	tttGTCGACgctacgccaaccaccaaacc
G956	GST-214 1991 C EcoRI F	tttGAATTCtagttccggcatttgtagcgc
G957	GST-214 2090 Ca Sall R	tttGTCGACgctacgccaaccaccgcta
G958	His214a4 1859 EcoRI F	tttGAATTCggattgttagcggtagcagcag
G959	His214a4 2090 Sall R	tttGTCGACggctacgccaaccaccgct
G970	GST-214 2090 N Sall R Stop	tttGTCGACtagctacgccaaccaccaaacc
G971	GST-214 2090 Ca Sall R Stop	tttGTCGACtagctacgccaaccaccgcta
G972	Nup214_mut_2090_r(Sall)	tttGTCGACtagctacgccaaccacc
G973	Nup214_wt_1859_f(EcoRI)	tttGAATTCggaatagctttggccagcaatcatcct
G974	Nup214_wt_2090_r(Sall)	tttGTCGACtagctacgccaaccaccaaacc
G985	Nup214_1916_f(NcoI)	tttCCATGGttcaaataccttaacctatttgaaacag
G986	Nup214_1916_f(NdeI)	tttCATATGtcaaataccttaacctatttgaaacag
G987	Nup214_2033_r(XhoI)	tttCTCGAGtggtggtgctgctgctcc
G988	Nup214_2090_r(XhoI)	tttCTCGAGgcttcgcccagccaccaaacc
G989	Nup214 1859 a1N EcoRI F	tttGAATTCtagctattgttttggtagcagagc
G990	Nup214 2090 a1N Sall R	tttGTCGACtagctacgccaaccaccaaacc
G991	Nup214 2090 a1A Sall R	tttGTCGACtagctacgccaaccacctgaac
G992	Nup214 1859 all EcoRI F	tttGAATTCtaggtattgttagcggtagcagaga
G993	Nup214 2090 all Sall R	tttGTCGACtagctacgccaaccaccgct
G994	Nup214 2090 WT Sall R	tttGTCGACtagcttcgcccagccaccaaacc
G1006	GST-214 1993 SallR	tttGTCGACtatgctggcaccctccaaacc
G1007	GST-214 1999 SallR	tttGTCGACtaggctggggctgaaccgaa
G1008	RFP-214 1993 SallR	tttGTCGACtgctggcaccctccaaacc
G1009	RFP-214 1999 SallR	tttGTCGACggctggggctgaaccgaa
G1050	Nup214_f_C1916(NdeI)	tttCATATGtcaaataccttaacctatttgaaacag
G1051	Nup214_r_2033C(XhoI)	tttCTCGAGacatgtggtgctgctgctcc
G1071	Nup214_1930_f_NdeI	tttCATATGttggtggatttgccagctc
G1072	Nup214_2021_r_XhoI	tttCTCGAGtgctgctggcagctg
G1075	Nup214_1916_f(EcoRI)	tttGAATTCtcaaataccttaacctatttgaaacag
G1118	Nup214_1930_f(EcoRI)	tttGAATTCttggtggatttgccagctgctg
G1119	Nup214_2021_r(Sall).xdna	tttGTCGACtatgctgctggcagctgagtg
G1126	Nup214_a1_f1916(NdeI)	tttCATATGagcaataccagcaacctgttg
G1127	Nup214_a1_r2033(XhoI)	tttCTCGAGggtggtattactgctgctac
G1128	Nup214_f1859(EcoRI)	tttGAATTCggaatagctttggccagca
G1129	Nup214_r2090(Sall)	tttGTCGACgcttcgcccagccaccaaacc
G1144	Nup214_2021r_6xHis_Sall	tttGTCGACtagtgatggtgatggtgatgctgctgagctgagct
G1147	Nup214_f1916_EcoRI	tttGAATTCtcaaataccttaacctatttgaa
G1148	Nup214_r2033_6xHis_Sall	tttGTCGACtagtgatggtgatggtgatggtggtgctgctgctcc
G1149	Nup214_r1929_Sall	tttGTCGACtatgcttgcccactgttt
G1150	Nup214_f2022_EcoRI	aaagcGAATTCggaggattcgggttg
G1151	Nup214_2090_6xHis_r	tttGTCGACtagtgatggtgatggtgatgcttcgcccagccaccaaacc
G1152	MBP-C-fragment1_f	atatatGGCGCCcaaatcgaaccgctct
G1153	MBP-C-fragment1_r	aaaGAATTCgtgatggtgatggtgatgcataatctatgctctgtggt
G1154	MBP-C-fragment2_f	atatatGTCGACatgaaaatcgaagaaggtaaactg
G1155	MBP-C-fragment2_r	atatatAAGCTTtaattagctcgcgctcttcag
G1156	RanBP3b_f_EcoRI	aaaaGAATTCatggcggacctggcgaac
G1157	RanBP3b_r_XhoI	aaaCTCGAGttatgtgctcccggctgctc
G1184	Nup214_K1916f_NdeI	tttCATATGaagtcaaataccttaacctatttgaaacag
G1187	RanBP3b_r_Sall	aaaaGTCGACttatgtgctcccggctgctc
G1198	RanBP3_f_HindIII	tttAAGCTTatggcggacctggcgaac

Number	Name	Sequence (5' → 3')
G1199	RanBP3_r_EcoRI	aaaGAATTCctgtgctcccggctcgtcgtg
G1211	PreScission_f_NcoI	aaaCCATGGaaaacgcccagaaaggtgaaa
G1256	RanBP3_His_r_Sall	tttGTCGACttagtgatggtgatggtgatgtgtgctcccggctcgtcgtg
G1257	CRM1_f_MunI	tttCAATTGatgccagcaattatgacaatgtag
G1258	CRM1_His_r_XhoI	tttCTCGAGttagtgatggtgatggtgatgatcacacatttcttctggaatctc
G1266	Nup214_f1906_EcoRI	tttGAATTCgccagtgggggccttgg
G1267	Nup214_r2042His_Sall	tttGTCGACttagtgatggtgatggtgatgattctgactcgcgagcgtg

Oligonucleotides for mutagenesis

Oligonucleotides were used for site-directed mutagenesis as well as for insertion of additional amino acids. Primers for site-directed mutagenesis were designed with the mutated bases in the middle flanked by 15-20 pairing bases on each side and usually not more than three amino acids changed at a time. Codons were chosen that needed the least amount of changed bases.

Table 16: Oligonucleotides for mutagenesis. Capital letters highlight the mutated or inserted codons.

Number	Name	Sequence (5' → 3')
G894	Nup214_a1_1961_f(EcoRI)	tttGAATTCtatttagctgcccgaataaaaccgg
G895	Nup214_wt_1961_f(EcoRI)	tttGAATTCtatttctctgccaacaaaacaggt
G1120	pMAL-c2_f(BglII)	tttAGATCTgctgccgaaccggccaaaaacctgg
G1121	pMal-c2_AAA2_r(EcoRI)	aatGAATTCggccgcgccattagctgctgctgctgccagggtgcatcgacagctc
G1122	a1.1_f	acaggtggcAGTggtgctgctccagtGAGTggcagccctcact
G1123	a1.1_r	agtaggagggctgccACTcactggagcagcaccACTgccacctgt
G1124	a1.2_f	agccctcactAGTgggggatcccctgggAGTggaggggtgccagca
G1125	a1.2_r	tgctggcaccctccACTcccaggggatccccACTtagtaggagggct
G1130	Nup214_K1928E_f	tttgaaacagtggggcccGAGacatttgggtgatttggc
G1131	Nup214_K1928E_r	ggcaaatccaccaaagtCTCggccccactgtttccaaa
G1132	Nup214_K1942E_f	tcgtgittggagagcagGAGcccactggcactttcagc
G1133	Nup214_K1942E_r	gctgaaagtgccagtgggCTCctgctcctccaaacgacga
G1134	Nup214_K1966E_f	gggtttctctccaaacGAGacaggtggcttcggtgct
G1135	Nup214_K1966E_r	agcaccgaagccacctgtCTCgtttggagaggaaaacc
G1136	Nup214_K2010E_f	ctgggctcgacgggagggcGAGgtgttcggagaggcact
G1137	Nup214_K2010E_r	agtgcctctccgaacacCTCgcctcccctcgagcccag
G1138	Nup214_D1896K_f	ggaggaaaaccagtcagAAGgcagccaacaaaacc
G1139	Nup214_D1896K_r	tgggttttggctgctCCTtctgactgggtttctcc
G1140	Nup214_E1940K_f	gccagctcgtgittggaAAGcagaaaccactggcact
G1141	Nup214_E1940K_r	agtgccagtggtttctgCTTtccaaacgacgagctggc
G1142	Nup214_E2014K_f	ggaggcaaagtgtcgaAAGggcactgcagctgcc
G1143	Nup214_E2014K_r	ggcagctgcagtgccCTTtccgaacactttgcctcc
G1145	Nup214_FG5_f	ggggtgccagcaAGTggttcagccccagcctttacaagccc
G1146	Nup214_FG5_r	gggctgttaaaggctggggctgaaccACTtgcctggcacc
G1185	Nup214_A1999K_f	gcattcgggtcagccccaAAGtttacaagccctctgggc
G1186	Nup214_A1999K_r	gcccagagggctgtaaaCTTtggggctgaaccgaatgc
G1188	Nup214_A1995K_f	cctgggttggaggggtgccaAAAttcggttcagccccagcctt
G1189	Nup214_A1995K_r	aaggctggggctgaaccgaaTTTtggcaccctccaaaccag
G1201	CRM1_mut1_f	ccctcacctacaagatTCTcaagtaaagTCCtttgtgacagggcttttc
G1202	CRM1_mut1_r	gaaaagccctgtcacaaaGGAActttactgAGAatctgtaggtgaggg
G1203	CRM1_mut2_f	gaagacacttctgattgTCTTCGgaagagagagaaatagcc
G1204	CRM1_mut2_r	ggctatttctctcttcCGAAGAcaaatcagaagtgtcttc

Number	Name	Sequence (5' → 3')
G1212	pMal-PreScission_r_EcoRI	tttgaattcGGGCCCTGGAACAGAACTTCCAGcccagggtgtgtattgtt
G1213	pMal-linkerAAA- PreScission_r_EcoRI	tttgaattcGGGCCCTGGAACAGAACTTCCAGggccgcggcattagtct
G1216	CRM1_mut3_f	ctgaaacaagaaGCGGCCaaacattggccaactttatcagtg
G1217	CRM1_mut3_r	cactgataaaagttggccaatgtttGGCCGcttctgtttcag
G1218	CRM1_mut4_f	cattgtttccagcattcgcctGCTattccacctacacag
G1219	CRM1_mut4_r	ctgtgtagggtgaatagcAGCgaatgctgggaacaatg
G1220	CRM1_mut5_f	gctattccacctacacagGCTaaactgttttgattcc
G1221	CRM1_mut5_r	ggaatccaaaacaagtttAGCctgtgtagggtgaatagc
G1222	CRM1_mut6_f	gttttgattccatcattGCGgctGCCaaacatactatgaggaatg
G1223	CRM1_mut6_r	cattcctcatagatgtttGGCagcCGCaatgatggaatccaaaac
G1224	CRM1_mut7_f	cagcttgaagaatttatGCAgatatgcttaatgtatac
G1225	CRM1_mut7_r	gtatacattaagcatatcTGcataaattctccaagctg
G1226	CRM1_mut8_f	gaagaatttatttagatagGCTaatgtatacaagtgcctc
G1227	CRM1_mut8_r	gaggcactgtatacattAGCcatatctaaataaattcttc
G1228	CRM1_mut9_f	gaaaattttgtccccctctgGCGgatgcagttctcattg
G1229	CRM1_mut9_r	caatgagaactgcatcCGCagagggggaacaaaatttc
G1230	CRM1_mut10_f	gtcgcgtgaaaattttgttGCCGCTctgttgatgcagttctc
G1231	CRM1_mut10_r	gagaactgcatccaacagAGCGGCaacaaaatttcagcgag
G1232	CRM1_mut11_f	gctgtcaattctcattgtGCCccagcattcctgtctattc
G1233	CRM1_mut11_r	gaatagcaaggaatgctggGGCacaatgagaattgacagc
G1234	CRM1_mut12_f	gtcaattctcattgtttcGCAgcatcctgtctattccac
G1235	CRM1_mut12_r	gtggaatagcaaggaatgcTGCgaaacaatgagaattgac
G1236	CRM1_mut13_f	gtttccagcattcctgtctGCTccacctacacagtttaaac
G1237	CRM1_mut13_r	gtttaaactgtgtagggtgAGCagcaaggaatgctgggaaac
G1238	CRM1_mut14_f	cccagcattcctgtctattGCAcctacacagtttaacttg
G1239	CRM1_mut14_r	caagtttaactgtgtaggTGCaatagcaaggaatgctggg
G1240	CRM1_mut15_f	cttcaaaaatgttgacaaGCAGCAGctgcagctcagagttt
G1241	CRM1_mut15_r	aaactctgagctgcagcTGCTGCTgtgcaacattttgtaag
G1242	CRM1_mut16_f	ataagtacatcattaaatGCTggaatccagttaacaac
G1243	CRM1_mut16_r	gttgtaactggatttccAGCatttaatgatgtacttat
G1244	CRM1_mut17_f	gaagaagatttggtgttAGCTGCatttccaggattaatgatg
G1245	CRM1_mut17_r	gaaatccagttaacaaccaaGCCtttctcaggaatatgtg
G1246	CRM1_mut18_f	cacatattcctgaagaaaGGCttggttgaactggatttc
G1247	CRM1_mut18_r	catcattaaatcctggaatGCAGCTaacaaccaaatcttcttc
G1248	CRM1_mut19_f	ccagttaacaaccaaatcGCTcttcaggaatatgtggc
G1249	CRM1_mut19_r	gccacatattcctgaagAGCGatttggttgaactgg
G1276	CRM1_L83F_f	cgaatactatggactacaaattTTTgaaaatgtataaaaacaag
G1277	CRM1_L83F_r	cttgttttatcacattttcAAAaattttagtccatagtatttcg
G1278	CRM1_L83R_f	cgaatactatggactacaaattCGGgaaaatgtataaaaacaag
G1279	CRM1_L83R_r	cttgttttatcacattttcCCGaattttagtccatagtatttcg
G1280	CRM1_I102Q_f	caaggaaccagtgcaaggaCAGaaaaatacgttgttggcct
G1281	CRM1_I102Q_r	aggccaacaacgtatttttCTGtccttcgactggttccttg
G1282	CRM1_I102W_f	caaggaaccagtgcaaggaTGaaaaatacgttgttggcct
G1283	CRM1_I102W_r	aggccaacaacgtatttttCCAtccttcgactggttccttg
G1284	CRM1_L134F_f	tcggaaaattaaatatgacTTTgttcagatactgaaacaaga
G1285	CRM1_L134F_r	tctgtttcagtaictgaacAAAgatcatatttaattttcga
G1286	CRM1_F149W_f	ggcccaaacattggccaactTGGatcagtgatattgttggagc
G1287	CRM1_F149W_r	gctccaacaatatcactgatCCAagttggccaatgtttgggcc
G1288	CRM1_D152W_f	cattggccaactttatcagtTGGattgttgagcaagtaggac
G1289	CRM1_D152W_r	gtcctactgtctccaacaatCCAactgataaaagttggccaatg

Number	Name	Sequence (5' → 3')
G1290	CRM1_A156F_f	ctttatcagtgatattgttgaTTTagtaggaccagcgaagctc
G1291	CRM1_A156F_r	gagacttctgctggctactAAAtccaacaatatcactgataaaag
G1292	CRM1_N167R_f	gcgaaagctctgtcaaaatCGTatggtgattctaaactcttg
G1293	CRM1_N167R_r	caagagtttaagaatcaccatACGatttgacagagactttcgc
G1294	CRM1_L679R_f	caacccaaaatgtggatataCGTaaagatcctgaaacagtcaagcag
G1295	CRM1_L679R_r	ctgcttgactgtttcaggatctttACGtatatccacattttggtg
G1296	CRM1_L679W_f	caacccaaaatgtggatataTGGaaagatcctgaaacagtcaagcag
G1297	CRM1_L679W_r	ctgcttgactgtttcaggatctttCCAatataccacattttggtg
G1298	CRM1_K680Q_f	caacccaaaatgtggatatactgCAAgatcctgaaacagtcaagcag
G1299	CRM1_K680Q_r	ctgcttgactgtttcaggatcTTGcagtataccacattttggtg
G1300	CRM1_K680R_f	caacccaaaatgtggatatactgAGAgatcctgaaacagtcaagcag
G1301	CRM1_K680R_r	ctgcttgactgtttcaggatcTCTcagtataccacattttggtg
G1302	CRM1_C723M_f	gatatgcttaatgtatacaagATGctcagtgaaaatattctgc
G1303	CRM1_C723M_r	gcgaaaatattttcactgagCATctgtatacattaagcatac
G1304	CRM1_A731Q_f	ctcagtgaaaatattctgcaCAGatccaagctaattggtgaaatg
G1305	CRM1_A731Q_r	catttcaccattagcttggatCTGtgcaaaaatattttcactgag
G1306	CRM1_L744W_f	gaaatggttacaaagcaaccaTGGattagaagtatgcaactgtaa
G1307	CRM1_L744W_r	ttacagttcgcatacttctaataCCAtggttgctttgtaaccatttc
G1308	CRM1_I745W_f	gaaatggttacaaagcaaccattgTGGagaagtatgcaactgtaa
G1309	CRM1_I745W_r	ttacagttcgcatacttctCCAcaatggttgctttgtaaccatttc
G1310	CRM1_M748R_f	gcaaccattgattagaagtAGGcgaactgaaaaagggaaac
G1311	CRM1_M748R_r	gtttcccttttacagttcgcCTTacttctaataatggttgc
G1312	CRM1_L679WK680R_f	caacccaaaatgtggatataTGGAGAgatcctgaaacagtcaagcag
G1313	CRM1_L679WK680R_r	ctgcttgactgtttcaggatcTCTCCAatataccacattttggtg
G1317	CRM1_C528W_f	taaaggatctattaggattaTGGgaacagaaaagaggcaaaga
G1318	CRM1_C528W_r	tctttgcctcttttctgttcCCAaatcctaatagatccttta
G1319	CRM1_A541K_f	aagataataaagctattattAAAtcaaatatcatgtacatagt
G1320	CRM1_A541K_r	actatgtacatgatattgaTTTaataatagctttattatctt
G1321	CRM1_D824K_f	ctgaaatacctcaaataatttAAAgctgttttgaatgcacattg
G1322	CRM1_D824K_r	caatgtgcattcaaaaacagcTTTaaatattgaggattttcag
G1323	CRM1_F823A_f	cagctgaaatacctcaaataGCTgatgctgttttgaatgcac
G1324	CRM1_F823A_r	gtgcattcaaaaacagcatcAGCtatttgaggattttcagctg
G1325	CRM1_H925W_f	cttattttgtgatattctccagTGGatctttctgttggacag
G1326	CRM1_H925W_r	ctgtcacaacagaaaagatCCActggagaatatcacaaaaataag
G1327	CRM1_S928K_f	gatattctccagcatatctttAAGgttggacagacacttcac
G1328	CRM1_S928K_r	gtgaagtgctgtcacaacCTTaaagatatgctggagaatatac
G1329	CRM1_T917E_f	cagctcagagttttatcaaGAGtatttttgatattctccagc
G1330	CRM1_T917E_r	gctggagaatatacaaaaaataCTCttgataaaaaactctgagctg
G1331	CRM1_W880A_f	ctgttttggattccatcattGCGgctttcaaacatactatgag
G1332	CRM1_W880A_r	ctcatagtatgtttgaaagcCGCaatgatggaatccaaaacaag
G1333	CRM1_Y918W_f	ctcagagttttatcaaactTGGttttgtgatattctccagcata
G1334	CRM1_Y918W_r	tatgctggagaatatacaaaaaCCAagtttgataaaaaactctgag
G1352	Nup214mut_f1916_Ndel	tttCATATGtcaaataccttaacctatctggaacag
G1353	Nup214mut_f1916_EcoRI	tttGAATTCtcaaataccttaacctatctggaacag

Oligonucleotides for sequencing

For sequencing of plasmids at GATC Biotech, standard primers from GATC were chosen via the PrimerScout tool on the GATC website (<http://www.gatc-biotech.com/>). For sequencing of pmRFP-cNLS plasmids or CRM1 mutants, the respective primers (10 μ M) were sent with the sample.

Table 17: Oligonucleotides for sequencing.

Number	Name	Sequence (5' → 3')
G387	Crm1-hs-39F	ATGCCAGCAATTATGACAATG
G388	Crm1-hs-200R	CTTTAAATGTGTCAGTACTTC
G389	Crm1-hs-501F	GGAGCAAGTAGGACCAGCGAA
G390	Crm1-hs-1001F	TCTCAGTTTGTCTCTGCAC
G391	Crm1-hs-1501F	AGTGGTCATGGAAAAATTTGA
G392	Crm1-hs-2001F	GAAAAGTACATGTTACTCCCT
G393	Crm1-hs-2495F	ACCTCAAATATTTGAATGCTG
G394	Crm1-hs-3001F	ACCTACAAGATGCTCAAGTAA
G545	pmCherry_seq_f	CGCTGAGGTCAAGACCACC
GATC	pGEX-5	CTGGCAAGCCACGTTTGG
GATC	pGEX-3	GGAGCTGCATGTGTCAGAG
GATC	pGEX5-FP	AACGTATTGAAGCTATCCC
GATC	pGEX3-RP	TCAAGAATTATACACTCCG
GATC	T7-981079	TAATACGACTCACTATAG
GATC	T7minus1	AATACGACTCACTATAGGG
GATC	pQE-FP	CGGATAACAATTTACACAG
GATC	pQE-RP	GTTCTGAGGTCATTACTGG
GATC	pMalE	TCAGACTGTGATGAAGC
GATC	pET-RP	CTAGTTATTGCTCAGCGG
GATC	pJET1-RP	TGAGGTGGTTAGCATAGTTC
GATC	pJET1-FP	ACTACTCGATGAGTTTTTCGG
GATC	PCR1	CGGGCCTCTTCGCTATT
GATC	PCR1minus1	GGGCCTCTTCGCTATT
GATC	EGF2	GGGGATGTGCTGCAAGG
GATC	UP-40	GTTTTCCCAGTCACGAC
GATC	pEGFP_C2-FP	GATCACATGGTCCTGCTG
GATC	pcDNA3.1-RP/1	CAAACAACAGATGGCTGGC
GATC	pcDNA3.1-FP	CTCTGGCTAACTAGAGAAC

2.1.11 Synthesized Genes

Synthesized genes were purchased either cloned into a pEX-A vector or as DNA fragment. The sequences of the synthesized genes can be found in the appendix (A) .

Table 18: Synthesized Genes.

Name	Type	Company
NdeI-Nup214K1942C-Xhol	cloned in pEX-A	eurofins
NdeI-Nup214K1966C-Xhol	cloned in pEX-A	eurofins
NdeI-Nup214K2010C-Xhol	cloned in pEX-A	eurofins

Name	Type	Company
NdeI-Nup214(1916-2033)KA-XhoI	cloned in pEX-A	eurofins
EcoRI-Nup214(1859-2090)KA-Sall	cloned in pEX-A	eurofins
EcoRI-Nup214(1859-2090)KAa1-Sall	cloned in pEX-A	eurofins
EcoRI-Nup214(1859-2090)KE-Sall	cloned in pEX-A	eurofins
EcoRI-Nup214(1859-2090)a1(5SGs)-Sall	cloned in pEX-A	eurofins
EcoRI-Nup214(1916-2033)a1(4SGs)-Sall	cloned in pEX-A	eurofins
SacI-CRM1_K680Q_A731Q-MssI	GeneArt Strings™ DNA Fragment	life technologies
SacI-CRM1_K680Q_A731Q_L679R-MssI	GeneArt Strings™ DNA Fragment	life technologies
SacI-CRM1_K680Q_A731Q_C723M-MssI	GeneArt Strings™ DNA Fragment	life technologies
Sall-CRM1_I102W_F149W-SacI	GeneArt Strings™ DNA Fragment	life technologies
Sall-CRM1_I102W_N167R-SacI	GeneArt Strings™ DNA Fragment	life technologies
Sall-CRM1_I102W_D152F-SacI	GeneArt Strings™ DNA Fragment	life technologies
EcoRI-Nup214(aa1859-2090)-Sall_mutant1	GeneArt Strings™ DNA Fragment	life technologies
EcoRI-Nup214(aa1859-2090)-Sall_mutant2	GeneArt Strings™ DNA Fragment	life technologies
EcoRI-Nup214(aa1859-2090)-Sall_mutant3	GeneArt Strings™ DNA Fragment	life technologies

2.1.12 Vectors

Table 19: Available Vectors.

Number	Name	Tag	Resistance	Application	Source
4	pET-28a	His (N/C-terminal)	kan	expression	Novagen
29	pMal-C2	MBP (N-terminal)	amp	expression	NEB
30	pEGFP-C1	EGFP	kan	transfection	Clontech
37	pETM41	MBP-His (N-terminal)	kan	expression	EMBL
46	pGex-6P-1	GST (N-terminal)	amp	expression	Amersham
47	pGex-6P-1-MCS	GST (N-terminal)	amp	expression	S. Hutten
52	pcDNA3.1(+)-HA	HA-Tag (C-terminal)	amp	transfection	S. Wälde

Table 20: Generated Vectors.

Number	Name	Tag	Cloning
74	pMal-linkerAAA	MBP (modified)	PCR(pMal-C2, G1120, G1121) cloned with BglII, EcoRI
75	pMal-PreScission	MBP	PCR(pMal-C2, G1211, G1212) cloned with EcoRI, NcoI
76	pMal-linkerAAA-PreScission	MBP (modified)	PCR(pMal-linkerAAA, G1211, G1213) cloned with EcoRI, NcoI
78	pMal-His-MCS-MBP	His, MBP (modified)	PCR(pMal-C2, G1152, G1153) cloned with Ehel, EcoRI and PCR(pMal-C2, G1154, G1155) cloned with HindIII, Sall

pMal-linkerAAA

The pMal-c2 vector was modified to resemble a vector used in [212]. The charged residues at the C-terminus of the MBP-tag were mutated to alanine and the linker length was shortened by PCR on pMal-c2 with a reverse primer containing the modified C-terminal region of MBP, a linker consisting of 3 alanines and an EcoRI recognition site.

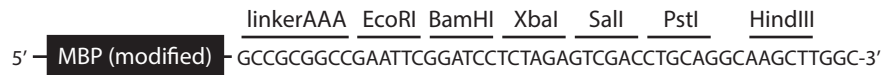


Figure 5: Multiple cloning site of the vector pMal-linkerAAA.

pMal-PreScission

The Factor Xa site of the pMal-c2 vector was changed to a PreScission protease site by PCR with a reverse oligo coding for the PreScission recognition site.

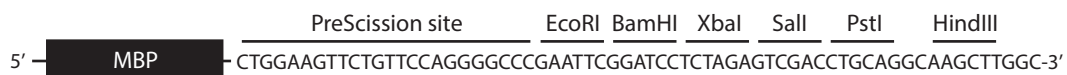


Figure 6: Multiple cloning site of the vector pMal-PreScission.

pMal-linkerAAA-PreScission

A PreScission protease recognition site was inserted between the modified MBP and the multiple cloning site of the pMal-linkerAAA vector by PCR with a reverse oligo coding for the PreScission recognition site.

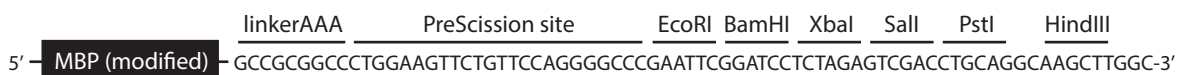


Figure 7: Multiple cloning site of the vector pMal-linkerAAA-PreScission.

pMal-His-MCS-MBP

The pMal-linkerAAA vector was modified by 2 cloning steps to yield a vector with an N-terminal His-tag and a C-terminal modified MBP-tag as described for the vector pMal-linkerAAA.

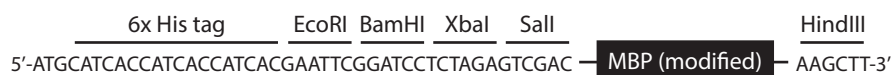


Figure 8: Multiple cloning site of the vector pMal-His-MCS-MBP.

2.1.13 Plasmids

Table 21: Available Plasmids.

Number	Name	Application	Source
1	pET11d-Ran	expression	
2	pET3d-RanQ69L	expression	
41	pGEX-PKI-NES	expression	S. Taylor
47	pBluescript-Nup214	transfection	G. Grosfeld
79	pGEX-6P-SPN1	expression	A. Dickmanns
145	pMAL-Nup214C	expression	R. Kehlenbach
146	pGEX3x-Rev	expression	J. Hauber
532	pcDNA3.1(+)-CRM1-HA	transfection	C. Spillner
628	pcDNA3.1(+)-CRM1(C528S)-HA	transfection	S. Roloff
736	pGEX-4T3-CRM1	expression	Y. M. Chook
856	pET30b-SPN1	expression	I. Waldmann
857	pEGFP-c1-SPN1	transfection	I. Waldmann
987	pmRFP-cNLS	transfection	C. Spillner
994	pmRFP-Nup214(1916-2033)a1-cNLS (5SGs)	transfection	C. Spillner
996	pmRFP-Nup214(1916-2033)a3-cNLS	transfection	C. Spillner
1007	pGEX-6P1-Nup214(1968-1990)	expression	S. Roloff
1008	pGEX-6P1-Nup214(1968-1990)a1	expression	S. Roloff
1009	pGEX-6P1-Nup214(1968-2033)	expression	S. Roloff
1010	pGEX-6P1-Nup214(1968-2033)a1 (5SGs)	expression	S. Roloff
1023	pmRFP-Nup214(1859-2090)F1982S-cNLS	transfection	C. Spillner
1024	pmRFP-Nup214(1859-2090)F1988S-cNLS	transfection	C. Spillner
1029	pmRFP-Nup214(1859-2090)F1976S-cNLS	transfection	C. Spillner
1030	pmRFP-Nup214(1859-2090)a1-cNLS	transfection	C. Spillner
1037	pmRFP-Nup214(1859-2090)a4-cNLS	transfection	C. Spillner
1064	pGEX-6P1-Nup214(1859-2090)	expression	C. Spillner
1065	pGEX-6P1-Nup214(1859-2090)a1 (4SG)	expression	C. Spillner
1066	pGEX-6P1-Nup214(1991-2090)	expression	C. Spillner
1069	pGEX-6P1-Nup214(1859-2090)FGless	expression	S. Roloff
1070	pGEX-6P1-Nup214(1968-2090)	expression	S. Roloff
1258	pTH24-TEV-SH	expression	A. Dickmanns
1316	pQE80-His-ZZ-RanQ69L(1-180)	expression	T. Güttler
1317	pGEX-6P1-RanBP3	expression	A. Dickmanns

Table 22: Generated Plasmids.

Number	Name	Cloning
1135	pET28a-His-Nup214(1930-2021)-His	PCR Nup214 (#47, G1071, G1072), cloned into vector #4 (NdeI, XhoI)
1136	pET28a-His-Nup214(1916-2033)KA-His	fragment from #1132 cloned into vector #4 (NdeI, XhoI)
1159	pQE60-CRM1(430AAA432)-His	fragment from #1160 cloned into plasmid #31 (SacI/SalI)
1160	pcDNA3.1(+)-CRM1(430AAA432 C528S)-HA	mutagenesis (G1073, G1074) on plasmid #628
1161	pGEX-6P1-Nup214(1968-2033)KA	PCR Nup214 (G851, G806), cloned into plasmid #47 (EcoRI/SalI)

Number	Name	Cloning
1162	pmRFP-Nup214(1968-2033)KA-cNLS	PCR Nup214 (#1136, G889, G833), cloned into plasmid #987 (EcoRI/ Sall)
1163	pmRFP-Nup214(1916-2033)-cNLS	PCR Nup214 (#47, G1075, G833), cloned into plasmid #987 (EcoRI/Sall)
1164	pmRFP-Nup214(1916-2033)KA-cNLS	PCR Nup214 (#1136, G1075, G833), cloned into plasmid #987 (EcoRI/Sall)
1169	pGEX-6P1-Nup214(1930-2021)	PCR Nup214 (#47, G1118, G1119), cloned into vector #46 (EcoRI/Sall)
1170	pMal-linkerAAA-Nup214(1930-2021)	PCR Nup214 (#47, G1118, G1144), cloned into vector #74 (EcoRI/Sall)
1174	pmRFP-Nup214(1859-2090)KA-cNLS	fragment from #1171 cloned into plasmid #987 (EcoRI, Sall)
1175	pmRFP-Nup214(1859-2090)KAa1-cNLS	fragment from #1172 cloned into plasmid #987 (EcoRI, Sall)
1176	pmRFP-Nup214(1859-2090)KE-cNLS	fragment from #1173 cloned into plasmid #987 (EcoRI, Sall)
1177	pmRFP-Nup214(1916-2033)KE-cNLS	PCR Nup214 (#1176, G1075, G833), cloned into plasmid #987 (EcoRI/Sall)
1178	pETM41-Nup214(1858-2090)KA	PCR Nup214 (#1174, G117, G118), cloned into vector #37 (NcoI/KpnI)
1179	pETM41-Nup214(1858-2090)KAa1	PCR Nup214 (#1175, G117, G118), cloned into vector #37 (NcoI/KpnI)
1180	pETM41-Nup214(1858-2090)KE	PCR Nup214 (#1176, G117, G118), cloned into vector #37 (NcoI/KpnI)
1184	pET28a-His-Nup214(1916-2033)a1-His	PCR Nup214 (#949, G1126, G1127), cloned into vector #4 (NdeI, XhoI)
1185	pmRFP-Nup214(1859-2090)-cNLS	PCR Nup214 (#47, G1128, G1129), cloned into plasmid #987 (EcoRI/Sall)
1188	pmRFP-Nup214(1859-2090)KE 2SG-cNLS	mutagenesis (G1122, G1123) on plasmid #1176
1189	pmRFP-Nup214(1859-2090) 5SG-cNLS	fragment from #1186 cloned into plasmid #987 (EcoRI, Sall)
1190	pmRFP-Nup214(1916-2033) 4SG-cNLS	fragment from #1187 cloned into plasmid #987 (EcoRI, Sall)
1192	pGEX-6P1-Nup214(2022-2033)	PCR Nup214(#47, G1147, G1149), cloned into vector #46 (EcoRI/Sall)
1193	pGEX-6P1-Nup214(1916-1929)	PCR Nup214(#47, G1150, G806), cloned into vector #46 (EcoRI/Sall)
1194	pMal-linkerAAA-Nup214(1930-2033)	PCR Nup214 (#47, G1118, G1148), cloned into vector #74 (EcoRI/Sall)
1195	pMal-linkerAAA-Nup214(1916-2033)	PCR Nup214 (#47, G1147, G1148), cloned into vector #74 (EcoRI/Sall)
1196	pMal-linkerAAA-Nup214(1916-2021)	PCR Nup214 (#47, G1147, G1144), cloned into vector #74 (EcoRI/Sall)
1273	pGEX-6P-Nup214(1961-2033) S1963C	PCR Nup214 (#948, G952, G806), cloned into vector #46 (EcoRI, Sall)
1277	pET28a-Nup214(1916-2033)-His	PCR Nup214 (#47, G985, G987), cloned into vector #4 (NcoI, XhoI)
1278	pET28a-His-Nup214(1916-2033)-His	PCR Nup214 (#47, G986, G987), cloned into vector #4 (NdeI, XhoI)
1279	pET28a-Nup214(1916-2090)-His	PCR Nup214 (#47, G985, G988), cloned into vector #4 (NcoI, XhoI)

Number	Name	Cloning
1280	pET28a-HisNup214(1916-2090)-His	PCR Nup214 (#47, G986, G988), cloned into vector #4 (NdeI, XhoI)
1281	pETM41-Nup214(1858-2033)	PCR Nup214 (#48, G117, G837), cloned into vector #37 (NcoI, EcoRI)
1282	pET28a-His-Nup214(C1916-2033)-His	PCR Nup214 (#47, G1050, G987), cloned into vector #4 (NdeI, XhoI)
1283	pET28a-His-Nup214(1916-2033C)-His	PCR Nup214 (#47, G986, G1051), cloned into vector #4 (NdeI, XhoI)
1287	pET28a-His-Nup214(1916-2033) K1942C-His	fragment from #1284 cloned into vector #4 (NdeI, XhoI)
1288	pET28a-His-Nup214(1916-2033) K1966C-His	fragment from #1285 cloned into vector #4 (NdeI, XhoI)
1289	pET28a-His-Nup214(1916-2033) K2010C-His	fragment from #1286 cloned into vector #4 (NdeI, XhoI)
1291	pmRFP-Nup214(1859-2090)K1928E-cNLS	mutagenesis (G1130, G1131) on plasmid #1185
1292	pmRFP-Nup214(1859-2090)K1942E-cNLS	mutagenesis (G1132, G1133) on plasmid #1185
1293	pmRFP-Nup214(1859-2090)KE 4SG-cNLS	mutagenesis (G1122, G1123) on plasmid #1176, then mutagenesis (G1124, G1125)
1294	pMal-linkerAAA-Nup214(1930-2021)-His	PCR Nup214 (#47, G1118, G1144) digested with EcoRI/Sall , cloned into vector #74 (EcoRI/Sall)
1295	pmRFP-Nup214(1859-2090)K1966D-cNLS	mutagenesis (G1134, G1135) on plasmid #1185
1296	pmRFP-Nup214(1859-2090)K2010E-cNLS	mutagenesis (G1136, G1137) on plasmid #1185
1297	pmRFP-Nup214(1859-2090)D1896K-cNLS	mutagenesis (G1138, G1139) on plasmid #1185
1298	pmRFP-Nup214(1859-2090)E2014K-cNLS	mutagenesis (G1142, G1143) on plasmid #1185
1299	pmRFP-Nup214(1859-2090)K1966E-cNLS	mutagenesis (G1134, G1135) on plasmid #1185
1300	pmRFP-Nup214(1859-2090)E1940K-cNLS	mutagenesis (G1140, G1141) on plasmid #1185
1301	pmRFP-Nup214(1859-2090)F1994S-cNLS	mutagenesis (G1145, G1146) on plasmid #1185
1302	pmRFP-Nup214(1859-2090)KA 5SG-cNLS	mutagenesis (G1145, G1146) on plasmid #1175
1303	pmRFP-Nup214(1859-2090)KE 5SG-cNLS	mutagenesis (G1145, G1146) on plasmid SAP604
1304	pmRFP-Nup214(1859-2090)KA(F1994S)-cNLS	mutagenesis (G1145, G1146) on plasmid #1174
1305	pmRFP-Nup214(1859-2090)KE(F1994S)-cNLS	mutagenesis (G1145, G1146) on plasmid #1176
1306	pmRFP-Nup214(1859-2090) D1896K E1940K-cNLS	mutagenesis (G1138, G1139) on plasmid #1300
1307	pmRFP-Nup214(1859-2090) DE/K-cNLS	mutagenesis (G1142, G1143) on plasmid #1306
1308	pMal-linkerAAA-Nup214(1859-2090)-His	PCR Nup214 (#47, G973, G1151), cloned into vector #74 (EcoRI/Sall)
1309	pMal-His-Nup214(1916-2033)-MBP(mod.)	PCR Nup214 (#47, G1147, G833), cloned into vector #78 (EcoRI/Sall)
1310	pmRFP-Nup214(1859-2090)DE/K 2SG-cNLS	mutagenesis (G1122, G1123) on plasmid #1307
1311	pmRFP-Nup214(1859-2090)DE/K F1976S-cNLS	mutagenesis (G1122, G1123) on plasmid #1307
1312	pmRFP-Nup214(1859-2090)DE/K F1994S-cNLS	mutagenesis (G1145, G1146) on plasmid #1307
1313	pmRFP-Nup214(1859-2090)DE/K 4SG-cNLS	mutagenesis (G1124, G1125) on plasmid #1310
1314	pmRFP-Nup214(1859-2090)DE/K 3SG-cNLS	mutagenesis (G1124, G1125) on plasmid #1310
1315	pmRFP-Nup214(1859-2090)DE/K 5SG-cNLS	mutagenesis (G1145, G1146) on plasmid #1313
1318	pMal-C2-Nup214(1859-2090)-His	PCR Nup214 (#47, G973, G1151), cloned into vector #29 (EcoRI/Sall)
1319	pET28a-His-Nup214(K1916-2033)-His	PCR Nup214 (#47, G1184, G987) , cloned into vector #4 (NdeI/XhoI)
1320	pET28a-His-Nup214(1916-2033)A1999K-His	mutagenesis (G1185, G1186) on plasmid #1278

Number	Name	Cloning
1321	pET28a-His-Nup214(1916-2033)A1995K-His	mutagenesis (G1188, G1189) on plasmid #1278
1322	pcDNA3.1(+)-CRM1(C528S A992S L996S)-HA	mutagenesis (G1201, G1202) on plasmid #628
1323	pcDNA3.1(+)-CRM1(C528S F1034S L1035S)-HA	mutagenesis (G1203, G1204) on plasmid #628
1325	pcDNA3.1(+)-CRM1(C528S L864A)-HA	mutagenesis (G1218, G1219) on plasmid #628
1326	pcDNA3.1(+)-CRM1(C528S F871A)-HA	mutagenesis (G1220, G1221) on plasmid #628
1327	pcDNA3.1(+)-CRM1(C528S L718)-HA	mutagenesis (G1226, G1227) on plasmid #628
1328	pcDNA3.1(+)-CRM1(C528S L781A)-HA	mutagenesis (G1228, G1229) on plasmid #628
1329	pcDNA3.1(+)-CRM1(C528S F860A)-HA	mutagenesis (G1232, G1233) on plasmid #628
1330	pcDNA3.1(+)-CRM1(C528S P861A)-HA	mutagenesis (G1234, G1235) on plasmid #628
1331	pcDNA3.1(+)-CRM1(C528S W142A P143A)-HA	mutagenesis (G1216, G1217) on plasmid #628
1332	pcDNA3.1(+)-CRM1(C528S W880A F882A)-HA	mutagenesis (G1222, G1223) on plasmid #628
1333	pcDNA3.1(+)-CRM1(C528S P964A)-HA	mutagenesis (G1242, G1243) on plasmid #628
1334	pcDNA3.1(+)-CRM1(C528S P967A V968A)-HA	mutagenesis (G1244, G1245) on plasmid #628
1335	pcDNA3.1(+)-CRM1(C528S F973A)-HA	mutagenesis (G1248, G1249) on plasmid #628
1336	pMal-PP-Nup214(1916-2033)-His	PCR Nup214 (#47, G1147, G1148), cloned into vector #75 (EcoRI/Sall)
1337	pMal-PP-Nup214(1859-2090)-His	PCR Nup214 (#47, G973, G1151), cloned into vector #75 (EcoRI/Sall)
1338	pMal-PP-linkerAAA-Nup214(1916-2033)-His	PCR Nup214 (#47, G1147, G1148), cloned into vector #76 (EcoRI/Sall)
1339	pMal-PP-linkerAAA-Nup214(1859-2090)-His	PCR Nup214 (#47, G973, G1151), cloned into vector #76 (EcoRI/Sall)
1340	pcDNA3.1(+)-CRM1(C528S P867A)-HA	mutagenesis (G1238, G1239) on plasmid #628
1341	pcDNA3.1(+)-CRM1(C528S E907A E908A)-HA	mutagenesis (G1240, G1241) on plasmid #628
1342	pcDNA3.1(+)-CRM1(C528S I972A)-HA	mutagenesis (G1246, G1247) on plasmid #628
1343	pcDNA3.1(+)-CRM1(C528S I866A)-HA	mutagenesis (G1236, G1237) on plasmid #628
1344	pMal-PP-RanBP3	PCR RanBP3 (SAP0666, G1156, G1256), cloned into vector #75 (EcoRI/Sall)
1345	pMal-linkerAAA-PP-RanBP3	PCR RanBP3 (SAP0666, G1156, G1256), cloned into vector #76 (EcoRI/Sall)
1346	pcDNA3.1(+)-CRM1(C528S L715A)-HA	mutagenesis (G1224, G1225) on plasmid #628
1347	pcDNA3.1(+)-CRM1(C528S P778A P779A)-HA	mutagenesis (G1230, G1231) on plasmid #628
1348	pMal-linkerAAA-Nup214(1916-2042)-His	PCR Nup214 (#47, G1147, G1267), cloned into vector #74 (EcoRI/Sall)
1349	pMal-linkerAAA-Nup214(1906-2033)-His	PCR Nup214 (#47, G1266, G1148), cloned into vector #74 (EcoRI/Sall)
1350	pMal-linkerAAA-Nup214(1906-2042)-His	PCR Nup214 (#47, G1266, G1267), cloned into vector #75 (EcoRI/Sall)
1355	pQE60-CRM1(L83F)-His	mutagenesis (G1276, G1277) on plasmid #31
1356	pQE60-CRM1(L83R)-His	mutagenesis (G1278, G1279) on plasmid #31
1357	pQE60-CRM1(I102Q)-His	mutagenesis (G1280, G1281) on plasmid #31
1358	pQE60-CRM1(A156F)-His	mutagenesis (G1290, G1291) on plasmid #31
1359	pQE60-CRM1(K680Q)-His	mutagenesis (G1298, G1299) on plasmid #31
1360	pQE60-CRM1(K680R)-His	mutagenesis (G1300, G1301) on plasmid #31
1361	pQE60-CRM1(L744W)-His	mutagenesis (G1306, G1307) on plasmid #31
1362	pQE60-CRM1(L679W K680R)-His	mutagenesis (G1312, G1313) on plasmid #31
1363	pQE60-CRM1(K680Q A731Q)-His	GeneArt fragment cloned into plasmid #31 (MssI/SacI)
1364	pQE60-CRM1(K680Q A731Q L679R)-His	GeneArt fragment cloned into plasmid #31 (MssI/SacI)

Number	Name	Cloning
1365	pQE60-CRM1(K680Q A731Q C723M)-His	GeneArt fragment cloned into plasmid #31 (MssI/SacI)
1366	pQE60-CRM1(L679R)-His	mutagenesis (G1294, G1295) on plasmid #31
1367	pQE60-CRM1(C723M)-His	mutagenesis (G1302, G1303) on plasmid #31
1368	pQE60-CRM1(M748R)-His	mutagenesis (G1310, G1311) on plasmid #31
1369	pQE60-CRM1(I102W N167R)-His	GeneArt fragment cloned into plasmid #31 (Sall/SacI)
1370	pQE60-CRM1(I102W)-His	mutagenesis (G1282, G1283) on plasmid #31
1371	pQE60-CRM1(L134F)-His	mutagenesis (G1284, G1285) on plasmid #31
1372	pQE60-CRM1(F149W)-His	mutagenesis (G1286, G1287) on plasmid #31
1373	pQE60-CRM1(D152W)-His	mutagenesis (G1288, G1289) on plasmid #31
1374	pQE60-CRM1(N167R)-His	mutagenesis (G1292, G1293) on plasmid #31
1375	pQE60-CRM1(L679W)-His	mutagenesis (G1296, G1297) on plasmid #31
1376	pQE60-CRM1(A731Q)-His	mutagenesis (G1304, G1305) on plasmid #31
1377	pQE60-CRM1(L83R F149W)-His	mutagenesis (G1286, G1287) on plasmid #1356
1378	pQE60-CRM1(I102Q F149W)-His	mutagenesis (G1286, G1287) on plasmid #1357
1379	pQE60-CRM1(L83F D152W)-His	mutagenesis (G1288, G1289) on plasmid #1355
1380	pQE60-CRM1(L83R D152W)-His	mutagenesis (G1288, G1289) on plasmid #1356
1381	pQE60-CRM1(L83F A156F)-His	mutagenesis (G1290, G1291) on plasmid #1355
1382	pQE60-CRM1(L679R L744W)-His	mutagenesis (G1294, G1295) on plasmid #1361
1383	pQE60-CRM1(L679W L744W)-His	mutagenesis (G1296, G1297) on plasmid #1361
1384	pQE60-CRM1(C723M L744W)-His	mutagenesis (G1302, G1303) on plasmid #1361
1385	pQE60-CRM1(I102W F149W)-His	GeneArt fragment cloned into plasmid #31 (Sall/SacI)
1386	pQE60-CRM1(C528W)-His	mutagenesis (G1317, G1318) on plasmid #31
1387	pQE60-CRM1(A541K)-His	mutagenesis (G1319, G1320) on plasmid #31
1388	pQE60-CRM1(L83F F149W)-His	mutagenesis (G1286, G1287) on plasmid #1355
1389	pQE60-CRM1(I102Q D152W)-His	mutagenesis (G1288, G1289) on plasmid #1357
1390	pQE60-CRM1(I102W D152F)-His	GeneArt fragment cloned into plasmid #31 (Sall/SacI)
1391	pQE60-CRM1(I102Q A156F)-His	mutagenesis (G1290, G1291) on plasmid #1357
1392	pQE60-CRM1(L83F D152W K680Q A731Q C723M)-His	cloning fragment from #1365 into #1379 (SacI/MssI)
1393	pQE60-CRM1(L83F D152W L679W L744W)-His	cloning fragment from #1383 into #1379 (SacI/MssI)
1394	pQE60-CRM1(L83F D152W C723M L744W)-His	cloning fragment from #1384 into #1379 (SacI/MssI)
1395	pQE60-CRM1(L83F A156F K680Q A731Q C723M)-His	cloning fragment from #1365 into #1381 (SacI/MssI)
1396	pQE60-CRM1(L83F A156F L679W L744W)-His	cloning fragment from #1383 into #1381 (SacI/MssI)
1397	pQE60-CRM1(L83F A156F C723M L744W)-His	cloning fragment from #1384 into #1381 (SacI/MssI)
1398	pQE60-CRM1(L83F L744W)-His	cloning fragment from #1361 into #1355 (SacI/MssI)
1399	pQE60-CRM1(L83F C723M)-His	cloning fragment from #1367 into #1355 (SacI/MssI)
1400	pQE60-CRM1(L83F K680Q A731Q L679R)-His	cloning fragment from #1364 into #1355 (SacI/MssI)
1401	pQE60-CRM1(I102Q F149W K680Q A731Q C723M)-His	cloning fragment from #1365 into #1378 (SacI/MssI)
1402	pQE60-CRM1(I102Q F149W L679W L744W)-His	cloning fragment from #1383 into #1378 (SacI/MssI)
1403	pQE60-CRM1(I102Q F149W C723M L744W)-His	cloning fragment from #1384 into #1378 (SacI/MssI)
1404	pQE60-CRM1(I102Q F149W L744W)-His	cloning fragment from #1361 into #1378 (SacI/MssI)

Number	Name	Cloning
1405	pQE60-CRM1(I102Q F149W C723M)-His	cloning fragment from #1367 into #1373 (Sacl/Mssl)
1406	pQE60-CRM1(L83R A156F)-His	mutagenesis (G1290, G1291) on plasmid #1356
1407	pQE60-CRM1(D824K)-His	mutagenesis (G1321, G1322) on plasmid #31
1408	pQE60-CRM1(F823A)-His	mutagenesis (G1323, G1324) on plasmid #31
1409	pQE60-CRM1(H925W)-His	mutagenesis (G1325, G1326) on plasmid #31
1410	pQE60-CRM1(S928K)-His	mutagenesis (G1327, G1328) on plasmid #31
1411	pQE60-CRM1(T917E)-His	mutagenesis (G1329, G1330) on plasmid #31
1412	pQE60-CRM1(W880A)-His	mutagenesis (G1331, G1332) on plasmid #31
1413	pQE60-CRM1(Y918W)-His	mutagenesis (G1333, G1334) on plasmid #31
1414	pET28a-His-Nup214(1916-2033)KAa1-His	PCR Nup214 (#1172, G986, G987), cloned into vector #4 (NdeI, XhoI)
1415	pET28a-His-Nup214(1916-2033)KE-His	PCR Nup214 (#1173, G986, G987), cloned into vector #4 (NdeI, XhoI)
1426	pmRFP-Nup214(1859-2090)X1-cNLS	GeneArt fragment cloned into plasmid #987 (EcoRI/Sall)
1427	pmRFP-Nup214(1859-2090)X2-cNLS	GeneArt fragment cloned into plasmid #987 (EcoRI/Sall)
1428	pmRFP-Nup214(1859-2090)X3-cNLS	GeneArt fragment cloned into plasmid #987 (EcoRI/Sall)
1429	pQE60-CRM1(D824K S928K)-His	mutagenesis (G1327, G1328) on plasmid #1407
1430	pQE60-CRM1(K680Q A731Q L679R F149W)-His	mutagenesis (G1286, G1287) on plasmid #1364
1431	pQE60-CRM1(K680Q A731Q L679R D824K)-His	mutagenesis (G1321, G1322) on plasmid #1364
1432	pQE60-CRM1(K680Q A731Q L679R S928K)-His	mutagenesis (G1327, G1328) on plasmid #1364
1433	pET28a-His-Nup214(1916-2033)X1-His	PCR Nup214 (#1426, G1352, G987), cloned into vector #4 (NdeI, XhoI)
1434	pET28a-His-Nup214(1916-2033)X2-His	PCR Nup214 (#1427, G1352, G987), cloned into vector #4 (NdeI, XhoI)
1435	pET28a-His-Nup214(1916-2033)X3-His	PCR Nup214 (#1428, G1352, G987), cloned into vector #4 (NdeI, XhoI)
1436	pMal-linkerAAA-Nup214(1916-2033)X1-His	PCR Nup214 (#1426, G1353, G1148), cloned into vector #74 (EcoRI/Sall)
1437	pMal-linkerAAA-Nup214(1916-2033)X2-His	PCR Nup214 (#1427, G1353, G1148), cloned into vector #74 (EcoRI/Sall)
1438	pMal-linkerAAA-Nup214(1916-2033)X3-His	PCR Nup214 (#1428, G1353, G1148), cloned into vector #74 (EcoRI/Sall)
1444	pcDNA3.1(+)-CRM1(K680Q A731Q L679R)-HA	PCR CRM1 (#1364, G275, G276), cloned into vector #52 (NheI, BamHI)
1445	pcDNA3.1(+)-CRM1(D824K)-HA	PCR CRM1 (#1407, G275, G276), cloned into vector #52 (NheI, BamHI)
1446	pcDNA3.1(+)-CRM1(K680Q A731Q L679R D824K)-HA	PCR CRM1 (#1431, G275, G276), cloned into vector #52 (NheI, BamHI)
1447	pcDNA3.1(+)-CRM1(K680Q A731Q L679R C528S)-HA	mutagenesis (G336, G337) on plasmid #1444
1448	pcDNA3.1(+)-CRM1(D824K C528S)-HA	mutagenesis (G336, G337) on plasmid #1445
1449	pcDNA3.1(+)-CRM1(K680Q A731Q L679R D824K C528S)-HA	mutagenesis (G336, G337) on plasmid #1446

2.2 Molecular Biology Methods

2.2.1 RbCl chemically competent cells

The protocol was adapted from [213] and used for preparing RbCl chemical competent TG1 cells.

4 ml LB was inoculated with half an aliquot of RbCl-competent TG1 clone #17 cells and incubated at 37 °C overnight. 100 ml LB supplemented with 10 mM MgSO₄ was inoculated with 1.5 ml of starter culture and incubated at 37 °C and 170 rpm until an OD₆₀₀ of 0.5-0.6 was reached. The culture was transferred to two pre-chilled 50 ml tubes and cooled down on ice for 15 minutes before harvesting in a pre-chilled centrifuge at 3000 g and 4 °C for 10 minutes.

All subsequent steps were performed on ice with pre-chilled reaction tubes.

The supernatant was discarded and the two cell pellets of each tube were resuspended in 20 ml of ice-cold TFB-I (30 mM KOAc, 10 mM CaCl₂, 50 mM MnCl₂, 100 mM RbCl, 15% glycerol, pH 5.8) by pipetting up and down. The resuspended cells were combined in one tube and incubated on ice for 15 minutes. The cells were pelleted in a pre-chilled centrifuge at 1000 g and 4 °C for 15 minutes. The supernatant was discarded and the cell pellet was resuspended in 4 ml of ice-cold TFB-II (100 mM MOPS, 75 mM CaCl₂, 10 mM RbCl, 15% glycerol, pH 6.5) by pipetting up and down. The resuspended cells were incubated on ice for 15 minutes. Aliquots of 40-100 µl were snap frozen in liquid nitrogen and stored at -80 °C until used.

2.2.2 Agarose gel electrophoresis

For separation of DNA fragments 0.7-2.0% agarose gels were prepared. The agarose was dissolved in 1x TAE buffer in an Erlenmeyer flask and boiled in a microwave oven until completely dissolved. 1 µl of SERVA DNA Stain Clear G (SERVA) per 100 ml gel was added to the solution prior to casting the gel.

The gel electrophoresis was run in 1x TAE buffer at 120 V for 20 to 50 minutes depending on the size of the gel and the intended resolution.

The GeneRuler 100bp DNA Ladder or the GeneRuler 1kb DNA Ladder (ThermoScientific) were used as molecular weight markers.

For extracting DNA fragments for further use, the bands were cut on an UV transilluminator with DNA Pick-Tips (Süd-Laborbedarf GmbH). The gel was documented with the GelSTICK "touch" system (INTAS Science Imaging Instruments).

2.2.3 Quantification of dsDNA

The concentration and purity of dsDNA was determined by measuring the UV absorbance at 260 nm and 280 nm with the NanoDrop 2000c (ThermoScientific).

2.2.4 Polymerase chain reaction (PCR)

PCR reactions were assembled with Phusion High-Fidelity DNA Polymerase (ThermoScientific) according to the manufacturer's instructions. Preparative PCR was done in 50 µl reactions. For control PCR of mini prep DNA the reaction was scaled down to 20 µl reactions. No additional DMSO or MgCl₂ was added. The PCR reaction was run for 35 cycles in standard conditions. Elongation time was adjusted to the expected size of the PCR product. The annealing temperature chosen was generally 2-4 °C below the initial primer melting temperature as calculated by the SerialCloner Software.

6x DNA sample buffer was added to the reactions after PCR. Depending on the expected size of the PCR products the sample was loaded on 0.7 - 2.0% agarose gels. PCR products were cut from agarose gels with DNA Pick-Tips (Süd-Laborbedarf GmbH) and purified with the NucleoSpin® Gel and PCR Clean-up kit (Macherey-Nagel). Purified DNA was eluted in 25 µl elution buffer.

2.2.5 Site-directed mutagenesis

Site-directed mutagenesis reactions were assembled with Pfu Ultra II polymerase (Agilent) according to the manufacturer's instructions. The PCR reaction was run for 35 cycles in standard conditions with an annealing temperature of 60 °C. Elongation time was adjusted to the size of the respective template plasmid. 1 µl DpnI was added to the reaction after PCR and the template plasmid was digested at 37 °C for 3 hours or overnight. 10-13 µl of the reaction was transformed into chemically competent DH5α cells or, in case of pQE60-CRM1 mutants, into chemically competent XL10 gold cells. The transformed cells were plated onto LB-agar plates with the respective antibiotic and incubated overnight at 37 °C. At least three clones were picked for inoculating 3 ml mini prep cultures. Plasmid from 2 ml of cultures was isolated with the NucleoSpin® Plasmid Kit (Macherey-Nagel). 20 µl plasmid was sent for sequencing at GATC Biotech.

2.2.6 Restriction enzyme digest

Restriction enzyme digest was performed in 20 µl reaction volume for plasmids and 30 µl reaction volume for purified PCR products. The buffer and restriction enzyme ratio was chosen as suggested by the DoubleDigest tool on the ThermoScientific website (<http://www.thermoscientificbio.com/webtools/doubledigest/>).

Control digest of mini prep DNA

14-16 µl of mini prep DNA was digested. The digest was performed for at least 1 hour at 37 °C. After digestion, 6x DNA sample buffer was added and the sample was loaded on a 0.7 - 2.0% agarose gel depending on the sizes of the expected fragments. The band pattern was documented with the GelSTICK "touch" system (INTAS Science Imaging Instruments).

Preparative digest of PCR products and plasmids

25 µl of purified PCR products or 5 µl of plasmid DNA was digested. The digest was performed for 2-3 hours at 37 °C. After digestion 6x DNA sample buffer was added and the sample was

loaded on a 0.7 - 2.0% agarose gel depending on the sized of the expected fragment. The DNA was visualized with an UV transilluminator and the intended bands were cut with DNA Pick-Tips (Süd-Laborbedarf GmbH). The gel was documented with the GelSTICK "touch" system (INTAS Science Imaging Instruments). The DNA was purified with the NucleoSpin® Gel and PCR Clean-up kit (Macherey-Nagel). Purified DNA was eluted in 25 µl elution buffer.

2.2.7 Ligation of DNA fragments

The ligation reaction was performed in 10 µl reaction volume containing 10 mM ATP, 1x T4 DNA Ligase Reaction Buffer (ThermoScientific) and 0.5 µl of T4 DNA Ligase (ThermoScientific). 20-30 ng of the vector DNA fragment was ligated with at least 5x molar excess of the insert DNA fragment. The reaction mixture was incubated at room temperature for 1 hour and subsequently transformed into chemically competent DH5α cells or, in case of pQE60-CRM mutants, into chemically competent XL10 gold cells.

2.2.8 Transformation of *E. coli* strains with plasmid DNA

An aliquot of RbCl competent cells was thawed on ice. 0.5 µg of plasmid or 5 µl of a ligation mixture was added to the cells. The cells were mixed thoroughly and incubated on ice for 30 minutes. A heat shock was performed at 42 °C for 90 seconds. The cells were cooled down on ice for 2 minutes before adding 500 µl ice-cold SOC medium (2% (w/v) tryptone, 0.5% (w/v) yeast extract, 10 mM NaCl, 2.5 mM KCl, 10 mM MgCl₂, 10 mM MgSO₄, 0.36% (w/v) glucose, pH 7.0). The mixture was incubated in a ThermoMixer (Eppendorf) at 37 °C, 850 rpm for 1 hour.

For ligations, cells were harvested by centrifugation (3000 rpm, 2.5 minutes). About 400 µl of the supernatant was removed and the cells were resuspended in the remaining liquid by pipetting up and down before plating on an LB-agar plate with an appropriate antibiotic.

In case of re-transformations, 70 µl of the cell suspension was plated directly on an LB-agar plate (LB supplemented with 1.5% (w/v) bacto-agar and the respective antibiotic).

The plates were incubated overnight at 37 °C.

2.2.9 Purification of plasmid DNA

Mini preps

3 ml of LB (1% (w/v) bacto-tryptone, 0.5% (w/v) yeast extract, 1% (w/v) NaCl (pH7.0)) supplemented with the appropriate antibiotic was inoculated with one colony picked from an LB-agar plate. Cultures were incubated overnight at 37 °C, 180 rpm.

2 ml of culture was transferred to a 2 ml reaction tube and cells were harvested by centrifugation (11000 g, 4 °C, 1 minute). DNA was extracted with the NucleoSpin® Plasmid (Macherey-Nagel) according to the manufacturer's instructions. The purified DNA was eluted with 50 µl of elution buffer.

Midi preps

200 ml of LB (1% (w/v) bacto-tryptone, 0.5% (w/v) yeast extract, 1% (w/v) NaCl (pH7.0)) supplemented with the appropriate antibiotic was inoculated with one colony picked from an LB-agar plate or with the rest of a mini prep culture. Cultures were incubated overnight at 37 °C, 180 rpm.

The cells were harvested by centrifugation (5250 g, 4 °C, 15 minutes). DNA was extracted with the NucleoBond™ Xtra Midi kit according to the manufacturer's instructions. The precipitated DNA was dissolved in 70 µl H₂O. The dsDNA concentration was determined with the NanoDrop 2000c (ThermoScientific) and adjusted to 1 mg/ml with H₂O.

2.2.10 DNA sequencing

Plasmids sequences were analyzed by GATC Biotech. 20 µl of mini prep DNA or 2 µg of midi prep DNA in a total volume of 20 µl were sent for sequencing.

Standard primers from GATC Biotech were chosen via the PrimerScout tool on the website (<http://www.gatc-biotech.com/>). For sequencing of pmRFP-cNLS plasmids or CRM1 mutants, 20 µl the respective primers (10 µM) were sent with the sample. A list of sequencing primers used in this work is found in section 2.1.10.

2.3 Biochemical Methods

2.3.1 SDS-PAGE

Proteins were separated by SDS-PAGE. According to the size of the proteins of interest resolving gels from 6% to 20% were chosen. SDS sample buffer was added to the sample. Cell lysates and pulldown samples were incubated at 98 °C for 5 minutes prior to loading on the gel. The gel electrophoresis was performed with Laemmli running buffer (25 mM Tris, 192 mM glycine, 0.05% SDS) in SE250 Mighty Small II Mini Vertical Electrophoresis Units (Hoefer) with 25 mA per gel and 300 V for 65 minutes.

For better visualization of samples containing small as well as large proteins NuPAGE® Novex® 4-12% Bis-Tris gradient gels were used with either NuPAGE® MES SDS or MOPS SDS running buffer. NuPAGE® sample buffer and 50 mM DTT was added to the samples prior to incubation at 70 °C for 10 minutes. The gel electrophoresis was performed in XCell SureLock® Mini-Cells at 200 V for 45 minutes.

The PageRuler Unstained, PageRuler Prestained or PageRuler Plus Prestained protein ladders were run next to the samples on every gel.

Gels were used either for Western blotting (see section 2.3.4) or proteins were visualized with Coomassie (see section 2.3.2) or silver staining (see section 2.3.3).

2.3.2 Coomassie staining of SDS-PAGE gels

The SDS-PAGE gel was rinsed in deionized water and then incubated with Coomassie fixing solution (40% ethanol, 10% acetic acid) for 5 minutes up to 1 hour. Coomassie staining solution (5% Aluminum sulfate-(14-18)-hydrate, 10% EtOH, 2% ortho-phosphoric acid, 0.02% CBB-G250) was applied for at least 15 minutes or overnight. As this method gives only minimal background, washing with deionized water for 15 minutes removed most of the residual background staining. Gels that were stained overnight were additionally incubated with Coomassie destaining solution (10% acetic acid) to speed up the destaining process.

Stained gels were documented using the LAS-3000 (Fujifilm) and imported to ImageJ software for editing and quantification.

2.3.3 Silver staining of SDS-PAGE gels

Low amounts of protein on gels were visualized by silver staining. Silver staining was performed with self-made solutions according to a protocol adapted from [214]. Alternatively the Pierce® Silver Stain Kit (ThermoScientific) was used according to the manufacturer's instructions. Novex® pre-cast gels were stained with the SilverQuest™ Staining Kit (Invitrogen) according to the manufacturer's instructions.

Stained gels were documented using the LAS-3000 (Fujifilm) and imported to ImageJ software for editing and quantification.

Protocol for Silver staining (adapted from [214]):

The SDS-PAGE or Tricine-SDS-PAGE gels were rinsed in deionized water and incubated in fixing solution (50% methanol, 10% acetic acid, 100 mM ammonium acetate) for at least 30 minutes or overnight. The gel was washed twice with deionized water and sensitized by incubating in sensitizing solution (0.005% sodium thiosulfate) for 60 minutes. Staining solution (0.1% silver nitrate) for 60 minutes, followed by a 10 second-rinse with water. Developing solution (0.037% formaldehyde, 2% sodium carbonate) was added to the gel until bands appeared (2- 3 minutes) and the development was stopped by adding stopping solution (50 mM EDTA) for 60 minutes. The gels were rinsed twice with water before documentation.

2.3.4 Western blotting

SDS-PAGE and Tricine-SDS-PAGE gels were blotted to nitrocellulose membrane. Amersham Hybond ECL Nitrocellulose Blotting Membrane (GE Healthcare) was used for detection of proteins with fluorophore-coupled secondary antibodies and Amersham Protran 0.45 μ m NC Nitrocellulose Blotting Membrane (GE Healthcare) was used for detection with HRP-coupled secondary antibodies.

The transfer was performed at 300 V, 400 mA in wet-blot chambers or at 150 V, 350 mA in a Mini Trans-Blot® Cell (Bio-Rad) with Western blot transfer buffer (25 mM Tris, 193 mM glycine, 0.02% SDS, 20% methanol). Blotting time was adjusted according to the size of the proteins and the percentage of the resolving gel and varied from 90 to 150 minutes.

Optionally, after transfer the membrane was stained with PonceauS staining solution for 1 minute. Excess staining solution was removed by several rinsing steps with 0.1% acetic acid. Stained membranes were documented using the LAS-3000 (Fujifilm) and imported to ImageJ software for editing.

To reduce unspecific binding, the membrane was blocked for 30 minutes with 4% milk powder in PBST (137 mM NaCl, 2.7 mM KCl, 10 mM Na₂HPO₄, 1.8 mM KH₂PO₄, 0.1% Tween-20) or 2% BSA in PBST depending on the primary antibody. Primary antibodies were diluted in freshly prepared blocking solution. A list of the primary antibodies used in this work and their respective dilutions can be found in section 2.1.9. Blots were incubated in a 50 ml tube with 5 ml of diluted antibody solution on a blot roller for 2 hours at room temperature or overnight at 4 °C. The antibody solution was recovered and could be reused several times when stored at -20 °C. The membrane was washed 3x 10 minutes with PBST. The secondary antibody was diluted in 20 ml of 4% milk powder in PBST and applied for 1 hour at room temperature. A list of the secondary antibodies used in this work and their respective dilutions can be found in section 2.1.9.

Protocol for detection with fluorophore-coupled secondary antibodies:

Western blot incubation boxes (LI-COR) were used for the blocking step, all washing steps and incubation with the secondary antibody.

After incubation with the secondary antibody the membrane was washed 1-3x for 10 minutes with PBST and then transferred to PBS (137 mM NaCl, 2.7 mM KCl, 10 mM Na₂HPO₄, 1.8 mM KH₂PO₄) until detection.

The signal was analyzed with the Odyssey® Sa Infrared Imaging System (LI-COR) using the ImageStudio software (version 4.0.21, LI-COR).

Protocol for detection with HRP-coupled secondary antibodies:

After incubation with the secondary antibody the membrane was washed 3x 10 minutes with PBST. Signals after addition of Immobilon™ Western Chemiluminescent HRP Substrate (Millipore) were detected with Amersham Hyperfilm™ ECL (GE Healthcare) or Medix XBU medical x-ray films (FOMA Bohemia). Films were developed with the developer machine CURIX60 (Agfa).

2.3.5 Chemically synthesized peptides

An NES peptide corresponding to the sequence CVDEMTKKFGTLTIHDTEK was obtained from Pepscan Presto B. V. (Lelystad, The Netherlands) with a purity of 63.8%.

2.3.6 Protein purification

Ran(1-180)Q69L [127] and SPN1(1-291) were purified by Thomas Monecke (Molecular Structural Biology, Universität Göttingen).

GST-PDCD2L wildtype and NES mutant were a gift from François Bachand (Université de Sherbrooke, Canada).

RanC4A [215], RanGAP [103], RanBP1 [216], GST-CCP1 [217] and GST-Rev [218] were available in the common laboratory stock.

Ran and RanQ69L were expressed and purified as described before [219].

GST-PKI-NES and GST-Rev-NES were purified with a standard protocol for purification of GST-fusion proteins [220, 221] in GST prep buffer (50 mM Tris pH 6.8, 300 mM NaCl, 1 mM MgCl₂, 0.25 mM EDTA, 1 mM DTT, 1 mM AP, 1 mM LP).

Importin α , importin β , importin 5, transportin and importin 13 were available in the common laboratory stock.

SPN1

His-SPN1 [222] and GST-SPN1 [217] were purified as described before.

CRM1-His

A glycerol stock of TG1 cells transformed with pQE60-CRM1-His [223] was plated on an LB-agar plate with ampicillin. The plate was incubated at 37 °C overnight. 200 ml 2YT (16 g/l tryptone, 10 g/l yeast extract, 5 g NaCl, pH 7.0) supplemented with ampicillin was inoculated with several colonies from the plate and incubated at 37 °C, 170 rpm overnight. 2 liters 2YT medium supplemented with ampicillin was inoculated with 10 ml starter culture in Erlenmeyer flasks without baffles. CRM1-His was expressed at 37 °C overnight without induction. Cells were harvested, washed once in PBS (137 mM NaCl, 2.7 mM KCl, 10 mM Na₂HPO₄, 1.8 mM KH₂PO₄) and stored at -80 °C until purification.

TG1 cells were transformed with pQE60-CRM1-His mutants and plated on an LB-agar plate with ampicillin. The plate was incubated at 37 °C overnight. 100 ml LB supplemented with ampicillin was inoculated with several colonies from the plate and incubated at 37 °C, 170 rpm overnight. 2 liters 2YT medium supplemented with ampicillin was inoculated with 10 ml starter culture in Erlenmeyer flasks without baffles. Expression was induced at an OD₆₀₀ of 0.5-0.7 with 100 μM Isopropyl β-D-1-thiogalactopyranoside. CRM1-His mutants were expressed at 37 °C for 5 hours. Cells were harvested, washed once in PBS and stored at -80 °C until purification.

For purification, a pellet from 2 liter culture was resuspended in 35 ml CRM1 prep buffer (50 mM HEPES pH 7.5, 500 mM NaCl, 2 mM MgCl₂, 20 mM β-mercaptoethanol, 100 μM PMSF, 1 μg/ml of each AP and LP). Cells were lysed with an EmulsiFlex-C3 (Avestin) and the lysate was cleared by centrifugation at 100000 g and 4 °C for 30-45 minutes. The supernatant was incubated with 1 ml Ni-NTA sepharose (Qiagen) equilibrated in CRM1 prep buffer at 4 °C for 1 hour. The beads were washed 4x with CRM1 prep buffer supplemented with 30 mM imidazole, transferred to an empty column and eluted with CRM1 prep buffer containing 300 mM imidazole. The eluted protein was changed into CRM1 desalting buffer (50 mM HEPES pH 7.5, 50 mM NaCl, 2 mM Mg(OAc)₂, 2 mM DTT) with PD-10 Desalting Columns (GE Healthcare) or a HiPrep 26/10 Desalting (Sephadex G-25) column (GE Healthcare) attached to an ÄKTApurifier (Amersham Biosciences). The protein solution was filtered with Minisart RC 15 single use syringe filters (0.2 μm, sartorius stedim biotech) before purification with a MonoQ anion exchanger column (GE Healthcare). CRM1-His was bound to the column in CRM1 desalting buffer and eluted with an increasing concentration of CRM1 high salt buffer (50 mM HEPES pH 7.5, 500 mM NaCl, 2 mM Mg(OAc)₂, 2 mM DTT). The peak fractions containing CRM1-His were pooled, aliquoted, snap-frozen in liquid nitrogen and stored at -80 °C. For subsequent complex formations for electron microscopy or crystallization CRM1-His was prepared freshly and the complex was formed immediately.

GST-Nup214 fragments

GST-Nup214 fragments were expressed and purified as described before [59]. Glutathione was removed from the eluted protein by buffer exchange into GST prep buffer (50 mM Tris pH 6.8, 300 mM NaCl, 1 mM MgCl₂, 0.25 mM EDTA, 1 mM DTT, 1 μg/ml of each AP and LP) with PD-10 Desalting Columns (GE Healthcare).

His-Nup214 fragments

His-Nup214 fragments were expressed and purified as described before [59]. After elution from Ni-NTA agarose (Qiagen), the protein was concentrated to a volume smaller than 5 ml with 20 ml/5 kDa Spin-XR concentrators (Corning), filtered with Minisart RC 15 single use syringe filters (0.2 μm , sartorius stedim biotech) before purification with a HiLoad 26/60 Superdex 75 prep grade column (GE Healthcare) attached to an ÄKTApurifier (Amersham Biosciences) in His prep buffer (50 mM Tris pH 6.8, 200 mM NaCl, 1 mM MgCl_2 , 10% glycerol, 4 mM β -mercaptoethanol, 100 μM PMSF, 1 $\mu\text{g/ml}$ of each AP and LP). The fractions containing the His-Nup214 were determined via SDS-PAGE, pooled and concentrated with 20 ml/5 kDa Spin-XR concentrators (Corning).

MBP-Nup214-His fragments

Plasmids coding for MBP-Nup214-His fragments were transformed into BL21 (DE3) codon+ cells and plated onto LB-agar plates supplemented with ampicillin and chloramphenicol. 200 ml MBP rich medium (10 g/l tryptone, 5 g/l yeast extract, 5 g/l NaCl, 2 g/l glucose) supplemented with ampicillin and chloramphenicol was inoculated with several colonies from an LB-agar plate and incubated overnight at 37 °C, 170 rpm. 1.5 liters MBP rich medium supplemented with ampicillin was inoculated with 15 ml starter culture, grown at 37 °C, 130 rpm to an OD600 of 0.5-0.7. Expression was induced with 300 μM Isopropyl β -D-1-thiogalactopyranoside and cells were grown overnight at 18 °C, 130 rpm. Cells were harvested, washed once in PBS (137 mM NaCl, 2.7 mM KCl, 10 mM Na_2HPO_4 , 1.8 mM KH_2PO_4) and stored at -80 °C until purification.

A pellet from 1.5 liters of culture was resuspended in 35 ml His prep buffer (50 mM Tris pH 6.8, 200 mM NaCl, 1 mM MgCl_2 , 10% glycerol, 4 mM β -mercaptoethanol, 100 μM PMSF, 1 $\mu\text{g/ml}$ of each AP and LP). Cells were lysed with the EmulsiFlex-C3 (Avestin) and the lysate was cleared by centrifugation at 100000 g, 4 °C for 30-45 minutes. The supernatant was added to 0.75 ml Ni-NTA sepharose and incubated at 4 °C for 1 hour. The beads were washed 3x with His prep buffer containing 30 mM imidazole and eluted with His prep buffer containing 300 mM imidazole. The eluted protein was diluted with His prep buffer to 10 ml, added to amylose resin and incubated at 4 °C for 1 hour. The protein was eluted with His prep buffer containing 15 mM maltose, aliquoted and stored at -80 °C.

2.3.7 Loading of Ran with GTP/GDP

Loading of Ran with GTP or GDP was performed with a protocol adapted from [24].

Ran was incubated with 20x molar excess of GTP or GDP and 15 mM EDTA in transport buffer (20 mM HEPES, 110 mM KOAc, 2 mM $\text{Mg}(\text{OAc})_2$, 1 mM EGTA, pH 7.3) for 30 minutes at room temperature. Afterwards 40 mM MgCl_2 was added and the mixture was incubated on ice for 15 minutes.

Loaded Ran was immediately used or snap-frozen in small aliquots and stored at -80 °C.

Aliquoted RanGTP was only thawed once.

RanGTP that was intended for loading with ^{32}P - γ -GTP was changed into transport buffer with 2 ml Zeba Desalting Spin Columns (Pierce) to remove unbound GTP. Afterwards the loading procedure was repeated to exchange the bound GTP with ^{32}P - γ -GTP. 10 μl of ^{32}P - γ -GTP (6000 Ci/mmol, 10 mCi/ml) was used for loading 150-200 μg of Ran in transport buffer containing 1 mg/ml BSA and 2 mM MgCl_2 . Unbound ^{32}P - γ -GTP was removed by PD-10 Desalting Columns (GE Healthcare).

2.3.8 *In vitro* binding assays

Pulldowns

Pulldowns were used to study the interaction of the nucleoporins with the CRM1 export complex. Per sample, 50 pmol GST or GST-fusion protein was immobilized on 25 μl glutathione sepharose High Performance beads (GE Healthcare) equilibrated in pulldown buffer (50 mM Tris pH 7.4, 200 mM NaCl, 1 mM MgCl_2 , 5% glycerol, 1 mM DTT) supplemented with 20 mg/ml BSA. Either the nucleoporin, a cargo or RanQ69L pre-loaded with GDP or GTP was immobilized. The beads were washed with 3 times 500 μl pulldown buffer supplemented with 20 mg/ml BSA and incubated with an equal or excess molar amount of the proteins of interest in a total volume of 400 μl pulldown buffer supplemented with 20 mg/ml BSA for 1 hour at 4 °C. The beads were washed with 3 times 500 μl pulldown buffer. Bound proteins were eluted in 2x SDS sample buffer before analysis by SDS-PAGE and optional Western blotting.

Halo assay

For the detection of low affinity interactions and better quantification a flow cytometry-based binding assay was developed (section 3.1).

CRM1 was labeled with Cy3 (Mono Reactive Dye Pack, GE Healthcare) according to the manufacturer's instructions. 50 pmol GST or GST-fusion protein was immobilized on 2.5 μl glutathione sepharose High Performance beads (GE Healthcare) equilibrated in transport buffer (20 mM HEPES pH7.3, 110 mM KOAc, 2 mM $\text{Mg}(\text{OAc})_2$, 1 mM EGTA, 1 mM DTT) supplemented with 10 mg/ml BSA. Either a nucleoporin, a cargo or Ran pre-loaded with GDP or GTP was immobilized. The beads were washed and incubated with 7.3 pmol CRM1-Cy3, an excess of the other proteins of interest and 5 μl 4x Halo mix (500 mM NaCl, 40 mg/ml BSA, 1 mM DTT, 2% 1,6-hexanediol) in a total volume of 20 μl transport buffer containing 10 mg/ml BSA for 1 hour at 4 °C. The beads were washed once in transport buffer and bound CRM1-Cy3 was analyzed by flow cytometry using a FACSCanto II (BD Biosciences) and FACS Diva 6.1.1 software. The median fluorescence of 10000 beads was measured (585/42 bandwidth and 556LP filter).

2.3.9 RanGAP assay

RanGAP assays were performed as described previously to quantitatively assess complex formation [24, 64]. CRM1 wildtype or mutants were incubated with Ran loaded with ^{32}P - γ -GTP and increasing concentrations of Nup214 or cargo or combinations thereof. GTP-hydrolysis of unbound RanGTP was initiated upon addition of 10 nM RanGAP and analyzed by determining free radioactive phosphate with a scintillation counter. Results were normalized to a reaction without RanGAP and plotted as percent GTP-hydrolysis.

2.3.10 Complex formation tests

About 200 μg of complex were prepared by mixing the purified proteins of interest at 4 °C for 1 hour and loading on a Superdex 200 10/300 GL column (GE Healthcare) equilibrated in export complex buffer (20 mM Tris pH 7.4, 50 mM NaCl, 1 mM $\text{Mg}(\text{OAc})_2$, 1 mM DTT). 1 ml fractions were collected and the protein content was analyzed by SDS-PAGE followed by Coomassie or silver staining or Western blotting.

2.3.11 Purification of Antibodies

Anti-Nup214 antibodies against an internal Nup214 peptide ((C)ASSSFGEQKPTGT) were raised in rabbit (Covalab). 10 ml rabbit serum (rabbit 1314036, Covalab project 3882) was diluted with 40 ml PBS (137 mM NaCl, 2.7 mM KCl, 10 mM Na_2HPO_4 , 1.8 mM KH_2PO_4) and incubated with immobilized antigen on beads (provided by Covalab) at 4 °C overnight. Beads were washed twice with 50 ml PBS supplemented with 0.5 M NaCl, transferred to a column and eluted with 0.2 M acetic acid (pH 2.7) containing 0.5 M NaCl. 500 μl fractions were collected and immediately neutralized with 100 μl 1M Tris/Base. The protein content of the fractions was tested by adding 5 μl of the fraction to 200 μl Bradford assay solution. The three fractions containing protein were pooled, changed into PBS with PD-10 Desalting Columns (GE Healthcare) and concentrated with 50 kDa/6 ml Concentrators (Corning) to 1.6 ml. The purified antibody was tested in immunofluorescence and Western blotting by Christiane Spillner.

2.4 Cell Biology Methods

2.4.1 Cultivation of mammalian cells

HeLa P4 cells and HeLa cells stably transfected with NFAT [60, 24] were grown at 37 °C and 5% CO₂ and 95% humidity on 10 cm or 15 cm diameter plates in Dulbecco's Modified Eagle Medium (DMEM) containing 10% fetal bovine serum (FBS), 2 mM L-glutamine and optionally 100 U/ml penicillin and 100 µg/ml streptomycin.

For passaging, cells were washed with PBS (137 mM NaCl, 2.7 mM KCl, 10 mM Na₂HPO₄, 1.8 mM KH₂PO₄) once and incubated with 0.025% Trypsin/ EDTA until detached. Medium was added and the cells were transferred to 10 cm, 15 cm or 24-well plates.

2.4.2 Transfection of DNA in mammalian cells

Plasmids were transfected with the calcium phosphate method [224]. For transfection in 24-well plates, cells were grown in 500 µl medium to a confluency of 40-50%. 1 µg plasmid DNA was transfected per well. 20 µl CaCl₂ (250 mM) was added to the DNA in a reaction tube followed by vortexing for 5 seconds. 20 µl 2x HEPES (50 mM HEPES, 250 mM NaCl, 1.5 mM Na₂HPO₄, pH 6.98) buffer was added followed by 10 seconds vortexing and incubation at room temperature for 25 minutes. After addition of the mixture, the cells were grown at 37 °C with 3% or 5% CO₂ for 24 hours.

For co-transfection experiments, HeLa cells were transfected with 0.3 µg of a plasmid coding for GFP-SPN1 [222] and 0.5-0.6 µg of plasmids coding for RFP-Nup214-cNLS fragments.

For transfection of 10 cm plates, the reaction mixture was upscaled using 15 µl DNA, 500 µl CaCl₂ and µl 2x HBS buffer.

2.4.3 *In vitro* export assays

In vitro export assays were adapted from [145]. GFP-NFAT spinner cells were grown in a 15 cm diameter plate to 40-50% confluency and expression of GFP-NFAT was induced by 1 µM trichostatin A in DMEM overnight. Import of GFP-NFAT into the nucleus was induced by 1 µM ionomycin in DMEM for 25 minutes. Cells were washed once with PBS (137 mM NaCl, 2.7 mM KCl, 10 mM Na₂HPO₄, 1.8 mM KH₂PO₄) and detached from the plate by addition of 0.025% Trypsin/ EDTA. Cells were resuspended in ice-cold transport buffer (20 mM HEPES, 110 mM KOAc, 2 mM Mg(OAc)₂, 1 mM EGTA, pH 7.3) supplemented with 10% FBS. Cells were counted with the CASY 1 (Schärfe System) and centrifuged at 300 g and 4 °C for 5 minutes. The pellet was resuspended in transport buffer, centrifuged again and resuspended in transport buffer at a concentration of 1x 10⁷ cells/ml. 0.7 µl of 1% digitonin was added per 1x 10⁶ cells for 3 minutes. 5 µl of cell suspension was mixed with 5 µl of a trypan blue solution on a cover slide to confirm sufficient permeabilization.

For transport assays with recombinant Nup214 fragments, cells were washed once with 50 ml transport buffer and resuspended in transport buffer at a concentration of 2x 10⁷ cells/ml. Transport reactions containing 200000 pre-incubated cells, Ran, an ATP-regenerating system

(1 mM ATP, 4 mM creatine phosphate, 10 U/ml creatine phosphokinase), NFAT oligo and the respective Nup214 protein of interest were assembled in reaction tubes and incubated at 30 °C in a thermomixer for 25 minutes. The samples were transferred to ice and the reaction was stopped with 500 µl ice-cold transport buffer.

For transport assays with recombinant CRM1 mutants, permeabilized cells were pre-treated to remove soluble transport factors and block endogenous CRM1. Cells were washed twice with 50 ml transport buffer and resuspended in transport buffer at a concentration of 0.5×10^7 cells/ml. 50000 cells per sample were incubated with ATP-regenerating system (1 mM ATP, 4 mM creatine phosphate, 10 U/ml creatine phosphokinase), and 100 nM LMB in a 30 °C water bath for 15 minutes. The cells were washed twice with 50 ml transport buffer and afterwards resuspended in transport buffer at a concentration of 0.5×10^7 cells/ml.

The export reactions were assembled on ice in FACS tubes. 50000 pre-incubated cells, Ran, ATP regenerating system, NFAT oligo and the respective CRM1 mutant were incubated in a 30 °C water bath for 25 minutes. The samples were transferred to ice and the reaction was stopped with 4 ml ice-cold transport buffer. After centrifugation at 300 g and 4 °C for 5 minutes, most of the supernatant was removed.

The efficiency of export was analyzed by measuring the fluorescence of GFP-NFAT in the nuclei by a FACSCanto™ II flow cytometer (BD Biosciences).

2.4.4 Detection of proteins by indirect immunofluorescence

For detection of endogenous or HA-tagged protein, cells were grown on coverslips in 24-well plates. The coverlids were washed with PBS and fixed with 4% formaldehyde in PBS containing 1 µg/ml Hoechst 33258 for 10 minutes at room temperature. After washing twice with PBS the coverslips were transferred to a dark humidity chamber and permeabilized with 0.5% Triton X-100 in PBS for 5 minutes. To reduce unspecific staining cells were afterwards blocked with 2% BSA in PBS for 10 minutes before incubation with the primary antibody diluted in 2% BSA in PBS for 1 hour. The coverslips were washed twice in PBS and once in 2% BSA in PBS and the secondary antibody was added for 1 hour. Unbound antibodies were removed by three washing steps with PBS. The coverslips were dried and mounted with mounting medium. A list of primary and secondary antibodies used for this work is found in section 2.1.9.

2.4.5 Quantification of GFP-SPN1 distribution

The effect of Nup214 or CRM mutants on nuclear export was analyzed by quantifying the distribution of overexpressed GFP-SPN1 [222]. The localization in 50-100 cells was divided into the three categories "N>C" (mainly nuclear), "N=C" (homogenous distribution throughout the cell) and "N<C" (mainly cytoplasmic). Results were presented as percent of the individual categories as a mean of at least three experiments as described previously [59].

2.5 Structural Biology Methods

2.5.1 Preparative purification of protein complexes

CRM1-SPN1-RanGTP or CRM1-SPN1-RanGTP-Nup214 complexes were prepared by mixing purified CRM1, RanQ69L-GTP, SPN1 and optionally a Nup214-fragment with at least 3 times molar excess of all components compared to CRM1 and incubation on ice for 1 hour. The assembled complex was further purified by gel filtration on a HiLoad 26/60 Superdex 200 prep grade column (GE Healthcare) in export complex buffer (20 mM Tris pH 7.4, 50 mM NaCl, 1 mM Mg(OAc)₂, 2 mM DTT). The fractions containing the purified complex were concentrated with 20 ml/50 kDa Concentrators (Corning) to a concentration of at least 3 mg/ml, flash frozen in liquid nitrogen and stored at -80 °C.

2.5.2 Cross-linking of protein complexes

The Nup214-Lys mutants were generated either with a PCR primer containing an additional codon for lysine or with site-directed mutagenesis yielding the plasmids pET28a-His-Nup214(K1916-2033)-His, pET28a-His-Nup214(1916-2033)A1995K-His and pET28a-His-Nup214(1916-2033)A1999K-His.

Pre-purified CRM1-SPN1-RanGTP-Nup214 complexes (see section 2.5.1) were changed into PBS (137 mM NaCl, 2.7 mM KCl, 10 mM Na₂HPO₄, 1.8 mM KH₂PO₄) with Zeba Desalting Spin columns (ThermoScientific) as the primary amines from the export complex buffer would hinder the function of all amine-reactive cross-linkers. Cross-linking of Nup214 complexes with BS³, BS²G and EGS was performed at 25 °C for 30 minutes.

A detailed description of the development of the different cross-linking strategies can be found in section 3.3.2.

2.5.3 Mass spectrometry

Cross-linked protein complexes either as a solution or on a Coomassie-stained SDS-PAGE were given to Romina Hofele (MPIIbpc, Göttingen) for further sample preparation and MS/MS analysis.

2.5.4 Electron microscopy

For electron microscopy experiments, only freshly prepared CRM1 was used. 500 pmol CRM1-SPN1-RanGTP-Nup214 complex were formed by incubating the individual purified proteins at a 1:1.2:1.5:2 molar ratio and an estimated complex concentration of ~1 mg/ml on ice for 1 hour. The complex was changed into EM buffer (20 mM HEPES pH 7.4, 50 mM NaCl, 1 mM Mg(OAc)₂, 1 mM DTT) with Zeba Desalting Spin columns (ThermoScientific).

Prepared complexes were given to David Haselbach (MPIIbpc, Göttingen) for further sample preparation and electron microscopy. GraFix was performed as described in [225], followed by negative stain- or cryo-electron microscopy.

2.5.5 Crystallography

The CRM1/SPN1(1-291)/RanQ69L(1-180)GTP/MBP-Nup214(1916-2033)-His complex was prepared as described in section 2.5.1 with a molar ratio of 1:3:5:5 and concentrated to 5 mg/ml. The Nup214 complex was crystallized in 24-well sitting drop crystallization plates by mixing 2 μ l of the protein solution with 1 μ l of the reservoir solution containing 5% (w/v) polyethylene glycol (PEG) 8000, 0.2 M L-proline, 0.1 M Tris/HCl pH 7.5, 4 mM D-maltose and 180 mM LiCl. Cross-seeding with older crystals of the same protein complex was used to control the number of crystals per well. Several seeds were added to the pre-incubated protein-reservoir mixture after 20 minutes. Crystals with dimensions of around 150 x 150 x 80 μ m grew at 20 °C after 5 days.

Crystals were optimized and analyzed and the model was built and refined by Thomas Monecke (Molecular Structural Biology, Universität Göttingen).

All crystals belonged to the orthorhombic space group C2221 and diffracted X-rays to a maximum resolution of 7 Å. In order to improve the diffraction quality, crystals were successively dehydrated by transferring to conditions with increasing PEG 8000 concentrations. The PEG 8000 concentration was increased from 5% to 45% in 5% steps with 15 minutes of incubation in between. Crystal dehydration resulted in a significant reduction of the unit cell lengths by ~10% for each axis (e.g. a-axis from 126 Å to 112 Å (13%), b-axis from 263 Å to 248 Å (6%) and c-axis from 229 Å to 210 Å (8%)) thereby decreasing the crystal solvent content from 69% to 59%. Dehydrated crystals were fished on micro meshes (MiTeGen) and mounted on beamline 14.3 (BESSY II, Berlin) equipped with an HC1c crystal humidifier [226]. Residual mother liquor was completely removed from the crystals using a paper wick. The crystals were flash frozen in liquid nitrogen and transferred to beamline 14.1 equipped with a 6M Pilatus detector for data collection (BESSY II, Berlin) [226]. Complete diffraction datasets of two treated crystals were collected. Data were processed using XDS and XSCALE [227].

Molecular replacement with PHASER [228] was used to solve the structure using the CRM1-RanGTP-SPN1 export complex (PDB ID: 3GJX) [127] as a starting model. Localization of the MBP (PDB ID: 1ANF) [229] by molecular replacement routines of PHASER did not provide an unambiguous solution and was therefore fitted manually into positive |Fo-Fc| difference electron density. After replacement and initial rigid body refinement, positive |Fo-Fc| difference electron density compared to the CRM1-RanGTP-SPN1 export complex structure (PDB ID: 3GJX) allowed for building of three regions of the Nup214 fragment. The structure refinement was done by iterative cycles of CNS [230] and manual model building in Coot [231].

Figures were generated with PyMOL.

3 Results

3.1 Development of a bead-based flow cytometry assay for protein-protein interactions (Halo assay)

A bead-based microscopy assay was previously described to analyze the interactions of different nucleoporins with each other [232]. In that assay, GST-nucleoporins were immobilized on beads and incubated with soluble CFP-fusions of other nucleoporins to test for interactions. The interaction was assessed with a microscope and a fluorescent halo could be observed around the dark beads in case the two nucleoporins interacted with each other [232].

Another study described a flow cytometry protein interaction assay (FCPIA), which used immobilized protein on polystyrene beads to detect interaction with a fluorescently labeled binding partner by flow cytometry [233]. FCPIA was used to calculate protein-protein interaction affinities and to perform competition experiments with unlabeled binding partners or small molecules [233].

In this work, both previously described assays were combined and developed into a stable, semi-quantitative assay to analyze the interaction of Cy3-labeled CRM1 with a variety of cargoes and Nup214 fragments.

When analyzing binding of Cy3-labeled CRM1 to immobilized Nup214 fragments by fluorescence microscopy, fluorescent halos appeared around the beads, similar as observed in [232], which led to the naming of the assay (appendix, figure S1).

3.1.1 Optimization of assay conditions

Optimization of the assay conditions included the composition of the buffer and additives as well as the amounts and ratios of the proteins. The two buffers commonly used for CRM1 *in vitro* binding assays are the Tris-based pulldown buffer and the HEPES-based transport buffer. In a first step, the two buffers were compared and their effect on the fluorescence signal was analyzed. Equal amounts of GST-RanGDP or GST-RanGTP were immobilized on beads and incubated with a constant amount of CRM1-Cy3 in the absence or presence of SPN1 and a Nup214 fragment. The fluorescence intensities measured in transport buffer were consistently higher than the intensities measured in Tris buffer (figure 9). This held true for samples with RanGDP or RanGTP and in the presence or absence of any other protein. Transport buffer was therefore used in all further experiments, as it showed consistently higher fluorescence intensities without increasing unspecific background binding.

Next, additives to the assay buffer were optimized. The described microscope assay used a 4x assay buffer containing 40 mM EDTA, 500 mM NaCl, 40 mg/ml BSA and 2% 1,6-hexanediol [232]. As EDTA is used to remove bound nucleotides from Ran, the effect of an assay buffer with and without EDTA was tested. A Nup214 fragment was immobilized and incubated with two different amounts of CRM1-Cy3 and NES peptides and increasing amounts of RanGTP with either the described buffer or the same buffer without EDTA (data not shown). No major difference between the two buffers was observed. Therefore EDTA was not used in future

experiments.

1,6-hexanediol was described as a reagent to minimize unspecific hydrophobic protein-protein interactions [232]. Its effect on the assay was tested by adding 2%, 5% or 10% 1,6-hexanediol to the 4x Halo mix (500 mM NaCl, 40 mg/ml BSA, 1 mM DTT) and probing the interaction of immobilized GST-SPN1 with a constant amount of CRM1-Cy3 in the absence or presence of RanGTP. No consistent effect could be observed (data not shown). 2% 1,6-hexanediol was anyway included in the assay buffer in accordance with the literature [232].

The optimized 4x Halo mix (500 mM NaCl, 40 mg/ml BSA, 1 mM DTT, 2% 1,6-hexanediol) was used for all subsequent experiments, leading to a total buffer concentration of 20 mM HEPES pH 7.3, 110 mM KOAc, 2 mM Mg(OAc)₂, 125 mM NaCl, 1 mM EGTA, 10 mg/ml BSA, 0.5% 1,6-hexanediol and 1.25 mM DTT in the samples.

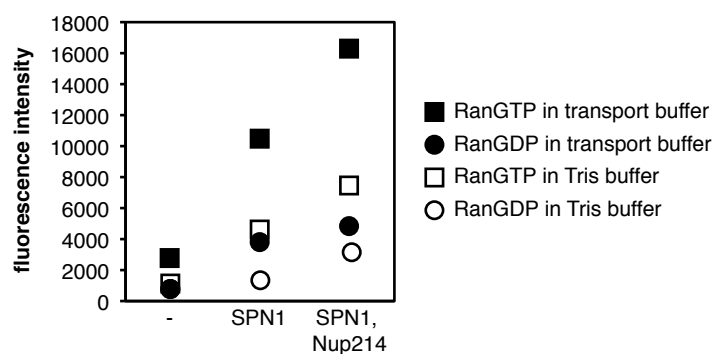


Figure 9: Transport buffer gave higher fluorescence signals in the bead-based flow cytometry assay. About 470 pmol of GST-RanGTP or GST-RanGDP were immobilized on 2.5 μ l glutathione sepharose. CRM1-Cy3 alone or with SPN1 or SPN1 and a Nup214(1916-2033) fragment were added to the beads. CRM1-binding was analyzed by flow cytometry. The absolute fluorescence intensities were plotted.

3.1.2 Biochemical verification of the novel CRM1-binding assay

In addition to the optimization of the assay conditions, the biochemical specificity of the assay had to be verified. First, it was tested if a saturation of CRM1-binding to immobilized GST-SPN1 could be reached. Increasing amounts from 2.5 pmol to 60 pmol CRM1-Cy3 were titrated to 50 pmol of immobilized GST-SPN1 in the presence of RanGTP. The detected fluorescence intensities increased with increasing CRM1-Cy3 amounts and a plateau was reached when SPN1 and CRM1-Cy3 were present at nearly equimolar levels, indicating specificity of the binding (figure 10A).

Next, the specificity of the binding was investigated by pre-incubating CRM1 with its inhibitor LMB to allow covalent modification of Cys528 and titrating increasing amounts of LMB-treated or mock-treated CRM1-Cy3 to immobilized GST-SPN1 in the presence of an excess of RanGTP. The samples with LMB-treated CRM1-Cy3 showed a decrease of more than 80% in fluorescence intensities for all CRM1 amounts tested (figure 10B).

The binding of Cy3-labeled CRM1 was compared to the binding of unlabeled CRM1 by titrating increasing amounts of unlabeled CRM1 to immobilized GST-cargoes, namely SPN1 and HIV-1 Rev, in the presence of a constant amount of CRM1-Cy3. Increasing amounts of unlabeled CRM1 lead to a decrease in fluorescence intensity, suggesting that the Cy3-labeling does not have major effect on the binding properties of CRM1. The relative decrease varied between SPN1 and Rev, indicating different on- and off-rates in the binding of CRM1 (figure 10C).

In the cellular context, the CRM1-RanGTP-cargo complex dissociates in the cytoplasm after translocation through the NPC upon hydrolysis of RanGTP. GTP-hydrolysis is mediated by RanBP1 and RanGAP. Therefore, it was tested if the binding of CRM1-Cy3-RanGTP-cargo complex was sensitive to the presence of RanBP1 and RanGAP. GST-SPN1 and GST-Rev were immobilized and CRM1-Cy3 and RanGTP were added. After incubation for 1 hour, RanGAP was added to the samples with RanBP1 and fluorescence intensities were compared to samples without RanBP1 and RanGAP. Addition of RanGTP increased the fluorescence intensity for by a factor of 2 for SPN1 and more than 20 for Rev. RanBP1 and RanGAP reduced the fluorescence intensities for both cargoes tested (figure 10D).

Taken together, CRM1-Cy3 binding in the assay can be saturated, blocked by LMB, competed with unlabeled CRM1 and reduced by the addition of RanGAP and RanBP1. The interactions of CRM1-Cy3 in the assay therefore seem specific and in accordance with known CRM1 properties.

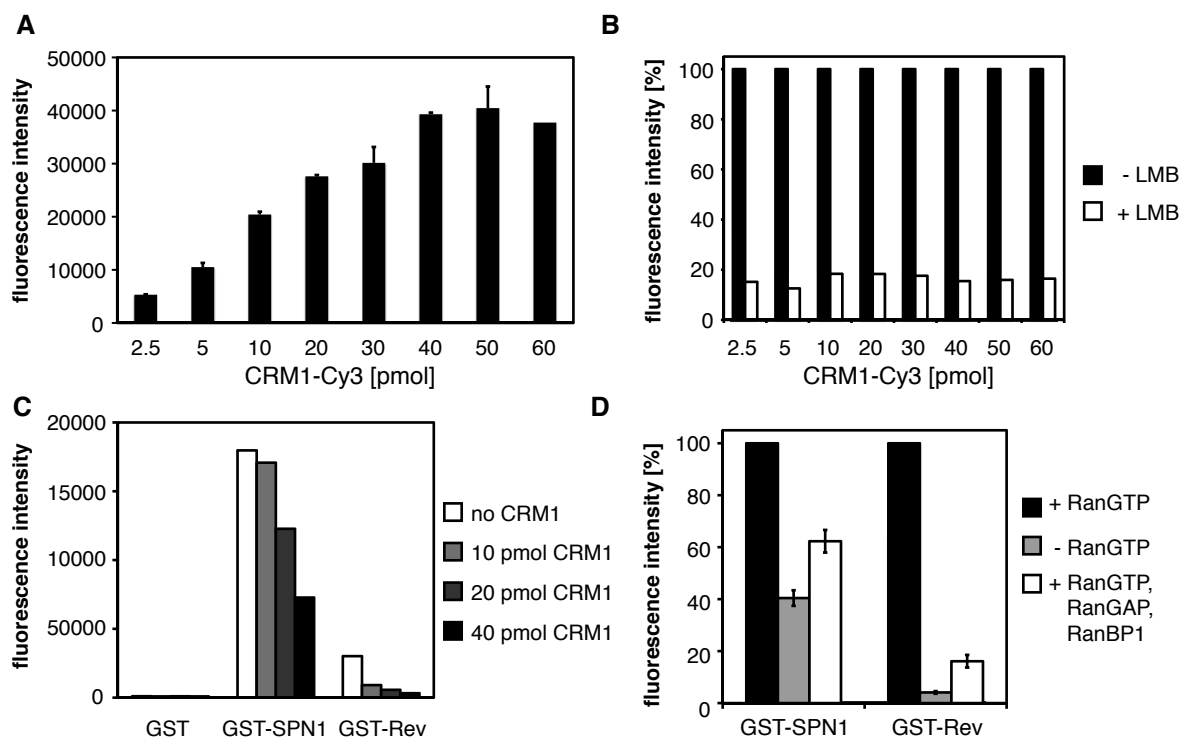


Figure 10: Controls verified the specificity of the Halo assay. (A-B) Increasing amounts of CRM1-Cy3 were titrated to 50 pmol immobilized GST-SPN1 in the presence of an excess amount of RanGTP. (A) The mean and standard deviation of duplicates were plotted. (B) CRM1-Cy3 was incubated with a 5x molar excess of LMB or ethanol as a solvent control at room temperature for 2.5 hours. Fluorescence intensities were normalized to the values of CRM1-Cy3 pre-incubated with ethanol as 100%. (C) 50 pmol GST or a GST-tagged cargo were immobilized on 2.5 μ l beads and incubated with 10 pmol of CRM1-Cy3 and an increasing amount of unlabeled CRM1 in the presence of RanGTP. Fluorescence intensities were normalized to the value of the sample without any competing unlabeled CRM1 as 100%. (D) 50 pmol of GST-tagged cargo was immobilized on 2.5 μ l beads and incubated with a constant amount of CRM1-Cy3 alone, in the presence of RanGTP or RanGTP and RanBP1. After 1 hour, RanGAP was added to the condition with RanBP1 and the samples were incubated for another 30 minutes. Fluorescence intensities were normalized to the value of the sample with RanGTP as 100%. The mean and standard deviation of two independent experiments were plotted.

3.1.3 Comparison of CRM1-binding to different Nup214 fragments reveals a detection range of 3 orders of magnitude

The newly developed assay was applied to quantify the binding of CRM1 to Nup214 fragments of different lengths. Several GST-Nup214 fragments were immobilized and incubated with CRM1-Cy3 in the absence or presence of RanGTP and CRM1-Cy3 binding was quantified by flow cytometry (figure 11). The observed fluorescence intensities increased with the size of the Nup214 fragments and were reduced when comparing fragments with mutated FG-repeats to non-mutated fragments of the same length.

The potency of the assay lies in the analysis of protein-protein interactions of very different strengths. Binding of CRM1-Cy3 to the different Nup214 fragments yields fluorescence intensities from ~90 to ~90000, therefore covering a range of 3 orders of magnitude, which is a lot more than with a conventional gel-based pulldown assay. The developed assay therefore allows the comparison of CRM1-binding to a variety of different Nup214 fragments.

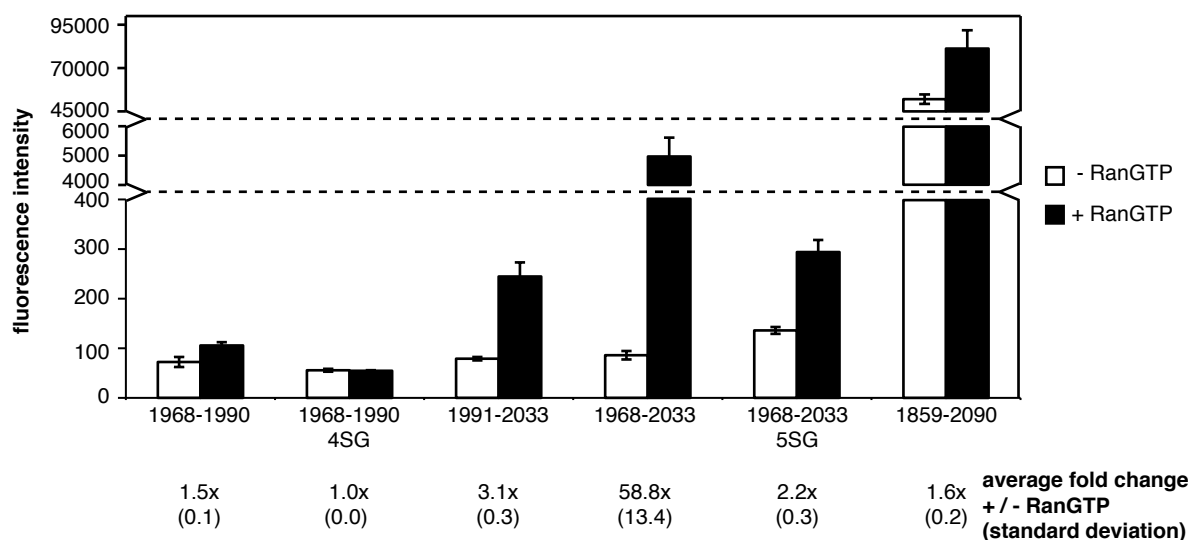


Figure 11: Comparison of CRM1 binding to different Nup214-fragments. 50 pmol of GST-tagged Nup214 fragments were immobilized on 2.5 μ l beads and incubated with a constant amount of CRM1-Cy3 and excess of an NES peptide in the presence or absence of RanGTP. The average fluorescence intensities and standard deviations of three independent experiments were plotted.

An increase of CRM1-binding upon addition of RanGTP was detected for all Nup214 fragments, except one, indicating a specific binding. Interestingly, the ratio of CRM1-binding in the presence of RanGTP compared to the absence of RanGTP varied for the different fragments. It was between a 1.5 and 3.0 fold change for very short as well as very long Nup214 fragments. Only a medium sized fragment containing the Nup214 residues 1968-2033 showed a ~60 fold increase of binding upon addition of RanGTP. The only fragment not showing an increase in fluorescence upon RanGTP addition was Nup214(1968-1990)4SG, which was expected as this fragment does not contain any FG-repeats. The fluorescence intensity of this fragment is the same as for GST (data not shown), indicating that the detected fluorescence results from non-specific background binding.

3.1.4 Application of the Halo assay to analyze CRM1-cargo interactions

As an application for the developed Halo assay, CRM1-binding to several of its cargoes was compared. Cytosolic carboxypeptidase 1 (CCP1) and programmed cell death protein 2-like protein (PDCD2L) were recently identified as novel CRM1 cargoes [217].

GST-fusions of SPN1 and a fragment of CCP1(1-120) were immobilized on glutathione sepharose and incubated with CRM1-Cy3 in the absence and presence of RanGTP (figure 12A). The increased binding of CRM1 to both of the cargoes in the presence of RanGTP reflects the specificity of the export complex formation. The detected fluorescence intensities indicate that the binding of CRM1 to SPN1 is very strong compared to the binding to the CCP1(1-120) fragment.

Binding of CRM1 to its cargo PDCD2L and a PDCD2L version with a mutated NES was compared (see figure 12B). GST, GST-PDCD2L and the GST-PDCD2L mutant were immobilized and incubated with CRM1-Cy3 alone, in the presence of RanGTP or RanGTP and a Nup214(1916-2033) fragment. The presence of RanGTP increased CRM1 binding to PDCD2L, but not the PDCD2L mutant, indicating that the mutated NES prevents specific interaction of PDCD2L with CRM1. Accordingly, the additional incubation with Nup214 lead to a massive increase of CRM1 binding to PDCD2L, but did not have an effect on CRM1-binding to the PDCD2L mutant.

To sum up, the Halo assay is a bead-based flow cytometry assay that is well suited for semi-quantitative analysis of CRM1-binding to nucleoporins and its cargoes. The application range of the assay could also be extended by labeling other proteins, for example import receptors.

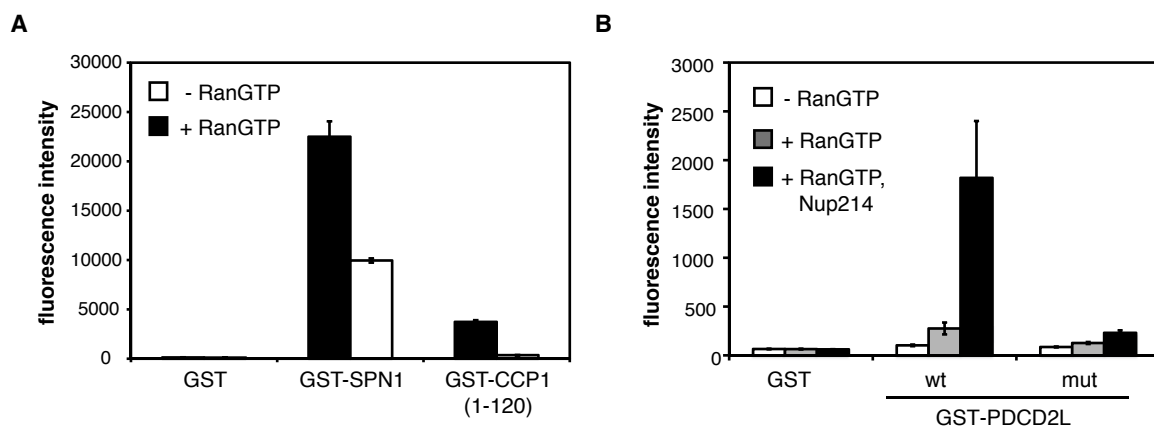


Figure 12: Analysis of CRM1-cargo interactions. (A) GST, GST-SPN1 and GST-CCP1(1-120) were immobilized on glutathione sepharose and incubated with CRM1-Cy3 in the absence or presence of RanGTP. Absolute fluorescence intensities and standard deviations of three experiments were plotted. The figure is modified from [217]. (B) GST, GST-PDCD2L and a GST-PDCD2L mutant with inactivated NES were immobilized on glutathione sepharose and incubated with CRM1-Cy3 alone or in the presence of RanGTP, with or without a Nup214(1916-2033) fragment. Absolute fluorescence intensities and standard deviations of 6 independent experiments were plotted.

3.2 Biochemical characterization of CRM1-Nup214 binding

3.2.1 CRM1 is the karyopherin with the highest avidity for Nup214

All current models of nuclear transport rely on an interaction of karyopherins with FG-nucleoporins to facilitate translocation through the nuclear pore complex. The C-terminal fragment of Nup214 (residues 1859-2090) contains a large number of FG-repeats and was previously shown to interact with CRM1 in a RanGTP-dependent manner [54, 58]. It was therefore investigated if this fragment could also interact with other nuclear transport receptors. The Nup214 C-terminus was immobilized on beads and incubated with a variety of nuclear transport receptors in the absence and presence of RanQ69L-GTP (figure 13). In addition to the export receptor CRM1, the import receptors importin α and importin β , individually or in combination, importin 5 and transportin were tested, as well as the bi-directional transport receptor importin 13. An interaction of Nup214 with CRM1 in the presence of RanQ69L-GTP could be observed, which could be further increased by addition of an NES peptide. None of the other receptors bound to the C-terminal Nup214 fragment. The specificity of Nup214-binding to CRM1 emphasizes the importance of Nup214 in the export of some CRM1-dependent cargoes [60]. The high avidity of the interaction is in accordance with observations that CRM1-export complexes get stalled in hydrogels derived from the Nup214 C-terminus, but not in hydrogels derived from other FG-Nups [234].

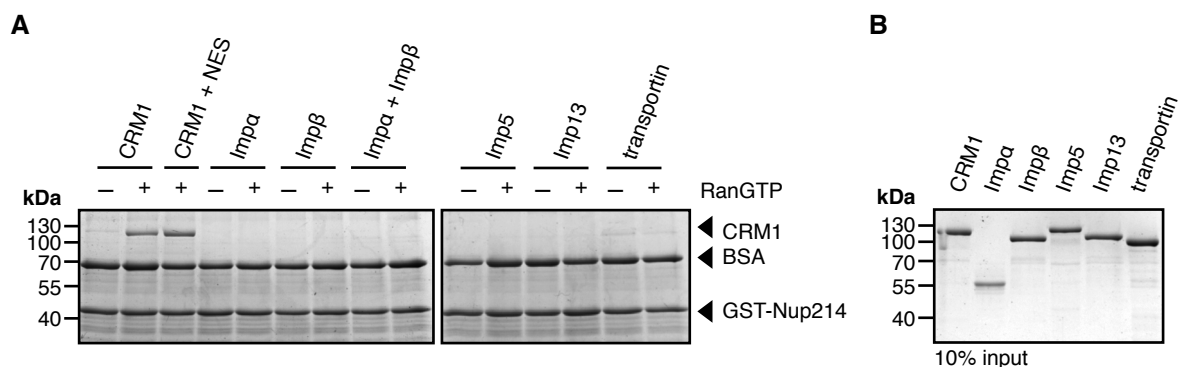


Figure 13: CRM1 is the karyopherin with the highest avidity for Nup214. 50 pmol GST-Nup214(1859-2090) were immobilized on glutathione beads and incubated with 50 pmol of the respective transport receptors in the absence or presence of 150 pmol RanQ69L-GTP and, for CRM1, an NES peptide. (A) Bound proteins were analyzed by SDS-PAGE, followed by Coomassie-staining. (B) shows 10% input samples of the transport receptors used in the assay.

3.2.2 Nup214 promotes the formation of CRM1 export complexes in a RanGTP-dependent manner

Nup214 was previously shown to have a stabilizing effect on CRM1 export complexes [60]. The relative effect of stabilization by Nup214 was further assessed with *in vitro* binding assays (figure 14). Immobilized GST-SPN1 or GST-Rev was incubated with CRM1 alone or in combination with RanGTP or a Nup214(1916-2033) fragment. No binding between CRM1 and any of the cargoes was observed in the absence of RanGTP in a pulldown assay (figure 14A). A clear binding of CRM1 to SPN1 was observed in the presence of RanGTP which was even stronger upon addition of the Nup214 fragment. For Rev, no increase in binding was observed

when incubated with only CRM1 and RanGTP. CRM1 binding to Rev could only be observed in the presence of the Nup214 fragment. Probing the same interactions with the Halo assay gave a more differentiated result (figure 14B). A specific interaction of SPN1 and CRM1 was observed even in the absence of RanGTP. This is in line with the fact that a CRM1-SPN1 complex was stable enough to crystallize [174]. Addition of RanGTP increased the binding of CRM1 to SPN1 by a factor of around 2 and addition Nup214 fragment increased the binding even further by a factor of around 1.5. The interaction of CRM1 with Rev is influenced the same way, but the extent of the effect of RanGTP and Nup214 differ a lot compared to SPN1. The interaction of CRM1 with Rev was only minimal in the absence of RanGTP. Addition of RanGTP led to a roughly 6-fold increase in CRM1 binding, which is increased even further by a factor of nearly 7 upon addition of the Nup214 fragment.

The relative effect of the stabilization by Nup214 observed in the assays is in accordance with the importance of Nup214 for the export of certain cargoes *in vivo*. The export of Rev by CRM1 is abolished in Nup214-knockdown cells [60] whereas Nup214-knockdown does not influence the cellular localization of SPN1 (data not shown).

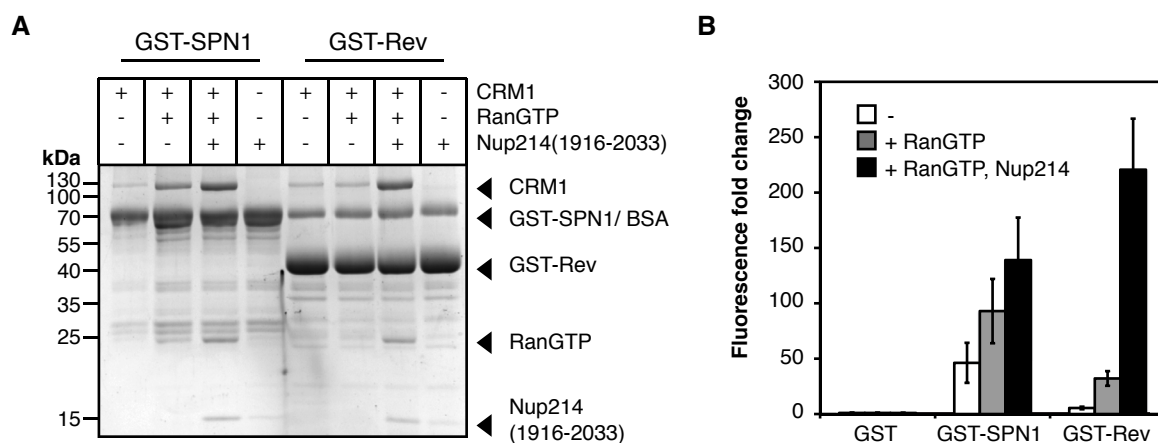


Figure 14: The relative effect of Nup214 varies with different cargoes. (A) 500 pmol of GST or GST-fusion protein was immobilized on glutathione beads and incubated with 250 pmol CRM1, RanGTP, Nup214(1916-2033) alone or with combinations thereof. Bound proteins were eluted with SDS sample buffer and analyzed by SDS-PAGE, followed by Coomassie-staining. (B) 50 pmol of GST or GST-fusion protein was immobilized on glutathione beads and incubated with 8.6 pmol CRM1-Cy3 and an excess of RanGTP or Nup214(1916-2033) alone or with combinations thereof. The bound fluorescence was analyzed by flow cytometry. Results were normalized against the sample with immobilized GST incubated with CRM1-Cy3, RanGTP and Nup214. The fold change of five independent experiments was plotted. Error bars indicate the standard deviation.

The stabilizing effect of Nup214 on export complexes was quantitatively assessed with RanGAP assays. CRM1 was incubated with Ran loaded with ^{32}P - γ -GTP and increasing amounts of SPN1 or an NES peptide in the absence or presence of a Nup214 fragment. GTP-hydrolysis was induced by addition of RanGAP. Hydrolysis of RanGTP by RanGAP releases radioactively labeled phosphate, which is analyzed by a scintillation counter. The more stable the complex, the less radioactively labeled phosphate gets released as RanGTP in a complex with CRM1 is resistant towards RanGAP-induced GTP-hydrolysis. The titration of a cargo, either SPN1 or an NES peptide in a RanGAP assay in the absence or presence of a Nup214 fragment confirms

that the tetrameric CRM1-RanGTP-cargo-Nup214 complex is clearly more resistant towards RanGAP-induced GTP-hydrolysis than the export complex alone (figure 15).

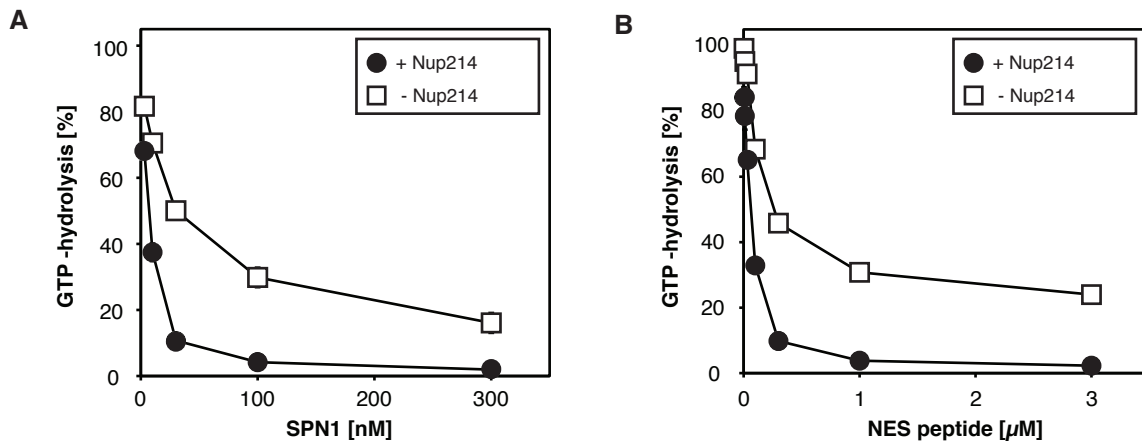


Figure 15: Nup214 increases stability of CRM1 export complexes towards RanGAP-induced GTP-hydrolysis. (A) SPN1 or (B) an NES peptide were titrated to CRM1 and Ran loaded with ^{32}P - γ -GTP in the absence or presence of 300 nM Nup214(1916-2033). GTP-hydrolysis was initiated by RanGAP. Counts were normalized to a sample without RanGAP and plotted as % GTP-hydrolysis. The mean of three independent experiments is shown. Error bars indicating the standard deviation are too small to be seen.

The interaction of CRM1 with its cargoes depends on the presence of RanGTP, as only the structural changes of CRM1 that follow upon binding of RanGTP open up the NES binding cleft on CRM1 and allow for cargo recognition. As it was established that Nup214 stabilizes CRM1 export complexes, it was investigated if the interaction of CRM1 and its cargoes could be stabilized by only Nup214 or if it was still dependent on RanGTP. Purified CRM1 was incubated with either SPN1 or an NES peptide, a Nup214 fragment and Ran loaded with GTP or GDP and complex formation was assessed by gel filtration (figure 16). No complex with Nup214 was formed in the presence of RanGDP, whereas RanGTP lead to the formation of Nup214-export complex for SPN1 as well as for the NES peptide. Therefore, Nup214 alone, at least the tested Nup214(1916-2033) fragment, is not able to promote CRM1-cargo interaction in the absence of RanGTP. It only stabilizes the already formed CRM1-RanGTP-cargo complexes.

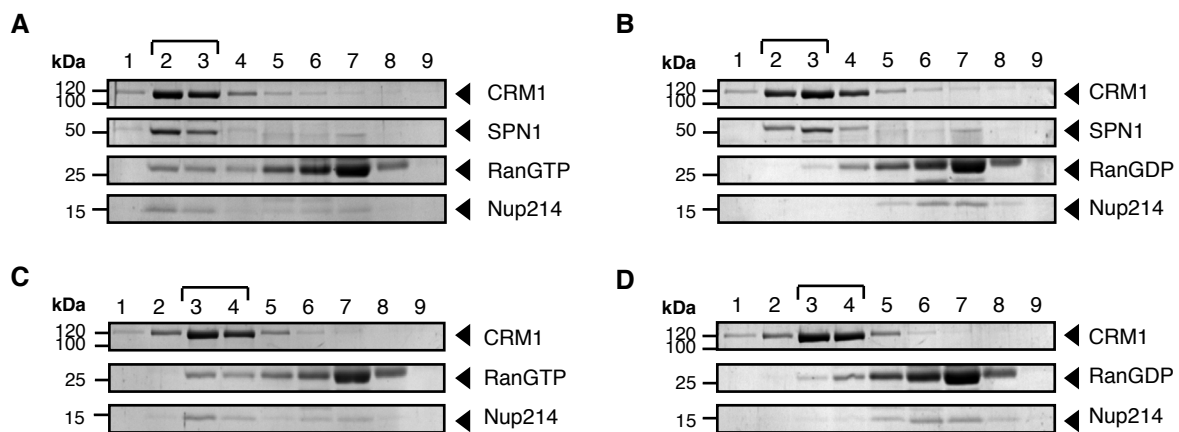


Figure 16: Nup214 binds to export complexes in the presence of RanGTP. 1.16 nmol of CRM1 and RanGTP or GDP were mixed with either an equimolar amount of SPN1 (A, B) or a 3-fold excess of the NES peptide (C, D) and incubated at 4 °C for 30 minutes. An equimolar amount of the Nup214(1916-2033) fragment was added and the complex was incubated at 4 °C for another 30 minutes before analysis on an analytical S200 gel filtration column in export complex buffer. 1ml fractions were collected and analyzed by SDS-PAGE, followed by Coomassie-staining. Arrows indicate the bands for the respective proteins. Brackets indicate the fractions in which a formed complex is expected.

3.2.3 Binding of Nup214 fragments to the export complex is independent of their stabilization effect in RanGAP assays

The binding of a large variety of Nup214 fragments to CRM1 export complexes was tested in this work. Most of the fragments were built around a conserved motif of FG-repeats between residues 1968 and 1996 [59]. The standard Nup214 fragment used for most of the assays and also for our structural analysis (see below) contained the residues from 1916-2033. Based on this standard fragment, several shorter constructs were generated to narrow down the binding sites and improve purification efficiency (appendix figure S9). An N- and C-terminal truncated fragment ranging from residues 1930 to 2021 showed similar purification efficiency as the standard fragment. Also the formation of a CRM1-RanGTP-SPN1-Nup214 complex worked with the same efficiency (figure 17).

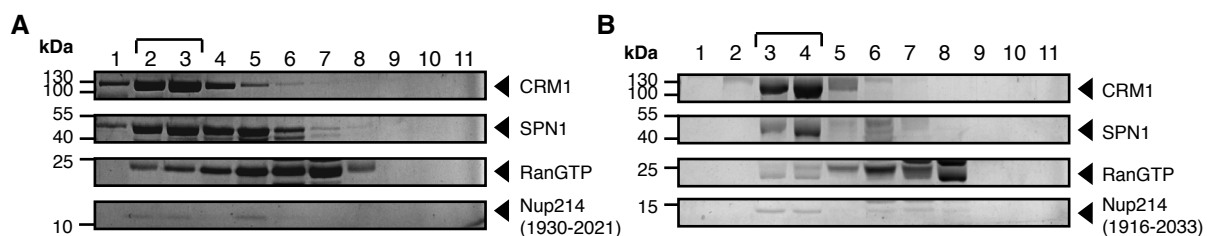


Figure 17: The Nup214-fragments 1930-2021 and 1916-2033 both bind stably to the export complex. 2.5 nmol of CRM1 were incubated with excess amounts of SPN1, RanQ69L-GTP and His-tagged (A) Nup214(1930-2021) or (B) Nup214(1916-2033) at 4 °C for 30 minutes. Complex formation was assessed by analytical gel filtration with a S200 column in export complex buffer. 1ml fractions were collected and analyzed by SDS-PAGE, followed by Coomassie-staining. Arrows indicate the bands for the respective proteins. Brackets indicate the fractions in which a formed complex is expected.

The comparison of the Nup214(1916-2033) fragment with the slightly truncated Nup214(1930-2021) fragment in RanGAP assays revealed unexpected differences in the ability of the Nup214 fragments to stabilize the CRM1-RanGTP complex towards RanGAP-induced GTP-hydrolysis. The addition of 300 nM of an MBP-tagged Nup214(1916-2033) standard fragment lead to a reduction of GTP-hydrolysis to 40%, whereas the MBP-tagged Nup214(1930-2021) did not show any stabilizing effect (figure 18A). This is remarkable, as Nup214(1930-2021) was able to form a stable tetrameric export complex (figure 17). Based on these results, several other constructs were designed (figure 18F). Fragments containing only the N- or the C-terminal truncation compared to the standard fragment, namely Nup214(1930-2033) and Nup214(1916-2021) showed increased GTP-hydrolysis with 300 nM of the Nup214(1930-2033) and Nup214(1916-2021) leading to around 60% and 80% GTP-hydrolysis, respectively (figure 18A). Comparing the same MBP-tagged Nup214 fragments in a pulldown assay revealed that the different ability of the Nup214 fragments to stabilize the complex in the RanGAP assay is only partially reflected by their ability to bind the CRM1 export complex. Incubating the fragments with immobilized GST-Rev and CRM1 in the absence or presence of RanQ69L-GTP revealed that all of the tested Nup214 fragments bind to the CRM1-RanGTP-Rev export complex in a RanGTP-dependent manner (figure 18B). The different stabilization effects from the RanGAP assay are partially reflected by decreased binding efficiencies of the Nup214 and CRM1 in the individual samples. The presence of residues 1916-1929 and 2022-2033 therefore has an obvious effect on the stability of the complex. Hence, it was investigated if these short peptides alone were able to bind and stabilize the complex. SPN1 was titrated in the presence of either GST or a GST-Nup214 fragment in a RanGAP assay (figure 18C). None of the short peptides showed any stabilizing effect compared to GST whereas the longer Nup214(1968-2033) fragment totally inhibited GTP-hydrolysis. This was confirmed by a pulldown assay in which the same constructs were immobilized on glutathione beads and incubated with pre-purified CRM1-RanGTP-SPN1 export complex. GST-Nup214(1968-2033) showed a clear binding of CRM1 and SPN1 whereas no CRM1-binding could be observed for immobilized GST-Nup214(1916-1929) and GST-Nup214(2022-2033) (figure 18D). Probing the different GST-Nup214 in a halo assay with CRM1-Cy3 and NES peptide in absence and presence of RanGTP confirmed the results from the previous pulldown assay (figure 18E).

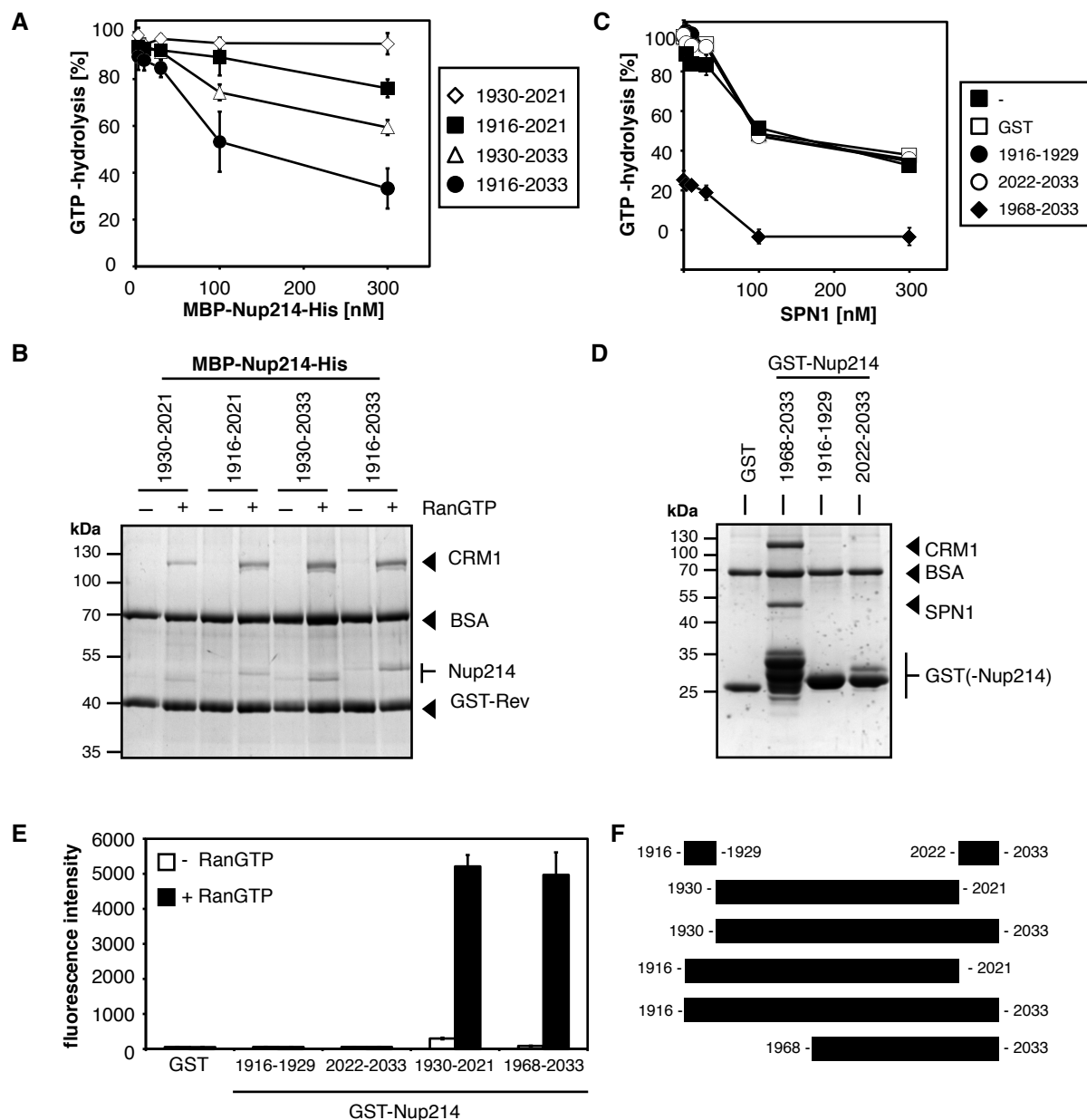


Figure 18: Binding of Nup214 fragments to CRM1 export complexes. (A) RanGAP assay: MBP-tagged Nup214 fragments were titrated to CRM1 and Ran loaded with ^{32}P - γ -GTP in the absence of cargo. GTP-hydrolysis was initiated by addition of RanGAP. Counts were normalized to a sample without RanGAP and plotted as % GTP-hydrolysis. The mean and standard deviation of three independent experiments are shown. (B) 50 pmol GST or GST-Rev were immobilized on beads and incubated with CRM1 and MBP-Nup214-His fragments in the absence or presence of RanGTP. Bound proteins were analyzed by SDS-PAGE, followed by Coomassie-staining. (C) RanGAP assay: SPN1 is titrated to CRM1 and ^{32}P - γ -GTP in the absence and presence of 2.5 μM GST or GST-Nup214 fragments as in (A). (D) 500 pmol GST or GST-Nup214 fragments were immobilized on beads and incubated with pre-purified CRM1-RanGTP-SPN1 export complex. Bound proteins were analyzed by SDS-PAGE, followed by Coomassie-staining. (E) 50 pmol GST- of GST-Nup214 fragments were immobilized on beads and incubated with CRM1-Cy3 and an NES peptide in absence or presence of RanGTP. Bound CRM1 was detected by flow cytometry. Average fluorescence intensities and standard deviations of three independent experiments were plotted. (F) Scheme of the Nup214 fragments used in the above assays.

The previous results showed that the binding of short Nup214 fragments to the export complex is independent of their stabilization effect in RanGAP assays. Therefore it was tested if longer Nup214 fragments would stabilize the CRM1-RanGTP-cargo export complex more effectively. GST-Nup214(1968-2033) and GST-Nup214(1859-2090) were immobilized on glutathione beads and incubated with either CRM1 alone or in combination with RanGTP, with or without an NES peptide. Whereas Nup214(1968-2033) could only form a complex with CRM1 in the presence of the NES cargo, Nup214(1859-2090) could also form a trimeric CRM1-RanGTP-Nup214 complex without cargo (figure 19A).

The obvious differences between the Nup214 fragments could be confirmed with a previously described *in vivo* interaction assay [59]. Nup214 fragments fused to RFP-cNLS were co-transfected with GFP-SPN1. The cNLS targeted the expressed Nup214 fragment to the nucleus. In case the transfected Nup214 fragment did not interact with CRM1, GFP-SPN1 was exported normally by CRM1 and localized exclusively to the cytoplasm. An interaction of the Nup214 fragment with CRM1 would trap CRM1 to the nucleus. Therefore, CRM1 would not be available for nuclear export and GFP-SPN1 would accumulate in the nucleus. The Nup214 fragments 1968-2033, 1916-2033 and 1859-2090 were compared for their effect on GFP-SPN1 localization (figure 19B). All three fragments had previously exhibited efficient binding to the export complex as well as export complex stabilization. Nup214(1968-2033) only exhibited minor effects when co-transfected with GFP-SPN1, shifting its localization in ~30% of the cells from an exclusively cytoplasmic to an equally distributed localization. The effect of Nup214(1916-2033) was more apparent. Nearly 80% of the cells showed a predominant nuclear GFP-SPN1 localization, in ~20% of the cells the GFP-SPN1 was distributed equally. Nup214(1859-2090) showed the most dramatic effect, as it apparently trapped all CRM1 in the nucleus thereby completely abolishing GFP-SPN1 export.

The observed effects on the stabilization of the export complex of the different Nup214 fragments therefore correlates in both *in vitro* and *in vivo* experiments.

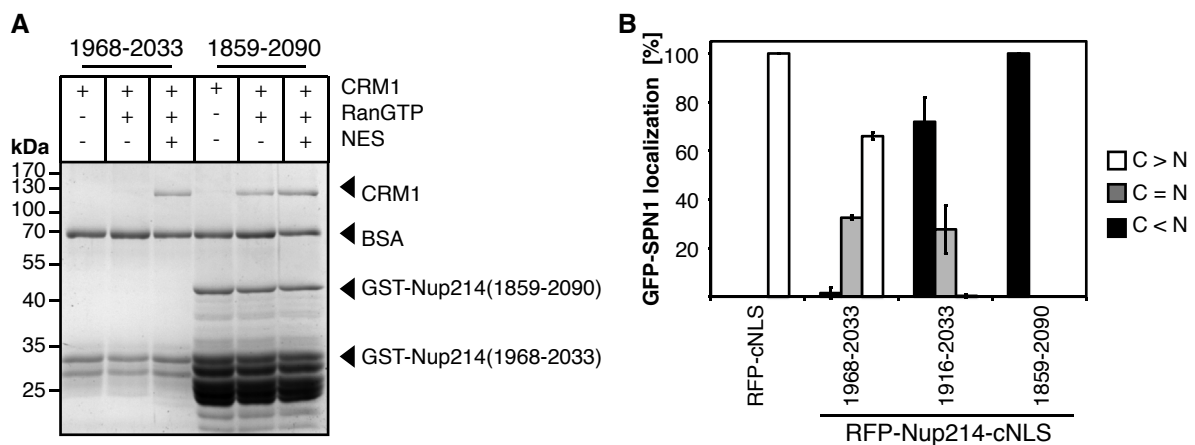


Figure 19: *In vivo* and *in vitro* binding assays indicate that the length of the Nup214 fragment influences the stability of CRM1-binding. (A) 50 pmol GST-Nup214(1968-2033) or GST-Nup214(1859-2090) was immobilized on beads and incubated with CRM1 in the absence or presence of RanGTP and NES peptide. Bound proteins were analyzed by SDS-PAGE, followed by Coomassie-staining. (B) Nup214 fragments 1968-2033, 1916-2033 and 1859-2090 fused to RFP-cNLS or the empty RFP-cNLS vector were co-transfected with GFP-SPN1 in HeLa P4 cells. Cells were analyzed by fluorescence microscopy after 24 hours. The localization of GFP-SPN1 in 100 cells was quantified for predominant cytoplasmic (C > N), equally distributed (C = N) and predominant nuclear (C < N) localization. Cells were transfected and localization was counted by Christiane Spillner. The mean and standard deviation of three independent experiments were plotted.

3.2.4 The Ran C-terminus destabilizes the CRM1-RanGTP-Nup214 complex

It was previously shown that the Ran C-terminus influences the stability of CRM1 export complexes by mediating its binding to RanBP1 [216, 235, 236]. An acid patch with the amino acid sequence DEDDDL at the Ran C-terminus was important for the binding of RanGTP to RanBP1, as its truncation abolished binding to RanBP1 completely [235, 236]. A Ran mutant named RanC4A in which 4 of these 5 acidic residues were mutated to alanine, yielding the sequence AAADAL, reduced the binding affinity to RanBP1 by a factor of around 20 [216].

The effect of wildtype Ran on CRM1-Nup214 complex stability was compared to RanC4A and truncated Ran(1-180). CRM1 and His-tagged Nup214(1916-2033) were incubated with the respective Ran species loaded with GTP in the absence or presence of SPN1. All three Ran species were able to form a tetrameric CRM1-Ran-SPN1-Nup214 complex (figure 20A,C,E). Interestingly, wildtype Ran was not able to complex with CRM1 in the absence of SPN1 (figure 20B), whereas a trimeric CRM1-Ran-Nup214 complex could be observed with RanC4A and Ran(1-180) (figure 20D,F) indicating a destabilizing effect of the Ran C-terminus on the Nup214 complex.

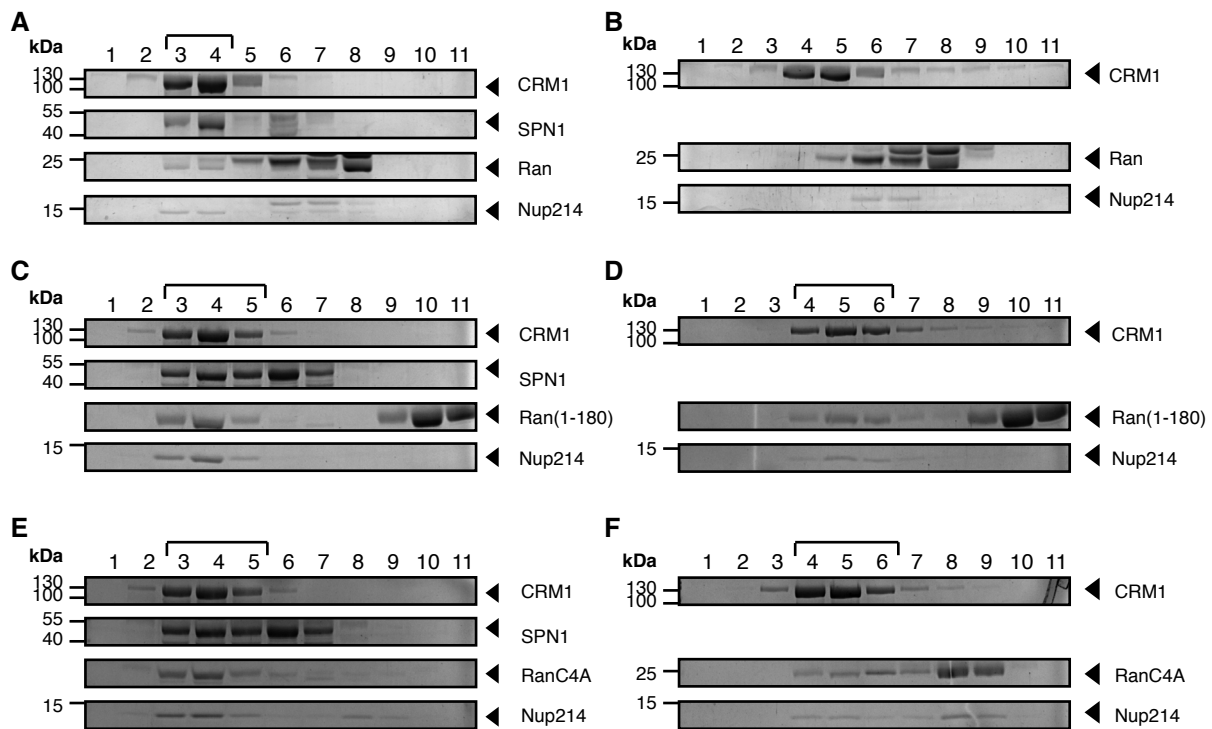


Figure 20: The C-terminus of Ran influences the stability of the CRM1-RanGTP-Nup214 complex. 2.5-3.0 nmol CRM1 were incubated with an excess amount of His-Nup214(1916-2033)-His and the respective Ran mutant loaded with GTP, in the presence or absence of SPN1. Complex formation was assessed by analytical gel filtration with a S200 column in export complex buffer. 1 ml fractions were collected and analyzed by SDS-PAGE, followed by Coomassie-staining. Arrows indicate the bands for the respective proteins. Brackets indicate the fractions in which a formed complex is observed. (A)-(B) show complex formations of the Ran wildtype in the (A) presence or (B) absence of SPN1. (C)-(D) show the same for Ran(1-180) and (E)-(F) for RanC4A.

3.3 Structural characterization of CRM1-RanGTP-SPN1-Nup214 complexes

Previous studies could narrow down the region on Nup214 that interacts with CRM1, but nothing was known about the interacting region on CRM1 [59]. The structure of CRM1, its cooperative binding mechanism and its sophisticated confirmation changes upon binding of RanGTP or cargo, made the use of CRM1 truncation mutants and therefore a biochemical approach unsuitable. Therefore, several structural approaches were applied to characterize the CRM1-Nup214 interaction on a molecular level.

3.3.1 Electron microscopy

Analysis of the protein complexes with single particle electron microscopy

In single particle electron microscopy (EM), a 3D structure of a macromolecule is calculated from thousands of 2D images of randomly oriented single macromolecules that are extracted from digitized micrographs. Technical advances in the field of electron microscopy, especially the development of direct electron detectors now allow the analysis of single particles at a near-atomic resolution. The major limit to resolution for biological samples is the damage of the sample by the beam itself. To preserve the sample, the beam intensity has to be very low, which on the other hand increases the noise level of the images and therefore also the challenges of data analysis [237, 238, 239].

Based on the single particle EM analysis of the unbound CRM1 [172], it was attempted to analyze the Nup214-CRM1-Ran-SPN1 complex accordingly.

The Nup214 fragment interacting with CRM1 is quite small (around 15 kDa) compared to the size of the export complex (around 184 kDa). Therefore, it was attempted to obtain two EM models, one of the export complex without Nup214 and one of the export complex with Nup214, and to identify Nup214 bound to CRM1 by subtracting the two density maps.

Sample preparation as a crucial step for EM sample quality

Sample preparation was the first crucial step. Gel filtration, concentration of the complex with spin concentrators or even thawing of frozen CRM1 had a massive negative effect on sample quality. Therefore, CRM1 was always prepared freshly and immediately used for EM sample preparation. Also, no additional purification step such as gel filtration was performed as this also decreased the quality of the obtained EM particles.

The complexes for EM were formed on ice for 1 hour, then the buffer was exchanged to EM buffer with Zeba Desalting Spin Columns (ThermoScientific). Afterwards the samples were given to David Haselbach (MPIbpc, Göttingen) for further sample preparation and analysis, starting with GraFix, a method developed by the same group [225]. GraFix combined a sucrose gradient for separation of the protein complex from unbound protein components with a glutaraldehyde gradient for simultaneous fixation of the complex. After GraFix Nup214 was bound covalently to the complex (see figure 21).

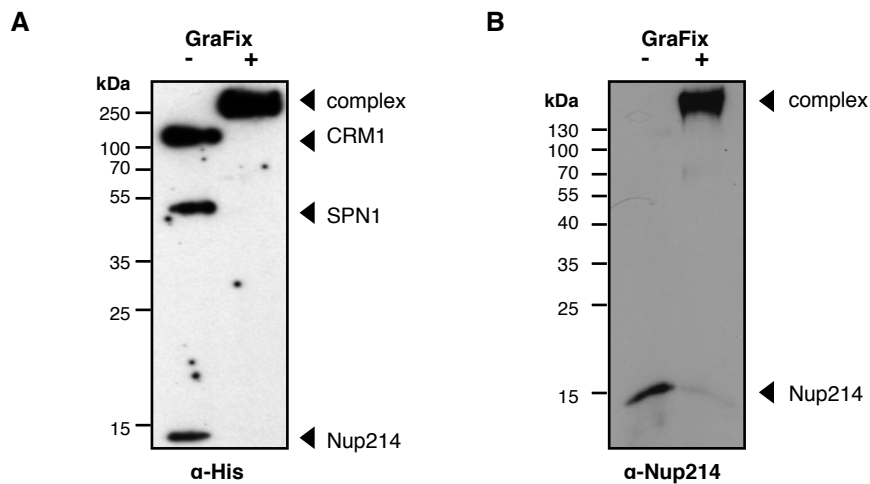


Figure 21: Nup214 bound to the export complex was fixed and purified with GraFix. (A) The α -His antibody recognizes the bands for CRM1, SPN1 and Nup214 before GraFix (-) and detects a band at the size of the complex after GraFix (+). (B) The α -Nup214 antibody detects a band at the size of the Nup214 fragment before GraFix (-), and a band at the size of the complex after GraFix (+).

Analysis of the Nup214-CRM1-RanGTP-SPN1 complex with EM

Single particles of the fixed complex were imaged by either negative stain- or cryo-electron microscopy. The ring- and S-shaped particles that are characteristic for CRM1 [172] could be readily identified (figure 22).

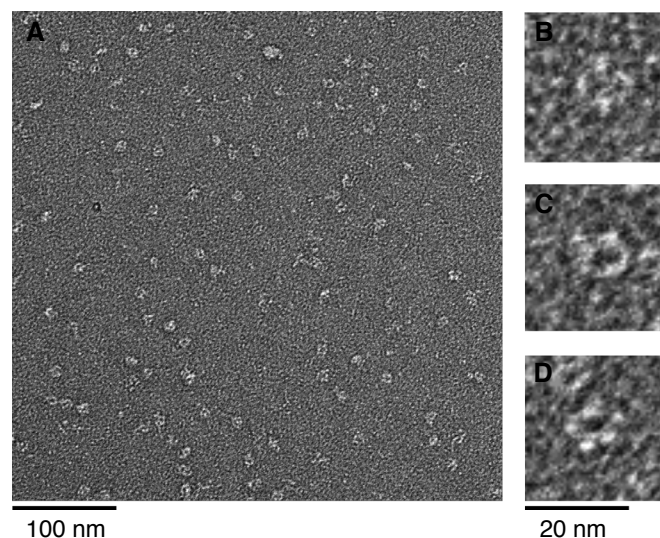


Figure 22: Single particles of the Nup214 complex. (A) Negative-stained particles were imaged and picked by an algorithm. (B-D) show randomly selected particles from (A).

Unfortunately, analysis of all obtained data sets, negative-stain or cryo images, was inconclusive. This was probably due to the resolution of around 20 Å combined with the small size of the Nup214 complex (around 200 kDa) and the small size of the Nup214 fragment in the complex. Another major problem seemed to be the flexibility of the Nup214 fragment and the high dynamic of the complex. Additional attempts were made to improve the stability of the complex and to increase the size of Nup214. This included using shorter or longer Nup214 fragments, GST- or MBP-tagged Nup214 fragments, the addition of Nup214 antibodies to the complex or Nup214 mutants that were labeled with an Mts-Atf-Biotin linker (ThermoScientific) and bound to NeutrAvidin or gold particles. None of the attempts could further improve the results and we concluded that the complex was not suited for EM analysis with the current methods available.

3.3.2 Cross-linking mass spectrometry

Cross-linking mass spectrometry is an established method to identify interacting regions in a protein complex. The protein complex is cross-linked with one of the various commercially available cross-linkers, trypsinized and analyzed by MS/MS analysis. Identified intermolecular cross-links, i.e. cross-linked peptides of two different proteins, allow conclusions about which regions of the proteins are in close proximity to each other. This method allows only for an approximate mapping of protein-protein interactions, it is not possible to identify interacting residues. Therefore, cross-linking mass spectrometry is the ideal method to give initial clues about the interacting regions of two proteins when no further information is available.

Efficient cross-linking of the Nup214-CRM1-RanGTP-SPN1 complex with various cross-linkers

There are a plethora of cross-linkers commercially available targeting amine (e.g. lysines), sulfhydryl (e.g. cysteines), carbohydrates (e.g. oxidized sugars) and carboxyls (e.g. C-terminus) groups or photoreactive cross-linkers that link nonspecifically. There are homobifunctional cross-linkers, meaning that both reactive groups target the same functional groups on the proteins or heterobifunctional cross-linkers with two different functional groups. Some of the cross-linkers can also be cleaved, for example by DTT, after cross-linking to leave only the individual proteins with modified residues or to reverse the linking.

The most common cross-linker for cross-linking mass spectrometry is BS³ (Bis[sulfosuccinimidyl] suberate), which is an amine-to-amine homobifunctional cross-linker that is water-soluble and non-cleavable. BS³ has amine-reactive N-hydroxysulfosuccinimide (NHS) groups linked by a 11.4 Å spacer arm. The sulfo-NHS esters interact with primary amines such as lysine side chains or the N-terminus of a protein by forming a stable amine bond upon release of N-hydroxysulfosuccinimide. The reaction is performed at pH 7-9 and as BS³ is soluble up to 100 mM in water it can be used in most commonly used buffers that do not contain free amines. Other common cross-linkers include BS²G (Bis[Sulfosuccinimidyl] glutarate), which is similar to BS³, but has a 7.7 Å spacer arm, EDC (1-Ethyl-3-[3-dimethylaminopropyl]carbodiimide hydrochloride), which is a zero-length heterobifunctional cross-linker that links carboxyl groups and primary amines, and EGS (Ethylene glycol bis[succinimidylsuccinate]), an amine-to-amine homobifunctional cross-linker with a 16.1 Å spacer arm.

For cross-linking, the initial step was to pre-purify the Nup214-CRM1-RanGTP-SPN1 complex by gel filtration. Subsequently, the buffer was changed to PBS with Zeba Desalting Spin columns as the primary amines from the export complex buffer would hinder the function of all amine-reactive cross-linkers.

13-23 pmol of the complex were incubated with increasing molar ratios of the respective cross-linker to find an optimal cross-linker to protein complex ratio (figure 23). An optimal ratio in this case is defined as the ratio that gives the most prominent and defined band on a Coomassie-stained SDS-gel at the expected size of the complex. If the ratio is too low, the band of the complex is not present or very faint and the bands of the individual proteins are still prominent. Too high a ratio leads to a blurred band of the complex, which indicates unspecific oligomerization.

Complexes with His-Nup214(1916-2033)-His (data not shown) and GST-Nup214(1968-2033) could be successfully linked with BS³, BS²G and EGS, the optimal ratio being 50:1 for BS³ and EGS, and between 50:1 to 100:1 for BS²G (figure 23).

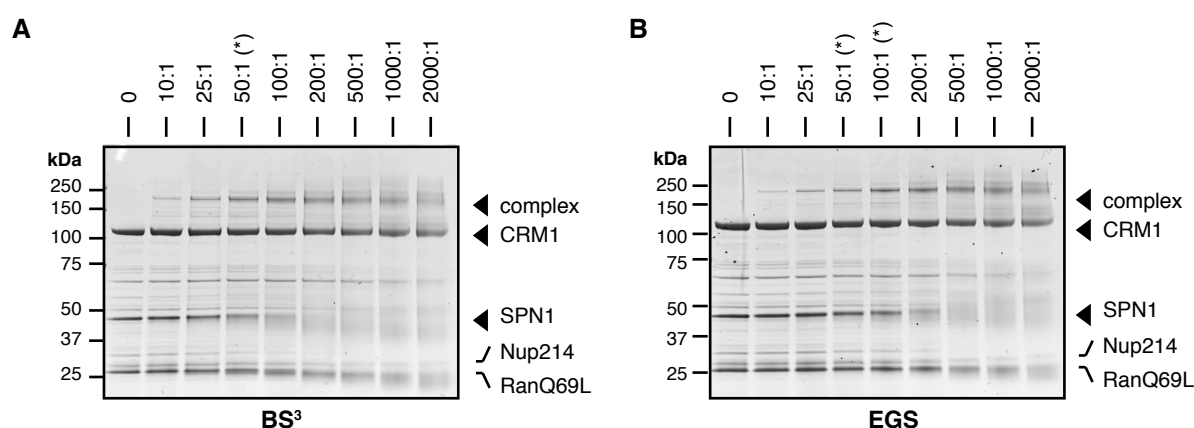


Figure 23: Titration of cross-linkers BS³ and EGS to GST-Nup214(1968-2033)-CRM1-RanGTP-SPN1 complex. (A) BS³ and (B) EGS were titrated to 22.8 pmol pre-formed GST-Nup214(1968-2033)-CRM1-RanGTP-SPN1 complex. The Coomassie-stained bands of the individual proteins as well as the complex are indicated with an arrow. The optimal concentration chosen for further experiments are marked by asterisks.

After the optimal ratio of cross-linker to protein complex had been determined, four samples each with 22.8 pmol of the GST-Nup214(1968-2033)-CRM1-RanGTP-SPN1 complex were linked with BS³ and EGS. For BS²G, 8 samples with 13 pmol complex per sample were incubated, one half with a cross-linker:protein ration of 50:1, the other half with a ratio of 100:1. The cross-linked samples were run on a SDS-gel, followed by Coomassie-staining. The gel was then given to Romina Hofele (MPIIbpc, Göttingen). The bands containing the complex were cut out of the gel and subjected to in-gel trypsin digestion before analysis by MS/MS.

The experiment with EGS did not give any results. The samples with BS³ and BS²G both gave a data set with a good sequence coverage of 73% for CRM1, 71% for SPN1 and 55% for Ran. The sequence coverage of the GST-Nup214(1968-2033) was 60%, but only peptides of the GST-tag were detected and no peptide for Nup214.

18 cross-links could be identified with BS³ and 13 with BS²G, thereof only five each were intermolecular cross-links coupling two different proteins from the complex. The complete list of identified cross-links can be found in the appendix (table S1).

Even though there were no cross-links to Nup214 identified, the data sets were used as a verification of the method itself. All obtained inter- and intra-molecular cross-links of CRM1, SPN1 and Ran were mapped on the available crystal structure of the export complex (PDB ID: 3GJX, [127])(figure 24). The C α -C α distances of the identified linked residues was measured in PyMOL. The maximum distance between two lysine side chains (8 Å each) and the 11.4 Å spacer of BS³ or the 7.7 Å spacer of BS²G is 27.4 Å and 23.7 Å, respectively. All identified distances cross-linked residues were within that range in the crystal structure, verifying the specificity of the approach (figure 24).

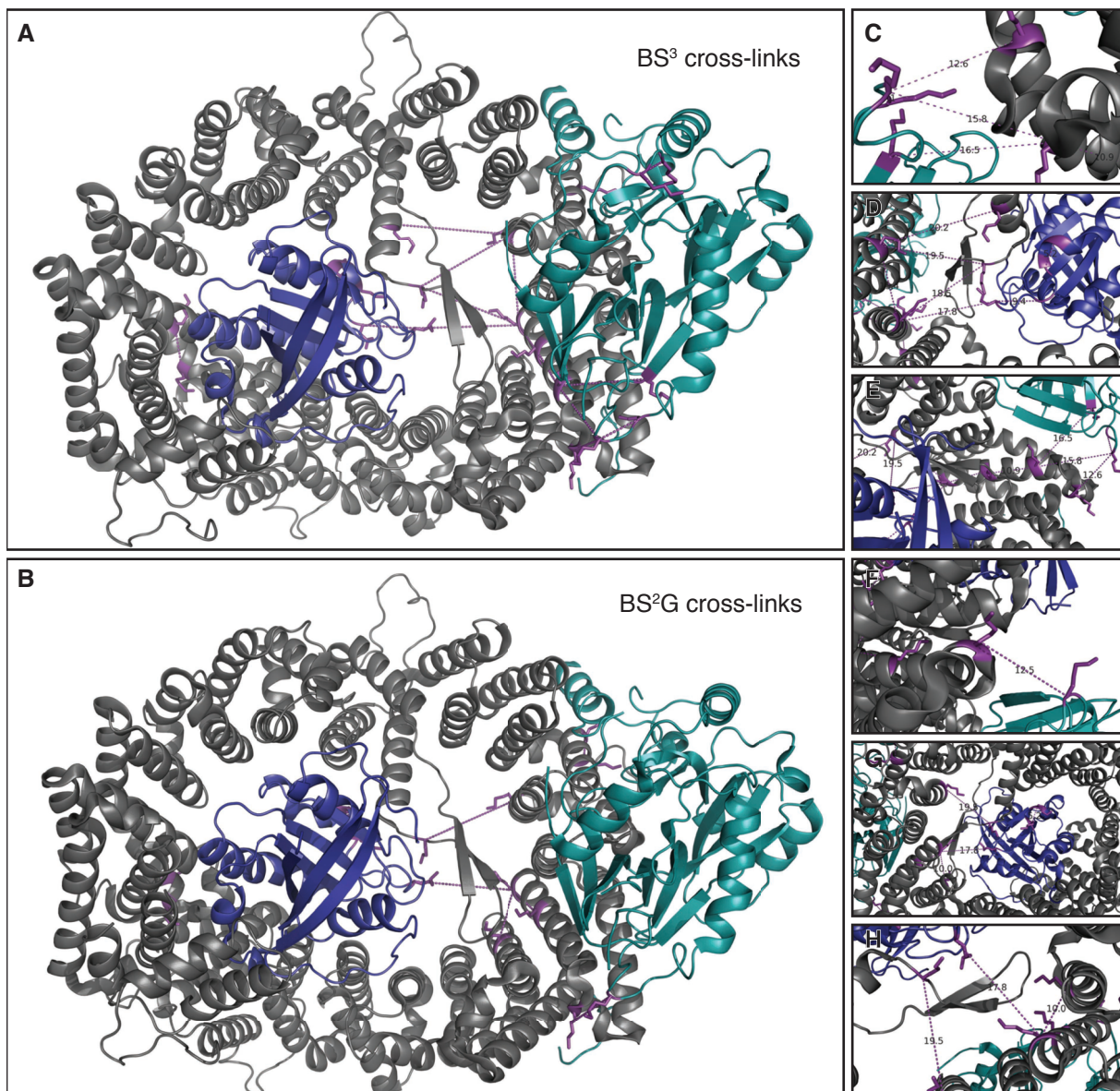


Figure 24: Cross-links of the GST-Nup214(1968-2033)-CRM1-RanGTP-SPN1 complex mapped on the crystal structure of the export complex. The structure shows CRM1 (gray), Ran (blue) and SPN1 (cyan) (PDB ID: 3GJX, [127]). Identified cross-linked residues are highlighted in purple. The cross-links obtained by (A) BS³ and (B) BS²G were mapped on the structure and C α -C α distances were calculated by PyMOL. (C)-(E) show selected regions of the structure in (A) and (F)-(H) show selected regions of the structure in (B).

Even though all four proteins of the complex were clearly cross-linked by BS³ and BS²G, no cross-linked Nup214 peptides could be identified. The analyzed Nup214-fragment was very hydrophobic due to its FG-repeat motives and in addition did not contain many sites for trypsin digestion. Both properties combined rendered detection of that specific Nup214 fragment by mass spectrometry highly unlikely.

Cross-linking of Nup214-CRM1-RanGTP-SPN1 complexes with BS³ and EDC indicates interacting regions

As the previous cross-linking strategy had failed due to limitations of the MS/MS analysis, the preparation of the MS sample after cross-linking was optimized by Romina Hofele (MPIbpc, Göttingen). In addition, Nup214 mutants were generated that contained an additional lysine and therefore an additional trypsin recognition site (Nup214-Lys mutants). This additional lysine should yield smaller, and therefore better detectable peptides after trypsinization.

The Nup214-Lys mutants were prepared and Nup214-CRM1-RanGTP-SPN1 complexes were assembled and purified by gel filtration at a preparative scale in PBS. The purified Nup214 complexes were then subjected to cross-linking with BS³. The optimal BS³:protein complex ratio was determined by titration of the cross-linker (figure 25). A cross-linker:protein ratio of 200:1 proved best for all tested Nup214-Lys mutant complexes.

For MS analysis, 1300 pmol of the Nup214 complexes were cross-linked with BS³ in a total volume of 1.5 ml in PBS. The cross-linked complex was directly subjected to in-solution trypsin digestion and MS/MS analysis by Romina Hofele (MPIbpc, Göttingen). Only the samples of the complexes with His-Nup214(1916-2033)-His and His-Nup214(K1916-2033)-His were analyzed by mass spectrometry.

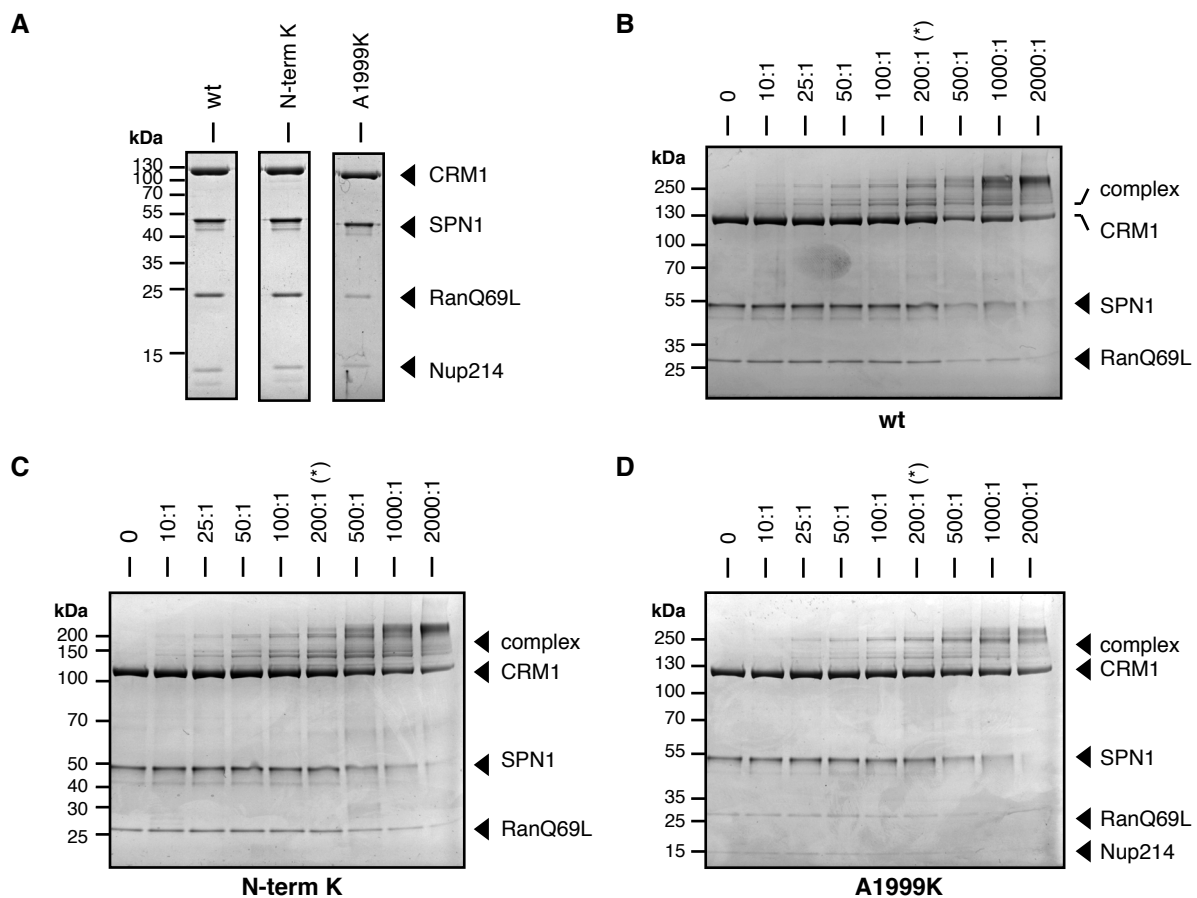


Figure 25: Cross-linking of His-Nup214(1916-2033)-His complexes by BS³. (A) The Nup214-CRM1-RanGTP-SPN1 complexes were purified and subsequently the CRM1-RanGTP-SPN1 complexes with (B) His-Nup214(1916-2033)-His, (C) His-Nup214(K1916-2033)-His and (D) His-Nup214(1916-2033)A1999K-His were incubated with increasing amounts of BS³. The Coomassie-stained bands of the individual proteins as well as of the complex are indicated with arrows. The optimal concentrations chosen for further experiments are marked by asterisks.

2848 and 2660 spectra were obtained for two technical replicates of the complex with the His-Nup214(1916-2033)-His and 2940 and 2882 for the complex with the His-Nup214(K1916-2033)-His, around 45% corresponding to intermolecular cross-links in all four replicates. The complete list of identified cross-links can be found in the appendix (tables S2, S3).

Many cross-links of the residues 1 and 2 of His-Nup214(1916-2033)-His and His-Nup214(K1916-2033)-His were identified. In addition, also the artificially introduced K22 of His-Nup214(K1916-2033)-His formed various cross-links. Mapping of the detected cross-links on the crystal structure of the export complex (PDB ID: 3GJX, [127]) revealed that these three N-terminal lysines cross-link unspecifically to the whole surface of the export complex (appendix, figures S2, S3). This suggests that the N-terminal region of the Nup214 fragments is flexible and not stably bound to CRM1. Residues 1 and 2 as well as the artificially inserted N-terminal lysine were therefore excluded from further analysis.

Analysis focused on the cross-links by the Nup214 residues K1928, K1942, K1966 and K2010 of the His-Nup214(1916-2033)-His wildtype and mutant fragments. The identified cross-links are summarized in table 23. The cross-links of the respective Nup214 residues to the export complex proteins partially overlap, suggesting that, for example, K1928 as well as K1942 can contact the CRM1 residue K680.

Table 23: Summary of the identified cross-links between His-Nup214(1916-2033)-His fragments and the export complex.

Nup214 residue	Linked protein	Linked residue
K1928	CRM1	K680
	SPN1	M1
		K223
		K314*
K1942	CRM1	K426
		K446
		K514
		K680
	SPN1	M1
		K223
		K323*
		K327*
		K343*
Ran	A2*	
K1966	CRM1	K22
		K426
K2010	CRM1	K22

The asterisk indicates residues that are not present in the crystal structure of the export complex (PDB ID: 3GJX, [127]).

Several cross-links of Nup214 to the export complex were identified with the previous approach. Therefore, the same strategy was used to cross-link the MBP-Nup214(1916-2033)-His fragment, which had also been used for electron microscopy and crystallization approaches, to the export complex CRM1-RanGTP-SPN1.

The optimal ratios of BS³ and EDC to the protein complex ratio were determined by titration of the cross-linker (figure 26). A BS³:protein ratio of 200:1 and EDC:protein ratio of 10000:1 proved best for the MBP-Nup214(1916-2033)-His complex.

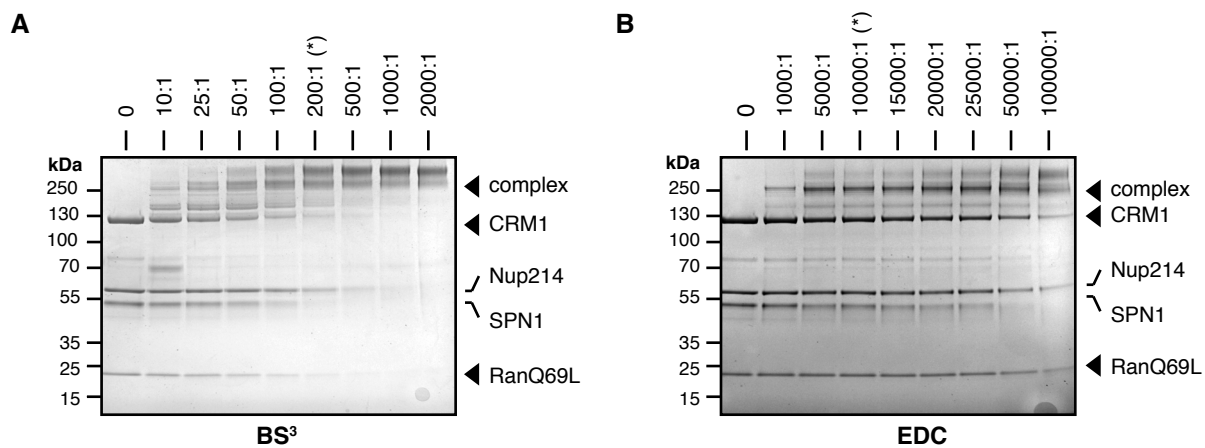


Figure 26: Cross-linking of the MBP-Nup214(1916-2033)-His complex by (A) BS³ and (B) EDC. The Coomassie-stained bands of the individual proteins as well as the complex are indicated by an arrow. The optimal concentration chosen for further experiments is marked with an asterisk.

For MS analysis, 1300 pmol of the MBP-Nup214(1916-2033) was cross-linked with BS³ or EDC to pre-purified CRM1-RanGTP-SPN1 export complex in a total volume of 1.5 ml PBS. The cross-linked complex was directly subjected to in-solution trypsin digestion and analyzed by Romina Hofele (MPIbpc, Göttingen).

2384 spectra were obtained for the complex cross-linked with BS³ and 598 for EDC. The reduced number of identified spectra for EDC can be explained by the fact that it is a zero-length cross-linker and therefore has a smaller operation radius. The complete list of identified cross-links can be found in the appendix (tables S4, S5).

The MBP-tag links indiscriminately to the complete surface of the export complex with BS³ as well as EDC (appendix, figure S4) indicating that the N-terminal MBP-tag is flexible, which could be expected from the previous results with the His-tagged Nup214 fragments. Cross-links of the MBP-tag were therefore excluded from further analysis and only cross-links of actual Nup214 residues were analyzed. Only six cross-links of Nup214 to any of the export complex proteins were identified in the two experiments, 4 cross-links with BS³ and 2 cross-links with EDC. The identified cross-links are summarized in table 24.

Table 24: Summary of the identified cross-links between MBP-Nup214(1916-2033)-His and the export complex.

Nup214 residue	Linked protein	Linked residue	Cross-linker
K1928	SPN1	K167	BS ³
		K223	BS ³
K1942	SPN1	K223	BS ³
	CRM1	D677	EDC
		E1013	EDC
K2010	CRM1	K22	BS ³

For verification, the identified cross-links of the His- and MBP-tagged Nup214(1916-2033) fragments to the export complex (tables 23, 24) were combined and mapped onto the crystal structure of the export complex (PDB ID: 3GJX, [127]) (figure 27). Note that not all cross-linked residues are actually present in the crystal structure. To assess the significance of the identified cross-links, the distances of the cross-linked residues of the export complex were measured in PyMOL.

The Nup214 residue K1928 links to CRM1 residue K680 as well as the SPN1 residues M1, K167, K223 and K314 (figure 27A). The C α -C α distances of CRM1 K680 and SPN1 K167 to SPN1 K223 in the export complex structure as measured by PyMOL are 12.6 Å and 14 Å, respectively. Therefore, it is likely that the same Nup214 residue could cross-link either one of them. On the other hand, the C α -C α distance of the SPN1 residues K223 and M1 is nearly 60 Å and they are located on completely opposite sides of the SPN1 protein. Therefore, these two residues are too far apart to be cross-linked by the same Nup214 residue unless there were significant structural changes in the Nup214 complex compared to the export complex.

Moreover, the Nup214 residue K1942 cross-links to SPN1 K223 as well as CRM1 residues D677 and E1013 (figure 27B). The C α -C α distance of SPN1 K223 and CRM1 D677 is around 40 Å, the distances of CRM1 E1013 to CRM1 D677 and SPN1 K223 are around 70 Å and 80 Å, respectively. Linking of the same Nup214 residue to all three of the identified residues, therefore is highly unlikely even if massive structural changes occur in the Nup214 complex compared to the export complex.

The same is true for linking of the Nup214 residue K1966 to CRM1 residues K22 and K426, which are nearly 65 Å apart in the export complex structure (figure 27C).

Interestingly, Nup214 K2010 cross-linked only to CRM1 K22 in all experiments with both the His- and MBP-tagged Nup214(1916-2033) fragments (figure 27D). Therefore it seems likely that Nup214 K2010 and CRM1 K22 are indeed in close proximity in the Nup214 complex.

Comparing the regions on the export complex to which the individual Nup214 proteins cross-link suggests that the more N-terminal Nup214 residues K1928 and K1942 are located close to the cargo-binding region on CRM1, whereas the more C-terminal residues K1966 and K2010 seem to be located in the region where the N- and C-termini of CRM1 come together. The ambiguous cross-links as well as the small number of identified cross-links did not allow for a definite conclusion of the binding of Nup214 to the export complex.

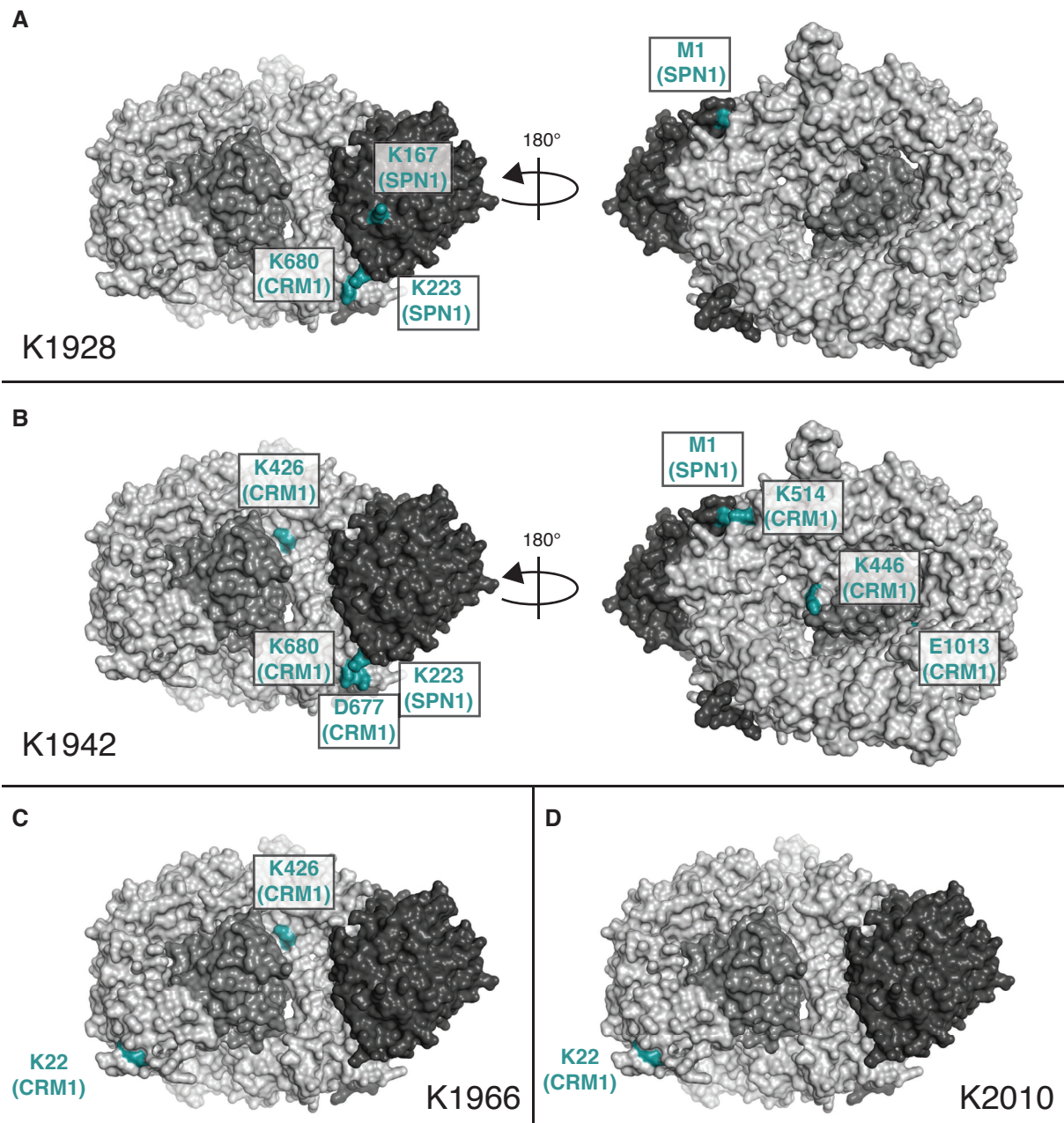


Figure 27: The identified cross-links of Nup214(1916-2033) were mapped on the crystal structure of the export complex (PDB ID: 3GJX, [127]). The structure shows CRM1 (light gray), RanGTP (medium gray) and SPN1 (dark gray). Cross-linked residues are highlighted in green. (A)-(D) show the cross-links of the Nup214 residues K1928, K1942, K1966 and K2010, respectively, to the export complex.

3.3.3 Crystallography

Cross-linking mass spectrometry only gave a very speculative hint of the orientation of the Nup214 fragment bound to CRM1 and electron microscopy did not identify the binding region either. The CRM1-RanGTP-SPN1-Nup214 complex was therefore crystallized to identify the interacting regions of Nup214 and CRM1.

Complex assembly and purification

As the CRM1-RanGTP-SPN1 export complex had been crystallized before (PDB ID: 3GJX, [127]), a special focus was put on identifying a Nup214 fragment suitable for crystallization. Nup214 fragments of various lengths and fused either to His-, GST- or MBP-tags were tested. The only Nup214 fragment that could be crystallized bound to the CRM1-RanGTP-SPN1 export complex was MBP-Nup214(1916-2033)-His. This fragment was expressed from a newly constructed vector, specifically designed for structural analysis as the original C-terminal end of the MBP as well as the linker between MBP and the multiple cloning site including the protease cleavage site had been removed and replaced by a short linker [212]. The short linker consisted of three alanines as well as a glutamate and a phenylalanine residue which were derived from the EcoRI restriction site used for cloning of the Nup214 fragment (compare figure 5). The intention of the vector modification was to decrease the flexibility of the MBP-tag fused to the Nup214 fragment. The more rigid linking should increase the chances of crystal formation. The presence and position of the MBP-tag turned out to be crucial for crystallization of the Nup214 complex, as attempts to crystallize complexes with the same Nup214(1916-2033) fragment with only a His-tag or with a C-terminally located MBP-tag did not produce any crystals. For complex formation, full-length SPN1 and truncated SPN1(1-291) were tested, as the C-terminus of SPN1 was prone to degradation not only as a single protein, but even in already formed complexes and crystals. The CRM1-RanGTP-SPN1-Nup214 complex was assembled and purified by gel filtration (figure 28). The gel filtration profiles of the complexes with full-length and truncated SPN1 both showed a peak at around 165 ml, corresponding to the respective complexes. In addition, peaks corresponding to excess MBP-Nup214, SPN1 and RanGTP were observed.

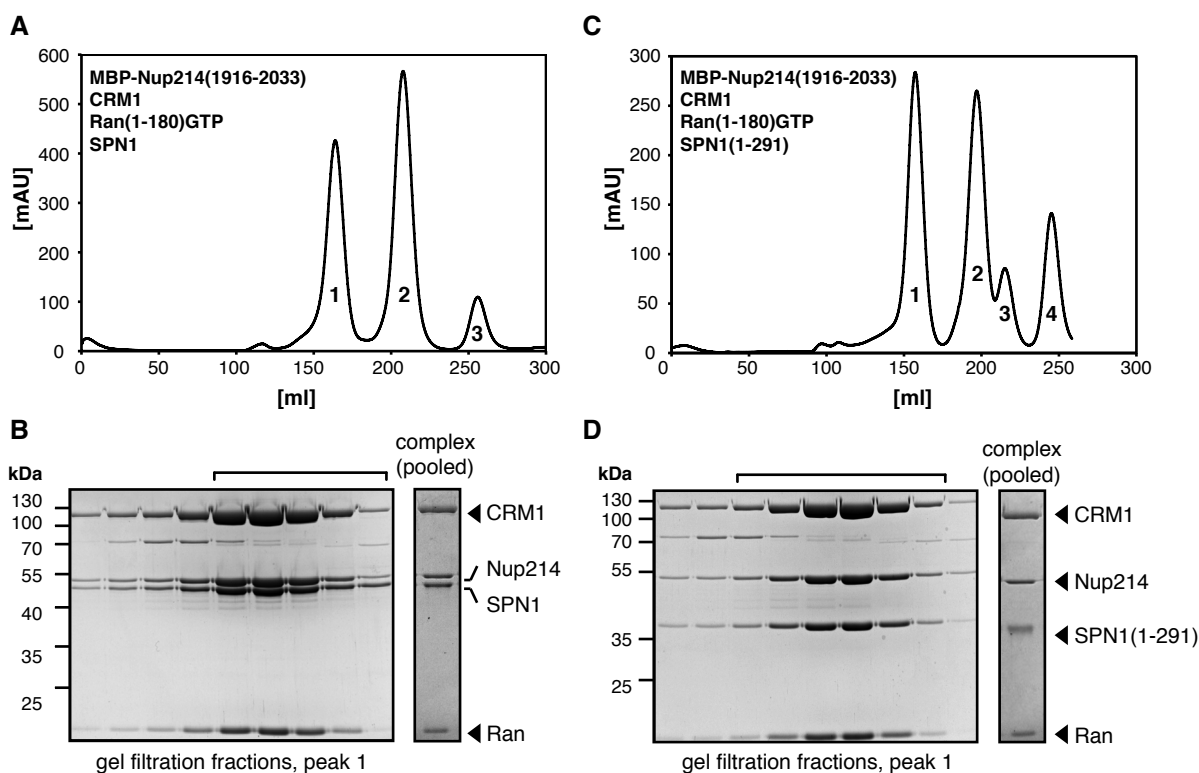


Figure 28: Purification of the CRM1-RanGTP-SPN1-Nup214 complex for crystallization. Complexes of CRM1-His, Ran(1-180)Q69L-GTP and MBP-Nup214(1916-2033)-His were assembled with full-length SPN1 and truncated SPN1(1-291). (A) Gel filtration profile of the CRM1-His/ Ran(1-180)Q69L-GTP/ MBP-Nup214(1916-2033)-His/ SPN1 complex. Peak 1 corresponds to the formed complex, peak 2 to excess SPN1 and Nup214 and peak 3 to excess Ran. (B) The collected fractions corresponding to gel filtration peak 1 from (A) were pooled and concentrated. (C) Gel filtration profile of the CRM1-His/ Ran(1-180)Q69L-GTP/ MBP-Nup214(1916-2033)-His/ SPN1(1-291) complex. Peak 1 corresponds to the formed complex, peak 2 to excess Nup214, peak 3 to excess SPN1(1-291) and peak 4 to excess Ran. (D) The collected fractions corresponding to gel filtration peak 1 from (C) were pooled and concentrated.

Crystallization screening and crystal optimizing

Initial crystallization screens were performed using the complex with full-length SPN1. Various commercially available screens, e.g. from Hampton Research or Molecular Dimensions, were tested either by manually setting up 24-well plates or with a crystallization robot. The only crystals were observed in a condition containing 0.1 M HEPES pH 7.5, 10% PEG3350 and 0.2 M L-proline (condition #61, Index™ screen, Hampton Research). Crystals appeared three days after setting up the plates. Crystals were small (figure 29A) and unstable as they dissolved again when left in the condition for more than a week. The crystallization condition was therefore optimized with respect to the proline concentration, PEG type and concentration, pH and additives. A condition containing 5% (w/v) polyethylene glycol (PEG) 8000, 0.2 M L-proline, 0.1 M Tris/HCl pH 7.5, 4 mM D-maltose and 180 mM LiCl proved most reliable in crystal formation of the Nup214 complex. Cross-seeding with crystals of the same protein complex was applied to reduce the number and increase the size of the formed crystals (figure 29B).

Complexes containing full-length and truncated SPN1 were subjected to crystallization and formed similar crystals under the same conditions. The complex with SPN1(1-291) diffracted to a higher resolution and was therefore used for crystal optimization.

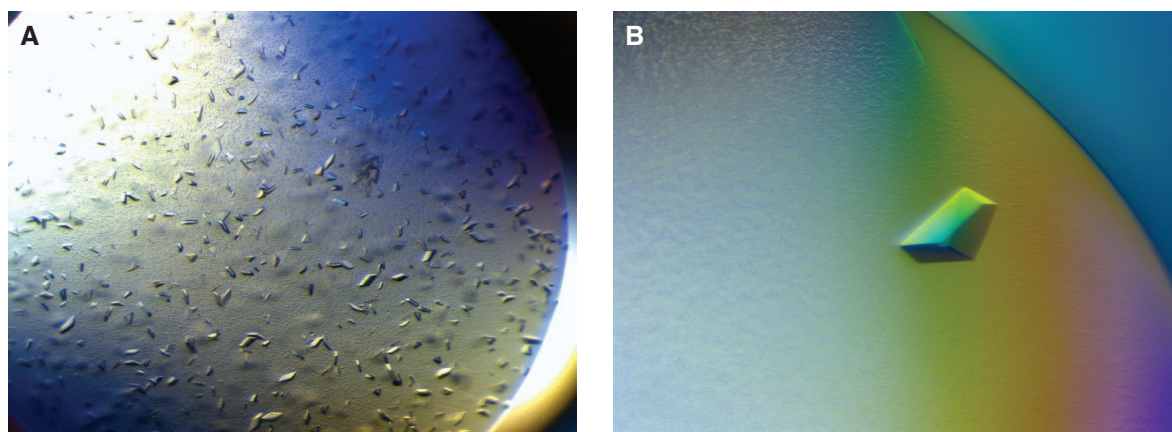


Figure 29: Optimization of crystal formation. (A) Crystals from the initial crystallization conditions were small and dissolved after a few days. (B) Crystals from the optimized condition grew to a size of 150 x 150 x 80 μm and diffracted to ~ 3 \AA after dehydration.

Crystals taken directly from the crystallization condition diffracted to a maximum resolution of 7 \AA . A sophisticated dehydration strategy was therefore developed by Thomas Monecke (Department of Molecular Structural Biology, Universität Göttingen) consisting of a stepwise increase of the PEG concentration as well as complete removal of mother liquor with an HC1c crystal humidifier (beamline 14.3, BESSY II, Berlin). Diffraction data was recorded and processed and the model was built and refined by Thomas Monecke.

The Nup214 complex crystallized in the space group $C222_1$. The model was built by molecular replacement using the export complex (PDB ID: 3GJX) as a search model. The final model had a resolution of 2.85 \AA and contained the CRM1 residues 5-1048, SPN1 residues 1-287 and the RanGTP residues 7-179, along with the MBP-tag and the three fragments of Nup214 corresponding to the residues 1916-1951, 1980-1988 and 2009-2027 (figure 30).

Overall structure of the Nup214 complex

The overall architecture of CRM1, RanGTP and SPN1 is similar to the structure of the export complex without Nup214 (PDB ID: 3GJX, [127]). Superposition of CRM1, RanGTP and SPN1 gave root mean square deviations (r.m.s.d.) of 0.68 \AA for 975 common $C\alpha$ atoms of CRM1, 0.33 \AA for 171 common $C\alpha$ atoms of RanGTP and 0.57 \AA for 248 common $C\alpha$ atoms of SPN1. The HEAT repeats of CRM1 form the same closed toroid in the export complex and Nup214 complex structures (appendix, figure S8A). Also the conformations of the three most variable features, the acidic loop, the NES binding cleft and the C-terminal helix is essentially unaltered (appendix, figures S8B,C,D, respectively). Corresponding to the conformation of CRM1, also the position and architecture of Ran(1-180)GTP and SPN(1-291) was similar in the Nup214 complex and the export complex. RanGTP interacts with CRM1 via the six N-terminal HEAT

repeats, the acidic loop and HEAT repeats 17 and 19. Binding of SPN1 to CRM1 occurs via the NES and the cap-binding domain to the outer surface of HEAT repeats 11-14. A third binding interface containing the 12 C-terminal residues of SPN1, which is present in the structure of the export complex is missing in the Nup214 complex as the truncated SPN1(1-291) instead of the full-length SPN1 was used for crystallization.

The MBP-tag makes contacts to RanGTP and CRM1 HEAT repeat 15. In addition, MBP also interacts with a symmetry-related Nup214 complex, thereby binding to CRM1 HEAT-repeats 12 and 13 as well the MBP-tag of the other molecule (data not shown).

Table 25: Crystal statistics.

	Crystal 1	Crystal 2
Data collection		
Space group	C2221	C2221
Number of complexes in a. u.	1	1
Wavelength [Å]	0.9184	0.9184
Cell dimensions		
a, b, c [Å]	111.57, 247.38, 209.98	112.33, 248.97, 210.57
α , β , γ [°]	90.0, 90.0, 90.0	90.0, 90.0, 90.0
Resolution [Å]	48.14-3.02 (3.12-3.02)*	48.49-2.85 (2.95-2.85)*
R_{merge}	0.058 (0.793)	0.055 (0.571)
$I / \sigma(I)$	15.34 (1.78)	15.52 (2.01)
Completeness [%]	98.4 (98.8)	98.2 (91.49)
Multiplicity	5.1 (5.2)	4.6 (4.1)
Refinement		
Resolution [Å]	48.14-3.02	30.00-2.85
No. reflections	56,383	67,922
R_{work}		0.242
R_{free}		0.283
No. atoms		14,933
B-factor		114.6
r.m.s.d.		
Bond lengths [Å]		0.017
Bond angles [°]		1.64

X-ray data collection, refinement and validation statistics for both crystals of the Nup214-CRM1-RanGTP-SPN1 complex. * Values in parentheses indicate the specific values in the particular highest resolution shell.

Interactions of the Nup214 fragment with CRM1

The Nup214(1916-2033) fragment binds to CRM1 via several FG-repeats targeting hydrophobic pockets located along a large fraction of the outer perimeter of the CRM1 ring (figure 30). We identified three prominent FG-repeat regions of Nup214 (termed FG-sites 1-3) in the structure. Each FG-site binds to CRM1 via at least two FG-repeats targeting a total of seven hydrophobic pockets (termed FG-pockets I-VII) on CRM1. A summary of all interactions between Nup214 and CRM1 can be found in the appendix (table S6).

The three FG-sites of Nup214 wind around the outer surface of CRM1, starting with N-terminus of the Nup214 fragment located close to HEAT repeats 14A and 15A and the C-terminus of the Nup214 fragment close to HEAT repeats 3A and 4A. The three Nup214 FG-sites bury a surface of 1331 Å², 408 Å² and 664 Å², respectively. Seven phenylalanines of Nup214 are buried in hydrophobic pockets of the CRM1 molecule, whereas the connecting residues lie loosely along the CRM1 surface. The linkers between the three identified Nup214 FG-sites are not defined in the structure, but long enough to connect the respective regions. It is therefore likely that all three Nup214 FG-sites derive from the same Nup214 fragment, although binding of symmetry related Nup214 molecules cannot be excluded completely.

The 36 residues of FG-site 1, ranging from S1916 to G1951, bind to a region between HEAT repeats 14-19. Three phenylalanines from FG-site 1 bind to hydrophobic pockets on CRM1. F1922 is buried in FG-pocket I between 14A and 15A, F1938 and F1947 bind between HEAT repeats 17A and 18A or 18A and 19A, respectively (figure 31B, E). F1992 is coordinated in FG-pocket I by hydrophobic interactions with the CRM1 residues I669, of HEAT 14 as well as Val720 and C723 of HEAT 15. Additionally, the main chain carbonyl of F1922 forms a hydrogen bond to the side chain amide of N719 on CRM1. Residues 1924-1928 form a short helical turn, and subsequently the Nup214 residues 1929-1936 wind along the surface of HEAT repeats 15A-17A. A pitched β -turn described by Nup214 residues 1937-1940 allows the phenyl side chain of F1938 to deeply insert into FG-pocket II between HEAT repeats 17A and 18A (figure 31B, E). F1938 forms hydrophobic interactions with F823 and F827, as well as a polar interaction with E828 on CRM1. The chain proceeds closely wrapped around HEAT repeat 18A and along the groove between HEAT repeats 18A and 19A where F1947 inserts into FG-pocket III by interacting with P868 and F871 of HEAT repeat 18A as well as A910, F914, S913 and Y918 of HEAT repeat 19A.

FG-site 2 encompasses nine Nup214 residues from 1980-1988 and lies across CRM1 HEAT repeat 17-19 (figure 31C, F). F1982 and F1988 within that stretch bind to hydrophobic pockets on CRM1. F1982 binds to FG-pocket IV, a shallow groove between HEAT repeats 17A and 18A, interacting with L831 on HEAT repeat 17A as well as S877, W880, D876 and L873 on HEAT repeat 18A. A type II β -turn is described by F1982 and the adjacent G1983, leading to another hydrophobic pocket which is occupied by F1988. Within this FG-pocket V, F1988 interacts with L872 and D876 of HEAT repeat 18A and F927, F928 and T931 of HEAT repeat 19A.

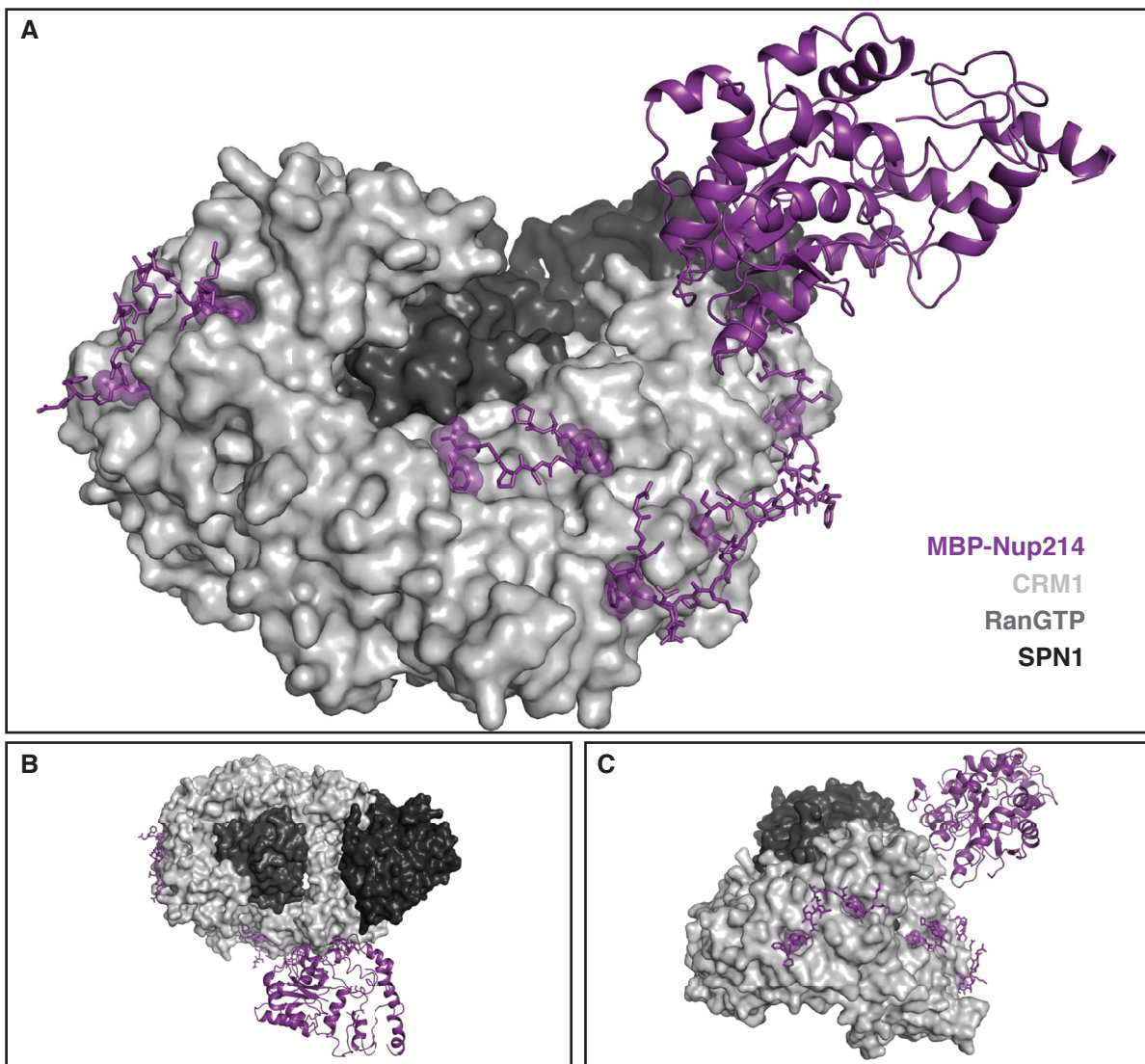


Figure 30: Nup214 interactions on the CRM1-RanGTP-SPN1 export complex. CRM1 (light gray), RanGTP (dark gray) and SPN1 (black) in surface representation. (A) Nup214 (in stick representation, purple) interacts with CRM1 via several regions on the outer surface of the ring. Interacting phenylalanines of Nup214 are highlighted by transparent spheres. (B)-(C) MBP is located between two symmetry-related Nup214 complexes.

The N-terminal CRM1 HEAT repeats 2-4 interact with FG-site 3 of Nup214 which is comprised of residues 2009-2027 (figure 31D, G). F2012 is inserted into a deep hydrophobic pocket (FG-pocket VI) between HEAT repeat 2-3 and forms interactions with V63 and D64 of HEAT repeat 2A and Q98, G101 and I102 of HEAT repeat 3A. The depth of the pocket and the insertion is reflected by an additional interaction of the F2012 phenyl group with L83 of HEAT repeat 2B. The Nup214 chain proceeds with a kink and a short α -helical segment, which crosses HEAT repeat 3 at a very close distance. F2024 is bound by I111 of HEAT repeat 3A and D152, as well as I153 of HEAT repeat 4A within FG-pocket VII.

In summary, the obtained structure is the first crystal structure of CRM1 bound to a nucleoporin fragment. Three FG-binding sites of Nup214 were identified, each binding via several phenylalanine residues to hydrophobic pockets along the CRM1 surface.

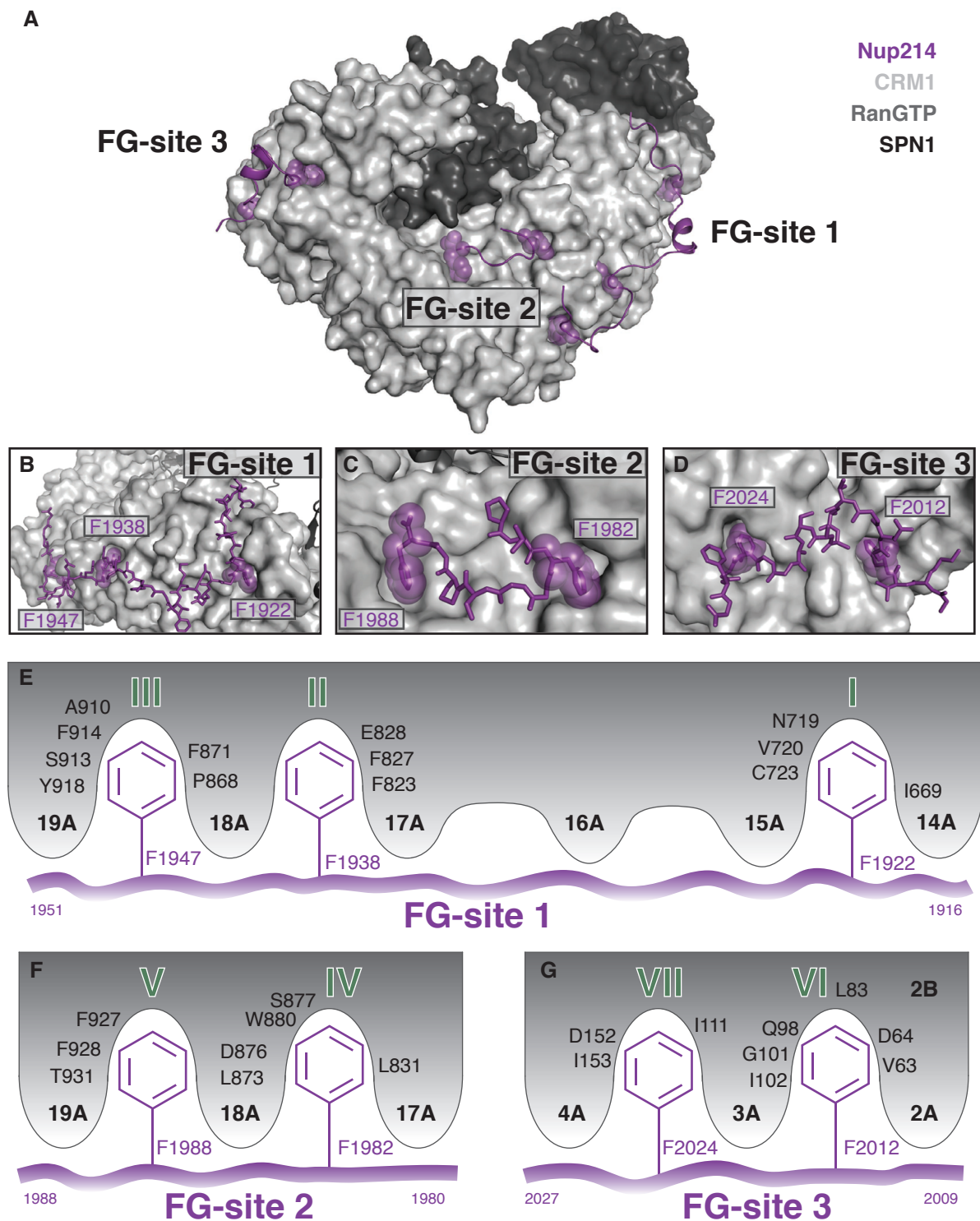


Figure 31: Nup214-binding sites on CRM1. The MBP-tag of Nup214 was omitted for clarity reasons. Nup214 (in stick representation, purple) interacts with CRM1 via three region on the outer surface of the ring. Interacting phenylalanines of Nup214 are highlighted by transparent spheres. (A) The localization of the three Nup214 FG-sites on the CRM1-RanGTP-SPN1 export complex. (B)-(D) Detailed view of (B) FG-site 1 (Nup214 residues 1916-1951), FG-site 2 (Nup214 residues 1980-1988) and (D) FG-site 3 (Nup214 residues 2009-2027). (E)-(G) Schematic representation of the interactions of Nup214 phenylalanines with hydrophobic pockets on CRM1 in FG-sites 1-3, respectively. FG-pockets I-VII on CRM1 are indicated in green.

3.4 Functional characterization of CRM1-Nup214 interactions

3.4.1 Analysis of prominent features of Nup214 revealed several FG-repeats important for CRM1-binding

It was previously shown that a conserved FG-repeat motif in Nup214 is important for its binding to CRM1 [59]. The effect of this motif on CRM1-Nup214 interaction was further investigated in this study by comparing the behavior of wildtype Nup214 to Nup214 mutants in which the FG-residues of the motif were changed to SG. A mutant in which the five FG-repeats of the motif, namely F1970, F1976, F1982, F1988 and F1994, were mutated to SG was termed "5SG" mutant. Mutants that had only the first four of the FGs (F1970, F1976, F1982 and F1988) mutated were called "4SG" mutants. Another feature frequently involved in protein-protein interactions are charged amino acids. Hence, charged amino acids in Nup214 were analyzed for their influence on binding to CRM1 in addition to FG-SG mutations. Single mutants were designed, in which a charged amino acid was exchanged for an amino acid with an opposite charge, e.g. Asp to Lys, or Lys to Glu. Furthermore, mutants in which all lysines were replaced by alanines ("KA" mutant) or glutamic acids ("KE" mutant) were constructed. Likewise, a mutant was constructed in which all acidic amino acids were mutated to lysine ("DE/K" mutant). For analysis in biochemical assays, the mutations were introduced into a plasmid coding for the recombinant fragment His-Nup214(1916-2033)-His.

All recombinant Nup214 mutants were expressed and purified with the standard Nup214 purification protocol. The purification yield of fragments in which phenylalanines were mutated to serines was much higher compared to the wildtype. First, the His-Nup214(1916-2033)-His fragments were tested for their ability to bind to the export complex. Five different His-Nup214(1916-2033)-His fragments, namely 5SG, KA, KA 4SG, KE and a non-mutated version (figure 32A), were incubated with pre-purified CRM1-RanGTP-SPN1 export complex. Subsequently, complex formation was assessed by analytical gel filtration. Complexes of all four Nup214 mutants eluted from the column at the same volume as the complex of the non-mutated Nup214 fragment (figure 32B). Only the elution profile of the KE mutant showed an asymmetric complex peak, indicating that the formed complex might not be as stable as the other complexes. That the complex peak indeed contained all the four proteins was confirmed by SDS-PAGE, followed by Coomassie-staining and Western blotting (data not shown). Analysis of the same Nup214 mutants in pulldown assays with immobilized GST-Rev showed more diverse binding of the different mutants. CRM1-binding to GST-Rev in a pulldown assay could only be observed in presence of RanGTP and Nup214, a complex of CRM1-RanGTP and Rev alone is not stable enough to be detected. Restricted binding of the Nup214 mutants to CRM1 would therefore lead to reduced binding of CRM1 to the immobilized GST-Rev. Indeed the sample with the Nup214 wildtype fragment and RanGTP showed the strongest binding of CRM1 to the immobilized GST-Rev (figure 32C). Also the binding of the Nup214 wildtype fragment was clearly detectable on the gel. By contrast, CRM1-binding in the samples with the Nup214 mutants was clearly reduced. The Nup214 KA mutant showed the strongest binding of the mutants indicated by a strong CRM1 band and clearly visible band for Nup214 KA on the gel. Nup214 5SG, KA 4SG and KE mutations are apparently more drastic.

CRM1-binding was even further reduced and the Nup214 fragments could hardly be detected on the gel.

For more quantitative analysis, RanGAP assays were performed. Titration of the five Nup214 fragments to CRM1 and Ran loaded with ^{32}P - γ -GTP in the absence of CRM1 cargo showed strong reduction of GTP-hydrolysis upon RanGAP addition for the Nup214 wildtype fragment (figure 32D). GTP-hydrolysis was reduced to $\sim 20\%$ for $3\ \mu\text{M}$ of the Nup214 wildtype fragment. The Nup214 KA fragment which had previously exhibited the strongest binding of all tested mutants in the pulldown assays (figure 32C), also resulted in the strongest reduction of GTP-hydrolysis. The Nup214 KE mutant reduced GTP-hydrolysis to $\sim 60\%$ for $3\ \mu\text{M}$ of the fragment. The two Nup214 mutants with mutated FG repeats, Nup214 5SG and Nup214 KA 4SG showed the weakest binding with more than 80% of the GTP hydrolyzed.

Next, the importance of the mutated residues in binding to CRM1 was assessed with an *in vitro* export assay using stably transfected GFP-NFAT cells. The cells were permeabilized and cytosol, ATP-regenerating system as well as increasing amounts of the Nup214 fragments were added to the cells. Export of GFP-NFAT from the nucleus was quantified by flow cytometry. Strong binding of the Nup214 fragment to CRM1 means that there is less CRM1 available for nuclear export, leading to reduced export of GFP-NFAT and a relative increase in the residual nuclear fluorescence. Nup214 5SG, KA, KA 4SG and KE mutants as well as the wildtype were titrated to the permeabilized cells. Flow cytometry analysis showed a clear reduction in nuclear export of GFP-NFAT for the non-mutated Nup214 fragment, whereas the export was hardly affected by all of the tested Nup214 mutants, indicating a reduced interaction between the Nup214 mutants and CRM1 (figure 32E).

Analysis of the Nup214 5SG, KA, KA 4SG, KE mutants in a variety of cellular and biochemical assays therefore revealed an important role of the FG-repeats as well as the lysines in Nup214 for CRM1-binding.

3.4.2 Analysis of the structure-derived Nup214 mutants confirms the importance of the identified phenylalanines in CRM1-binding

Several interactions between CRM1 and Nup214 were identified by X-ray crystallography (see section 3.3.3). Two of the phenylalanine residues of the previously investigated conserved motif, F1982 and F1988, were visible in the crystal structure and were found to bind to hydrophobic pockets on the CRM1 surface. In addition, several other phenylalanines were identified that bound to different hydrophobic pockets on CRM1. To verify the molecular interactions identified by the crystal structure, another set of Nup214 mutants were designed. A Nup214 mutant in which all the phenylalanines that bound to the C-terminal arch of CRM1 in the crystal structure (F1922, F1930, F1938, F1947, F1982 and F1988) were mutated to serine was termed "X1". Accordingly, the phenylalanines that bound to the N-terminal arch of CRM1 in the crystal structure (F2012, F2024 and F2026) were mutated to serine in the Nup214 "X2" mutant. The Nup214 "X3" mutant is a combination of X1 and X2. In accordance with the previous set of Nup214 mutants, these structure-derived mutants were also introduced into the plasmid coding for the recombinant fragment His-Nup214(1916-2033)-His. Additionally, the mutations were also introduced into the plasmid coding for the Nup214 fragment that was used in the crystallographic studies, MBP-Nup214(1916-2033)-His (figure 33A).

Pulldown assays showed reduced binding of CRM1 to GST-Rev in the presence of the the X1 and X2 mutant. In presence of the Nup214 X3 mutant, hardly any binding of CRM1 to GST-Rev was detected (figure 33B).

For a more quantitative analysis, binding of the Nup214-X mutants to CRM1 was assessed by RanGAP assays (figure 33C, D). The recombinant His-Nup214(1916-2033)-His and MBP-Nup214(1916-2033)-His X-mutants were titrated to CRM1 and ^{32}P - γ -GTP in the absence of CRM1 cargo. The wildtype Nup214 fragments led to a strong resistance of the complex towards RanGAP-induced GTP-hydrolysis. By contrast, more than 60% of the GTP was hydrolyzed when titrating the His- or MBP-tagged Nup214 X1 or X2 mutants, implying a strongly reduced binding of these Nup214 mutants to CRM1. Strikingly, the combinatorial Nup214 mutants in which all of the phenylalanines that bound to CRM1 in the crystal structure were mutated did not lead to any stabilization of the CRM1-RanGTP complex towards RanGAP, indicating that this mutant is unable to bind CRM1.

Interestingly, results of the binding assays with the Nup214-X mutants resemble the results of the binding assays of the truncated Nup214 fragments as described above (section 3.2.3). Even though the truncated Nup214 fragments were able to bind the export complex, they did not have a stabilizing effect on the complex (figure 18). In addition, the importance of the mutated residues in binding to CRM1 was assessed with an *in vitro* export assay as described above. Nup214 X1, X2 and X3 mutants as well as the wildtype were titrated to permeabilized GFP-NFAT cells. Flow cytometry analysis showed a clear reduction in nuclear export of GFP-NFAT for the non-mutated Nup214 fragment, whereas the export was hardly affected for the Nup214 X2 and X3 mutants, indicating a reduced interaction of the Nup214 mutants with CRM1 (figure 32E). Interestingly, the effect of Nup214 X1 on nuclear export was more prominent.

3.4.3 Importance of the identified binding residues in cellular context

For the above described biochemical analysis of Nup214 mutants, fragments containing the residues 1916-2033 were used. To anticipate the relevance of the identified interacting residues within the whole FG-repeat domain of Nup214, cellular binding assays were performed. The mutations were introduced into a transfection plasmid coding for Nup214(1859-2090) fused to RFP-cNLS for analysis in cellular assays. A scheme of all used RFP-Nup214-cNLS constructs can be found in the appendix (figure S10).

The plasmids were co-transfected with GFP-SPN1 and the distribution of GFP-SPN1 localization was counted in at least 100 cells (see figure 34). Exchange of the charged amino acids alone did not have a strong effect on SPN1 localization, only the exchange of the lysines to glutamic acid lead to a redistribution of GFP-SPN1 in ~30% of the cells. Also the exchange of a single phenylalanine (F1994S mutant) or conserved FG-repeat motif (4SG mutant) did not affect GFP-SPN1 localization. Interestingly, the effect of combinatorial mutants was a lot stronger than it could have been expected from the effect of the individual mutants. 5SG, the combination of F1994S and 4SG, showed predominantly an equal distribution of GFP-SPN1 between the cytoplasm and the nucleus compared to a clear nuclear localization with both individual mutants. Similar effects could be observed for mutants combining mutations of hydrophobic as well as charged amino acids. The mutant showing the least binding to CRM1 was KE 5SG in which the lysines were mutated to glutamic acid and 5FGs were mutated to SG. Localization of GFP-SPN1 was not affected at all when co-transfected with this mutant. This is remarkable, as the Nup214(1859-2090) fragment contains 25 additional phenylalanines. The crystal structure-derived Nup214-X mutants showed very diverse effects on CRM1-interaction. Nup214 X2 did not alter GFP-SPN1 localization, Nup214 X1 led to some redistribution of GFP-SPN1 in about 20% of the cells. The combination mutant Nup214 X3 led to cytoplasmic localization of GFP-SPN1 in about 50% of the cells and an equal distribution in the remaining 50% of the cells, indicating the importance of the mutated residues in CRM1-binding.

From these results, it can be concluded that binding of CRM1 to Nup214 is indeed mediated by phenylalanine residues, but is also affected by basic residues. Furthermore, the combination of several mutations can have a synergistic effect on CRM1-binding.

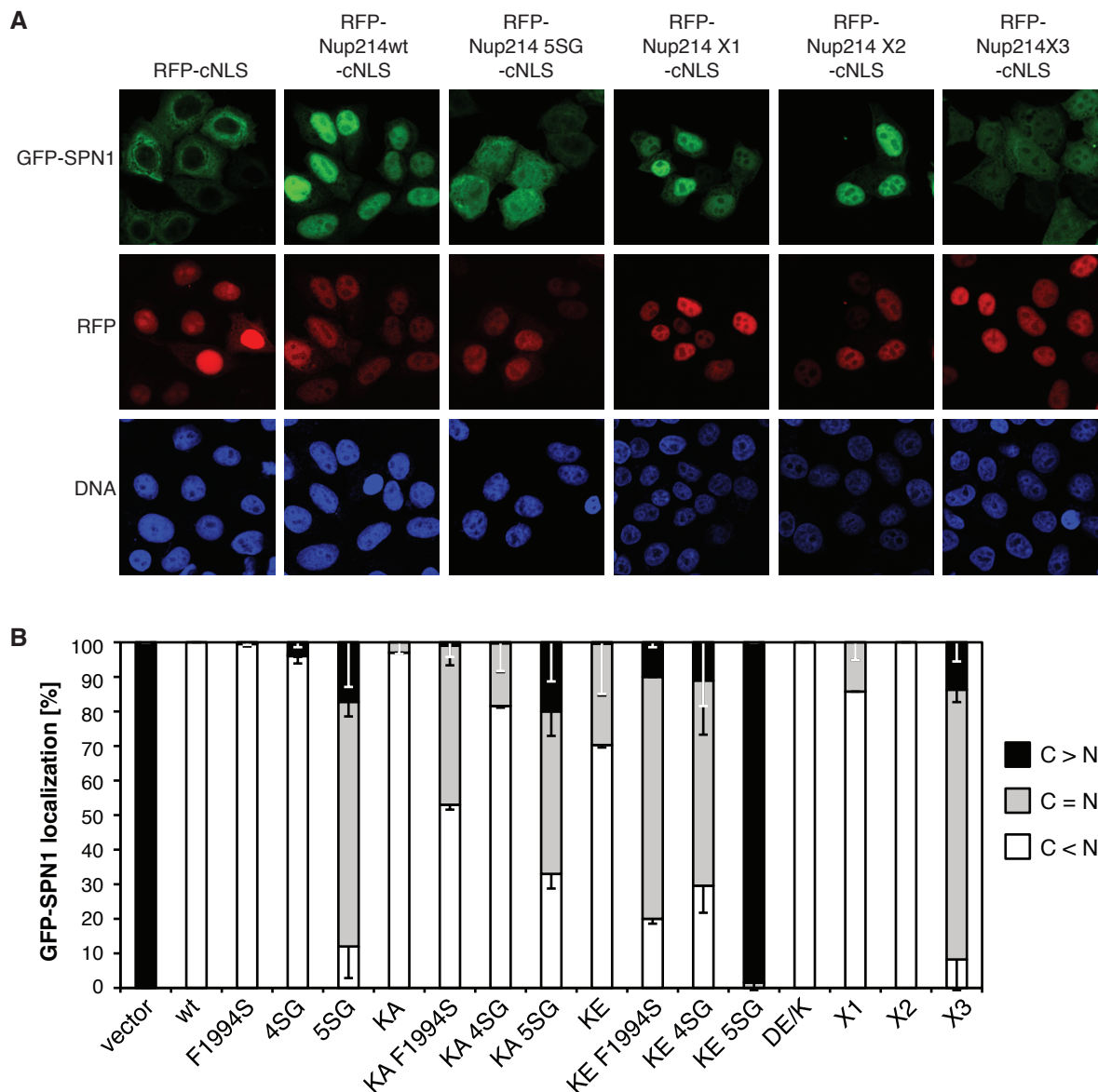


Figure 34: Co-transfection of Nup214 mutants with GFP-SPN1. HeLa P4 cells were transfected with plasmids coding for the Nup214(1859-2090) fragment fused to RFP-cNLS or the empty RFP-cNLS vector were co-transfected with GFP-SPN1. Cells were analyzed by fluorescence microscopy after 24 hours. (A) shows a subset of the tested Nup214 mutants. All RFP-Nup214-cNLS constructs (red) localized in the nucleus (blue). Localization of GFP-SPN1 is altered depending on the co-transfected Nup214 construct (green). (B) The localization of GFP-SPN1 in 100 cells was quantified for predominant cytoplasmic (C > N), equally distributed (C = N) and predominant nuclear (C < N) localization. The mean and standard deviation of at least three independent experiments were plotted. Cells were transfected and localization was determined by Christiane Spillner.

3.4.4 Characterization of structure-derived CRM1 mutants

The crystal structure revealed multiple Nup214-binding pockets on CRM1 (figure 31, table S6). CRM1 mutants were designed to obstruct that binding and therefore verify the identified Nup214-binding sites. Seven binding pockets were identified that bound phenylalanines of MBP-Nup214 in the crystal structure. Binding pockets were numbered from I to VII. An additional pocket "L" binds a phenylalanine derived from the linker between the MBP and the Nup214. It was nevertheless included in the analysis as there are various phenylalanines in Nup214 upstream of the used aa1916-2033 fragment that could potentially interact with this binding pocket. The binding pockets were predominantly hydrophobic, but for most of the pockets no obvious interacting residue could be identified. The strategy for mutagenesis was therefore to introduce larger residues into the binding pockets of CRM1 with the intention to block access of the phenylalanine to the pocket (see figures 35 and 36). The complete list of mutated CRM1 residues can be found in table 26.

Table 26: Mutated residues in CRM1.

FG-site #	FG-Pocket #	Residue #	Original Residue	Mutated Residue
1 (aa1916-1951)	L (linker)	680	K	Q, R
		731	A	Q
		744	L	W
		745	I	W
		748	M	R
	I (F1922)	679	L	R, W
		723	C	M
	II (F1938)	823	F	A
		824	D	K
	III (F1947)	917	T	E
		918	Y	W
2 (aa1980-1988)	IV (F1982)	880	W	A
	V (F1988)	925	H	W
		928	S	K
3 (aa2009-2027)	VI (F2012)	83	L	F, R
		102	I	Q, W
	VII (F2024)	134	L	F
		149	F	W
		152	D	W
		156	A	F
		167	N	R

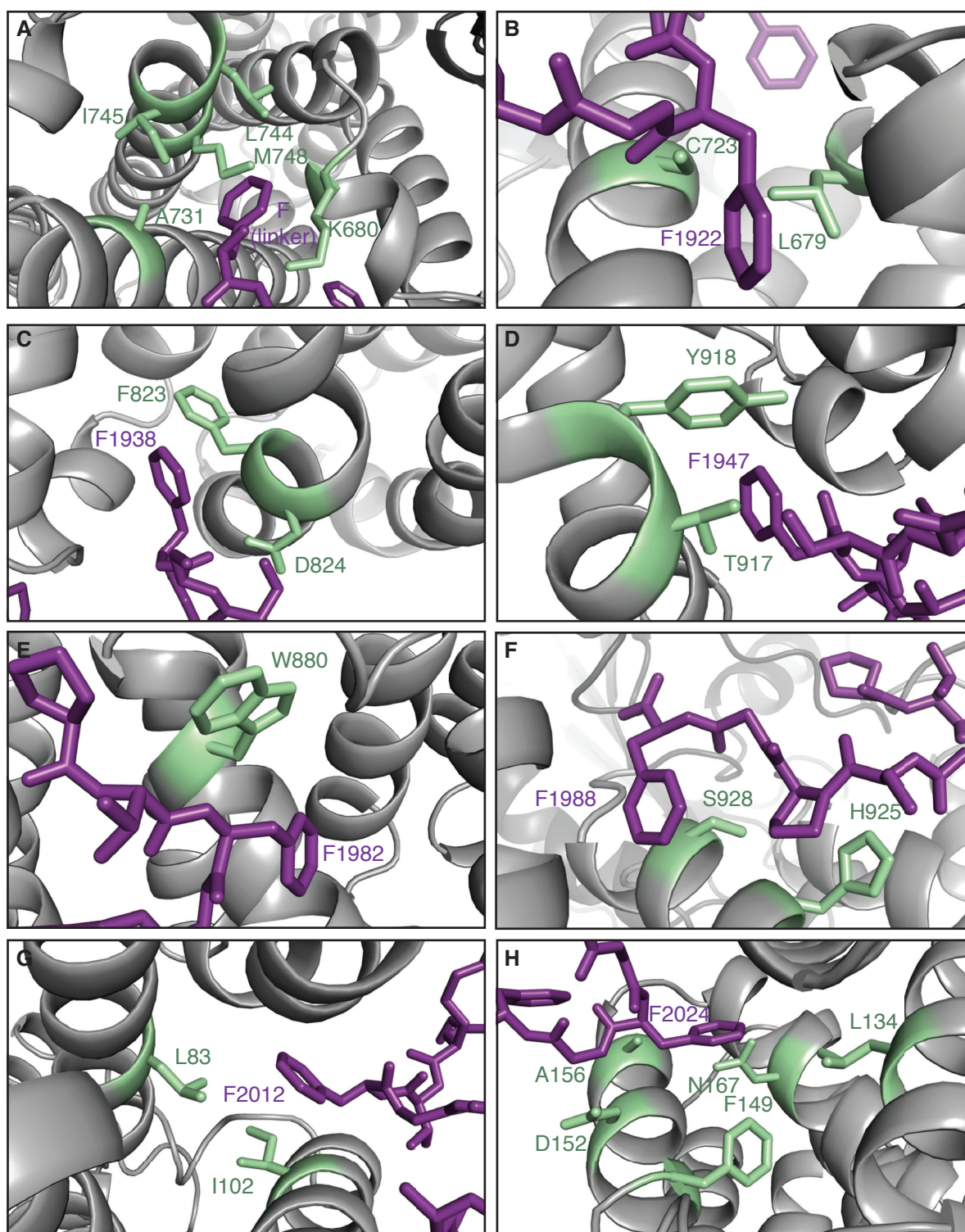


Figure 35: Phenylalanine-binding pockets on CRM1. Eight hydrophobic pockets on CRM1 were identified from the crystal structure of the Nup214 complex. Selected residues were mutated to larger amino acids to obstruct binding of Nup214 to the pockets. The CRM1 backbone is colored in gray, the respective residues chosen for mutagenesis are highlighted in green. Nup214 is depicted in purple. (A) Binding pocket L binds a phenylalanine from the linker between the MBP-tag and Nup214. (B)-(H) show the binding pockets I-VII of F1922, F1938, F1947, F1982, F1988, F2012 and F2024, respectively.

CRM1 single mutants were generated by site-directed mutagenesis on the pQE60-CRM1-His plasmid. Double or multiple mutants were generated either by site-directed mutagenesis, by cloning of synthesized gene fragments or by combining CRM1 fragments containing the desired mutations. A selection of mutants were expressed. The purification was performed with the same protocol as for the wildtype CRM1. All CRM1 mutants were readily expressed, but only a subset were soluble and could be purified. Interestingly, especially mutation of N-terminal residues led to insoluble protein. This includes mutations of the residues L83, I102 and L134, alone as well as in combination with any other mutations of the protein. The yield of soluble protein was significantly lower in the mutants compared to the wildtype, yielding as little as 15 μg from 12 liters of expression cultures in the case of the K680Q A731Q L679R D824K mutant compared to several mg per liter expression culture for the wildtype. A complete list of all generated CRM1 mutants and their expression and purification efficiency can be found in the appendix (table S7).

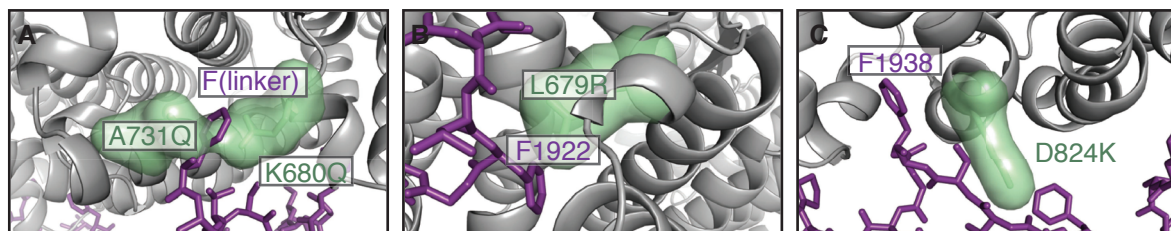


Figure 36: Selected mutations of CRM1 were introduced into the structure *in silico* with PyMOL to analyze their potential to block phenylalanine-binding to the respective hydrophobic pockets. The mutations (A) K680Q A731Q, (B) L679R and (C) D824K are shown. The CRM1 backbone is colored in gray, the respective mutated residues are highlighted in green. Nup214 is depicted in purple.

Based on the large number of binding pockets on CRM1 involved in the interaction with Nup214, it was highly unlikely that a mutation of a single FG-pocket would have an drastic effect on Nup214-CRM1 binding. First, purified CRM1 mutants were tested for their ability to bind phenylsepharose. Phenylsepharose is commonly used as a mimic of hydrophobic FG-repeats. CRM1 mutants were incubated with phenylsepharose in the absence or presence of RanGTP and NES peptide. In accord with the expectations, no significant difference in binding could be observed between the different tested CRM1 mutants (figure 37). Furthermore, binding to phenylsepharose was also independent of RanGTP and NES.

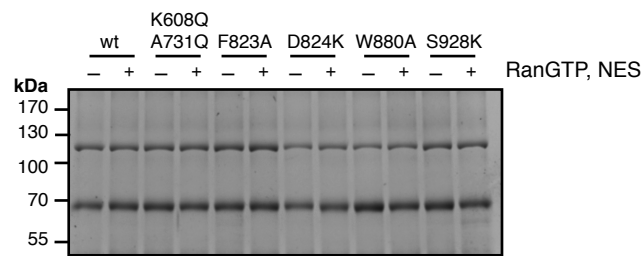


Figure 37: CRM1 mutants show no differences in binding to phenylsepharose. 25 pmol CRM1 mutants were incubated with 5 μ l phenylsepharose in absence or presence of an excess of RanGTP and NES peptide. Bound proteins were analyzed by SDS-PAGE, followed by Coomassie staining.

No difference in binding to phenylsepharose was observed for any of the CRM1 mutants. Therefore, it was proceeded with a more sensitive analysis by RanGAP assays.

Available crystal structures of CRM1 show that conformational changes in the molecule are mutually influenced by binding of RanGTP and cargo. To rule out that the mutations of CRM1 changed the affinity for RanGTP or cargo, an NES peptide was titrated to the respective CRM1 mutants and Ran loaded with 32 P- γ -GTP. The stability of the complex was analyzed. Strikingly, even though the CRM1 mutants were designed to inhibit Nup214-binding, most CRM1 mutants also showed altered binding to NES peptide and/ or RanGTP (figure 38, left panel). Some mutants like CRM1 S928K showed reduced NES-binding whereas CRM1 K680Q A731Q showed an increase in NES-binding. The only mutants that exhibited unaltered NES complex stability were CRM1 D824K, Y918W and W880A.

Titration of Nup214 to the respective CRM1 mutants and Ran loaded with 32 P- γ -GTP revealed that most of the tested CRM1 mutants were indeed impaired in their binding to Nup214 as as levels of GTP-hydrolysis were increased upon addition of RanGAP compared to the wildtype (figure 38, middle panel). Only CRM1 K680Q A731Q did not lead to increased GTP-hydrolysis.

Next, the CRM1 mutants were analyzed in a cellular context by *in vitro* export assays. Cells stably transfected with GFP-NFAT were permeabilized and pre-incubated with an ATP-regenerating system and LMB to remove or inactivate most of the endogenous CRM1. After extensive washing, recombinant CRM1 mutants were added to a final concentration of 30 nM and nuclear fluorescence at 0, 5, 10 and 25 minutes was analyzed by flow cytometry. Most of the CRM1 mutants showed a somewhat slower nuclear export compared to the wildtype (figure 38, right panel). The observed effects were small, but reproducible. Only CRM1 A156F was able to export GFP-NFAT at the same rate of the non-mutated CRM1. In contrast, kinetics with 100 nM of the CRM1 mutants did not show any variation (appendix, figure S13), indicating that binding defects of the mutants are only relevant in conditions with low, rate-limiting CRM1 concentrations.

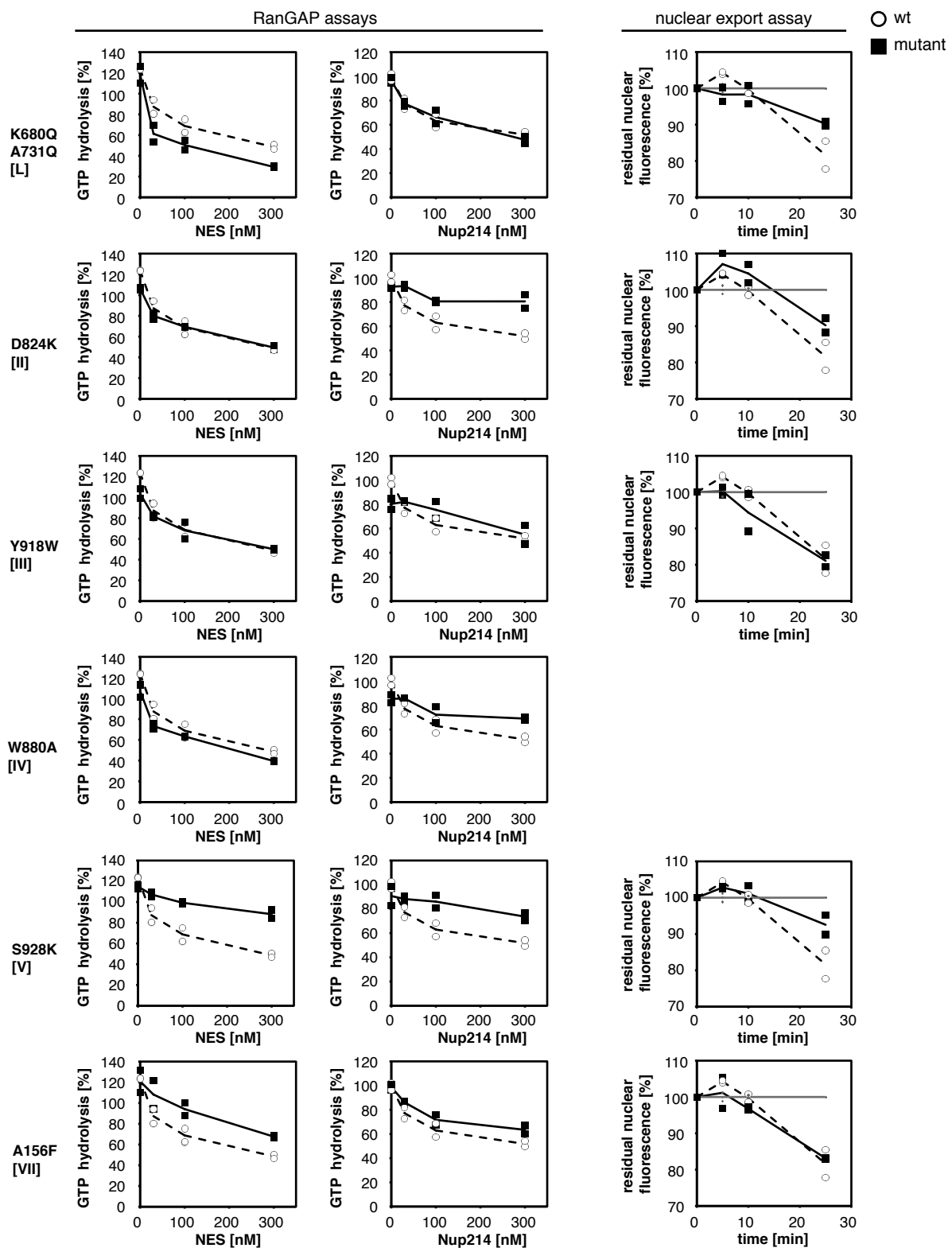


Figure 38: CRM1 mutants showed diverse binding to NES/ RanGTP and Nup214. The CRM1 mutants were plotted (black square) individually in comparison to the wildtype CRM1 (white circle). The average of the values is indicated by the black line for the CRM1 mutants and the dashed line for the CRM1 wildtype. The individual values and averages of two independent experiments were plotted. Square brackets indicate the altered FG-binding pocket of the CRM1 mutant. (left panel) NES peptide or (middle panel) MBP-Nup214(1916-2033)-His was titrated to 100 nM of the CRM1 mutants and Ran loaded with ^{32}P - γ -GTP in RanGAP assays. (right panel) Permeabilized GFP-NFAT cells were incubated with 30 nM of the respective CRM1 mutants. Residual nuclear fluorescence was analyzed by flow cytometry. Values were normalized to fluorescence intensities at 0 minutes and plotted in relation to a kinetic without added CRM1 (gray).

As some single mutants showed an effect on Nup214 binding and nuclear export, it was tested if these effects would be additive in CRM1 mutants with more than one mutated hydrophobic pocket. A set of CRM1 mutants including D824K (FG binding pocket III) and K680Q A731Q L679R (FG binding pockets L and I) as well as a combinatorial mutant of the two, namely K680Q A731Q L679R D824K was analyzed for their binding of NES peptide and Nup214 in RanGAP assays and furthermore for their effect on export of GFP-NFAT. Again, only D824K exhibited nearly unaltered binding to an NES peptide and RanGTP. The K680Q A731Q L679R mutant as well as the K680Q A731Q L679R D824K mutant, bound to the NES peptide stronger than the wildtype (figure 39, left panel). K680Q A731Q L679R binding to Nup214 was comparable to the wildtype, whereas CRM1 D824K showed decreased binding to Nup214. Surprisingly, the effect on Nup214 binding was not additive for the K680Q A731Q L679R D824K mutant. On the contrary, the decrease in Nup214 binding was slightly smaller as compared to the D824K single mutant (figure 39, middle panel). Also the effect of the respective CRM1 mutants on nuclear export of GFP-NFAT was not additive, although all three mutants showed reduced export kinetics compared to the wildtype (figure 39, right panel).

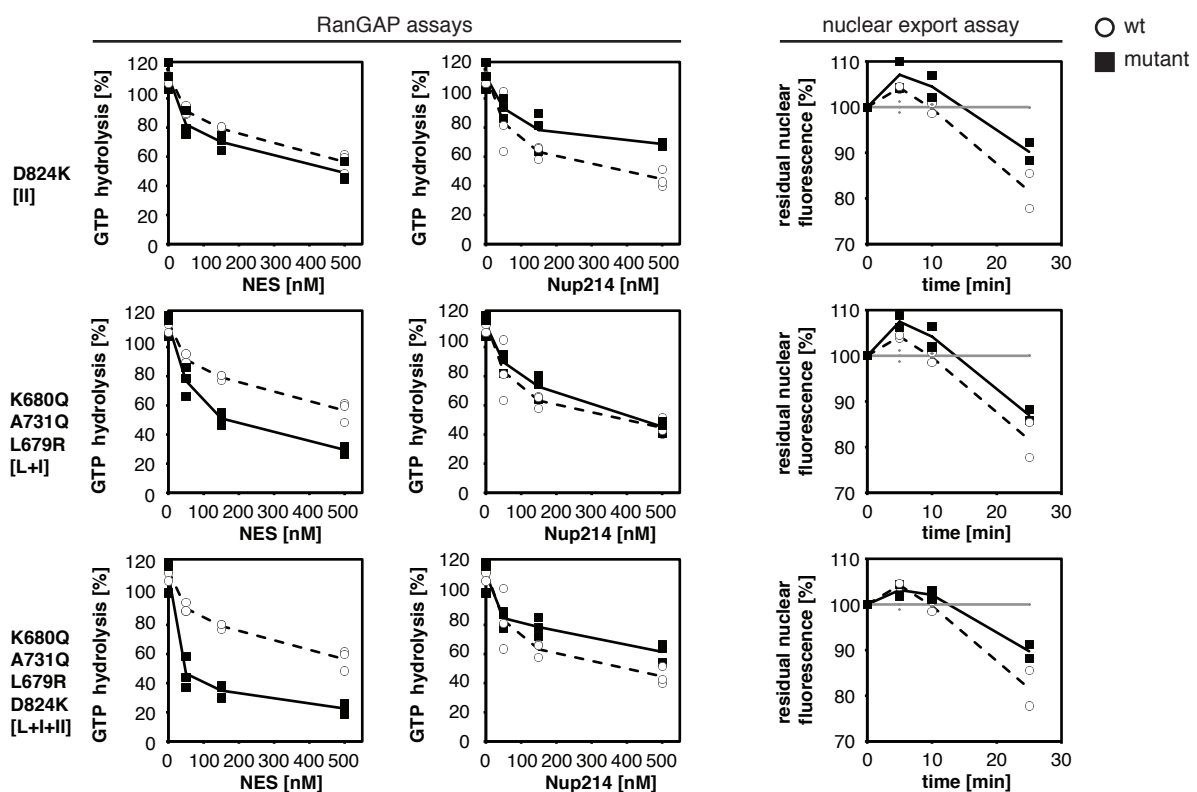


Figure 39: Differences in NES and Nup214 are not additive for the tested CRM1 double and triple mutants. The CRM1 mutants were plotted (black square) individually in comparison to the wildtype CRM1 (white circle). The average of the values is indicated by the black line for the CRM1 mutants and the dashed line for the CRM1 wildtype. The individual values and averages of three (RanGAP assays) or two (export assay) independent experiments were plotted. Square brackets indicate the altered FG-binding pocket of the CRM1 mutant. (left panel) NES peptide or (middle panel) MBP-Nup214(1916-2033)-His was titrated to 30 nM of the CRM1 mutants and Ran loaded with ^{32}P - γ -GTP in RanGAP assays. (right panel) Permeabilized GFP-NFAT cells were incubated with 30 nM of the respective CRM1 mutants. Residual nuclear fluorescence was analyzed by flow cytometry. Values were normalized to fluorescence intensities at 0 minutes and plotted in relation to a kinetic without added CRM1 (gray). Note that the plotted export kinetic for CRM1 D824 is the same as in figure 38

The description of additional mutants can be found in the appendix, figures S11 and S12.

The effects of the CRM1 mutants as observed in the described assays are summarized in table 27. For CRM1 mutants that showed altered NES/ RanGTP binding, no reliable conclusion about Nup214 binding could be drawn as it would not be clear if reduced binding to Nup214 could be attributed to actual impaired Nup214 binding or a general conformational change in CRM1. Nevertheless, a role of the mutated binding pockets in Nup214 binding cannot be ruled out. Five of the tested CRM1 mutants showed unaltered binding to an NES peptide and RanGTP. At the same time, only two out of the five mutants showed reduced binding to Nup214 in RanGAP assays. These mutations were D824K and W880K, corresponding to the binding pockets of Nup214 F1938 and F1982, respectively. It can therefore be concluded that the binding pockets II and IV on CRM1 indeed play an important role in CRM1-Nup214 interaction.

Table 27: Purified CRM1 mutants and their effect on NES binding, Nup214 binding and export.

Mutated residues	FG-pockets	Binding to NES	Binding to Nup214	Effect on export
L744W	L	=	=	not tested
K680Q A731Q	L	>	=	<
F823A	II	<	<	not tested
D824K	II	=	<	<
T917E	III	=	=	not tested
Y918W	III	=	=	=
W880A	IV	=	<	not tested
S928K	V	<	<	<
F149W	VII	<	<	not tested
A156F	VII	<	<	=
L679W K680R	L+I	<	<	not tested
K680Q A731Q L679R	L+I	>	<	<
K680Q A731Q C723M	L+I	>	=	not tested
L679R L744W	L+I	=	=	not tested
C723M L744W	L+I	<	<	not tested
K680Q A731Q L679R D824K	L+I+II	>	<	<

Summary of the results from figures 38 and 39 as well as S11 and S12. "=" indicates comparable binding/ export by the CRM1 mutant compared to the wildtype. ">" indicates increased and "<" decreased binding/ export by the CRM1 mutant.

3.5 Analysis of RanBP3-CRM1 interactions

3.5.1 The stabilization of export complexes by RanBP3 is concentration-dependent

RanBP3 had previously been identified as a co-factor that stimulates CRM1-export complex formation [240, 241]. The effect of RanBP3 on CRM1-export complex formation depended on the kind of cargo as well as on the concentration of RanBP3. The effect of different RanBP3 concentrations on the stability of different export complex was therefore analyzed by RanGAP assays, using either an NES peptide or SPN1 as cargo (figure 40). NES peptide or SPN1 were titrated to CRM1 and Ran loaded with ^{32}P - γ -GTP in the presence of absence of either a Nup214 fragment or different concentrations of RanBP3. Both tested concentrations of RanBP3 showed an increased resistance of the NES peptide-CRM1-RanGTP complex as well as of the SPN1-CRM1-RanGTP complex towards RanGAP-mediated GTP-hydrolysis. The strongest stabilization was observed when Nup214 had been added. Interestingly, the lower RanBP3 concentration led to an increased stabilization compared to the higher RanBP3 concentration for the NES peptide- as well as the SPN1-export complex. The observation that high concentrations of RanBP3 might have a relatively destabilizing effect is in agreement with published data [240]. It was recently suggested to arise from a weak interaction of the Ran binding domain of RanBP3 with the acidic loop of CRM1 [176]. The published structure showed that the NES binding cleft was closed when RanBP3 was bound to CRM1, but could be displaced by binding of an NES. High concentrations of RanBP3 would therefore outcompete NES binding, leading to a relative destabilization of the export complex [176].

Similar stabilization of the export complex by Nup214 and RanBP3 indicated that they might have similar binding modes on CRM1.

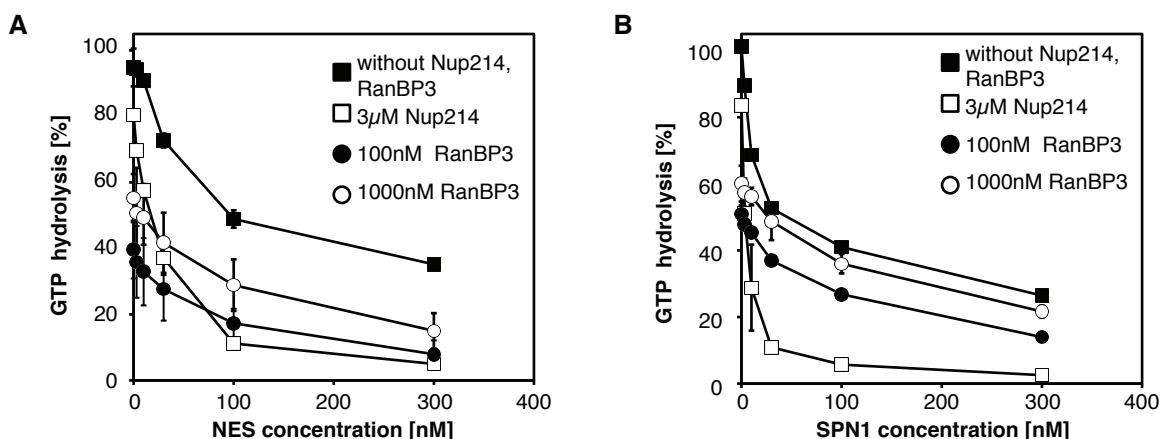


Figure 40: RanBP3 stabilizes export complexes. (A) SPN1 or (B) NES was titrated to CRM1 and Ran loaded with ^{32}P - γ -GTP in the presence of absence of either 3 μM MBP-Nup214(1930-2021)-His, 100 nM or 1000 nM RanBP3. 100 nM RanBP3 corresponded to a 1:5 molar ratio compared to CRM1 whereas 1000 nM RanBP3 was equivalent to a 2:1 molar ratio. The mean and standard deviation of two independent experiments are shown. Some error bars are too small to be seen.

3.5.2 RanBP3 and Nup214 compete for binding to CRM1 export complexes

Our crystal structures of the Nup214 complex as well as the recently published complex of the yeast homologues of CRM1, RanGTP and RanBP3 ([176]) suggest overlapping binding sites for Nup214 and RanBP3 on CRM1. It was therefore tested if Nup214 and RanBP3 competed for CRM1-binding. GST-Nup214(1930-2021) was immobilized on beads and incubated with pre-purified CRM1-RanGTP-SPN1 export complex and increasing amounts of RanBP3. Addition of 20% molar amount of RanBP3 did not significantly affect binding of the export complex to immobilized Nup214 fragment, whereas equimolar amounts of RanBP3 resulted in considerably less binding of CRM1 and SPN1 (figure 41A).

For a more quantitative analysis, Halo assays were performed. The comparison of different immobilized Nup214 fragments revealed that equimolar RanBP3 amounts nearly abolished binding of CRM1 to shorter Nup214 fragments (residues 1930-2021 and 1968-2033) whereas it only reduced CRM1-binding to Nup214(1859-2090) by 50% (figure 41B).

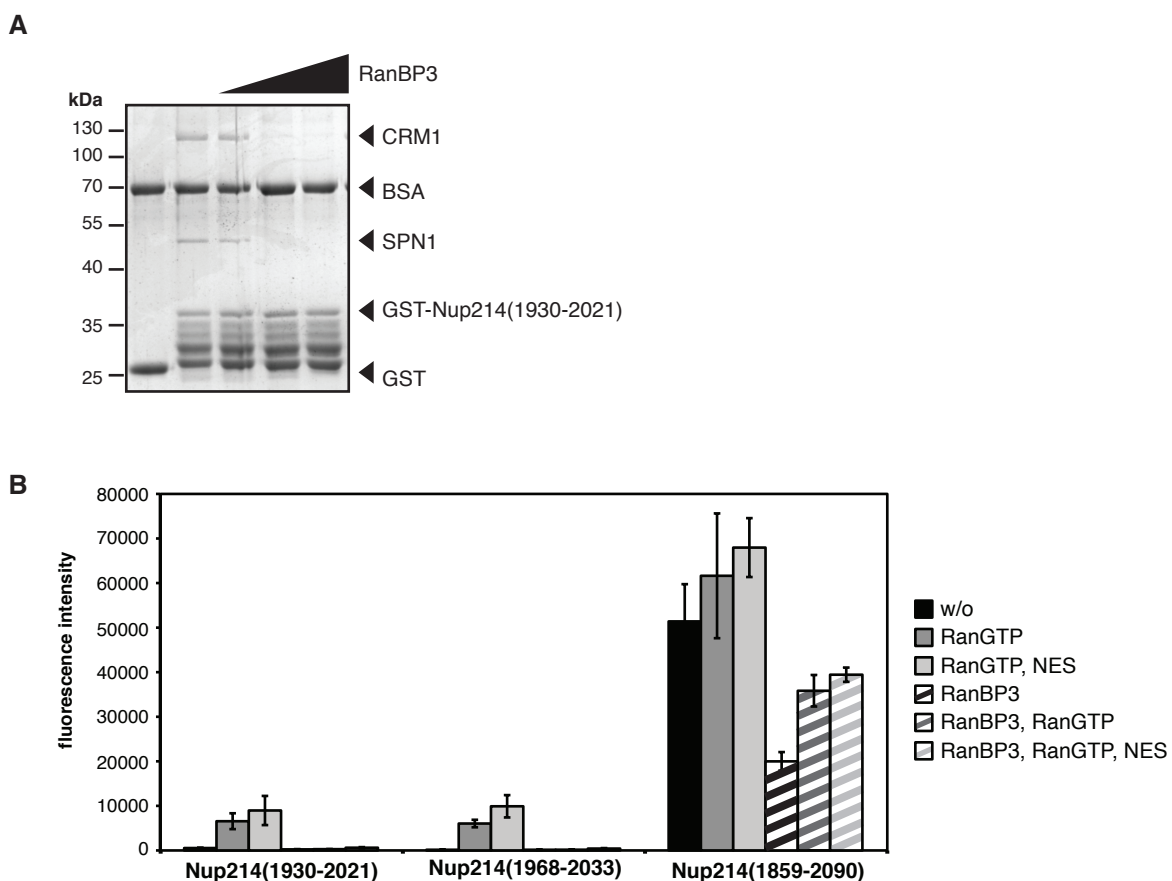


Figure 41: RanBP3 and Nup214 compete for binding to CRM1 export complexes. (A) 250 pmol GST or GST-Nup214(1930-2021) were immobilized on beads and incubated with pre-purified CRM1-RanGTP-SPN1 export complex and increasing amounts of RanBP3 (50/250/500 pmol). Bound proteins were analyzed by SDS-PAGE, followed by Coomassie-staining. (B) 50 pmol GST-Nup214(1930-2021), GST-Nup214(1968-2033) or GST-Nup214(1859-2090) were immobilized on beads and incubated with CRM1-Cy3, RanGTP or NES peptides in the absence or presence of 50 pmol RanBP3. Bound CRM1-Cy3 was quantified by flow cytometry analysis. Absolute fluorescence intensities and standard deviations of 3 independent experiments were plotted.

3.5.3 RanBP3 and Nup214 can bind free CRM1 simultaneously, but not the CRM1 export complex

Next, it was tested if binding of Nup214 and RanBP3 was mutually exclusive. GST-RanBP3 was immobilized and incubated either with pre-purified CRM1-RanGTP-SPN1 export complex or CRM1 alone in the presence or absence of Nup214. Interestingly, binding of Nup214 to immobilized RanBP3 could only be detected in the presence of free CRM1, but not in the presence of the export complex (figure 42). Furthermore, the tested Nup214(1916-2033) fragment reduced binding of the export complex to immobilized RanBP3 in agreement with the results described above (figure 41).

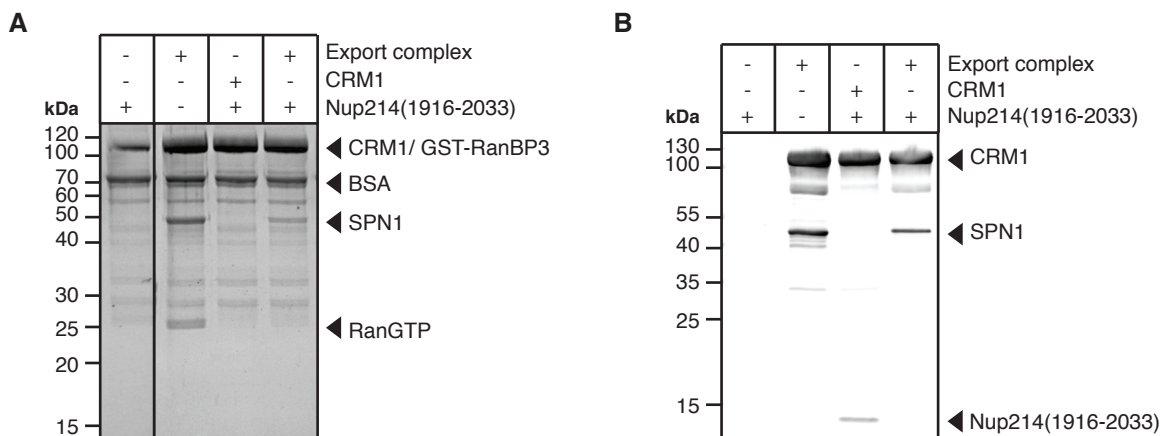


Figure 42: RanBP3 and Nup214 can bind free CRM1, but no CRM1 export complexes, simultaneously. 100 pmol GST-RanBP3 were immobilized and incubated with pre-purified CRM1-RanGTP-SPN1 export complex or CRM1 in absence or presence of His-Nup214(1916-2033)-His. Bound proteins were analyzed by SDS-PAGE, followed by (A) Coomassie-staining and (B) Western blotting with an α -His antibody to detect the His-tagged CRM1, SPN1 and Nup214.

It can therefore be concluded that Nup214 and RanBP3 compete for similar binding sites on the CRM1 export complex, but might be able to interact simultaneously with unbound CRM1 in its open conformation.

4 Discussion

4.1 The Halo assay is a novel, semi-quantitative assay for the analysis of protein-protein interactions

The Halo assay is a stable, semi-quantitative assay for the analysis of interactions between CRM1 and a variety of cargoes and Nup214 fragments. The main advantages of the assay compared to conventional gel-based pulldown assays are the easy quantification of the binding by flow cytometry and the large detection range.

Binding of Cy3-labeled CRM1 to various Nup214 fragments was probed. This included short fragments with a very low affinity like the Nup214(1868-1990) fragment as well as very long, high affinity fragments such as Nup214(1859-2090). Binding of CRM1 to Nup214(1968-1990) could not be detected in previously described conventional pulldown assays [59] whereas with the Halo assay a clear RanGTP-dependent binding was observed (figure 11). Compared to this fragment, CRM1-binding of CRM1 to the Nup214(1859-2090) fragment was $\sim 1000x$ higher.

Conventional pulldown assays rely on the analysis of the interacting proteins by SDS-PAGE followed by Coomassie- or silver staining or Western blotting. The detection limit of Coomassie staining is generally set at 100 ng protein and 10 ng for colloidal Coomassie. Silver staining allows for a detection of 1 ng [242]. Even though stains with a high sensitivity would allow the detection of very low affinity binding, direct comparison with 1000x stronger binding fragment would be difficult due to saturation of the staining.

The Halo assay therefore offers an advantage in comparison with conventional gel-based assays, as it has a detection range of at least 3 orders of magnitude.

The application range of the assay can easily be extended by fluorescence labeling of other proteins of interest, for example import receptors or any other protein. Before using a new protein in the assay, it should be ensured that the binding properties of the fluorescently labeled protein are the same as of the unlabeled protein. It is also possible to use two or more differently labeled proteins in the same assay to allow for parallel quantification of the binding.

4.2 Structural analysis of a CRM1 export complex bound to long segments of FG-repeats from Nup214

A complex containing CRM1-RanGTP-SPN1 and a Nup214(1916-2033) fragment was crystallized in this work. The obtained crystal structure of the Nup214 complex is the first structure of CRM1, or export receptors in general, with a nucleoporin-fragment. It also contains the longest FG-repeat fragment observed in any available crystal structure. The crystallization of FG-repeat-containing peptides is challenging as the fragments themselves are very hydrophobic due to their sequence and also natively unfolded [34]. In addition, the interaction of transport receptors with nucleoporins has to be transient in order for transport complexes to translocate through the nuclear pore. Therefore, interactions of karyopherins with some fragments of nucleoporins might not be stable enough to be captured in protein crystals.

Of all ten available crystal structures that contain FG-repeats, half were crystallized with short FXFG- or GLFG-peptides that contained one or two phenylalanine residues. A crystal structure of p15 and TAP bound to a 6-residue peptide derived from Nup214 (aa1810-1815) shows an

interaction with one phenylalanine (PDB ID: 1JN5, [209]). Only four out of the ten structures describe interactions between karyopherins and actual nucleoporin fragments. A structure of truncated human importin β with a 7-residue fragment of *S. cerevisiae* Nsp1p (PDB ID: 1O6O, [206]) identified one FG-binding pocket. Another crystal structure of *S. cerevisiae* importin β bound to a 39-residues fragment of *S. cerevisiae* Nup1p (PDB ID: 2BPT, [207]) contained three FG-binding pockets between the N-terminal HEAT repeats of importin β .

The only structure of CRM1 interacting with FG-repeats is the recently published structure of the yeast Yrb2 complex (PDB ID: 3WYF, [176]) with two short FG-binding regions, each binding three phenylalanine residues of Yrb2.

By contrast, our crystal structure of the Nup214 complex contains three FG-sites bound to CRM1, each with several FG-motifs. FG-site 1 is the longest of the three sites, encompassing 34 residues including three phenylalanine residues bound to CRM1. Furthermore, this FG-site is not observed in the structure of the Yrb2p complex and therefore might be exclusive for Nup214-CRM1 interaction. FG-site 2 and 3 are 8 and 18 residues long, respectively, and each bind to CRM1 with two FG-repeats. These two binding sites overlap with the binding sites of Yrb2 on CRM1.

4.3 CRM1 conformation and function is highly sensitive towards manipulation

Crystal structures of CRM1 revealed that it is a highly flexible molecule that changes its conformation upon binding to other proteins like RanGTP, cargoes as well as assembly and dissociation factors [127, 172, 177, 176]. Interaction with RanGTP and cargo leads CRM1 to change from an open, S-shaped conformation [172], to a closed- ring-like structure [127]. This massive structural change is accompanied by conformational changes within the most flexible structural features of the CRM1 molecule, the acidic loop, the NES binding cleft and the C-terminal helix. It is not surprising that the conformational changes that occur are closely interconnected. Folding-back of the acidic loop for example, triggers closing of the NES binding cleft. In the same manner, manipulation of the CRM1 molecule by mutagenesis of individual residues might trigger changes within the molecule that exceed the intended function. 63 structure-derived CRM1 mutants were cloned in this work which were designed to interfere with Nup214-binding (appendix, table S7). Of the 38 tested constructs, only 20 expressed a soluble CRM1 mutant, but many of them with a very low yield compared to the wildtype. 18 mutants were insoluble. Remarkably, solubility was not correlated with the number of mutated residues. Several single mutants were insoluble whereas several double and triple mutants were soluble and could be purified. Strikingly, mutations within the N-terminus, in particular residues L83, I102 and L134, led to insoluble protein.

Aside from the expression and purification efficiency, also the properties of the soluble CRM1 mutants varied. The 20 purified CRM1 mutants exhibited very different tolerance towards freezing and thawing as well as buffer exchanges. CRM1 H925W, for example, was completely precipitated after thawing, independent from the buffer it was frozen in.

16 purified CRM1 mutants could be tested in RanGAP assay for their binding to an NES peptide, RanGTP and Nup214 (table 27). Only six of them (five single mutants and one double mutant) exhibited an unaltered binding to RanGTP and an NES peptide. This is remarkable, as all the

mutants were designed to only block access of the Nup214 phenylalanine side chains to the hydrophobic pockets of CRM1. Even though some of the mutations chosen might appear quite drastic, e.g. leucine to tryptophan or alanine to glutamine, those combinations were specifically chosen, because according to the structure of the Nup214 complex, they seemed to be the only amino acids large enough to inhibit phenylalanine-binding to the respective hydrophobic pocket. Nevertheless, from the observed effects it is obvious that the introduced mutation led to conformational changes within the CRM1 molecule, thereby altering its affinities to RanGTP and/ or an NES peptide, even though the binding regions of RanGTP and cargoes are in distinctly different region on the CRM1 molecule compared to the mutated residues. Perhaps, some introduced large amino acids act as a wedge between the two HEAT repeats forming the respective hydrophobic pocket, thereby changing the plasticity of the whole molecule. This could lead to decreased flexibility and sterical hinderance within the molecule when changing from its open to its closed conformation. On the other hand, also the introduction of small amino acids. e.g. F823A altered binding to NES/ RanGTP whereas the introduction of larger or charged amino acids did not alter binding in case of the L679L L744W double mutant (table 27). Regarding their intended effect, most CRM1 mutants were indeed decreased in their binding to Nup214. For CRM1 mutants showing altered NES or RanGTP binding, it is difficult to interpret their effect on interaction with Nup214 and overall nuclear export.

Overall, it can be concluded that the CRM1 structure is very sensitive towards manipulation due to its sophisticated conformational changes and cooperative binding mechanisms. Mutants of CRM1 and probably other karyopherins as well, should therefore be characterized carefully and surveyed for unaltered binding to RanGTP and cargo before conclusions with respect to any other interaction partner can be drawn.

4.4 Integrative structural and functional analysis reveals that Nup214 stabilizes CRM1 export complexes by acting as a molecular clamp

4.4.1 Integration of electron microscopy, cross-linking mass spectrometry and crystallography data suggests flexible regions of Nup214 between anchored phenylalanine residues in binding pockets of CRM1

The cross-linking mass spectrometry data suggested that the more N-terminally located Nup214 residues are located closer to the cargo binding region on CRM1, whereas the more C-terminal Nup214 residues are located in the region where the N- and C-termini of CRM1 come together. All identified cross-links from the above described datasets are summarized in table 28. On the Nup214 fragments, only cross-links to the residues K1928, K1942, K1966 and K2010 were identified. The obtained cross-links were mapped on the crystal structure of the Nup214 complex and the C α -C α distances of the cross-linked residues were measurement by PyMOL (figure 43).

Table 28: Summary of the identified cross-links between Nup214 and the export complex.

Nup214 residue	Linked protein	Linked residue	Cross-linker
K1928	CRM1	K680	BS ³
		M1	BS ³
	SPN1	K167	BS ³
		K223	BS ³
		K314	BS ³
K1942	CRM1	K426	BS ³
		K446	BS ³
		K514	BS ³
		D677	EDC
		K680	BS ³
		E1013	EDC
	SPN1	M1	BS ³
		K223	BS ³
		K323	BS ³
		K327	BS ³
		K343	BS ³
	Ran	A2	BS ³
	K1966	CRM1	K22
K426			BS ³
K2010	CRM1	K22	BS ³

Some of the cross-links confirmed the crystal structure of the Nup214 complex, others should not have been linked judging from their position in the crystal structure. Even though false positive cross-links can not be excluded completely, the good compliance of the obtained intra- and intermolecular cross-links of CRM1, RanGTP and SPN1 with the crystal structure of the export complex suggest that most of the identified cross-links are specific.

Nup214 residue K1928 and CRM1 residue K680 are 27.1 Å apart in the crystal structure of the Nup214 complex and therefore within the range that can be covered by the cross-linker (figure 43A). On the other hand, SPN1 residue K167 is 57.0 Å apart from the Nup214 residue K1928 in the crystal structure and therefore the cross-linker should not be able to cover the distance between them (figure 43B).

Nup214 K1942 targets six residues on two sides of the CRM1 molecule as well as five residues on SPN1 and one on RanGTP (figure 43C). Most of these residues are too far away from K1942 in the crystal structure to be linked. K1942 lies within FG-site 1 on a loosely attached 8-residue stretch between two hydrophobic pockets on CRM1 that anchor Nup214 residues F1938 and F1947. From the cross-linking mass spectrometry data, one could speculate that this stretch might be flexible when the complex is in solution, thereby allowing K1942 to cross-link to the identified residues. Nevertheless, as long as Nup214 residues F1938 and F1947 are inserted in the binding pockets of CRM1, the flexibility would not be high enough to explain all the identified interactions.

The same holds true for Nup214 residue K1966 (figure 43D). K1966 could not be identified in the crystal structure of the Nup214 complex. It is located on a 29 residue-stretch between FG-sites 1 and 2. That fact that no density could be observed for these residues in the X-ray crystallography data already indicated a high flexibility of the region. This flexibility could account for cross-links between K1966 and CRM1 residues K22 as well as K426.

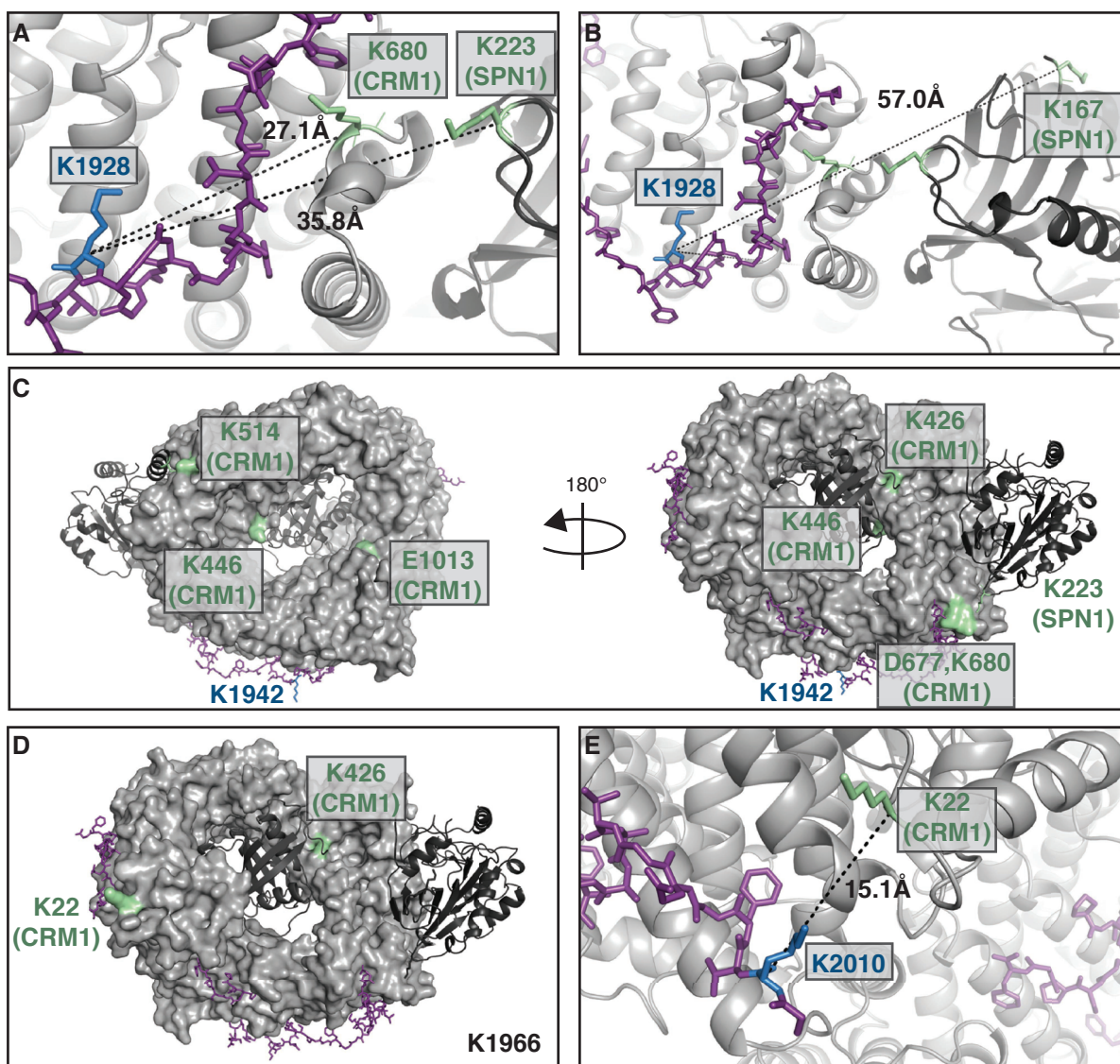


Figure 43: The cross-linking results were mapped on the crystal structure of the Nup214 complex. Nup214 (purple) in stick representation. Cross-linked residues of Nup214 are highlighted in blue. (A)-(B) CRM1 is shown in gray as a cartoon representation. Cross-linked residues of CRM1 are highlighted in green and as stick representation. Cross-links of the Nup214 residue K1928 to (A) CRM1 K680 and SPN1 K223 and (B) SPN1 K167 are shown. Cross-links are shown with a dashed line, respective $C\alpha$ - $C\alpha$ distances are indicated. (C)-(D) CRM1 is shown in gray as a cartoon representation. Cross-linked residues of CRM1 are highlighted in green. (C) Nup214 K1942 cross-links to the indicated residues of the export complex. (D) K1966 is not present in the crystal structure, but was shown to link to CRM1 residues K22 and K426 on opposite sides of the CRM1 ring. (E) Nup214 K2010 links to CRM1 K22. The cross-link is indicated by a dashed line, the $C\alpha$ - $C\alpha$ distance between the two residues is 15.1 Å.

Nup214 residue K2010 links only to CRM1 residue K22 which is 15.1 Å away in the crystal structure (figure 43E). As K2010 is very close to F2012, which is deeply inserted into a

hydrophobic pocket on CRM1, it is not surprising that the position of K2010 seems fixed as well, therefore allowing it only to cross-link to residues in close proximity.

The results of the cross-linking mass spectrometry and crystallization only partially match. It is likely that the obtained crystal structure represents only one possible conformation of the Nup214 complex. The Nup214 fragment contains many residues that are only loosely attached to the CRM1 surface or cannot be observed by X-ray crystallography, because they are too flexible. It is plausible that these flexible regions might behave differently when the complex is in solution as in the cross-linking samples, compared to the crystal environment.

The flexibility of several region of CRM1 as suggested by missing densities in crystallography data as well as cross-links all over the export complex by some Nup214 residues in the mass spectrometry data, could also explain the challenge to obtain meaningful data with electron microscopy. As single particle electron microscopy relies on averaging several thousands of micrographs, flexible regions in a protein cannot be observed by electron microscopy. The cross-linking data suggested high flexibility at the N-terminus of the Nup214 fragment including its N-terminal tags, explaining why all tested tags could not be observed by electron microscopy. Furthermore, the epitope of the Nup214 antibody used in electron microscopy samples ranges from 1934-1946, a region including and adjoining the residues F1938 and F1947 which are bound by hydrophobic pockets. The epitope might therefore not be accessible to the antibody when Nup214 is bound to CRM1.

In summary, the structural data suggest that Nup214 binds to CRM1 mainly via the phenylalanine side chain that insert into hydrophobic pockets on the CRM1 molecule. The residues between these bound phenylalanines are either loosely attached to the outer surface of CRM1 or flexible in solution.

4.4.2 Nup214 couples the N- and C-terminal arch of CRM1

The crystal structure of the Nup214 complex revealed that Nup214 winds along the outer surface of the CRM1 molecule from HEAT repeat 14 close to the cargo binding region on CRM1, across the contact region of the CRM1 C- and N-termini up to HEAT repeat 4. Three binding regions of Nup214 were identified on CRM1 and even though there was no density for Nup214 residues in the crystal structure that directly interact with the N- and C- terminal HEAT repeats of CRM1, the structural data suggests that Nup214 stabilizes CRM1 export complexes by coupling the N- and C-terminal arches of CRM1 through interactions of phenylalanine side chains with hydrophobic pockets on both halves of the molecule.

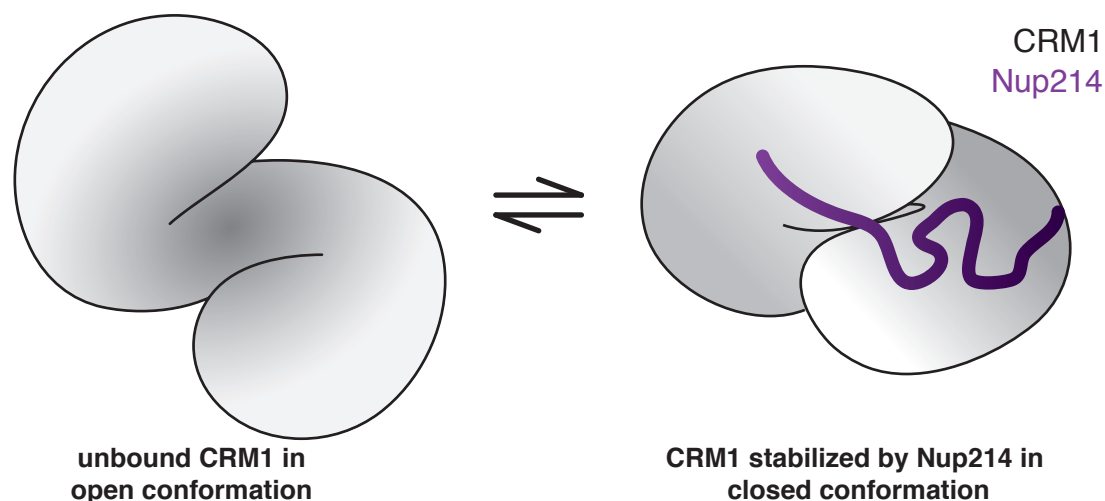


Figure 44: Nup214 stabilizes the closed conformation of CRM1 by acting as a molecular clamp. Unbound CRM1 (gray) occurs mainly in the open conformation. CRM1 adapts a closed conformation upon binding to RanGTP and/ or cargo which can be stabilized by Nup214 (purple).

This hypothesis could be reinforced by the binding assays with the structure-derived Nup214 mutants X1, X2 and X3. In the Nup214 X1 mutant all phenylalanine residues that bound to CRM1 in the C-terminal half were mutated, whereas all phenylalanine residues that bound to the N-terminal HEAT repeats of CRM1 were mutated in X2. While Nup214 X1 showed reduced binding in pulldown assays, binding of Nup214 X2 was only slightly altered. Only the combination of the mutations in the Nup214 X3 mutant abolished binding to CRM1 completely. Also the effect of the Nup214 X1 and X2 mutations compared to the wildtype in cellular binding assays was rather minimal. Nup214(1859-2090) X2 fused to RFP-cNLS did not have any effect on the localization of the co-transfected GFP-SPN1 compared to the wildtype, the respective X1 construct only led to re-localization of GFP-SPN1 in ~30% of the cells. The binding assays therefore indicate that binding of the Nup214 phenylalanines to either one of the CRM1 halves is enough to mediate a stable binding. This is in strong contrast to the observed effects of the X1 and X2 fragments in RanGAP assays. Even though both fragments clearly bind to CRM1 in the binding assays, they hardly stabilize the CRM1-RanGTP complex towards RanGAP-mediated hydrolysis. This indicates that Nup214 can bind stably to CRM1 by interacting with either one of the arches, but needs binding to both the C-terminal and the N-terminal halves of CRM1 in order to stabilize the complex and protect it from RanGAP-induced GTP-hydrolysis. This suggestion is in agreement with the observed binding behaviors and stabilization effect of truncated Nup214 fragments. Nup214(1916-2033) and Nup214(1930-2021) fragments both form stable export complexes with SPN1 (figure17). Truncation of residues 1916-1929 of the N-terminus of the Nup214 standard fragment removes F1922, which is inserted in FG-pocket I in the crystal structure of the Nup214 complex. On the other hand, truncation of residues 2022-2033 from the C-terminus of the standard fragment removes F2024, which was found inserted into FG-pocket VII in the structure. The removal of either one of these interacting phenylalanine residues led to a decrease in the stabilization against RanGAP-mediated complex dissociation in RanGAP assays (figure 18A). Judging from the RanGAP assays, the truncation of F1922 is less drastic than the truncation of F2024, which can be explained by the

fact that the respective truncations contain four more phenylalanine residues binding to CRM1 in the C-terminal half of CRM1 and two more in the N-terminal half, respectively. Truncation of the N- and the C-terminus as in the Nup214(1930-2021) fragment did not show any stabilization of the CRM1-RanGTP complex in RanGAP assays, similar to the Nup214(1916-2033) X3 mutant, in which all binding phenylalanines were mutated to serine. In the absence of cargo, as shown with the RanGAP assays, binding of the remaining phenylalanines is apparently not strong enough to counteract the opening of the CRM1 molecule as initiated by interaction of the Ran C-terminus with the acidic loop of CRM1. In the presence of a cargo, CRM1 is held in the closed conformation by NES binding to the cleft. Nup214 does not have to counteract conformational changes and therefore also the X1 and X2 mutant as well as the truncated Nup214(1930-2021) can stably bind the export complex.

In summary, the crystal structure of the Nup214 complex combined with the Nup214 mutant binding assay data suggest that Nup214 stabilizes the export complex by binding to hydrophobic pockets on the C- and N-terminal halves of CRM1, thereby acting as a molecular clamp. The N- and C-terminus of CRM1 are held together by the clamp thereby defending the closed conformation of the CRM1 molecule against intrinsic and extrinsic stimuli for complex dissociation. This would suggest that Nup214 has to detach from CRM1 before the dissociation of the export complex can be induced by RanBP1 or Ran-binding domains of Nup358 [24].

4.5 Interaction of FG-nucleoporins and karyopherins might rely on overlapping as well as specific binding sites

4.5.1 Comparison of binding sites from Nup214 and RanBP3 on CRM1

Crystal structures of FG-repeats bound to importin β revealed binding of GLFG and FXFG repeats via phenylalanine side chains to overlapping hydrophobic pockets between HEAT repeats 5/6, 6/7 and 7/8 indicating that these pockets bind phenylalanines most stably in importin β [122, 206, 207].

A crystal structure of the RanBP3 yeast homologue Yrb2p in complex with the yeast homologues of CRM1 (Xpo1p) and Ran-GTP (Gsp1p-GTP) was published recently [176]. RanBP3 contains two FG-repeat motifs and a C-terminal Ran binding domain. Comparison of the Nup214-CRM1-RanGTP-SPN1 crystal structure with the crystal structure of Xpo1p-Gsp1pGTP-Yrb2p revealed partially overlapping binding sites for Nup214 and the RanBP3 homologue on CRM1 in a similar manner as shown for the GLFG and FXFG repeats in importin β . Alignments for CRM1/Xpo1 and RanBP3/Yrb2 can be found in the appendix (figures S5, S7).

The overall crystal structure of human CRM1 as found by us and others is also similar to the *S. cerevisiae* Xpo1p protein (appendix, figure S14A). The HEAT repeats of CRM1 within the Nup214 complex structure and Xpo1p within the Yrb2 complex align very well and form the characteristic ring-shaped structure. The major difference in CRM1 conformation of the structures can be observed in two distinct regions, the acidic loop and the C-terminal helix (appendix, figure S14B,C). In the structure of the Nup214 complex, the acidic loop of CRM1 is

folded across its ring and interacts with residues on the inner surface of HEAT repeat 15. The C-terminal helix (HEAT repeat 21B) is folded back onto the ring and located in a stack with the other HEAT repeats. The position of the acidic loop as well as the C-terminal helix is in accordance with other cargo-containing crystal structures of CRM1, e.g. in [127]. On the other hand, the structure of Xpo1p in complex with Yrb2p shows distinctly different conformations of these structural features. Here, the acidic loop of Xpo1p is folded back onto the inside of the ring, its residues interacting with the inner surface of HEAT repeats 11 and 12. This is similar to the position of the acidic loop in unligated CRM1 as well as CRM1 bound to RanBP1 [172, 177]. Strikingly different is the position of the C-terminal helix of Xpo1p. In all previously available crystal structures in which the C-terminal helix had not been truncated, it was either located in a stack with the other HEAT-repeats or spanning across the ring of the molecule and interacting with the inner surface of HEAT repeats 10. The C-terminal helix of Xpo1p in complex with Yrb2p is folded away from the ring, in exactly the opposite direction as found in other structures (appendix, figure S14C) .

Comparison of the binding of Nup214 and Yrb2p to CRM1 or Xpo1p, respectively, reveals similarities as well as differences in the interacting regions (figure 45). FG-repeats from Nup214 and the RanBP3 homologue both bind to hydrophobic pockets on CRM1/ Xpo1p. The Nup214 fragments wraps around the outer surface of the CRM1 toroid, starting at FG-site 1 between HEAT repeat 14 and 15 and continuing to FG-site 2 between HEAT repeat 19 and 20 and further more to FG-site 3 along HEAT repeats 2 to 4. Apart from the Ran binding domain, only two short FG-repeat containing segments could be identified from Yrb2. The binding regions of Yrb2 correspond to the Nup214 FG-site 2 and 3. The Yrb2 FG-fragments spanned residues 97-110 and 141-155 and contained four and three phenylalanines, respectively. Phenylalanines F98, F100 and F106 of the first segment and F142, F148 and F152 of the second segment were shown to bind to hydrophobic pockets on Xpo1p. Yrb2p residue F100 binds to the same cavity as Nup214 residue F1982. The same is true for Yrb2p residues F106, F142 and F152 binding to the same hydrophobic pockets as Nup214 residues F1988, F2012 and F2024, respectively. On the other hand, Yrb2p residues F98 and F148 do not have a corresponding phenylalanine on Nup214. Furthermore the bound Nup214 residues F1922, F1938 and F1947 do not have a corresponding phenylalanine on Yrb2p.

In agreement with these overlapping interaction sites of the RanBP3 homologue and Nup214 on CRM1 are the observations from the binding assays that suggested a mutually exclusive binding for RanBP3 and Nup214 to the CRM1 export complex (figure 41). The comparison of Nup214 and Yrb2 binding to CRM1 and Xpo1, respectively, suggests that the set of hydrophobic pockets on CRM1 used to interact with nucleoporins overlaps, but is not identical.

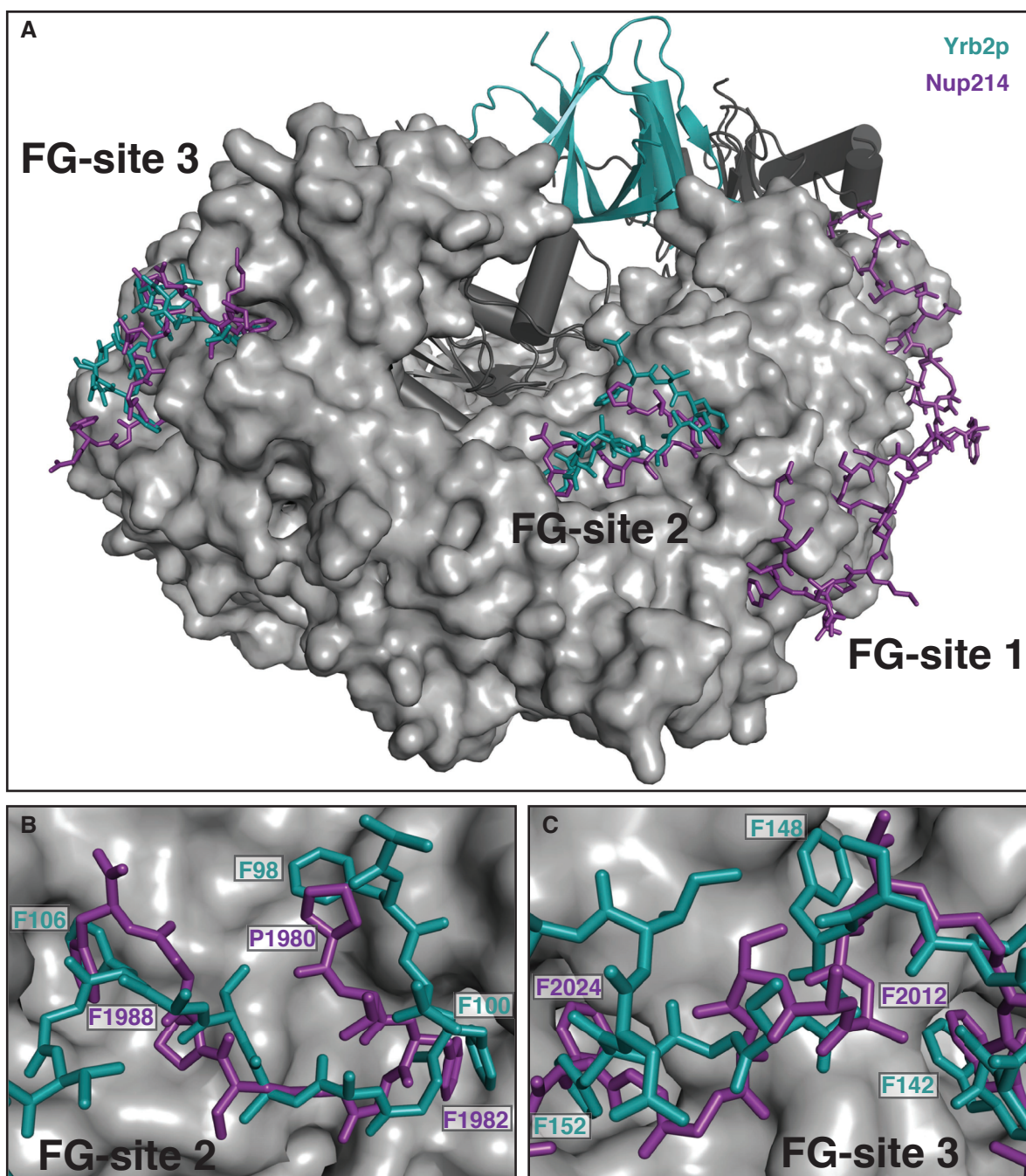


Figure 45: Comparison of the crystal structures of the Nup214-CRM1-RanGTP-SPN1 complex and the Xpo1p-Gsp1pGTP-Yrb2p complex. Yrb2 is superimposed on the crystal structure of the Nup214 complex. CRM1 (light gray, surface representation), RanGTP and SPN1 (dark gray, cartoon representation) and Nup214 (purple, stick representation) from the Nup214 complex and Yrb2 (cyan, stick representation) from the Yrb2 complex are shown. (A) The superposition of the two complexes reveals that Yrb2 and Nup214 share FG-site 2 and 3 on CRM1, while FG-site 1, the longest Nup214 segment, is exclusive for Nup214. (B)-(C) Detail views of FG-site 2 and 3. Although the binding of Nup214 and Yrb2 to hydrophobic pockets overlaps for some phenylalanine residues (e.g. Yrb2 F142 and Nup214 F2012 in (C)), the backbone trace and side chain positioning varies for most parts of the two proteins.

4.5.2 Implications for the interaction of CRM1 with other nucleoporins

It was shown that some binding sites for Nup214 and RanBP3 on CRM1 overlap, while others are specific for the respective protein (figure 45). Therefore, it could be speculated that this is true for the interaction of CRM1 with other FG-nucleoporins as well. CRM1 mutants impaired for binding to Nup214 might therefore also be altered in their binding to other FG-Nups, e.g. Nup62. This would have several implications on the interpretation of *in vitro* transport assays with CRM1 mutants as described above (figures 38, 39). On one hand, the observed export defect of some CRM1 mutants could not be attributed solely to a defect in Nup214-binding. It could be an accumulation of binding defects to FG-nucleoporins in general that slows down the export of the cargo. On the other hand, not only the export might be altered in CRM1 mutants with reduced binding affinities to FG-nucleoporins, also the re-import of CRM1 into the nucleus relies on the interaction of CRM1 with FG-nucleoporins. Reduced export of NFAT in the described transport assays can therefore not be equated with reduced binding of the respective CRM1 mutants to Nup214. More likely, it can be ascribed to reduced binding to FG-nucleoporins in general, leading to decreased export and re-import of the respective mutants. The probability that a CRM1 mutant shows impaired binding to several FG-Nups increases with every additional FG-pocket mutated. Nevertheless, keeping in mind that there might not only be overlapping, but also exclusive FG-sites for binding of nucleoporins to CRM1, it cannot be excluded that an observed transport defect is indeed a consequence of reduced binding to Nup214 only.

4.6 Regulation of nuclear transport by nucleoporin-karyopherin interactions

All current models of nucleocytoplasmic transport rely on the interaction of transport receptors with FG-nucleoporins. Our crystal structure revealed seven FG-binding pockets on CRM1. From the distribution of hydrophobicity on the structure it is likely that there are several more pockets that did not bind the Nup214 fragment used in this study. It could be speculated that the additional binding pockets interact with other FG-repeat regions in Nup214 that were previously described [234].

The large number of FG-binding pockets on CRM1 is in accordance with previous molecular dynamics studies, which suggested up to 14 binding sites for FG-repeats in the yeast transport receptor Cse1p [243]. Therefore, the question arises why transport receptors have so many different binding pockets. The results of this work indicate that the binding sites of FG-nucleoporins to transport receptors overlap partially, but not completely. Therefore, it could be speculated that transport receptors do not indiscriminately bind any nucleoporin with any hydrophobic pocket on their surface. The pattern of phenylalanine residues within the nucleoporins, as well as the residues that connect them might be an important factor for the affinity of a transport receptor to a nucleoporin. Furthermore, also the pattern of hydrophobic FG-binding pockets on a respective transport receptor could increase its affinity to a nucleoporin with a corresponding pattern of phenylalanine residues. The need for a matching pattern of phenylalanine residues in the FG-Nups and FG-binding pockets on the transport receptor would explain why, for example, Nup214 interacts specifically with CRM1, but not with other transport receptors (figure 13). In addition, the matching patterns of the FG-binding pockets on CRM1 and the phenylalanines within Nup214 could explain why the tested Nup214 fragment and CRM1 interact with such high an avidity.

Furthermore, the patterns of FG-binding pockets on the surface of transport receptors are likely to vary, depending on the conformation of the transport receptor. Extensive structural changes between unbound receptors and RanGTP- or cargo-loaded transport receptors as observed for CRM1 [127, 172], could induce different sets of hydrophobic pockets on their surface. This could lead to a changed affinity of the receptors to specific nucleoporins in their unbound and bound state. The interaction of transport receptors with different sets of nucleoporins in case they are unbound, loaded with cargo or bound to any other transport factor, could have direct consequences on the directionality of their translocation through the nuclear pore complex. Therefore, it could be speculated that a changed affinity of transport receptors to nucleoporins due to conformational changes upon binding to different proteins, could prime the receptors for nuclear import or export, in which case models of nucleocytoplasmic transport should be revised to include a component accounting for the directionality of the translocation through the nuclear pore complex.

4.7 Outlook

First, it should be tested if a combination of the two CRM1 mutations that exhibited unaltered binding of CRM1 to NES and RanGTP, but reduced binding to a Nup214 fragment (CRM1 D824K and W800A mutants), would have a cumulative effect on Nup214-binding. Therefore, the double mutant should be cloned and tested in RanGAP assays and an export assay as described above for the other CRM1 mutants.

It was shown that the FG-binding sites for Nup214 and RanBP3 on CRM1 partially overlap. It would therefore be interesting to test if this is also the case for other FG-nucleoporins. A first step would be to check if different FG-nucleoporins compete for binding to CRM1. This could be done by *in vitro* binding assays with different nucleoporins immobilized and titration of other FG-nucleoporins, for example Nup62 or Nup98. Next, it could be tested if CRM1 mutants that showed a defect in Nup214 binding, like CRM1 D824K, are also impaired in their binding to other FG-nucleoporins. For this, RanGAP assays could be performed with CRM1 mutants and titration of different FG-Nups in the same manner as described above for Nup214. Moreover, possible CRM1-interacting FG-repeats in the other FG-nucleoporins could be identified by analyzing different Nup-mutants or truncations. It could also be attempted to get crystal structures of the CRM1 export complex with other FG-nucleoporins to ultimately identify the respective binding sites.

Once there is a first idea of where on CRM1 the other FG-nucleoporins bind to and which residues on the nucleoporins mediate the binding, it would be interesting to see if other nucleoporins also stabilize the export complex by acting as a molecular clamp or if that is a specific and novel mechanism of Nup214. With respect to the molecular clamp mechanism, analysis should also focus on the Nup214(1859-2090) fragment, which corresponds to the major FG-repeat region. The affinity of this Nup214 fragment to CRM1 is a lot higher compared to the fragment used for the crystallization of the Nup214 complex. The Nup214(1859-2090) fragment can form stable complexes with CRM1 and RanGTP even in the absence of cargo. Information about which additional residues of this fragments are also involved in the binding to CRM1 and moreover about the region on CRM1 that they interact with, could not only verify the molecular clamp mechanism, but maybe also give an idea about how CRM1 export complexes bound to Nup214 are actually able to dissociate.

Taken together, all these aspects would help to further elucidate the complex cycle of nucleocytoplasmic transport.

References

- [1] M. Breeuwer and D. S. Goldfarb, Facilitated nuclear transport of histone H1 and other small nucleophilic proteins, *Cell* **60**(6), 999–1008 (1990).
- [2] M. Kurz, D. Doenecke, and W. Albig, Nuclear transport of H1 histones meets the criteria of a nuclear localization signal—mediated process, *Journal of Cellular Biochemistry* **64**(4), 573–578 (1997).
- [3] K. Schwamborn, W. Albig, and D. Doenecke, The Histone H1(0) Contains Multiple Sequence Elements for Nuclear Targeting, *Experimental Cell Research* **244**(1), 206–217 (1998).
- [4] M. Kumeta, H. Yamaguchi, S. H. Yoshimura, and K. Takeyasu, Karyopherin-independent spontaneous transport of amphiphilic proteins through the nuclear pore, *Journal of Cell Science* **125**(21), 4979–4984 (2012).
- [5] T. U. Schwartz, Modularity within the architecture of the nuclear pore complex, *Curr Opin Struct Biol* **15**(2), 221–226 (2005).
- [6] J. G. Gall, Octagonal Nuclear Pores, *J Cell Biol* **32**(2), 391–399 (1967).
- [7] J. E. Hinshaw, B. O. Carragher, and R. A. Milligan, Architecture and design of the nuclear pore complex, *Cell* **69**(7), 1133–1141 (1992).
- [8] C. Akey and M. Radermacher, Architecture of the *Xenopus* nuclear pore complex revealed by three-dimensional cryo-electron microscopy, *J Cell Biol* **122**(1), 1–19 (1993).
- [9] D. Stoffler, B. Feja, B. Fahrenkrog, J. Walz, D. Typke, and U. Aebi, Cryo-electron tomography provides novel insights into nuclear pore architecture: implications for nucleocytoplasmic transport, *J Mol Biol* **328**(1), 119–130 (2003).
- [10] M. Beck, F. Förster, M. Ecke, J. M. Plitzko, F. Melchior, G. Gerisch, W. Baumeister, and O. Medalia, Nuclear Pore Complex Structure and Dynamics Revealed by Cryoelectron Tomography, *Science* **306**, 1387–1390 (2004).
- [11] J. M. Cronshaw, A. N. Krutchinsky, W. Zhang, B. T. Chait, and M. J. Matunis, Proteomic analysis of the mammalian nuclear pore complex, *J Cell Biol* **158**(5), 915–927 (2002).
- [12] J. Fiserova, E. Kiseleva, and M. W. Goldberg, Nuclear envelope and nuclear pore complex structure and organization in tobacco BY-2 cells, *Plant J* **59**(2), 243–255 (2009).
- [13] Q. Yang, M. P. Rout, and C. W. Akey, Three-Dimensional Architecture of the Isolated Yeast Nuclear Pore Complex: Functional and Evolutionary Implications, *Mol Cell* **1**(2), 223–234 (1998).
- [14] M. P. Rout, J. D. Aitchison, A. Suprapto, K. Hjertaas, Y. Zhao, and B. T. Chait, The yeast nuclear pore complex: composition, architecture, and transport mechanism, *J Cell Biol* **148**(4), 635–651 (2000).
- [15] K. H. Bui, A. von Appen, A. L. DiGuilio, A. Ori, L. Sparks, M.-T. Mackmull, T. Bock, W. Hagen, A. Andrés-Pons, J. S. Glavy, and M. Beck, Integrated Structural Analysis of the Human Nuclear Pore Complex Scaffold, *Cell* **155**, 1233–1243 (2013).
- [16] C. W. Akey, Structural Plasticity of the Nuclear Pore Complex, *J Mol Biol* **248**, 273–293 (1995).
- [17] G. Rabut, V. Doye, and J. Ellenberg, Mapping the dynamic organization of the nuclear pore complex inside single living cells, *Nat Cell Biol* **6**(11), 1114–1121 (2004).
- [18] A. Hoelz, E. W. Debler, and G. Blobel, The structure of the nuclear pore complex, *Annu Rev Biochem* **80**, 613–643 (2011).
- [19] K.-C. Hsia, P. Stavropoulos, G. Blobel, and A. Hoelz, Architecture of a Coat for the Nuclear Pore Membrane, *Cell* **131**(7), 1313–1326 (2007).
- [20] D. Devos, S. Dokudovskaya, R. Williams, F. Alber, N. Eswar, B. T. Chait, M. P. Rout, and A. Sali, Simple fold composition and modular architecture of the nuclear pore complex, *Proc Natl Acad Sci U S A* **103**(7), 2172–2177 (2006).
- [21] K. J. Ryan and S. R. Wentz, The nuclear pore complex: a protein machine bridging the nucleus and cytoplasm, *Curr Opin Cell Biol* **12**(3), 361–371 (2000).
- [22] A. Radu, M. S. Moore, and G. Blobel, The peptide repeat domain of nucleoporin Nup98 functions as a docking site in transport across the nuclear pore complex, *Cell* **81**(2), 215–222 (1995).

- [23] J. Katahira, K. Strässer, A. Podtelejnikov, M. Mann, J. U. Jung, and E. Hurt, The Mex67p-mediated nuclear mRNA export pathway is conserved from yeast to human, *EMBO J* **18**(9), 2593–2609 (1999).
- [24] R. H. Kehlenbach, A. Dickmanns, A. Kehlenbach, T. Guan, and L. Gerace, A Role for RanBP1 in the Release of CRM1 from the Nuclear Pore Complex in a Terminal Step of Nuclear Export, *J Cell Biol* **145**(4), 645–657 (1999).
- [25] B. Hülsmann, A. Labokha, and D. Görlich, The Permeability of Reconstituted Nuclear Pores Provides Direct Evidence for the Selective Phase Model, *Cell* **150**(4), 738–751 (2012).
- [26] B. Fahrenkrog and U. Aebi, The nuclear pore complex: nucleocytoplasmic transport and beyond, *Nat Rev Mol Cell Biol* **4**(10), 757–766 (2003).
- [27] M. P. Rout, J. D. Aitchison, M. O. Magnasco, and B. T. Chait, Virtual gating and nuclear transport: the hole picture, *Trends Cell Biol* **13**(12), 622–628 (2003).
- [28] D. J. Dilworth, A. Suprpto, J. C. Padovan, B. T. Chait, R. W. Wozniak, M. P. Rout, and J. D. Aitchison, Nup2p Dynamically Associates with the Distal Regions of the Yeast Nuclear Pore Complex, *J Cell Biol* **153**(7), 1465–1478 (2001).
- [29] L. A. Strawn, T. Shen, N. Shulga, D. S. Goldfarb, and S. R. Wentz, Minimal nuclear pore complexes define FG repeat domains essential for transport, *Nat Cell Biol* **6**, 197–206 (2004).
- [30] S. Krull, J. Thyberg, B. Björkroth, H.-R. Rackwitz, and V. C. Cordes, Nucleoporins as components of the nuclear pore complex core structure and Tpr as the architectural element of the nuclear basket, *Mol Biol Cell* **15**, 4261–4277 (2004).
- [31] E. R. Griffis, S. Xu, and M. A. Powers, Nup98 Localizes to Both Nuclear and Cytoplasmic Sides of the Nuclear Pore and Binds to Two Distinct Nucleoporin Subcomplexes, *Mol Biol Cell* **14**(2), 600–610 (2003).
- [32] B. Fahrenkrog, J. Köser, and U. Aebi, The nuclear pore complex: a jack of all trades?, *Trends Biochem Sci* **29**(4), 175–182 (2004).
- [33] B. Fahrenkrog, B. Maco, A. M. Fager, J. Köser, U. Sauder, K. S. Ullman, and U. Aebi, Domain-specific antibodies reveal multiple-site topology of Nup153 within the nuclear pore complex, *J Struct Biol* **140**(1-3), 254 – 267 (2002).
- [34] D. P. Denning, S. S. Patel, V. Uversky, A. L. Fink, and M. Rexach, Disorder in the nuclear pore complex: the FG repeat regions of nucleoporins are natively unfolded, *Proc Natl Acad Sci U S A* **100**(5), 2450–2455 (2003).
- [35] N. P. Allen, S. S. Patel, L. Huang, R. J. Chalkley, A. Burlingame, M. Lutzmann, E. C. Hurt, and M. Rexach, Deciphering Networks of Protein Interactions at the Nuclear Pore Complex, *Mol Cell Proteomics* **1**(12), 930–946 (2002).
- [36] L. Huang, M. A. Baldwin, D. A. Maltby, K. F. Medzihradzky, P. R. Baker, N. Allen, M. Rexach, R. D. Edmondson, J. Campbell, P. Juhasz, S. A. Martin, M. L. Vestal, and A. L. Burlingame, The Identification of Protein-Protein Interactions of the Nuclear Pore Complex of *Saccharomyces cerevisiae* Using High Throughput Matrix-assisted Laser Desorption Ionization Time-of-Flight Tandem Mass Spectrometry, *Mol Cell Proteomics* **1**, 434–450 (2002).
- [37] R. Bernad, H. van der Velde, M. Fornerod, and H. Pickersgill, Nup358/RanBP2 attaches to the nuclear pore complex via association with Nup88 and Nup214/CAN and plays a supporting role in CRM1-mediated nuclear protein export, *Mol Cell Biol* **24**(6), 2373–2384 (2004).
- [38] S. G. Brohawn and T. U. Schwartz, Molecular architecture of the Nup84-Nup145C-Sec13 edge element in the nuclear pore complex lattice, *Nat Struct Mol Biol* **16**(11), 1173–1177 (2009).
- [39] N. Belgareh, G. Rabut, S. W. Bai, M. van Overbeek, J. Beaudouin, N. Daigle, O. V. Zatssepina, F. Pasteau, V. Labas, M. Fromont-Racine, J. Ellenberg, and V. Doye, An evolutionarily conserved NPC subcomplex, which redistributes in part to kinetochores in mammalian cells, *J Cell Biol* **154**(6), 1147–1160 (2001).
- [40] S. Vasu, S. Shah, A. Orjalo, M. Park, W. H. Fischer, and D. J. Forbes, Novel vertebrate nucleoporins Nup133 and Nup160 play a role in mRNA export, *J Cell Biol* **155**(3), 339–354 (2001).

- [41] T. C. Walther, A. Alves, H. Pickersgill, I. Loïodice, M. Hetzer, V. Galy, B. B. Hülsmann, T. Köcher, M. Wilm, T. Allen, I. W. Mattaj, and V. Doye, The Conserved Nup107-160 Complex Is Critical for Nuclear Pore Complex Assembly, *Cell* **113**(2), 195–206 (2003).
- [42] T. Boehmer, J. Enninga, S. Dales, G. Blobel, and H. Zhong, Depletion of a single nucleoporin, Nup107, prevents the assembly of a subset of nucleoporins into the nuclear pore complex, *Proc Natl Acad Sci U S A* **100**(3), 981–985 (2003).
- [43] A. Harel, A. V. Orjalo, T. Vincent, A. Lachish-Zalait, S. Vasu, S. Shah, E. Zimmerman, M. Elbaum, and D. J. Forbes, Removal of a Single Pore Subcomplex Results in Vertebrate Nuclei Devoid of Nuclear Pores, *Mol Cell* **11**(4), 853–864 (2003).
- [44] I. Loïodice, A. Alves, G. Rabut, M. van Overbeek, J. Ellenberg, J.-B. Sibarita, and V. Doye, The Entire Nup107-160 Complex, Including Three New Members, Is Targeted as One Entity to Kinetochores in Mitosis, *Mol Biol Cell* **15**, 3333–3344 (2004).
- [45] T. Stuwe, A. R. Correia, D. H. Lin, M. Paduch, V. T. Lu, A. A. Kossiakoff, and A. Hoelz, Architecture of the nuclear pore complex coat, *Science* **347**(6226), 1148–1152 (2015).
- [46] B. Fahrenkrog, E. C. Hurt, U. Aebi, and N. Panté, Molecular Architecture of the Yeast Nuclear Pore Complex: Localization of Nsp1p Subcomplexes, *J Cell Biol* **143**(3), 577–588 (1998).
- [47] M. Cohen, Y. B. Tzur, E. Neufeld, N. Feinstein, M. R. Delannoy, K. L. Wilson, and Y. Gruenbaum, Transmission electron microscope studies of the nuclear envelope in *Caenorhabditis elegans* embryos, *J Struct Biol* **140**(1–3), 232–240 (2002).
- [48] M. Suntharalingam and S. R. Wenthe, Peering through the Pore: Nuclear Pore Complex Structure, Assembly, and Function, *Dev Cell* **4**(6), 775–789 (2003).
- [49] D. Kraemer, R. W. Wozniak, G. Blobel, and A. Radu, The human CAN protein, a putative oncogene product associated with myeloid leukemogenesis, is a nuclear pore complex protein that faces the cytoplasm, *Proc Natl Acad Sci U S A* **91**(4), 1519–1523 (1994).
- [50] T. C. Walther, H. S. Pickersgill, V. C. Cordes, M. W. Goldberg, T. D. Allen, I. W. Mattaj, and M. Fornerod, The cytoplasmic filaments of the nuclear pore complex are dispensable for selective nuclear protein import, *J Cell Biol* **158**(1), 63–77 (2002).
- [51] C. S. Weirich, J. P. Erzberger, J. M. Berger, and K. Weis, The N-terminal domain of Nup159 forms a beta-propeller that functions in mRNA export by tethering the helicase Dbp5 to the nuclear pore, *Mol Cell* **16**(5), 749–60 (2004).
- [52] J. Napetschnig, G. Blobel, and A. Hoelz, Crystal structure of the N-terminal domain of the human protooncogene Nup214/CAN, *Proc Natl Acad Sci U S A* **104**(6), 1783–1788 (2007).
- [53] H. von Moeller, C. Basquin, and E. Conti, The mRNA export protein DBP5 binds RNA and the cytoplasmic nucleoporin NUP214 in a mutually exclusive manner, *Nat Struct Mol Biol* **16**(3), 247–254 (2009).
- [54] M. Fornerod, J. van Deursen, S. van Baal, A. Reynolds, D. Davis, K. G. Murti, J. Fransen, and G. Grosveld, The human homologue of yeast CRM1 is in a dynamic subcomplex with CAN/Nup214 and a novel nuclear pore component Nup88, *EMBO J* **16**(4), 807–816 (1997).
- [55] C. Schmitt, C. von Kobbe, A. Bachi, N. Panté, J. P. Rodrigues, C. Boscheron, G. Rigaut, M. Wilm, B. Séraphin, M. Carmo-Fonseca, and E. Izaurralde, Dbp5, a DEAD-box protein required for mRNA export, is recruited to the cytoplasmic fibrils of nuclear pore complex via a conserved interaction with CAN/Nup159p, *EMBO J* **18**(15), 4332–4347 (1999).
- [56] J. Napetschnig, S. A. Kassube, E. W. Debler, R. W. Wong, G. Blobel, and A. Hoelz, Structural and functional analysis of the interaction between the nucleoporin Nup214 and the DEAD-box helicase Ddx19, *Proc Natl Acad Sci U S A* **106**(9), 3089–3094 (2009).
- [57] R. Bastos, L. R. d. Pouplana, M. Enarson, K. Bodoor, and B. Burke, Nup84, A Novel Nucleoporin That Is Associated With CAN/Nup214 on the Cytoplasmic Face of the Nuclear Pore Complex, *J Cell Biol* **137**(5), 989–1000 (1997).

- [58] M. Fornerod, J. Boer, S. van Baal, H. Morreau, and G. Grosveld, Interaction of cellular proteins with the leukemia specific fusion proteins DEK-CAN and SET-CAN and their normal counterpart, the nucleoporin CAN, *Oncogene* **13**(8), 1801–1808 (1996).
- [59] S. Roloff, C. Spillner, and R. H. Kehlenbach, Several phenylalanine-glycine motives in the nucleoporin Nup214 are essential for binding of the nuclear export receptor CRM1, *J Biol Chem* **288**, 3952–3963 (2012).
- [60] S. Hutten and R. H. Kehlenbach, Nup214 Is Required for CRM1-Dependent Nuclear Protein Export In Vivo, *Mol Cell Biol* **26**(18), 6772–6785 (2006).
- [61] J. Moroianu, M. Hijikata, G. Blobel, and A. Radu, Mammalian karyopherin alpha 1 beta and alpha 2 beta heterodimers: alpha 1 or alpha 2 subunit binds nuclear localization signal and beta subunit interacts with peptide repeat-containing nucleoporins, *Proc Natl Acad Sci U S A* **92**(14), 6532–6536 (1995).
- [62] N. Bonifaci, J. Moroianu, A. Radu, and G. Blobel, Karyopherin beta2 mediates nuclear import of a mRNA binding protein, *Proc Natl Acad Sci U S A* **94**(10), 5055–5060 (1997).
- [63] N. R. Yaseen and G. Blobel, Cloning and characterization of human karyopherin beta 3, *Proc Natl Acad Sci U S A* **94**(9), 4451–4456 (1997).
- [64] P. Askjaer, A. Bachi, M. Wilm, F. R. Bischoff, D. L. Weeks, V. Ogniewski, M. Ohno, C. Niehrs, J. Kjems, I. W. Mattaj, and M. Fornerod, RanGTP-regulated interactions of CRM1 with nucleoporins and a shuttling DEAD-box helicase, *Mol Cell Biol* **19**(9), 6276–6285 (1999).
- [65] C. A. Hodge, H. V. Colot, P. Stafford, and C. N. Cole, Rat8p/Dbp5p is a shuttling transport factor that interacts with Rat7p/Nup159p and Gle1p and suppresses the mRNA export defect of xpo1-1 cells, *EMBO J* **18**(20), 5778–5788 (1999).
- [66] R. Bernad, D. Engelsma, H. Sanderson, H. Pickersgill, and M. Fornerod, Nup214-Nup88 Nucleoporin Sub-complex Is Required for CRM1-mediated 60 S Preribosomal Nuclear Export, *J Biol Chem* **281**(28), 19378–19386 (2006).
- [67] A. Bachi, I. C. Braun, J. P. Rodrigues, N. Panté, K. Ribbeck, C. von Kobbe, U. Kutay, M. Wilm, D. Görlich, M. Carmo-Fonseca, and E. Izaurralde, The C-terminal domain of TAP interacts with the nuclear pore complex and promotes export of specific CTE-bearing RNA substrates, *RNA* **6**(1), 136–158 (2000).
- [68] J. van Deursen, J. Boer, L. Kasper, and G. Grosveld, G2 arrest and impaired nucleocytoplasmic transport in mouse embryos lacking the proto-oncogene CAN/Nup214., *EMBO J* **15**(20), 5574–5583 (1996).
- [69] J. M. Cronshaw and M. J. Matunis, The nuclear pore complex: disease associations and functional correlations, *Trends Endocrinol Metab* **15**(1), 34–39 (2004).
- [70] M. von Lindern, M. Fornerod, S. van Baal, M. Jaegle, T. de Wit, A. Buijs, and G. Grosveld, The translocation (6;9), associated with a specific subtype of acute myeloid leukemia, results in the fusion of two genes, *dek* and *can*, and the expression of a chimeric, leukemia-specific *dek-can* mRNA, *Mol Cell Biol* **12**(4), 1687–1697 (1992).
- [71] M. von Lindern, S. van Baal, J. Wiegant, A. Raap, A. Hagemeyer, and G. Grosveld, *Can*, a putative oncogene associated with myeloid leukemogenesis, may be activated by fusion of its 3' half to different genes: characterization of the *set* gene., *Mol Cell Biol* **12**(8), 3346–3355 (1992).
- [72] G. K. Fu, G. Grosveld, and D. M. Markovitz, DEK, an autoantigen involved in a chromosomal translocation in acute myelogenous leukemia, binds to the HIV-2 enhancer, *Proc Natl Acad Sci U S A* **94**(5), 1811–1815 (1997).
- [73] C. Graux, J. Cools, C. Melotte, H. Quentmeier, A. Ferrando, R. Levine, J. R. Vermeesch, M. Stul, B. Dutta, N. Boeckx, A. Bosly, P. Heimann, A. Uyttebroeck, N. Mentens, R. Somers, R. A. F. MacLeod, H. G. Drexler, A. T. Look, D. G. Gilliland, L. Michaux, P. Vandenberghe, I. Wlodarska, P. Marynen, and A. Hagemeyer, Fusion of NUP214 to ABL1 on amplified episomes in T-cell acute lymphoblastic leukemia, *Nat Genet* **36**(10), 1084–1089 (2004).
- [74] J. Z. Levin, M. F. Berger, X. Adiconis, P. Rogov, A. Melnikov, T. Fennell, C. Nusbaum, L. A. Garraway, and A. Gnirke, Targeted next-generation sequencing of a cancer transcriptome enhances detection of sequence variants and novel fusion transcripts, *Genome Biol* **10**(10), R115 (2009).

- [75] P. Gorello, R. La Starza, D. Di Giacomo, M. Messina, M. C. Puzzolo, B. Crescenzi, A. Santoro, S. Chiaretti, and C. a. Mecucci, SQSTM1-NUP214: a new gene fusion in adult T-cell acute lymphoblastic leukemia, *Haematologica* **95**(12), 2161–2163 (2010).
- [76] S. Xu and M. A. Powers, Nuclear pore proteins and cancer, *Semin Cell Dev Biol* **20**(5), 620–630 (2009).
- [77] M.-H. Zhou and Q.-M. Yang, NUP214 fusion genes in acute leukemia (Review), *Oncol Lett* **8**(3), 959–962 (2014).
- [78] H. Fried and U. Kutay, Nucleocytoplasmic transport: taking an inventory, *Cell Mol Life Sci* **60**, 1659–1688 (2003).
- [79] I. W. Mattaj and L. Englmeier, Nucleocytoplasmic transport: The Soluble Phase, *Annu Rev Biochem* **67**(1), 265–306 (1998).
- [80] B. Talcott and M. M. S., Getting across the nuclear pore complex, *Trends Cell Biol* **9**(8), 312–318 (1999).
- [81] K. Ribbeck and D. Görlich, Kinetic analysis of translocation through nuclear pore complexes, *EMBO J* **20**(6), 1320–1330 (2001).
- [82] I. G. Macara, Transport into and out of the nucleus, *Microbiol Mol Biol Rev* **65**(4), 570–594 (2001).
- [83] S. Wälde and R. H. Kehlenbach, The Part and the Whole: functions of nucleoporins in nucleocytoplasmic transport, *Trends Cell Biol* **20**(8), 461–469 (2010).
- [84] J. Bednenko, G. Cingolani, and L. Gerace, Importin beta contains a COOH-terminal nucleoporin binding region important for nuclear transport, *J Cell Biol* **162**(3), 391–401 (2003).
- [85] D. Görlich and U. Kutay, Transport between the Cell Nucleus and the Cytoplasm, *Annu Rev Cell Dev Biol* **15**(1), 607–660 (1999).
- [86] A. Cook, F. Bono, M. Jinek, and E. Conti, Structural Biology of Nucleocytoplasmic Transport, *Annu Rev Biochem* **76**(1), 647–671 (2007).
- [87] N. Mosammamarast and L. F. Pemberton, Karyopherins: from nuclear-transport mediators to nuclear-function regulators, *Trends Cell Biol* **14**(10), 547–556 (2004).
- [88] L. F. Pemberton and B. M. Paschal, Mechanisms of Receptor-Mediated Nuclear Import and Nuclear Export, *Traffic* **6**(3), 187–198 (2005).
- [89] J.-M. Mingot, S. Kostka, R. Kraft, E. Hartmann, and D. Görlich, Importin 13: a novel mediator of nuclear import and export, *EMBO J* **20**(14), 3685–3694 (2001).
- [90] K. Yoshida and G. Blobel, The Karyopherin Kap142p/Msn5p Mediates Nuclear Import and Nuclear Export of Different Cargo Proteins, *J Cell Biol* **152**(4), 729–740 (2001).
- [91] C. Gontan, T. Güttler, E. Engelen, J. Demmers, M. Fornerod, F. G. Grosveld, D. Tibboel, D. Görlich, Dirkrlich, R. A. Poot, and R. J. Rottier, Exportin 4 mediates a novel nuclear import pathway for Sox family transcription factors, *J Cell Biol* **185**(1), 27–34 (2009).
- [92] M. Rexach and G. Blobel, Protein import into nuclei: association and dissociation reactions involving transport substrate, transport factors, and nucleoporins, *Cell* **83**(5), 683–692 (1995).
- [93] D. Görlich, N. Panté, U. Kutay, U. Aebi, and F. R. Bischoff, Identification of different roles for RanGDP and RanGTP in nuclear protein import., *EMBO J* **15**(20), 5584–5594 (1996).
- [94] M. Fornerod, M. Ohno, M. Yoshida, and I. W. Mattaj, CRM1 Is an Export Receptor for Leucine-Rich Nuclear Export Signals, *Cell* **90**(6), 1051–1060 (1997).
- [95] U. Kutay, F. R. Bischoff, S. Kostka, R. Kraft, and D. Görlich, Export of Importin alpha from the Nucleus Is Mediated by a Specific Nuclear Transport Factor, *Cell* **90**(6), 1061–1071 (1997).
- [96] Y. M. Chook and G. Blobel, Karyopherins and nuclear import, *Curr Opin Struct Biol* **11**(6), 703–715 (2001).
- [97] K. Weis, Regulating Access to the Genome: Nucleocytoplasmic Transport throughout the Cell Cycle, *Cell* **112**(4), 441–451 (2003).
- [98] E. Izaurralde, U. Kutay, C. von Kobbe, I. W. Mattaj, and D. Görlich, The asymmetric distribution of the constituents of the Ran system is essential for transport into and out of the nucleus, *EMBO J* **16**(21), 6535–6547 (1997).

- [99] A. E. Smith, B. M. Slepchenko, J. C. Schaff, L. M. Loew, and I. G. Macara, Systems analysis of Ran transport, *Science* **295**(5554), 488–491 (2002).
- [100] P. Kalab, K. Weis, and R. Heald, Visualization of a Ran-GTP gradient in interphase and mitotic *Xenopus* egg extracts, *Science* **295**(5564), 2452–2456 (2002).
- [101] T. Güttler and D. a. Görlich, Ran-dependent nuclear export mediators: a structural perspective, *EMBO J* **30**(17), 3457–3474 (2011).
- [102] F. R. Bischoff, C. Klebe, J. Kretschmer, A. Wittinghofer, and H. Ponstingl, RanGAP1 induces GTPase activity of nuclear Ras-related Ran, *Proc Natl Acad Sci U S A* **91**(7), 2587–2591 (1994).
- [103] R. Mahajan, C. Delphin, T. Guan, L. Gerace, and F. Melchior, A Small Ubiquitin-Related Polypeptide Involved in Targeting RanGAP1 to Nuclear Pore Complex Protein RanBP2, *Cell* **88**(1), 97–107 (1997).
- [104] M. J. Matunis, E. Coutavas, and G. Blobel, A novel ubiquitin-like modification modulates the partitioning of the Ran-GTPase-activating protein RanGAP1 between the cytosol and the nuclear pore complex., *J Cell Biol* **135**(6), 1457–1470 (1996).
- [105] R. D. Makde, J. R. England, H. P. Yennawar, and S. Tan, Structure of RCC1 chromatin factor bound to the nucleosome core particle, *Nature* **467**(7315), 562–566 (2010).
- [106] F. R. Bischoff and H. Ponstingl, Catalysis of guanine nucleotide exchange on Ran by the mitotic regulator RCC1, *Nature* **354**(6348), 80–82 (1991).
- [107] M. S. Moore and G. Blobel, Purification of a Ran-interacting protein that is required for protein import into the nucleus, *Proc Natl Acad Sci U S A* **91**(21), 10212–10216 (1994).
- [108] B. M. Paschal and L. Gerace, Identification of NTF2, a cytosolic factor for nuclear import that interacts with nuclear pore complex protein p62., *J Cell Biol* **129**(4), 925–937 (1995).
- [109] A. Smith, A. Brownawell, and I. G. Macara, Nuclear import of Ran is mediated by the transport factor NTF2, *Curr Biol* **8**(25), 1403–1406 (1998).
- [110] K. Ribbeck, G. Lipowsky, H. M. Kent, M. Stewart, and D. a. Görlich, NTF2 mediates nuclear import of Ran, *EMBO J* **17**(22), 6587–6598 (1998).
- [111] M. Stewart, H. M. Kent, and A. J. McCoy, Structural basis for molecular recognition between nuclear transport factor 2 (NTF2) and the GDP-bound form of the ras-family GTPase ran, *J Mol Biol* **277**(3), 635–646 (1998).
- [112] M. Ohtsubo, R. Kai, N. Furuno, T. Sekiguchi, M. Sekiguchi, H. Hayashida, K. Kuma, T. Miyata, S. Fukushige, and T. Murotsu, Isolation and characterization of the active cDNA of the human cell cycle gene (RCC1) involved in the regulation of onset of chromosome condensation., *Genes Dev* **1**(6), 585–593 (1987).
- [113] M. E. Nemergut, C. A. Mizzen, T. Stukenberg, C. D. Allis, and I. G. Macara, Chromatin Docking and Exchange Activity Enhancement of RCC1 by Histones H2A and H2B, *Science* **292**(5521), 1540–1543 (2001).
- [114] G. Cingolani, C. Petosa, K. Weis, and C. W. Muller, Structure of importin- β bound to the IBB domain of importin- α , *Nature* **399**(6733), 221–229 (1999).
- [115] S. J. Lee, Y. Matsuura, S. M. Liu, and M. Stewart, Structural basis for nuclear import complex dissociation by RanGTP, *Nature* **435**(7042), 693–696 (2005).
- [116] Y. M. Chook and G. Blobel, Structure of the nuclear transport complex karyopherin- β 2-Ran•GppNHp, *Nature* **399**(6733), 230–237 (1999).
- [117] C. Petosa, G. Schoehn, P. Askjaer, U. Bauer, M. Moulin, U. Steuerwald, M. Soler-López, F. Baudin, I. W. Mattaj, and C. W. Müller, Architecture of CRM1/Exportin1 suggests how cooperativity is achieved during formation of a nuclear export complex, *Mol Cell* **16**(5), 761–775 (2004).
- [118] Y. Matsuura and M. Stewart, Structural basis for the assembly of a nuclear export complex, *Nature* **432**(7019), 872–877 (2004).
- [119] M. A. Andrade and P. Bork, HEAT repeats in the Huntington's disease protein, *Nat Genet* **11**(2), 115–116 (1995).
- [120] M. A. Andrade, C. Perez-Iratxeta, and C. P. Ponting, Protein Repeats: Structures, Functions, and Evolution, *J Struct Biol* **134**(2–3), 117–131 (2001).

- [121] I. R. Vetter, C. Nowak, T. Nishimoto, J. Kuhlmann, and A. Wittinghofer, Structure of a Ran-binding domain complexed with Ran bound to a GTP analogue: implications for nuclear transport, *Nature* **398**, 39–46 (1999).
- [122] R. Bayliss, T. Littlewood, and M. Stewart, Structural Basis for the Interaction between FxFG Nucleoporin Repeats and Importin beta in Nuclear Trafficking, *Cell* **102**(1), 99–108 (2000).
- [123] G. Cingolani, J. Bednenko, M. T. Gillespie, and L. Gerace, Molecular basis for the recognition of a nonclassical nuclear localization signal by importin beta, *Mol Cell* **10**(6), 1345–1353 (2002).
- [124] S. J. Lee, T. Sekimoto, E. Yamashita, E. Nagoshi, A. Nakagawa, N. Imamoto, M. Yoshimura, H. Sakai, K. T. Chong, T. Tsukihara, and Y. Yoneda, The structure of importin-beta bound to SREBP-2: nuclear import of a transcription factor, *Science* **302**(5650), 1571–1575 (2003).
- [125] G. Mitrousis, A. S. Olia, N. Walker-Kopp, and G. Cingolani, Molecular Basis for the Recognition of Snurportin 1 by Importin β , *J Biol Chem* **283**(12), 7877–7884 (2008).
- [126] D. Wohlwend, A. Strasser, A. Dickmanns, and R. Ficner, Structural Basis for RanGTP Independent Entry of Spliceosomal U snRNPs into the Nucleus, *Journal of Molecular Biology* **374**(4), 1129–1138 (2007).
- [127] T. Monecke, T. Güttler, P. Neumann, A. Dickmanns, D. Görlich, and R. Ficner, Crystal Structure of the Nuclear Export Receptor CRM1 in Complex with Snurportin1 and RanGTP, *Science* **324**(5930), 1087–1091 (2009).
- [128] U. Fischer, J. Huber, W. C. Boelens, I. W. Mattaj, and R. Lührmann, The HIV-1 Rev Activation Domain is a nuclear export signal that accesses an export pathway used by specific cellular RNAs, *Cell* **82**(3), 475–483 (1995).
- [129] W. Wen, J. L. Meinkoth, R. Y. Tsien, and S. S. Taylor, Identification of a signal for rapid export of proteins from the nucleus, *Cell* **82**(3), 463–473 (1995).
- [130] K. Stade, C. S. Ford, C. Guthrie, and K. Weis, Exportin 1 (Crm1p) Is an Essential Nuclear Export Factor, *Cell* **90**(6), 1041–1050 (1997).
- [131] E. Paraskeva, E. Izaurralde, F. R. Bischoff, J. Huber, U. Kutay, E. Hartmann, R. Lührmann, and D. Görlich, CRM1 mediated recycling of snurportin 1 to the cytoplasm, *J Cell Biol* **145**(2), 255–264 (1999).
- [132] M. Ohno, A. Segref, A. Bachi, M. Wilm, and I. W. Mattaj, PHAX, a Mediator of U snRNA Nuclear Export Whose Activity Is Regulated by Phosphorylation, *Cell* **101**(2), 187–198 (2000).
- [133] A. W. Johnson, E. Lund, and J. Dahlberg, Nuclear export of ribosomal subunits, *Trends Biochem Sci* **27**(11), 580–585 (2002).
- [134] E. Conti, M. Uy, L. Leighton, G. Blobel, and J. Kuriyan, Crystallographic Analysis of the Recognition of a Nuclear Localization Signal by the Nuclear Import Factor Karyopherin α , *Cell* **94**(2), 193–204 (1998).
- [135] Y. Matsuura and M. Stewart, Nup50/Npap60 function in nuclear protein import complex disassembly and importin recycling, *EMBO J* **24**(21), 3681–3689 (2005).
- [136] M. Peifer, S. Berg, and A. B. Reynolds, A repeating amino acid motif shared by proteins with diverse cellular roles, *Cell* **76**(5), 789–791 (1994).
- [137] B. Kobe, Autoinhibition by an internal nuclear localization signal revealed by the crystal structure of mammalian importin α , *Nat Struct Mol Biol* **6**(4), 388–397 (1999).
- [138] M. R. Fontes, T. Teh, and B. Kobe, Structural basis of recognition of monopartite and bipartite nuclear localization sequences by mammalian importin- α , *J Mol Biol* **297**(5), 1183–1194 (2000).
- [139] M. R. M. Fontes, T. Teh, D. Jans, R. I. Brinkworth, and B. Kobe, Structural Basis for the Specificity of Bipartite Nuclear Localization Sequence Binding by Importin- α , *J Biol Chem* **278**(30), 27981–27987 (2003).
- [140] M. T. Harreman, T. M. Kline, H. G. Milford, M. B. Harben, A. E. Hodel, and A. H. Corbett, Regulation of Nuclear Import by Phosphorylation Adjacent to Nuclear Localization Signals, *J Biol Chem* **279**(20), 20613–20621 (2004).
- [141] N. Kudo, S. Khochbin, K. Nishi, K. Kitano, M. Yanagida, M. Yoshida, and S. Horinouchi, Molecular Cloning and Cell Cycle-dependent Expression of Mammalian CRM1, a Protein Involved in Nuclear Export of Proteins, *J Biol Chem* **272**(47), 29742–29751 (1997).
- [142] M. Fukuda, S. Asano, T. Nakamura, M. Adachi, M. Yoshida, M. Yanagida, and E. Nishida, CRM1 is responsible for intracellular transport mediated by the nuclear export signal, *Nature* **390**(6657), 308–311 (1997).

- [143] M. Neville, F. Stutz, L. Lee, L. I. Davis, and M. Rosbash, The importin-beta family member Crm1p bridges the interaction between Rev and the nuclear pore complex during nuclear export, *Curr Biol* **7**(10), 767–775 (1997).
- [144] B. Ossareh-Nazari, F. Bachelierie, and C. Dargemont, Evidence for a role of CRM1 in signal-mediated nuclear protein export, *Science* **278**(5335), 141–144 (1997).
- [145] R. H. Kehlenbach, A. Dickmanns, and L. Gerace, Nucleocytoplasmic Shuttling Factors Including Ran and CRM1 Mediate Nuclear Export of NFAT In Vitro, *J Cell Biol* **141**(4), 863–874 (1998).
- [146] M. T. Bohnsack, K. Regener, B. Schwappach, R. Saffrich, E. Paraskeva, E. Hartmann, and D. Görlich, Exp5 exports eEF1A via tRNA from nuclei and synergizes with other transport pathways to confine translation to the cytoplasm, *EMBO J* **21**(22), 6205–6215 (2002).
- [147] S.-C. Fu, H.-C. Huang, P. Horton, and H.-F. Juan, ValidNESs: a database of validated leucine-rich nuclear export signals, *Nucleic Acids Res* **41**(D1), D338–D343 (2013).
- [148] D. Xu, A. Farmer, G. Collett, N. V. Grishin, and Y. M. Chook, Sequence and structural analyses of nuclear export signals in the NESdb database, *Mol Biol Cell* (2012).
- [149] Y. Adachi and M. Yanagida, Higher order chromosome structure is affected by cold-sensitive mutations in a *Schizosaccharomyces pombe* gene *crm1+* which encodes a 115-kD protein preferentially localized in the nucleus and its periphery., *J Cell Biol* **108**(4), 1195–1207 (1989).
- [150] T. Hamamoto, S. Gunji, H. Tsuji, and T. Beppu, Leptomycins A and B, new antifungal antibiotics. I. Taxonomy of the producing strain and their fermentation, purification and characterization, *J Antibiot* **36**(6), 639–645 (1983).
- [151] K. Nishi, M. Yoshida, D. Fujiwara, M. Nishikawa, S. Horinouchi, and T. Beppu, Leptomycin B targets a regulatory cascade of *crm1*, a fission yeast nuclear protein, involved in control of higher order chromosome structure and gene expression., *J Biol Chem* **269**(9), 6320–6324 (1994).
- [152] B. Wolff, J.-J. Sanglier, and Y. Wang, Leptomycin B is an inhibitor of nuclear export: inhibition of nucleo-cytoplasmic translocation of the human immunodeficiency virus type 1 (HIV-1) Rev protein and Rev-dependent mRNA, *Chem Biol* **4**(2), 139–147 (1997).
- [153] N. Kudo, B. Wolff, T. Sekimoto, E. P. Schreiner, Y. Yoneda, M. Yanagida, S. Horinouchi, and M. Yoshida, Leptomycin B Inhibition of Signal-Mediated Nuclear Export by Direct Binding to CRM1, *Exp Cell Res* **242**(2), 540–547 (1998).
- [154] N. Kudo, N. Matsumori, H. Taoka, D. Fujiwara, E. P. Schreiner, B. Wolff, M. Yoshida, and S. Horinouchi, Leptomycin B inactivates CRM1/exportin 1 by covalent modification at a cysteine residue in the central conserved region, *Proc Natl Acad Sci U S A* **96**(16), 9112–9117 (1999).
- [155] T. Meissner, E. Krause, and U. Vinkemeier, Ratjadone and leptomycin B block CRM1-dependent nuclear export by identical mechanisms, *FEBS Lett* **576**(1–2), 27–30 (2004).
- [156] Q. Sun, Y. P. Carrasco, Y. Hu, X. Guo, H. Mirzaei, J. MacMillan, and Y. M. Chook, Nuclear export inhibition through covalent conjugation and hydrolysis of Leptomycin B by CRM1, *Proc Natl Acad Sci U S A* (2013).
- [157] J. G. Turner, J. Dawson, and D. M. Sullivan, Nuclear export of proteins and drug resistance in cancer, *Biochem Pharmacol* **83**(8), 1021 – 1032 (2012), *Drug Resistance in Cancer*.
- [158] F. Lu, A. B. Gladden, and J. A. Diehl, An Alternatively Spliced Cyclin D1 Isoform, Cyclin D1b, Is a Nuclear Oncogene, *Cancer Res* **63**(21), 7056–7061 (2003).
- [159] L. Chen, J. E. Moore, C. Samathanam, C. Shao, E. Cobos, M. S. Miller, and W. Gao, CRM1-dependent p53 nuclear accumulation in lung lesions of a bitransgenic mouse lung tumor model, *Oncology Reports* **26**, 223–228 (2011).
- [160] M. Kanai, K. Hanashiro, S.-H. Kim, S. Hanai, A. H. Boulares, M. Miwa, and K. Fukasawa, Inhibition of Crm1-p53 interaction and nuclear export of p53 by poly(ADP-ribosyl)ation, *Nat Cell Biol* **9**(10), 1175–1183 (2007).
- [161] K. T. Nguyen, M. P. Holloway, and R. A. Altura, The CRM1 nuclear export protein in normal development and disease, *Int J Biochem Mol Biol* **3**(2), 137–151 (2012).

- [162] R. Lapalombella, Q. Sun, K. Williams, L. Tangeman, S. Jha, Y. Zhong, V. Goettl, E. Mahoney, C. Berglund, S. Gupta, A. Farmer, R. Mani, A. J. Johnson, D. Lucas, X. Mo, D. Daelemans, V. Sandanayaka, S. Shechter, D. McCauley, S. Shacham, M. Kauffman, Y. M. Chook, and J. C. Byrd, Selective inhibitors of nuclear export show that CRM1/XPO1 is a target in chronic lymphocytic leukemia, *Blood* **120**(23), 4621–4634 (2012).
- [163] J. Etchin, Q. Sun, A. Kentsis, A. Farmer, Z. C. Zhang, T. Sanda, M. R. Mansour, C. Barcelo, D. McCauley, M. Kauffman, S. Shacham, A. L. Christie, A. L. Kung, S. J. Rodig, Y. M. Chook, and A. T. Look, Antileukemic activity of nuclear export inhibitors that spare normal hematopoietic cells, *Leukemia* **27**(1), 66–74 (2013).
- [164] K. Zhang, M. Wang, A. T. Tamayo, S. Shacham, M. Kauffman, J. Lee, L. Zhang, Z. Ou, C. Li, L. Sun, R. J. Ford, and L. V. Pham, Novel selective inhibitors of nuclear export CRM1 antagonists for therapy in mantle cell lymphoma, *Exp Hematol* **41**(1), 67–78.e4 (2013).
- [165] P. Ranganathan, X. Yu, C. Na, R. Santhanam, S. Shacham, M. Kauffman, A. Walker, R. Klisovic, W. Blum, M. Caligiuri, C. M. Croce, G. Marcucci, and R. a. Garzon, Preclinical activity of a novel CRM1 inhibitor in acute myeloid leukemia, *Blood* **120**(9), 1765–1773 (2012).
- [166] A. S. Azmi, A. Aboukameel, B. Bao, F. H. Sarkar, P. A. Philip, M. Kauffman, S. Shacham, and R. M. Mohammad, Selective Inhibitors of Nuclear Export Block Pancreatic Cancer Cell Proliferation and Reduce Tumor Growth in Mice, *Gastroenterology* **144**(2), 447–456 (2013).
- [167] J. Etchin, T. Sanda, M. R. Mansour, A. Kentsis, J. Montero, B. T. Le, A. L. Christie, D. McCauley, S. J. Rodig, M. Kauffman, S. Shacham, R. Stone, A. Letai, A. L. Kung, and A. Thomas Look, KPT-330 inhibitor of CRM1 (XPO1)-mediated nuclear export has selective anti-leukaemic activity in preclinical models of T-cell acute lymphoblastic leukaemia and acute myeloid leukaemia, *Br J Haematol* **161**(1), 117–127 (2013).
- [168] H. Inoue, M. Kauffman, S. Shacham, Y. Landesman, J. Yang, C. P. Evans, and R. H. Weiss, CRM1 Blockade by Selective Inhibitors of Nuclear Export Attenuates Kidney Cancer Growth, *J Urol* **189**(6), 2317–2326 (2012).
- [169] K. Kojima, S. M. Kornblau, V. Ruvolo, A. Dilip, S. Duvvuri, R. E. Davis, M. Zhang, Z. Wang, K. R. Coombes, N. Zhang, Y. H. Qiu, J. K. Burks, H. Kantarjian, S. Shacham, M. Kauffman, and M. a. Andreeff, Prognostic impact and targeting of CRM1 in acute myeloid leukemia, *Blood* **121**(20), 4166–4174 (2013).
- [170] T. Monecke, A. Dickmanns, and R. Ficner, Allosteric control of the exportin CRM1 unraveled by crystal structure analysis, *FEBS J* (2014).
- [171] D. Görlich, M. Dabrowski, F. R. Bischoff, U. Kutay, P. Bork, E. Hartmann, S. Prehn, and E. Izaurralde, A Novel Class of RanGTP Binding Proteins, *J Cell Biol* **138**(1), 65–80 (1997).
- [172] T. Monecke, D. Haselbach, B. Voß, A. Russek, P. Neumann, E. Thomson, E. Hurt, U. Zachariae, H. Stark, H. Grubmüller, A. Dickmanns, and R. Ficner, Structural basis for cooperativity of CRM1 export complex formation, *Proc Natl Acad Sci U S A* **110**(3), 960–965 (2013).
- [173] C. Dian, F. Bernaudat, K. Langer, M. F. Oliva, M. Fornerod, G. Schoehn, C. W. Müller, and C. Petosa, Structure of a Truncation Mutant of the Nuclear Export Factor CRM1 Provides Insights into the Auto-Inhibitory Role of Its C-Terminal Helix, *Structure* **21**, 1–12 (2013).
- [174] X. Dong, A. Biswas, K. E. Suel, L. K. Jackson, R. Martinez, H. Gu, and Y. M. Chook, Structural basis for leucine-rich nuclear export signal recognition by CRM1, *Nature* **458**(7242), 1136–1141 (2009).
- [175] T. Güttler, T. Madl, P. Neumann, D. Deichsel, L. Corsini, T. Monecke, R. Ficner, M. Sattler, and D. Gorlich, NES consensus redefined by structures of PKI-type and Rev-type nuclear export signals bound to CRM1, *Nat Struct Mol Biol* **17**(11), 1367–1376 (2010).
- [176] M. Koyama, N. Shirai, and Y. Matsuura, Structural Insights into How Yrb2p Accelerates the Assembly of the Xpo1p Nuclear Export Complex, *Cell Rep* **9**, 983–995 (2014).
- [177] M. Koyama and Y. Matsuura, An allosteric mechanism to displace nuclear export cargo from CRM1 and RanGTP by RanBP1, *EMBO J* **29**(12), 2003–2013 (2010).
- [178] N. Dölker, C. E. Blanchet, B. Voß, D. Haselbach, C. Kappel, T. Monecke, D. I. Svergun, H. Stark, R. Ficner, U. Zachariae, H. Grubmüller, and A. Dickmanns, Structural Determinants and Mechanism of Mammalian CRM1 Allostery, *Structure* **21**, 1–11 (2013).
- [179] N. Saito and Y. Matsuura, A 2.1-Å-Resolution Crystal Structure of Unliganded CRM1 Reveals the Mechanism of Autoinhibition, *J Mol Biol* **425**(2), 350–364 (2013).

- [180] C. Senay, P. Ferrari, C. Rocher, K.-J. Rieger, J. Winter, D. Platel, and Y. Bourne, The Mtr2-Mex67 NTF2-like Domain Complex: Structural Insights into a Dual Role of Mtr2 for Yeast Nuclear Export, *J Biol Chem* **278**(48), 48395–48403 (2003).
- [181] L. A. Strawn, T. Shen, and S. R. Wentz, The GLFG Regions of Nup116p and Nup100p Serve as Binding Sites for Both Kap95p and Mex67p at the Nuclear Pore Complex, *J Biol Chem* **276**(9), 6445–6452 (2001).
- [182] T. A. Isgro and K. Schulten, Binding Dynamics of Isolated Nucleoporin Repeat Regions to Importin- β , *Structure* **13**(12), 1869–1879 (2005).
- [183] N. C. Chi and S. A. Adam, Functional domains in nuclear import factor p97 for binding the nuclear localization sequence receptor and the nuclear pore., *Mol Biol Cell* **8**(6), 945–956 (1997).
- [184] S. Kose, N. Imamoto, T. Tachibana, T. Shimamoto, and Y. Yoneda, Ran-unassisted Nuclear Migration of a 97-kD Component of Nuclear Pore-targeting Complex, *J Cell Biol* **139**(4), 841–849 (1997).
- [185] U. Kutay, E. Izaurralde, F. R. Bischoff, I. W. Mattaj, and D. Görlich, Dominant-negative mutants of importin-beta block multiple pathways of import and export through the nuclear pore complex, *EMBO J* **16**(6), 1153–1163 (1997).
- [186] I. C. Braun, A. Herold, M. Rode, and E. Izaurralde, Nuclear Export of mRNA by TAP/NXF1 Requires Two Nucleoporin-Binding Sites but Not p15, *Mol Cell Biol* **22**(15), 5405–5418 (2002).
- [187] S. Kuersten, G.-J. Arts, T. C. Walther, L. Englmeier, and I. W. Mattaj, Steady-State Nuclear Localization of Exportin-t Involves RanGTP Binding and Two Distinct Nuclear Pore Complex Interaction Domains, *Mol Cell Biol* **22**(16), 5708–5720 (2002).
- [188] J. Morrison, J.-C. Yang, M. Stewart, and D. Neuhaus, Solution NMR Study of the Interaction Between NTF2 and Nucleoporin FxFG Repeats, *J Mol Biol* **333**(3), 587 – 603 (2003).
- [189] L. Miao and K. Schulten, Transport-Related Structures and Processes of the Nuclear Pore Complex Studied Through Molecular Dynamics, *Structure* **17**(3), 449–459 (2009).
- [190] R. Gamini, W. Han, J. E. Stone, and K. Schulten, Assembly of Nsp1 nucleoporins provides insight into nuclear pore complex gating, *PLoS Comput Biol* **10**(3), e1003488 (2014).
- [191] N. Wilken, J. Senécal, U. Scheer, and M. C. Dabauvalle, Localization of the Ran-GTP binding protein RanBP2 at the cytoplasmic side of the nuclear pore complex, *Eur J Cell Biol* **68**(3), 211–219 (1995).
- [192] N. Yokoyama, N. Hayashi, T. Seki, N. Pante, T. Ohba, K. Nishii, K. Kuma, T. Hayashida, T. Miyata, U. Aebi, M. Fukui, and T. Nishimoto, A giant nucleopore protein that binds Ran/TC4, *Nature* **376**(6536), 184–188 (1995).
- [193] C. Delphin, T. Guan, F. Melchior, and L. Gerace, RanGTP Targets p97 to RanBP2, a filamentous protein localized at the cytoplasmic periphery of the nuclear pore complex, *Mol Biol Cell* **8**(12), 2379–2390 (1997).
- [194] T. Hu, T. Guan, and L. Gerace, Molecular and Functional Characterization of the p62 Complex, an Assembly of Nuclear Pore Complex Glycoproteins, *J Cell Biol* **134**(3), 589–601 (1996).
- [195] J. Sukegawa and G. Blobel, A nuclear pore complex protein that contains zinc finger motifs, binds DNA, and faces the nucleoplasm, *Cell* **72**(1), 29–38 (1993).
- [196] S. Shah and D. J. Forbes, Separate nuclear import pathways converge on the nucleoporin Nup153 and can be dissected with dominant-negative inhibitors, *Curr Biol* **8**(25), 1376–1386 (1998).
- [197] Y. Matsuura, A. Lange, M. T. Harreman, A. H. Corbett, and M. Stewart, Structural basis for Nup2p function in cargo release and karyopherin recycling in nuclear import, *EMBO J* **22**(20), 5358–5369 (2003).
- [198] C. Rollenhagen, P. Mühlhäusser, U. Kutay, and N. Panté, Importin beta-depending Nuclear Import Pathways: Role of the Adapter Proteins in the Docking and Releasing Steps, *Mol Biol Cell* **14**, 2104–2115 (2003).
- [199] S. Wälde, K. Thakar, S. Hutten, C. Spillner, A. Nath, U. Rothbauer, S. Wiemann, and R. H. Kehlenbach, The nucleoporin Nup358/RanBP2 promotes nuclear import in a cargo and transport receptor-specific manner, *Traffic* **13**, 218–233 (2012).
- [200] S. Hutten, A. Flotho, F. Melchior, and R. H. Kehlenbach, The Nup358-RanGAP Complex Is Required for Efficient Importin alpha/beta-dependent Nuclear Import, *Mol Biol Cell* **19**(5), 2300–2310 (2008).

- [201] S. Hutten, S. Wälde, C. Spillner, J. Hauber, and R. H. Kehlenbach, The nuclear pore component Nup358 promotes transportin-dependent nuclear import, *J Cell Sci* **122**(8), 1100–1110 (2009).
- [202] R. A. Pumroy, J. D. Nardozzi, D. J. Hart, M. J. Root, and G. Cingolani, Nucleoporin Nup50 Stabilizes Closed Conformation of Armadillo repeat 10 in Importin α 5, *J Biol Chem* **287**(3), 2022–2031 (2012).
- [203] J. Kobayashi and Y. Matsuura, Structural Basis for Cell-Cycle-Dependent Nuclear Import Mediated by the Karyopherin Kap121p, *J Mol Biol* **425**, 1852–1868 (2013).
- [204] R. P. Grant, D. Neuhaus, and M. Stewart, Structural Basis for the Interaction Between the Tap/NXF1 UBA Domain and FG Nucleoporins at 1 Å Resolution, *J Mol Biol* **326**(3), 849–858 (2003).
- [205] M. Hobeika, C. Brockmann, F. Gruessing, D. Neuhaus, G. Divita, M. Stewart, and C. Dargemont, Structural Requirements for the Ubiquitin-associated Domain of the mRNA Export Factor Mex67 to Bind Its Specific Targets, the Transcription Elongation THO Complex Component Hpr1 and Nucleoporin FXFG Repeats, *J Biol Chem* **284**(26), 17575–17583 (2009).
- [206] R. Bayliss, T. Littlewood, L. A. Strawn, S. R. Wentz, and M. Stewart, GLFG and FxFG Nucleoporins Bind to Overlapping Sites on Importin-beta, *J Biol Chem* **277**(52), 50597–50606 (2002).
- [207] S. M. Liu and M. Stewart, Structural Basis for the High-affinity Binding of Nucleoporin Nup1p to the *Saccharomyces cerevisiae* Importin- β Homologue, Kap95p, *J Mol Biol* **349**(3), 515–525 (2005).
- [208] M. A. Powers, D. J. Forbes, J. E. Dahlberg, and E. Lund, The Vertebrate GLFG Nucleoporin, Nup98, Is an Essential Component of Multiple RNA Export Pathways, *J Cell Biol* **136**(2), 241–250 (1997).
- [209] S. Fribourg, I. C. Braun, E. Izaurralde, and E. Conti, Structural Basis for the Recognition of a Nucleoporin FG Repeat by the NTF2-like Domain of the TAP/p15 mRNA Nuclear Export Factor, *Mol Cell* **8**(3), 645–656 (2001).
- [210] R. Bayliss, S. W. Leung, R. P. Baker, B. B. Quimby, A. H. Corbett, and M. a. Stewart, Structural basis for the interaction between NTF2 and nucleoporin FxFG repeats, *EMBO J* **21**(12), 2843–2853 (2002).
- [211] P. Charneau, G. Mirambeau, P. Roux, S. Paulous, H. Buc, and F. Clavel, HIV-1 Reverse Transcription A Termination Step at the Center of the Genome, *J Mol Biol* **241**(5), 651–662 (1994).
- [212] D. R. Smyth, M. K. Mrozkiewicz, W. J. McGrath, P. Listwan, and B. Kobe, Crystal structures of fusion proteins with large-affinity tags, *Protein Sci* **12**(7), 1313–1322 (2003).
- [213] D. Hanahan, *DNA Cloning, a Practical Approach*, volume 1, chapter Techniques for transformation of *E. coli*, page 109, IRL Press, Ltd., 1985.
- [214] H. Schagger, Tricine-SDS-PAGE, *Nat Protoc* **1**(1), 16–22 (2006).
- [215] M. Geyer, R. Assheuer, C. Klebe, J. Kuhlmann, J. Becker, A. Wittinghofer, and H. R. Kalbitzer, Conformational states of the nuclear GTP-binding protein Ran and its complexes with the exchange factor RCC1 and the effector protein RanBP1, *Biochemistry* **38**(35), 11250–11260 (1999).
- [216] R. H. Kehlenbach, R. Assheuer, A. Kehlenbach, J. Becker, and L. Gerace, Stimulation of Nuclear Export and Inhibition of Nuclear Import by a Ran Mutant Deficient in Binding to Ran-binding Protein 1, *J Biol Chem* **276**(17), 14524–14531 (2001).
- [217] K. Thakar, S. Karaca, S. A. Port, H. Urlaub, and R. H. Kehlenbach, Identification of CRM1-dependent nuclear export cargos using quantitative mass spectrometry, *Mol Cell Proteomics* **12**, 664–678 (2013).
- [218] M. Arnold, A. Nath, J. Hauber, and R. H. Kehlenbach, Multiple Importins Function as Nuclear Transport Receptors for the Rev Protein of Human Immunodeficiency Virus Type 1, *J Biol Chem* **281**(30), 20883–20890 (2006).
- [219] F. Melchior, D. J. Sweet, and L. Gerace, Analysis of Ran/TC4 function in nuclear protein import, *Methods Enzymol* **257**, 279–291 (1995).
- [220] K. L. Guan and J. E. Dixon, Eukaryotic proteins expressed in *Escherichia coli*: an improved thrombin cleavage and purification procedure of fusion proteins with glutathione S-transferase, *Anal Biochem* **192**(2), 262–267 (1991).
- [221] A. T. Harootunian, S. R. Adams, W. Wen, J. L. Meinkoth, S. S. Taylor, and R. Y. Tsien, Movement of the Free Catalytic Subunit of cAMP-dependent Protein Kinase into and out of the Nucleus Can Be Explained by Diffusion, *Mol Biol Cell* **4**, 993–1002 (1993).

- [222] I. Waldmann, C. Spillner, and R. H. Kehlenbach, The nucleoporin-like protein NLP1 (hCG1) promotes CRM1-dependent nuclear protein export, *J Cell Sci* **125**(Pt 1), 144–154 (2012).
- [223] T. Guan, R. H. Kehlenbach, E. C. Schirmer, A. Kehlenbach, F. Fan, B. E. Clurman, N. Arnheim, and L. Gerace, Nup50, a Nucleoplasmically Oriented Nucleoporin with a Role in Nuclear Protein Export, *Mol Cell Biol* **20**(15), 5619–5630 (2000).
- [224] F. M. Ausubel, R. Brent, R. E. Kingston, D. D. Moore, J. G. Seidman, J. A. Smith, and K. Struhl, *Current protocols in molecular biology*, Greene Publishing Associates and Wiley-Interscience, 1994.
- [225] B. Kastner, N. Fischer, M. M. Golas, B. Sander, P. Dube, D. Boehringer, K. Hartmuth, J. Deckert, F. Hauer, E. Wolf, H. Uchtenhagen, H. Urlaub, F. Herzog, J. M. Peters, D. Poerschke, R. Luhrmann, and H. Stark, GraFix: sample preparation for single-particle electron cryomicroscopy, *Nat Meth* **5**(1), 53–55 (2008).
- [226] U. Mueller, N. Darowski, M. R. Fuchs, R. Forster, M. Hellmig, K. S. Paithankar, S. Puhringer, M. Steffien, G. Zocher, and M. S. Weiss, Facilities for macromolecular crystallography at the Helmholtz-Zentrum Berlin, *J Synchrotron Radiat* **19**(3), 442–449 (2012).
- [227] W. Kabsch, XDS, *Acta Crystallogr D Biol Crystallogr* **66**(Pt 2), 125–132 (02 2010).
- [228] A. J. McCoy, R. W. Grosse-Kunstleve, P. D. Adams, M. D. Winn, L. C. Storoni, and R. J. Read, Phaser crystallographic software, *J Appl Crystallogr* **40**(4), 658–674 (2007).
- [229] F. A. Quijcho, J. C. Spurlino, and L. E. Rodseth, Extensive features of tight oligosaccharide binding revealed in high-resolution structures of the maltodextrin transport/chemosensory receptor, *Structure* **5**(8), 997–1015 (1997).
- [230] A. T. Brunger, Version 1.2 of the Crystallography and NMR system, *Nat Protoc* **2**(11), 2728–2733 (2007).
- [231] P. Emsley, B. Lohkamp, W. G. Scott, and K. Cowtan, Features and development of Coot, *Acta Crystallogr D Biol Crystallogr* **66**(4), 486–501 (2010).
- [232] S. S. Patel, B. J. Belmont, J. M. Sante, and M. F. Rexach, Natively Unfolded Nucleoporins Gate Protein Diffusion across the Nuclear Pore Complex, *Cell* **129**(1), 83–96 (2007).
- [233] L. L. Blazer, D. L. Roman, M. R. Muxlow, and R. R. Neubig, Use of Flow Cytometric Methods to Quantify Protein-Protein Interactions, *Curr Protoc Cytom* **51**(13.11), 1–15 (2001).
- [234] A. A. Labokha, S. Gradmann, S. Frey, B. B. Hülsmann, H. Urlaub, M. Baldus, and D. Görlich, Systematic analysis of barrier-forming FG hydrogels from *Xenopus* nuclear pore complexes, *EMBO J* **32**(2), 204–218 (11 2012).
- [235] J. Kuhlmann, I. Macara, and A. Wittinghofer, Dynamic and Equilibrium Studies on the Interaction of Ran with Its Effector, RanBP1, *Biochemistry* **36**(40), 12027–12035 (1997).
- [236] C. I. Villa Braslavsky, C. Nowak, D. Görlich, A. Wittinghofer, and J. Kuhlmann, Different Structural and Kinetic Requirements for the Interaction of Ran with the Ran-Binding Domains from RanBP2 and Importin- β , *Biochemistry* **39**(38), 11629–11639 (2000).
- [237] J. R. Harris, Transmission electron microscopy in molecular structural biology: A historical survey, *Arch Biochem Biophys* (2014).
- [238] J. L. S. Milne, M. J. Borgnia, A. Bartesaghi, E. E. H. Tran, L. A. Earl, D. M. Schauder, J. Lengyel, J. Pierson, A. Patwardhan, and S. Subramaniam, Cryo-electron microscopy – a primer for the non-microscopist, *FEBS J* **280**(1), 28–45 (2013).
- [239] X.-c. Bai, G. McMullan, and S. H. W. Scheres, How cryo-EM is revolutionizing structural biology, *Trends Biochem Sci* **40**(1), 49–57 (2015).
- [240] L. Englmeier, M. Fornerod, F. R. Bischoff, C. Petosa, I. W. Mattaj, and U. Kutay, RanBP3 influences interactions between CRM1 and its nuclear protein export substrates, *EMBO Rep* **2**(10), 926–932 (2001).
- [241] M. E. Lindsay, J. M. Holaska, K. Welch, B. M. Paschal, and I. G. Macara, Ran-binding protein 3 is a cofactor for Crm1-mediated nuclear protein export, *J Cell Biol* **153**(7), 1391–1402 (2001).
- [242] J. Reinders, A. Sickmann, W. Weiss, F. Weiland, and A. Görg, *Methods in Molecular Biology™*, volume 564, pages 59–82, Humana Press, 2009.
- [243] T. A. Isgro and K. Schulten, Cse1p-Binding Dynamics Reveal a Binding Pattern for FG-Repeat Nucleoporins on Transport Receptors, *Structure* **15**(8), 977–991 (2007).

List of Figures

1. Nucleoporins	9
2. Secondary structure of Nup214	11
3. The Ran cycle in nucleocytoplasmic transport	13
4. Comparison of import and export complexes	15
5. Multiple cloning site of the vector pMal-linkerAAA	35
6. Multiple cloning site of the vector pMal-PreScission	35
7. Multiple cloning site of the vector pMal-linkerAAA-PreScission	35
8. Multiple cloning site of the vector pMal-His-MCS-MBP	35
9. Transport buffer gave higher fluorescence signals in the bead-based flow cytometry assay	58
10. Controls verified the specificity of the Halo assay	60
11. Comparison of CRM1 binding to different Nup214-fragments	61
12. Analysis of CRM1-cargo interactions	62
13. CRM1 is the karyopherin with the highest avidity for Nup214	63
14. The relative effect of Nup214 varies with different cargoes	64
15. Nup214 increases the stability of CRM1 export complexes towards RanGAP-induced GTP-hydrolysis	65
16. Nup214 binds to export complexes in the presence of RanGTP	66
17. The Nup214-fragments 1930-2021 and 1916-2033 both bind stably to the export complex	66
18. Binding of Nup214 fragments to CRM1 export complexes	68
19. <i>In vivo</i> and <i>in vitro</i> binding assays indicate that the length of the Nup214 fragment influ- ences the stability of CRM1-binding	70
20. The C-terminus of Ran influences the stability of the CRM1-RanGTP-Nup214 complex . .	71
21. Nup214 bound to the export complex was fixed and purified with GraFix	73
22. Single particles of the Nup214 complex	73
23. Titration of cross-linkers BS ³ and EGS to GST-Nup214(1968-2033)-CRM1-RanGTP- SPN1 complex	76
24. Cross-links of the GST-Nup214(1968-2033)-CRM1-RanGTP-SPN1 complex mapped on the crystal structure of the export complex	77
25. Cross-linking of His-Nup214(1916-2033)-His complexes by BS ³	79
26. Cross-linking of the MBP-Nup214(1916-2033)-His complex by BS ³ and EDC	81
27. The identified cross-links of Nup214(1916-2033) were mapped on the crystal structure of the export complex (PDB ID: 3GJX, [127])	83
28. Purification of the CRM1-RanGTP-SPN1-Nup214 complex for crystallization	85
29. Optimization of crystal formation	86
30. Nup214 interactions on the CRM1-RanGTP-SPN1 export complex	89
31. Nup214-binding sites on CRM1	90
32. Analysis of Nup214 SG and charge exchange mutants in a variety of assays reveals an importance for FG-repeats and lysines in CRM1-binding	93
33. Analysis of the structure-derived Nup214 mutants confirms the importance of the identi- fied phenylalanines in CRM1-binding	95
34. Co-transfection of Nup214 mutants with GFP-SPN1	97
35. Phenylalanine-binding pockets on CRM1	99
36. Selected mutations of CRM1 were introduced into the structure <i>in silico</i> with PyMOL . . .	100
37. CRM1 mutants show no differences in binding to phenylsepharose	101
38. CRM1 mutants showed diverse binding to NES/ RanGTP and Nup214	102
39. Differences in NES and Nup214 are not additive for the tested CRM1 double and triple mutants	103

40. RanBP3 stabilizes export complexes	105
41. RanBP3 and Nup214 compete for binding to CRM1 export complexes	106
42. RanBP3 and Nup214 can bind free CRM1, but no CRM1 export complexes, simultaneously	107
43. The cross-links were mapped on the crystal structure of the Nup214 complex	112
44. Nup214 stabilizes the closed conformation of CRM1 by acting as a molecular clamp . . .	114
45. Comparison of the crystal structures of the Nup214-CRM1-RanGTP-SPN1 complex and the Xpo1p-Gsp1pGTP-Yrb2p complex	117
S1. CRM1-Cy3 binding to a subset of Nup214 fragments can be compared by the intensities of the fluorescent halos	141
S2. The N-terminus of His-Nup214(1916-2033)-His unspecifically cross-links residues across the surface of the export complex	151
S3. The N-terminus of His-Nup214(K1916-2033)-His unspecifically cross-links residues across the surface of the export complex	160
S4. The MBP-tag of Nup214(1916-2033) cross-links indiscriminately to the surface of the ex- port complex	165
S5. Alignment of <i>H. sapiens</i> CRM1 and <i>S. cerevisiae</i> Xpo1p	166
S6. Alignment of <i>H. sapiens</i> Nup214 and <i>S. cerevisiae</i> Nup159	168
S7. Alignment of <i>H. sapiens</i> RanBP3 and <i>S. cerevisiae</i> Yrb2p	169
S8. Comparison of the CRM1-RanGTP-SPN1 architecture in the crystal structure of the Nup214 complex and the export complex	172
S9. Nup214 fragments of different lengths used in this study	173
S10. Nup214 mutants used in this study	173
S11. CRM1 single mutants showed diverse binding to NES and Nup214	176
S12. CRM1 double and triple mutants showed diverse binding to NES and Nup214	177
S13. Export kinetic	178
S14. Comparison of CRM1 from the Nup214 complex crystal structure to Xpo1p from the Yrb2 complex	179

List of Tables

1. Overview of structures of transport factors with FG-repeats	19
2. Software	21
3. Technical equipment	21
4. Consumables	22
5. Kits	23
6. Chemicals and Reagents	23
7. Enzymes	24
8. Buffers and Solutions	25
9. Stock solutions	26
10. Bacterial media	26
11. Cell lines	26
12. <i>E. coli</i> strains	27
13. Primary antibodies	27
14. Secondary antibodies	28
15. Oligonucleotides for cloning	28
16. Oligonucleotides for mutagenesis	30
17. Oligonucleotides for sequencing	33
18. Synthesized Genes	33
19. Available Vectors	34
20. Generated Vectors	34
21. Available Plasmids	36
22. Generated Plasmids	36
23. Summary of the identified cross-links between His-Nup214(1916-2033)-His fragments and the export complex	80
24. Summary of the identified cross-links between MBP-Nup214(1916-2033)-His and the ex- port complex	81
25. Crystal statistics	87
26. Mutated residues in CRM1	98
27. Purified CRM1 mutants and their effect on NES binding, Nup214 binding and export . . .	104
28. Summary of the identified cross-links between Nup214 and the export complex	111
S1. Cross-linking of GST-Nup214 complex with BS ³ and BS ² G	142
S2. Cross-linking of His-Nup214(1916-2033)-His complex with BS ³	143
S3. Cross-linking of His-Nup214(K1916-2033)-His complex with BS ³	152
S4. Cross-linking of the MBP-Nup214(1916-2033)-His complex with BS ³	161
S5. Cross-linking of the MBP-Nup214(1916-2033)-His complex with EDC	164
S6. Interactions of Nup214 to CRM1 in the crystal structure	170
S7. CRM1 mutants designed to impair binding to Nup214	174
S8. Abbreviations	180
S9. Amino acid codes	181

Appendix

A Synthesized genes

The sequences of synthesized genes as ordered from the companies. Capital letters highlight the respective restriction sites as well as the mutated residues as compared to the wildtype.

NdeI-Nup214K1942C-XhoI

1916-2033

5'-CATATGtcaaatacctctaacctatttgaaacagtggggccaagacatttggaggattgccagctcgtcgtttggagagcagTGTccc actggcactttcagctctggaggaggaagtgtggcatccaaggctttgggtttcctctccaaacaaaacagggtggcttcggtgctgctccaggtt tggcagccctcctactttgggggatcccctgggtttggaggggtgccagcattcgggtcagccccagcctttacaagccctctgggctcgacgg gaggcaaagtgttcggagagggcactgcagctgccagcgcaggaggattcgggtttgggagcagcagcaacaccacaCTCGAG-3'

NdeI-Nup214K1966C-XhoI

1916-2033

5'-CATATGtcaaatacctctaacctatttgaaacagtggggccaagacatttggaggattgccagctcgtcgtttggagagcagaaaccc actggcactttcagctctggaggaggaagtgtggcatccaaggctttgggtttcctctccaaacTGTacaggtggcttcggtgctgctccagtg tttggcagccctcctactttgggggatcccctgggtttggaggggtgccagcattcgggtcagccccagcctttacaagccctctgggctcgacgg gaggcaaagtgttcggagagggcactgcagctgccagcgcaggaggattcgggtttgggagcagcagcaacaccacaCTCGAG-3'

NdeI-Nup214K2010C-XhoI

1916-2033

5'-CATATGtcaaatacctctaacctatttgaaacagtggggccaagacatttggaggattgccagctcgtcgtttggagagcagaaaccc actggcactttcagctctggaggaggaagtgtggcatccaaggctttgggtttcctctccaaacaaaacagggtggcttcggtgctgctccaggtt tggcagccctcctactttgggggatcccctgggtttggaggggtgccagcattcgggtcagccccagcctttacaagccctctgggctcgacgg gaggcTGTgttcggagagggcactgcagctgccagcgcaggaggattcgggtttgggagcagcagcaacaccacaCTCGAG-3'

NdeI-Nup214(1916-2033)KA-XhoI

K1928A K1942A K1966A K2010A

5'-CATATGtcaaatacctctaacctatttgaaacagtggggccGCGacatttggaggattgccagctcgtcgtttggagagcagGCGc ccactggcactttcagctctggaggaggaagtgtggcatccaaggctttgggtttcctctccaaacGCGacaggtggcttcggtgctgctcca gtgtttggcagccctcctactttgggggatcccctgggtttggaggggtgccagcattcgggtcagccccagcctttacaagccctctgggctcga cgggagggcGCGgtgttcggagagggcactgcagctgccagcgcaggaggattcgggtttgggagcagcagcaacaccacaCTCGAG -3'

EcoRI-Nup214(1859-2090)KA-SalI

K1892A K1900A K1928A K1942A K1966A K2010A

5'-GAATTCtggaaatagctttggccagcaatcatcctctccagtggtagcgtgtttgggtctggaacactggaagagggggagggtttctca gtggccttgagggaGCGcccagtcaggatgcagccaacGCGaaccattcagctcggccagtgggggctttggatccacagctacctca aatacctctaacctatttgaaacagtggggccGCGacatttggaggattgccagctcgtcgtttggagagcagGCGcccactggcactttc agctctggaggaggaagtgtggcatccaaggctttgggtttcctctccaaacGCGacaggtggcttcggtgctgctccaggtttggcagccc tctactttgggggatcccctgggtttggaggggtgccagcattcgggtcagccccagcctttacaagccctctgggctcgacgggagggcGCG gtgttcggagagggcactgcagctgccagcgcaggaggattcgggtttgggagcagcagcaacaccacatccttcggcagcgtcgcgagtc agaatgccccactttcggatcactgtcccaacagactctggtttgggaccagagtagcggattctcgtgtttggatcaggcacaggagggtt cagctttgggtcaaataactcgtctgtccagggtttgtggctggcgaagcGTTCGAC-3'

EcoRI-Nup214(1859-2090)KAa1-Sall

K1892A K1900A K1928A K1942A K1966A K2010A F1970S F1976S F1982S F1988S

5'-GAATTCtgaatagtcttggccagcaatcatcctctccagtggtagcgtgttgggtctggaaacactggaagagggggaggttctca
gtggccttgagggaGCGcccagtcaggatgcagccaacGCGaacccattcagctcggccagtgggggccttggatccacagctacctca
aataccttaacctatttggaaacagtgggggccGCGacatttgggtgatttgcagctcgtcgttggagagcagGCGcccactggcactttc
agctctggaggaggaagtgtggcatccaaggccttgggtttcctcctcaaacGCGacaggtggcAGTggtgctgtccagtgAGTggc
agccctcctactAGTgggggatcccctgggAGTggaggggtgccagcattcgggtcagccccagcctttacaagccctctgggctcgacgg
gaggcGCGgttctggagagggcactgcagctgccagcgcaggaggattcgggttgggagcagcagcaaacaccacatcctcggcagc
ctcgcgagtcagaatgccccactttcgatcactgtcccaacagacttctggttgggaccagagtagcggattctctggtttggatcaggca
caggaggggtcagcttgggtcaataactcgtctgtccagggtttgggtggcgaagcGTTCGAC-3'

EcoRI-Nup214(1859-2090)KE-Sall

K1892E K1900E K1928E K1942E K1966E K2010E

5'-GAATTCtgaatagtcttggccagcaatcatcctctccagtggtagcgtgttgggtctggaaacactggaagagggggaggttctca
gtggccttgagggaGAGcccagtcaggatgcagccaacGAGaacccattcagctcggccagtgggggccttggatccacagctacctcaa
ataccttaacctatttggaaacagtgggggccGAGacatttgggtgatttgcagctcgtcgttggagagcagGAGcccactggcactttcag
ctctggaggaggaagtgtggcatccaaggccttgggtttcctcctcaaacGAGacaggtggctcgggtcgtcctcagtggttggcagccctc
ctactttgggggatcccctgggttggaggggtgccagcattcgggtcagccccagcctttacaagccctctgggctcgacgggagggcGAGgt
gttcggagagggcactgcagctgccagcgcaggaggattcgggttgggagcagcagcaaacaccacatcctcggcagcgtcgcgagtcag
aatgccccactttcgatcactgtcccaacagacttctggttgggaccagagtagcggattctctggttggatcaggcacaggaggggtca
gcttgggtcaataactcgtctgtccagggtttgggtggcgaagcGTTCGAC-3'

EcoRI-Nup214(1859-2090)a1(5SGs)-Sall

F1970S F1976S F1982S F1988S F1994S

5'-GAATTCtgaatagtcttggccagcaatcatcctctccagtggtagcgtgttgggtctggaaacactggaagagggggaggttctca
gtggccttgaggaaagcccagtcaggatgcagccaacaagaaccattcagctcggccagtgggggccttggatccacagctacctcaaat
accttaacctatttggaaacagtggggccaagacatttgggtgatttgcagctcgtcgttggagagcagaaacccactggcactttcagctc
ggaggaggaagtgtggcatccaaggccttgggtttcctcctcaaaaacaggtggcAGTggtgctgtccagtgAGTggcagccctc
ctactAGTgggggatcccctgggAGTggaggggtgccagcaAGTggtcagccccagcctttacaagccctctgggctcgacgggagg
caaagtgttcggagagggcactgcagctgccagcgcaggaggattcgggttgggagcagcagcaaacaccacatcctcggcagcgtcgcg
agtcagaatgccccactttcgatcactgtcccaacagacttctggttgggaccagagtagcggattctctggttggatcaggcacaggga
gggtcagcttgggtcaataactcgtctgtccagggtttgggtggcgaagcGTTCGAC-3'

EcoRI-Nup214(1916-2033)a1(4SGs)-Sall

F1970S F1976S F1982S F1988S

5'-GAATTCtcaaataccttaacctatttggaaacagtggggccaagacatttgggtgatttgcagctcgtcgttggagagcagaaacc
actggcactttcagctcgtggaggaggaagtgtggcatccaaggccttgggtttcctcctcaaaaacaggtggcAGTggtgctgtccag
tgAGTggcagccctcctactAGTgggggatcccctgggAGTggaggggtgccagcattcgggtcagccccagcctttacaagccctctgg
gctcgacgggagggcaaagtgttcggagagggcactgcagctgccagcgcaggaggattcgggttgggagcagcagcaaacaccacaGT
TCGAC-3'

SacI-CRM1_K680Q_A731Q-MssI

5'-aaaaaaaGAGCTCactggaaatttctgaagactgtagttaacaagctgttcaattatcatgatgagaccatgatggagtccaggatat
ggctgtgatactttcattaaaaatagcccaaaaatgccgcaggcatttctgtcaggttccaggttggagaagtgatccatttattgatgaaattttaa
caacattaacactatttattgtatctcagcctcaacagggtcatacgtttatgaagctgtgggtacatgattggtgcacaaacagatcaaacag
tacaagaacacttgatagaaaagtacatgttactccctaatcaagtgtgggatagataatccagcaggcaacaaaaaatgtggatatactgC
AAGatcctgaaacagtcaagcagcttggtagcatttggaaacaaatgtgagagcctgcaaagctgttggacaccccttgaattcagcttgg
agaatttattgatagatgcttaatgtatacaagtcctcagtgaaaatatttctgcaCAGatccaagctaatggtgaaatggttcaaaagcaacca
ttgattagaagtatgccaactgtaaaaagggaaactttaaagtaatatctggttgggtgagccgatccaatgatccacagatggtcgtgaaaat

ttgttccccctctgttggatgcagttctcattgattatcagagaaatgtcccagctgctagagaaccagaagtgttagtactatggccataattgtca
acaagttagggggacatataacagctgaaatacctcaaatattgtatgctgttttgaatgcacattgaatatgataaataaggactttgaagaata
tctgaacatagaacgaacttttctactactcaggctgtcaattctcattgttcccagcattccttctattccacctacacaGTTTAAACaaa
aaa-3'

Sacl-CRM1_K680Q_A731Q_L679R-Mssl

5'-aaaaaaGAGCTCactggaatttctgaagactgtagtaacaagctgttccaattcatgcatgagaccatgatggagtccaggat
ggcttggatattcattaaaaatagcccaaaaatgccgcagcattcgttcagggtcagggtggagaagtgtaccatttattgatgaaatttgaa
caacattaacactattatttggatcttcagcctcaacaggttcatacgtttatgaagctgtgggtacatgattgggtgcacaaacagatcaaacag
tacaagaacacttgatagaaaagtacatgttactcccaatcaagtggtggatagataatccagcaggcaacaaaaatgtggatataCGT
CAAgatcctgaaacagtcagcagctgttagcattttgaaaacaaatgtgagagcctgcaaagctgtggacacccttgaattcagctgg
aagaatttattagatagcttaagtatacaagtgccctcagtgaaaatattctgcaCAGatccaagctaagtggaatgggtacaaagcaacc
attgattagaagtatgcgaactgtaaaaagggaaactttaaagtaatatctggttgggtgagccgatccaatgatccacagatggctgctgaaa
atttgtccccctctgttggatgcagttctcattgattatcagagaaatgtcccagctgctagagaaccagaagtgttagtactatggccataattgt
caacaagttagggggacatataacagctgaaatacctcaaatattgtatgctgttttgaatgcacattgaatatgataaataaggactttgaagaa
tatcctgaacatagaacgaacttttctactactcaggctgtcaattctcattgttcccagcattccttctattccacctacacaGTTTAAACa
aaaaa-3'

Sacl-CRM1_K680Q_A731Q_C723M-Mssl

5'-aaaaaaGAGCTCactggaatttctgaagactgtagtaacaagctgttccaattcatgcatgagaccatgatggagtccaggat
ggcttggatattcattaaaaatagcccaaaaatgccgcagcattcgttcagggtcagggtggagaagtgtaccatttattgatgaaatttgaa
caacattaacactattatttggatcttcagcctcaacaggttcatacgtttatgaagctgtgggtacatgattgggtgcacaaacagatcaaacag
tacaagaacacttgatagaaaagtacatgttactcccaatcaagtggtggatagataatccagcaggcaacaaaaatgtggatatactgC
AAGatcctgaaacagtcagcagctgttagcattttgaaaacaaatgtgagagcctgcaaagctgtggacacccttgaattcagctgga
agaatttattagatagcttaagtatacaagATGctcagtgaaaatattctgcaCAGatccaagctaagtggaatgggtacaaagcaacc
attgattagaagtatgcgaactgtaaaaagggaaactttaaagtaatatctggttgggtgagccgatccaatgatccacagatggctgctgaaa
atttgtccccctctgttggatgcagttctcattgattatcagagaaatgtcccagctgctagagaaccagaagtgttagtactatggccataattgt
caacaagttagggggacatataacagctgaaatacctcaaatattgtatgctgttttgaatgcacattgaatatgataaataaggactttgaagaa
tatcctgaacatagaacgaacttttctactactcaggctgtcaattctcattgttcccagcattccttctattccacctacacaGTTTAAACa
aaaaa-3'

Sall-CRM1_I102W_F149W-Sacl

5'-aaaaaaGTCGACacaatttggaaatttctcagaatataaatacgaatactatggactacaaatttggaaaatgtgataaaaacaagg
tgaagattctccaaggaaccagtgcaaggaTGaaaaaatacgttggcctcattatcaagacgtcatctgacccaacttgttagag
aaagaaaaggtgtatatacgaaaataaataatgatcctgttcagatactgaaacaagaatggcccaaacattggccaactTGatcagtgat
attgttggagcaagtaggaccagcgaaagtctctgcaaaaataatggtgattcttaactctgagtgagaagtatttatttctctagtggaca
gataaccaagtcacaaatctaaagcattttaaagacagcaatgcaatgaattctcacagatattcaactgtgtagttgtaatgaaaattctcaa
aatgctccactgtacatgcaacctggaacattgctcagatttctgaactggattcccctgggataatatttggagacaaataatcagcacattg
attataagttcctgaaatgttccaatgttccgaatgtctctcgaagtgcctcactgagattgctgggtgagtgtaagccaatataagaacaattt
taacactatttactctgacaatgatgcaactaaagcagatgctcctttaaataccaatattcgaacttgcgtactcaaatggaaaagatgatgaaca
gaacttcattcaaaatctcagttgttctctgcaccttcttaaggaacatgatcaacttatagaaaaagattaaatctcagggaaactctatgga
ggccctcattatattgttggatctgaaagtagaagaactgaaatctttaaattgtcttgaatactggaatcatttggctgctgaactctatagag
agagtcattctctacatctgcctcctcgttgccttctggaagtcaacattttagatttctcccaggagacagctatattgccatgttattcaaggctc
gttattaatggttagtgaatggctaaaccagaggaagtattggtttagagaatgatcaaggagaagtgtgagagaattatgaaggatata
gattccataaattgtataagaatagagggaaacattggttattctactcatctggattatgtagatacagaaagaataatgacagagaagcttc
acaatcaagtgaatggtacagagtggtcatggaaaaattgaatacattgttggcaataggctcattagtgagcaatgcatgaagagga
cgaaaaacgatttctgttactgttataaaggatctattaggattatgtaacagaaaagaggcaaaagataataaagctatttattgcatcaaatatc
atgtacatagtaggcaataccacgtttttgaGAGCTCaaaaaa-3'

Sall-CRM1_I102W_N167R-Sacl

5'-aaaaaaGTCGACacaatttggaaatttctcagaatataaatacgaatactatggactacaaatttggaaaatgtgataaaaacaagg
tgaagattctccaaggaaccagtgcaaggaTGaaaaaatacgttggcctcattatcaagacgtcatctgacccaacttgttagag
aaagaaaaggtgtatatacgaaaataaataatgatcctgttcagatactgaaacaagaatggcccaaacattggccaactttatcagtgatatt
gttggagcaagtaggaccagcgaaagtctctgcaaaaatCGTatggtgattcttaactctgagtgagaagtatttatttctctagtggacag

ataaccaagtc aaatctaagc atttaaaagacagc atgtgcaatgaattctcacagatattcaactgtgtcagtttgaatggaaaattctcaa
atgtccactgtgacatgcaacctggaaacattgtctcagatttctgaactggattcccctgggatataatgttgagacc aaattaatcagcacattgat
ttataagttcctgaaatgttccaatgttctgaaatgtctctcgaagtgcctcactgagattgtctggtgtgagtgtaagccaatataagaacaatttga
acactatttactctgacaatgatgcaactaaagcagatgcttccittaaataccaatattcgacttgcgtactcaaagaaaagatgatgaacag
aacttcattcaaaatctcagttgttctctgcaccttcttaaggaacatgatcaactatagaaaaaagattaaatctcagggaaactcttatggag
gcccttcattatagtgttggtatctgaagtagaagaactgaaatctttaaattgtcttgaatactggaatcattggctgtgactctatagaga
gagtcacattctacatctgcctctccgttcttctggaagtc aacatttgaatgttctctccaggagacagctatattgccatgttattcaaggctcg
tttaataatggttagtgaatggctaaaccagaggaagtattggtgtagagaatgatcaaggagaagtgtgagagaattcatgaaggatacag
attccataaattgtataagaatagagggaaacattggttacttactcatctggattatgtagatacagaaagaataatgacagagaagctcac
aatcaagtgaatggtacagagtggtcatggaaaaattgaatacattgttggcaataggctccattagtgagcaatgcatgaagaggacg
aaaaacgatttctgttactgttataaaggatctattaggattatgtgaacagaaaagaggcaagataataaagctattattgcatcaaatatcat
gtacatagtaggtcaataccacgtttttgaGAGCTCaaaaaa-3'

Sall-CRM1_I102W_D152F-SacI

5'-aaaaaaGTCGACacaatttggaaatttctcagaatataatgaatacgaataactatggactacaaatttggaaaatgtgataaaaaaagg
tgaagattctccaaggaaccagtgcaaggaTGGaaaaaatacgttggcctcattatcaagacgtcatctgaccaacttgtgtagag
aaagaaaagggtgatatcggaaaataatgatccttgttcagatactgaaacaagaatggcccaaacattggccaactttatcagTTTTat
tgttgagcaagtaggaccagcgaaagtctctgcaaaataatggtgattcttaaactctgagtgagaagaagtatttgattctctagtggacaga
taaccaagtcaaatctaagcatttaaaagacagc atgtgcaatgaattctcacagatattcaactgtgtcagtttgaatggaaaattctcaaaat
gtcaccattgtacatgcaaccttggaaacattgtcagatttctgaactggattcccctgggatataatgttgagacc aaattaatcagcacattgatt
ataagttcctgaatgttccaatgttctgaaatgtctctcgaagtgcctcactgagattgtctggtgtgagtgtaagccaatataagaacaatttga
cactatttactctgacaatgatgcaactaaagcagatgcttccittaaataccaatattcgacttgcgtactcaaagaaaagatgatgaacaga
acttcattcaaaatctcagttgttctctgcaccttcttaaggaacatgatcaactatagaaaaaagattaaatctcagggaaactcttatggagg
cccttcattatagtgttggtatctgaagtagaagaactgaaatctttaaattgtctgaatactggaatcatttggctgtgactctatagagag
agtcacattctacatctgcctctccgttcttctggaagtc aacatttgaatgttctctccaggagacagctatattgccatgttattcaaggctcgtt
tattaatggttagtgaatggctaaaccagaggaagtattggtgtagagaatgatcaaggagaagtgtgagagaattcatgaaggatacagat
tcataaatttgtataagaatagagggaaacattggttacttactcatctggattatgtagatacagaaagaataatgacagagaagcttaca
atcaagtgaatggtacagagtggtcatggaaaaattgaatacattgttgggcaataggctccattagtgagcaatgcatgaagaggacga
aaaacgatttctgttactgttataaaggatctattaggattatgtgaacagaaaagaggcaagataataaagctattattgcatcaaatatcatgt
acatagtaggtcaataccacgtttttgaGAGCTCaaaaaa-3'

EcoRI-Nup214(aa1859-2090)-Sall_mutant1

F1922S, F1930S, F1938S, F1947S, F1982S, F1988S

5'-aaaaaaGAATTCcggaaatagctttggccagcaatcatcctcttccagtggttagcgtgttgggtctggaaacactggaagaggggga
ggtttctcagtgcccttgaggaaaaccagtcaggatgagccaaacaaaaccattcagctcggccagtgggggcttggatccacagct
acctcaaataccttaacctTCTggaacagtgggccaagacaTCTggtgatttccagctcgtcTCTggagagcagaaacca
ctggcactTCCagctctggaggaggaagtgtggcatccaaggcttgggttctctcacaacaaaacaggtggctcgggtctgtccagt
gttggcagccctctactTCTgggggatcccctgggTCTggaggggtccagcattcgggtcagcccagccttacaagccctctgggctc
gacgggaggcaaatgttcggagagggcactgcagctgccagcgcaggaggattcgggttgggagcagcagcaacaccacatcctcgg
cacgctcgcgagtcagaatgccccacttccgatcactgtccaacagactctggttgggaccagagtagcggattctctggttggatca
ggcacaggaggggtcagcttgggtcaataactcgtctgtccagggtttgggtggctggcgaagcGTCGACaaaaaa-3'

EcoRI-Nup214(aa1859-2090)-Sall_mutant2

F2012S, F2024S, F2026S

5'-aaaaaaGAATTCcggaaatagctttggccagcaatcatcctcttccagtggttagcgtgttgggtctggaaacactggaagaggggga
ggtttctcagtgcccttgaggaaaaccagtcaggatgagccaaacaaaaccattcagctcggccagtgggggcttggatccacagct
acctcaaataccttaacctatttggaaacagtgggccaagacatttgggtgatttccagctcgtcgttggagagcagaaaccactggcac
ttcagctctggaggaggaagtgtggcatccaaggcttgggttctctcacaacaaaacaggtggctcgggtctgtcctcagtttggcagc
ctcctacttttgggggatcccctgggttggaggggtgccagcattcgggtcagcccagccttacaagccctctgggctcagcgggagggcaa
agtTCCggagagggcactgcagctgccagcgcaggaggaTCCgggTCTgggagcagcagcaacaccacatcctcggcacgctc
gcgagtcagaatgccccacttccgatcactgtccaacagactctggttgggaccagagtagcggattctctggttggatcaggcaca
ggaggggtcagcttgggtcaataactcgtctgtccagggtttgggtggctggcgaagcGTCGACaaaaaa-3'

EcoRI-Nup214(aa1859-2090)-Sall_mutant3

F1922S, F1930S, F1938S, F1947S, F1982S, F1988S, F2012S, F2024S, F2026S

5'-aaaaaaGAATTCcggaatagtcttggccagcaatcatcctcttccagtggtagcgtgtttgggtctggaacactggaagaggggga
ggtttctcagtgcccttgaggaaaaccagtcaggatgcagccaacaaaaaccattcagctcggccagtgggggcttggatccacagct
acctcaaatacctctaacctTCTggaaacagtggggccaagacaTCTggtggatttgcagctcgtcgTCTggagagcagaaacca
ctggcactTCCagctctggaggaggaagtgtggcatccaaggcttgggtttcctctccaaacaaaacaggtggcttcggtgctcctcagt
gtttggcagccctctactTCTgggggatcccctgggTCTggaggggtgccagcattcggttcagcccagcctttacaagccctctgggctc
gacgggaggcaaagtTCCggagagggcactgcagctgccagcgcaggaggaTCCgggTCTgggagcagcagcaacaccacat
cctcggcagctcgcgagtcagaatgccccacttccgatcactgtccaacagactctggtttgggaccagagtagcggattctctggttt
ggatcaggcacaggaggggtcagcttgggtcaaataactcgtctgtccagggtttggtggctggcgaagcGTCGACaaaaaa-3'

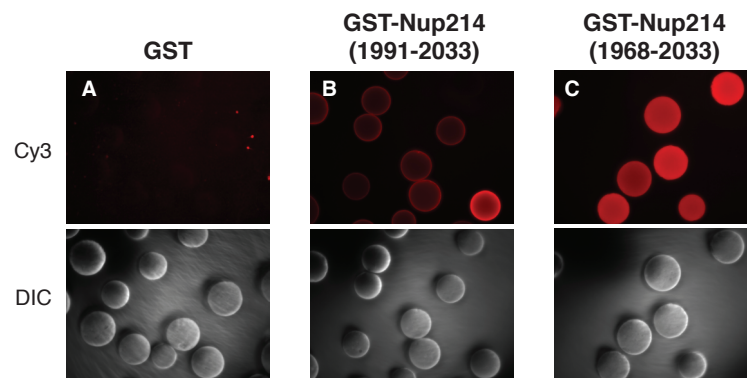
B Halo assay - analysis with fluorescence microscopy

Figure S1: CRM1-Cy3 binding to a subset of Nup214 fragments can be compared by the intensities of the fluorescent halos. 25 μg of GST or GST-Nup214 was immobilized on 2.5 μl glutathione sepharose High Performance beads (GE Healthcare) equilibrated in transport buffer containing 10 mg/ml BSA. The beads were washed twice with transport buffer containing 10 mg/ml BSA and incubated with 6.0 pmol CRM1-Cy3 and optionally 22.5 pmol RanGTP and 2.9 μl 4x assay buffer (500 mM NaCl, 40 mg/ml BSA, 1 mM DTT) in a total volume of 11.7 μl transport buffer + 10 mg/ml BSA at 4 $^{\circ}\text{C}$ for 55 minutes. The beads were washed once and subsequently mounted on a microscope slide. The samples were analyzed by fluorescence microscopy with a filter for Cy3 (upper panel) or transmitted light only (lower panel).

C Cross-linking mass spectrometry data

C.1 Cross-linking of the GST-Nup214(1968-2033) complex with BS³ and BS²G

Table S1: Cross-linking of GST-Nup214 complex with BS³ and BS²G.

Linker	XL Type	Protein 1	Protein 2	Residue 1	Residue 2	Distance [Å] in 3GJX
BS ³	intra	CRM1	CRM1	190	195	8.3
BS ³	intra	CRM1	CRM1	455	594	20.2
BS ³	intra	CRM1	CRM1	446	594	19.5
BS ³	intra	CRM1	CRM1	446	700	18.5
BS ³	intra	CRM1	CRM1	594	700	15.4
BS ³	intra	CRM1	CRM1	686	693	10.9
BS ³	intra	CRM1	CRM1	693	700	10.7
BS ³	intra	SPN1	SPN1	75	77	not in structure
BS ³	intra	SPN1	SPN1	95	97	5.4
BS ³	intra	SPN1	SPN1	264	266	7.1
BS ³	intra	SPN1	SPN1	366	370	not in structure
BS ³	intra	Ran	Ran	127	130	5.2
BS ³	intra	Ran	Ran	132	134	9.4
BS ³	inter	CRM1	SPN1	563	75	not in structure
BS ³	inter	CRM1	SPN1	680	266	12.6
BS ³	inter	CRM1	SPN1	686	266	15.8
BS ³	inter	CRM1	SPN1	686	271	16.5
BS ³	inter	CRM1	Ran	700	127	17.8
BS ² G	intra	CRM1	CRM1	190	192	5.5
BS ² G	intra	CRM1	CRM1	700	757	10.0
BS ² G	intra	CRM1	CRM1	446	594	19.5
BS ² G	intra	CRM1	CRM1	560	563	5.3
BS ² G	intra	CRM1	CRM1	693	700	10.7
BS ² G	intra	SPN1	SPN1	75	77	not in structure
BS ² G	intra	SPN1	SPN1	366	370	not in structure
BS ² G	intra	Ran	Ran	132	134	5.2
BS ² G	inter	CRM1	SPN1	594	18	not in structure
BS ² G	inter	CRM1	SPN1	594	24	not in structure
BS ² G	inter	CRM1	SPN1	560	75	not in structure
BS ² G	inter	CRM1	SPN1	680	266	12.6
BS ² G	inter	CRM1	Ran	700	127	17.8

As the used His-SPN1 construct is elongated at the N-terminus due to the cloning strategy, the Met3 from the SPN1 from 3GJX corresponds to Met44 in the cross-linking data.

C.2 Cross-linking of His-Nup214(1916-2033)-His complexes with BS³

Table S2: Cross-linking of His-Nup214(1916-2033)-His complex with BS³.

Replicate	Type	Protein 1	Protein 2	Residue 1	Residue 2	Spectrum Count
A	inter	Nup214	Ran	1	134	1
A	inter	Nup214	Ran	1	142	1
A	inter	Nup214	Ran	2	2	29
A	inter	Nup214	Ran	2	28	3
A	inter	Nup214	Ran	2	37	12
A	inter	Nup214	Ran	2	38	1
A	inter	Nup214	Ran	2	99	6
A	inter	Nup214	Ran	2	127	3
A	inter	Nup214	Ran	2	134	3
A	inter	Nup214	Ran	2	142	1
A	inter	Nup214	Ran	2	152	4
A	inter	Nup214	Ran	2	159	7
A	inter	Nup214	SPN1	1	80	1
A	inter	Nup214	SPN1	1	223	2
A	inter	Nup214	SPN1	1	313	1
A	inter	Nup214	SPN1	1	323	3
A	inter	Nup214	SPN1	2	32	3
A	inter	Nup214	SPN1	2	34	1
A	inter	Nup214	SPN1	2	52	4
A	inter	Nup214	SPN1	2	93	19
A	inter	Nup214	SPN1	2	144	1
A	inter	Nup214	SPN1	2	211	1
A	inter	Nup214	SPN1	2	223	32
A	inter	Nup214	SPN1	2	228	1
A	inter	Nup214	SPN1	2	314	9
A	inter	Nup214	SPN1	2	317	1
A	inter	Nup214	SPN1	2	321	1
A	inter	Nup214	SPN1	2	323	10
A	inter	Nup214	SPN1	2	327	8
A	inter	Nup214	SPN1	2	343	3
A	inter	Nup214	SPN1	34	223	2
A	inter	Nup214	SPN1	48	323	1
A	inter	Nup214	SPN1	48	343	1
A	inter	Nup214	CRM1	1	686	1
A	inter	Nup214	CRM1	2	122	1
A	inter	Nup214	CRM1	2	192	2
A	inter	Nup214	CRM1	2	426	5
A	inter	Nup214	CRM1	2	531	2
A	inter	Nup214	CRM1	2	534	8
A	inter	Nup214	CRM1	2	568	1
A	inter	Nup214	CRM1	2	594	3
A	inter	Nup214	CRM1	2	680	3
A	inter	Nup214	CRM1	2	686	2
A	inter	Nup214	CRM1	2	693	1
A	inter	Nup214	CRM1	2	700	7
A	inter	Nup214	CRM1	2	741	3
A	inter	Nup214	CRM1	2	757	1
A	inter	Nup214	CRM1	2	1049	3
A	inter	Nup214	CRM1	48	446	1
A	inter	Nup214	CRM1	116	22	2
A	intra	Nup214	Nup214	1	48	1
A	intra	Nup214	Nup214	2	2	2
A	intra	Nup214	Nup214	2	48	25
A	intra	Ran	Ran	1	2	5
A	intra	Ran	Ran	2	23	1
A	intra	Ran	Ran	2	28	3
A	intra	Ran	Ran	2	37	4
A	intra	Ran	Ran	2	38	5
A	intra	Ran	Ran	2	99	1
A	intra	Ran	Ran	2	159	1
A	intra	Ran	Ran	2	167	2
A	intra	Ran	Ran	12	37	1
A	intra	Ran	Ran	12	38	7
A	intra	Ran	Ran	12	99	2
A	intra	Ran	Ran	23	37	13
A	intra	Ran	Ran	23	38	1
A	intra	Ran	Ran	23	159	1
A	intra	Ran	Ran	28	37	3
A	intra	Ran	Ran	28	38	10
A	intra	Ran	Ran	28	99	2
A	intra	Ran	Ran	28	134	1
A	intra	Ran	Ran	28	152	1
A	intra	Ran	Ran	28	159	2
A	intra	Ran	Ran	37	127	1

Replicate	Type	Protein 1	Protein 2	Residue 1	Residue 2	Spectrum Count
A	intra	Ran	Ran	37	152	14
A	intra	Ran	Ran	38	99	3
A	intra	Ran	Ran	99	123	5
A	intra	Ran	Ran	99	130	2
A	intra	Ran	Ran	99	132	19
A	intra	Ran	Ran	99	134	30
A	intra	Ran	Ran	99	141	5
A	intra	Ran	Ran	99	142	11
A	intra	Ran	Ran	99	159	1
A	intra	Ran	Ran	123	130	4
A	intra	Ran	Ran	123	134	5
A	intra	Ran	Ran	123	141	1
A	intra	Ran	Ran	123	142	2
A	intra	Ran	Ran	123	152	2
A	intra	Ran	Ran	123	159	2
A	intra	Ran	Ran	127	130	9
A	intra	Ran	Ran	127	132	25
A	intra	Ran	Ran	127	134	2
A	intra	Ran	Ran	127	152	20
A	intra	Ran	Ran	127	159	1
A	intra	Ran	Ran	134	141	2
A	intra	Ran	Ran	134	142	3
A	intra	Ran	Ran	134	152	1
A	intra	Ran	Ran	134	159	3
A	intra	Ran	Ran	142	159	6
A	intra	SPN1	SPN1	32	34	1
A	intra	SPN1	SPN1	32	93	3
A	intra	SPN1	SPN1	32	144	4
A	intra	SPN1	SPN1	32	223	1
A	intra	SPN1	SPN1	32	314	13
A	intra	SPN1	SPN1	32	317	6
A	intra	SPN1	SPN1	32	321	3
A	intra	SPN1	SPN1	32	323	10
A	intra	SPN1	SPN1	32	327	4
A	intra	SPN1	SPN1	32	343	5
A	intra	SPN1	SPN1	34	80	1
A	intra	SPN1	SPN1	34	93	2
A	intra	SPN1	SPN1	34	144	6
A	intra	SPN1	SPN1	34	314	4
A	intra	SPN1	SPN1	34	323	4
A	intra	SPN1	SPN1	34	327	1
A	intra	SPN1	SPN1	52	93	1
A	intra	SPN1	SPN1	52	314	4
A	intra	SPN1	SPN1	52	323	6
A	intra	SPN1	SPN1	52	327	1
A	intra	SPN1	SPN1	52	343	1
A	intra	SPN1	SPN1	80	80	8
A	intra	SPN1	SPN1	80	92	6
A	intra	SPN1	SPN1	80	93	6
A	intra	SPN1	SPN1	80	323	1
A	intra	SPN1	SPN1	81	93	2
A	intra	SPN1	SPN1	93	144	5
A	intra	SPN1	SPN1	128	144	3
A	intra	SPN1	SPN1	144	314	4
A	intra	SPN1	SPN1	144	317	1
A	intra	SPN1	SPN1	144	321	1
A	intra	SPN1	SPN1	144	323	6
A	intra	SPN1	SPN1	144	343	1
A	intra	SPN1	SPN1	167	211	2
A	intra	SPN1	SPN1	211	223	2
A	intra	SPN1	SPN1	211	314	2
A	intra	SPN1	SPN1	211	323	1
A	intra	SPN1	SPN1	211	327	1
A	intra	SPN1	SPN1	221	228	5
A	intra	SPN1	SPN1	223	223	4
A	intra	SPN1	SPN1	223	314	3
A	intra	SPN1	SPN1	223	323	4
A	intra	SPN1	SPN1	223	327	7
A	intra	SPN1	SPN1	223	343	6
A	intra	SPN1	SPN1	228	314	2
A	intra	SPN1	SPN1	298	314	5
A	intra	SPN1	SPN1	314	321	1
A	intra	SPN1	SPN1	314	327	20
A	intra	SPN1	SPN1	314	343	6
A	intra	SPN1	SPN1	314	345	3
A	intra	SPN1	SPN1	317	323	2
A	intra	SPN1	SPN1	317	327	2
A	intra	SPN1	SPN1	321	327	4
A	intra	SPN1	SPN1	314	323	8
A	intra	SPN1	SPN1	323	343	13
A	intra	SPN1	SPN1	327	345	1

Replicate	Type	Protein 1	Protein 2	Residue 1	Residue 2	Spectrum Count
A	intra	CRM1	CRM1	1	1	2
A	intra	CRM1	CRM1	1	122	1
A	intra	CRM1	CRM1	1	144	1
A	intra	CRM1	CRM1	1	537	1
A	intra	CRM1	CRM1	2	122	2
A	intra	CRM1	CRM1	2	531	1
A	intra	CRM1	CRM1	54	88	16
A	intra	CRM1	CRM1	54	129	5
A	intra	CRM1	CRM1	54	522	1
A	intra	CRM1	CRM1	76	122	2
A	intra	CRM1	CRM1	88	92	13
A	intra	CRM1	CRM1	92	103	1
A	intra	CRM1	CRM1	92	144	26
A	intra	CRM1	CRM1	92	190	18
A	intra	CRM1	CRM1	92	192	7
A	intra	CRM1	CRM1	103	122	1
A	intra	CRM1	CRM1	103	144	6
A	intra	CRM1	CRM1	103	192	2
A	intra	CRM1	CRM1	103	1049	1
A	intra	CRM1	CRM1	104	144	1
A	intra	CRM1	CRM1	104	1049	3
A	intra	CRM1	CRM1	122	129	2
A	intra	CRM1	CRM1	144	190	6
A	intra	CRM1	CRM1	144	192	6
A	intra	CRM1	CRM1	144	312	1
A	intra	CRM1	CRM1	144	415	2
A	intra	CRM1	CRM1	144	492	3
A	intra	CRM1	CRM1	144	680	1
A	intra	CRM1	CRM1	172	192	1
A	intra	CRM1	CRM1	190	192	1
A	intra	CRM1	CRM1	190	522	1
A	intra	CRM1	CRM1	190	1049	4
A	intra	CRM1	CRM1	192	1049	7
A	intra	CRM1	CRM1	312	590	3
A	intra	CRM1	CRM1	331	534	1
A	intra	CRM1	CRM1	331	1049	1
A	intra	CRM1	CRM1	415	479	2
A	intra	CRM1	CRM1	415	674	3
A	intra	CRM1	CRM1	426	455	1
A	intra	CRM1	CRM1	426	492	2
A	intra	CRM1	CRM1	446	594	8
A	intra	CRM1	CRM1	446	700	11
A	intra	CRM1	CRM1	455	594	6
A	intra	CRM1	CRM1	455	1049	1
A	intra	CRM1	CRM1	492	522	5
A	intra	CRM1	CRM1	514	522	5
A	intra	CRM1	CRM1	514	560	11
A	intra	CRM1	CRM1	522	534	1
A	intra	CRM1	CRM1	522	560	43
A	intra	CRM1	CRM1	522	563	2
A	intra	CRM1	CRM1	531	534	14
A	intra	CRM1	CRM1	531	537	1
A	intra	CRM1	CRM1	531	680	2
A	intra	CRM1	CRM1	534	594	3
A	intra	CRM1	CRM1	537	563	1
A	intra	CRM1	CRM1	560	568	6
A	intra	CRM1	CRM1	560	594	1
A	intra	CRM1	CRM1	563	594	1
A	intra	CRM1	CRM1	594	700	18
A	intra	CRM1	CRM1	594	1049	8
A	intra	CRM1	CRM1	594	1051	1
A	intra	CRM1	CRM1	680	693	5
A	intra	CRM1	CRM1	680	741	2
A	intra	CRM1	CRM1	686	700	2
A	intra	CRM1	CRM1	693	700	11
A	intra	CRM1	CRM1	693	741	18
A	intra	CRM1	CRM1	693	757	19
A	intra	CRM1	CRM1	700	757	25
A	intra	CRM1	CRM1	752	757	2
A	inter	CRM1	SPN1	1	211	1
A	inter	CRM1	SPN1	1	223	1
A	inter	CRM1	SPN1	92	32	1
A	inter	CRM1	SPN1	92	323	1
A	inter	CRM1	SPN1	103	314	1
A	inter	CRM1	SPN1	339	93	1
A	inter	CRM1	SPN1	339	298	1
A	inter	CRM1	SPN1	367	223	1
A	inter	CRM1	SPN1	415	32	7
A	inter	CRM1	SPN1	426	93	2
A	inter	CRM1	SPN1	446	144	1
A	inter	CRM1	SPN1	446	223	1

Replicate	Type	Protein 1	Protein 2	Residue 1	Residue 2	Spectrum Count
A	inter	CRM1	SPN1	492	93	1
A	inter	CRM1	SPN1	522	1	1
A	inter	CRM1	SPN1	522	32	9
A	inter	CRM1	SPN1	522	34	9
A	inter	CRM1	SPN1	531	81	1
A	inter	CRM1	SPN1	531	93	2
A	inter	CRM1	SPN1	534	34	1
A	inter	CRM1	SPN1	534	93	7
A	inter	CRM1	SPN1	534	144	2
A	inter	CRM1	SPN1	534	223	1
A	inter	CRM1	SPN1	534	323	1
A	inter	CRM1	SPN1	537	34	2
A	inter	CRM1	SPN1	537	54	1
A	inter	CRM1	SPN1	560	32	6
A	inter	CRM1	SPN1	560	34	1
A	inter	CRM1	SPN1	560	314	1
A	inter	CRM1	SPN1	563	32	5
A	inter	CRM1	SPN1	568	223	1
A	inter	CRM1	SPN1	594	314	2
A	inter	CRM1	SPN1	594	323	3
A	inter	CRM1	SPN1	594	327	1
A	inter	CRM1	SPN1	594	343	3
A	inter	CRM1	SPN1	674	223	6
A	inter	CRM1	SPN1	674	228	5
A	inter	CRM1	SPN1	680	223	24
A	inter	CRM1	SPN1	686	1	1
A	inter	CRM1	SPN1	686	128	1
A	inter	CRM1	SPN1	686	223	9
A	inter	CRM1	SPN1	700	223	1
A	inter	CRM1	SPN1	700	327	1
A	inter	CRM1	SPN1	741	223	10
A	inter	CRM1	SPN1	1049	32	1
A	inter	CRM1	SPN1	1049	34	1
A	inter	CRM1	SPN1	1051	32	1
A	inter	CRM1	Ran	1	1	2
A	inter	CRM1	Ran	1	123	1
A	inter	CRM1	Ran	2	2	7
A	inter	CRM1	Ran	2	60	8
A	inter	CRM1	Ran	122	2	4
A	inter	CRM1	Ran	122	99	1
A	inter	CRM1	Ran	144	142	1
A	inter	CRM1	Ran	144	152	1
A	inter	CRM1	Ran	331	134	8
A	inter	CRM1	Ran	339	132	1
A	inter	CRM1	Ran	426	159	6
A	inter	CRM1	Ran	446	127	2
A	inter	CRM1	Ran	446	132	1
A	inter	CRM1	Ran	446	134	1
A	inter	CRM1	Ran	455	123	2
A	inter	CRM1	Ran	455	132	2
A	inter	CRM1	Ran	455	134	2
A	inter	CRM1	Ran	492	159	4
A	inter	CRM1	Ran	563	159	1
A	inter	CRM1	Ran	674	167	2
A	inter	CRM1	Ran	700	127	30
A	inter	CRM1	Ran	700	159	1
A	inter	CRM1	Ran	741	28	1
A	inter	CRM1	Ran	741	37	3
A	inter	CRM1	Ran	757	37	13
A	inter	CRM1	Ran	757	60	1
A	inter	CRM1	Ran	757	127	19
A	inter	CRM1	Ran	757	152	14
A	inter	CRM1	Ran	1012	99	9
A	inter	CRM1	Ran	1049	99	3
A	inter	CRM1	Ran	1049	134	1
A	inter	SPN1	Ran	2	123	1
A	inter	SPN1	Ran	32	1	1
A	inter	SPN1	Ran	34	37	1
A	inter	SPN1	Ran	34	60	1
A	inter	SPN1	Ran	92	1	2
A	inter	SPN1	Ran	93	1	2
A	inter	SPN1	Ran	93	159	2
A	inter	SPN1	Ran	96	2	1
A	inter	SPN1	Ran	211	2	1
A	inter	SPN1	Ran	223	2	1
A	inter	SPN1	Ran	223	159	2
A	inter	SPN1	Ran	223	167	2
A	inter	SPN1	Ran	323	134	1
A	inter	SPN1	Ran	327	2	1
A	inter	SPN1	Ran	343	132	1
A	inter	SPN1	Ran	343	134	1

Replicate	Type	Protein 1	Protein 2	Residue 1	Residue 2	Spectrum Count
A	inter	SPN1	Ran	343	152	1
A	inter	SPN1	Ran	345		1
B	intra	Nup214	Nup214	1	2	1
B	intra	Nup214	Nup214	2	2	6
B	intra	Nup214	Nup214	2	48	25
B	intra	Nup214	Nup214	48	116	1
B	intra	Ran	Ran	1	2	6
B	intra	Ran	Ran	2	28	3
B	intra	Ran	Ran	2	37	3
B	intra	Ran	Ran	2	38	5
B	intra	Ran	Ran	2	99	1
B	intra	Ran	Ran	2	134	1
B	intra	Ran	Ran	2	159	2
B	intra	Ran	Ran	2	167	1
B	intra	Ran	Ran	12	38	6
B	intra	Ran	Ran	23	37	13
B	intra	Ran	Ran	23	38	5
B	intra	Ran	Ran	28	37	2
B	intra	Ran	Ran	28	38	7
B	intra	Ran	Ran	28	99	1
B	intra	Ran	Ran	28	159	2
B	intra	Ran	Ran	37	127	1
B	intra	Ran	Ran	37	134	2
B	intra	Ran	Ran	37	152	14
B	intra	Ran	Ran	38	99	4
B	intra	Ran	Ran	38	159	1
B	intra	Ran	Ran	99	123	2
B	intra	Ran	Ran	99	130	3
B	intra	Ran	Ran	99	132	15
B	intra	Ran	Ran	99	134	26
B	intra	Ran	Ran	99	141	4
B	intra	Ran	Ran	99	142	11
B	intra	Ran	Ran	99	159	1
B	intra	Ran	Ran	123	130	5
B	intra	Ran	Ran	123	134	3
B	intra	Ran	Ran	123	152	1
B	intra	Ran	Ran	123	159	2
B	intra	Ran	Ran	127	130	10
B	intra	Ran	Ran	127	132	23
B	intra	Ran	Ran	127	134	2
B	intra	Ran	Ran	127	152	21
B	intra	Ran	Ran	127	159	2
B	intra	Ran	Ran	134	141	2
B	intra	Ran	Ran	134	142	2
B	intra	Ran	Ran	134	159	3
B	intra	Ran	Ran	142	142	2
B	intra	Ran	Ran	142	159	7
B	intra	Ran	Ran	159	159	2
B	intra	SPN1	SPN1	32	52	1
B	intra	SPN1	SPN1	32	93	3
B	intra	SPN1	SPN1	32	144	4
B	intra	SPN1	SPN1	32	314	12
B	intra	SPN1	SPN1	32	317	3
B	intra	SPN1	SPN1	32	321	1
B	intra	SPN1	SPN1	32	323	10
B	intra	SPN1	SPN1	32	327	4
B	intra	SPN1	SPN1	32	343	3
B	intra	SPN1	SPN1	34	52	1
B	intra	SPN1	SPN1	34	93	1
B	intra	SPN1	SPN1	34	144	5
B	intra	SPN1	SPN1	34	223	1
B	intra	SPN1	SPN1	34	314	3
B	intra	SPN1	SPN1	34	323	6
B	intra	SPN1	SPN1	34	327	3
B	intra	SPN1	SPN1	34	343	1
B	intra	SPN1	SPN1	52	93	1
B	intra	SPN1	SPN1	52	314	4
B	intra	SPN1	SPN1	52	323	5
B	intra	SPN1	SPN1	52	327	2
B	intra	SPN1	SPN1	52	343	2
B	intra	SPN1	SPN1	80	81	1
B	intra	SPN1	SPN1	80	92	6
B	intra	SPN1	SPN1	81	93	1
B	intra	SPN1	SPN1	81	96	1
B	intra	SPN1	SPN1	93	144	4
B	intra	SPN1	SPN1	93	314	1
B	intra	SPN1	SPN1	128	144	2
B	intra	SPN1	SPN1	144	314	4
B	intra	SPN1	SPN1	144	317	1
B	intra	SPN1	SPN1	144	323	5
B	intra	SPN1	SPN1	144	343	1

Replicate	Type	Protein 1	Protein 2	Residue 1	Residue 2	Spectrum Count
B	intra	SPN1	SPN1	167	211	5
B	intra	SPN1	SPN1	211	223	1
B	intra	SPN1	SPN1	211	343	1
B	intra	SPN1	SPN1	221	228	6
B	intra	SPN1	SPN1	223	223	4
B	intra	SPN1	SPN1	223	314	3
B	intra	SPN1	SPN1	223	323	4
B	intra	SPN1	SPN1	223	327	7
B	intra	SPN1	SPN1	223	343	4
B	intra	SPN1	SPN1	223	345	1
B	intra	SPN1	SPN1	228	314	1
B	intra	SPN1	SPN1	298	314	4
B	intra	SPN1	SPN1	314	323	7
B	intra	SPN1	SPN1	314	327	14
B	intra	SPN1	SPN1	314	343	6
B	intra	SPN1	SPN1	314	345	1
B	intra	SPN1	SPN1	317	323	4
B	intra	SPN1	SPN1	321	323	1
B	intra	SPN1	SPN1	321	327	2
B	intra	SPN1	SPN1	323	343	14
B	intra	SPN1	SPN1	327	345	2
B	intra	CRM1	CRM1	1	22	1
B	intra	CRM1	CRM1	1	537	1
B	intra	CRM1	CRM1	2	122	2
B	intra	CRM1	CRM1	2	531	1
B	intra	CRM1	CRM1	54	88	17
B	intra	CRM1	CRM1	54	129	2
B	intra	CRM1	CRM1	76	122	1
B	intra	CRM1	CRM1	76	741	1
B	intra	CRM1	CRM1	88	92	13
B	intra	CRM1	CRM1	92	103	1
B	intra	CRM1	CRM1	92	144	23
B	intra	CRM1	CRM1	92	190	13
B	intra	CRM1	CRM1	92	192	7
B	intra	CRM1	CRM1	92	1049	1
B	intra	CRM1	CRM1	103	144	7
B	intra	CRM1	CRM1	103	192	2
B	intra	CRM1	CRM1	103	1049	1
B	intra	CRM1	CRM1	104	144	2
B	intra	CRM1	CRM1	104	560	1
B	intra	CRM1	CRM1	104	752	1
B	intra	CRM1	CRM1	104	1049	2
B	intra	CRM1	CRM1	122	129	2
B	intra	CRM1	CRM1	124	172	3
B	intra	CRM1	CRM1	144	190	6
B	intra	CRM1	CRM1	144	192	7
B	intra	CRM1	CRM1	144	492	1
B	intra	CRM1	CRM1	190	1049	3
B	intra	CRM1	CRM1	192	1049	8
B	intra	CRM1	CRM1	312	590	1
B	intra	CRM1	CRM1	312	594	1
B	intra	CRM1	CRM1	367	693	1
B	intra	CRM1	CRM1	415	479	4
B	intra	CRM1	CRM1	415	674	1
B	intra	CRM1	CRM1	426	492	1
B	intra	CRM1	CRM1	446	594	8
B	intra	CRM1	CRM1	446	700	10
B	intra	CRM1	CRM1	455	594	3
B	intra	CRM1	CRM1	479	492	1
B	intra	CRM1	CRM1	492	522	7
B	intra	CRM1	CRM1	514	522	4
B	intra	CRM1	CRM1	514	560	13
B	intra	CRM1	CRM1	522	534	3
B	intra	CRM1	CRM1	522	560	38
B	intra	CRM1	CRM1	522	563	2
B	intra	CRM1	CRM1	531	534	11
B	intra	CRM1	CRM1	531	537	1
B	intra	CRM1	CRM1	534	594	2
B	intra	CRM1	CRM1	560	568	4
B	intra	CRM1	CRM1	560	594	1
B	intra	CRM1	CRM1	563	594	2
B	intra	CRM1	CRM1	594	700	18
B	intra	CRM1	CRM1	594	1049	6
B	intra	CRM1	CRM1	680	693	3
B	intra	CRM1	CRM1	680	741	2
B	intra	CRM1	CRM1	686	700	1
B	intra	CRM1	CRM1	693	700	14
B	intra	CRM1	CRM1	693	741	12
B	intra	CRM1	CRM1	693	757	18
B	intra	CRM1	CRM1	700	757	20
B	inter	Nup214	Ran	1	1	1

Replicate	Type	Protein 1	Protein 2	Residue 1	Residue 2	Spectrum Count
B	inter	Nup214	Ran	1	134	1
B	inter	Nup214	Ran	2	2	24
B	inter	Nup214	Ran	2	28	3
B	inter	Nup214	Ran	2	37	9
B	inter	Nup214	Ran	2	38	2
B	inter	Nup214	Ran	2	99	6
B	inter	Nup214	Ran	2	127	4
B	inter	Nup214	Ran	2	132	1
B	inter	Nup214	Ran	2	134	1
B	inter	Nup214	Ran	2	152	2
B	inter	Nup214	Ran	2	159	6
B	inter	Nup214	SPN1	1	223	1
B	inter	Nup214	SPN1	1	323	2
B	inter	Nup214	SPN1	2	32	4
B	inter	Nup214	SPN1	2	34	3
B	inter	Nup214	SPN1	2	52	6
B	inter	Nup214	SPN1	2	93	19
B	inter	Nup214	SPN1	2	96	1
B	inter	Nup214	SPN1	2	144	2
B	inter	Nup214	SPN1	2	221	1
B	inter	Nup214	SPN1	2	223	30
B	inter	Nup214	SPN1	2	228	3
B	inter	Nup214	SPN1	2	314	10
B	inter	Nup214	SPN1	2	317	1
B	inter	Nup214	SPN1	2	323	12
B	inter	Nup214	SPN1	2	327	7
B	inter	Nup214	SPN1	2	343	4
B	inter	Nup214	SPN1	48	223	1
B	inter	Nup214	SPN1	48	323	1
B	inter	Nup214	SPN1	48	327	1
B	inter	Nup214	CRM1	1	568	1
B	inter	Nup214	CRM1	1	594	1
B	inter	Nup214	CRM1	2	2	1
B	inter	Nup214	CRM1	2	192	2
B	inter	Nup214	CRM1	2	426	4
B	inter	Nup214	CRM1	2	531	1
B	inter	Nup214	CRM1	2	534	9
B	inter	Nup214	CRM1	2	568	2
B	inter	Nup214	CRM1	2	594	3
B	inter	Nup214	CRM1	2	680	2
B	inter	Nup214	CRM1	2	686	4
B	inter	Nup214	CRM1	2	693	1
B	inter	Nup214	CRM1	2	700	4
B	inter	Nup214	CRM1	2	741	2
B	inter	Nup214	CRM1	2	757	1
B	inter	Nup214	CRM1	2	1049	3
B	inter	Nup214	CRM1	48	426	1
B	inter	Nup214	CRM1	48	446	1
B	inter	Nup214	CRM1	48	514	1
B	inter	Nup214	CRM1	116	22	4
B	inter	CRM1	SPN1	1	96	1
B	inter	CRM1	SPN1	1	211	1
B	inter	CRM1	SPN1	1	221	1
B	inter	CRM1	SPN1	144	93	1
B	inter	CRM1	SPN1	331	52	1
B	inter	CRM1	SPN1	415	32	2
B	inter	CRM1	SPN1	426	93	2
B	inter	CRM1	SPN1	426	327	1
B	inter	CRM1	SPN1	446	144	1
B	inter	CRM1	SPN1	492	93	1
B	inter	CRM1	SPN1	514	1	1
B	inter	CRM1	SPN1	522	32	7
B	inter	CRM1	SPN1	522	34	11
B	inter	CRM1	SPN1	531	80	2
B	inter	CRM1	SPN1	531	81	2
B	inter	CRM1	SPN1	534	1	1
B	inter	CRM1	SPN1	534	32	1
B	inter	CRM1	SPN1	534	34	2
B	inter	CRM1	SPN1	534	93	9
B	inter	CRM1	SPN1	534	144	1
B	inter	CRM1	SPN1	534	223	1
B	inter	CRM1	SPN1	534	314	1
B	inter	CRM1	SPN1	534	323	1
B	inter	CRM1	SPN1	537	2	1
B	inter	CRM1	SPN1	537	34	3
B	inter	CRM1	SPN1	537	96	1
B	inter	CRM1	SPN1	560	32	11
B	inter	CRM1	SPN1	560	314	1
B	inter	CRM1	SPN1	563	32	2
B	inter	CRM1	SPN1	568	34	1
B	inter	CRM1	SPN1	594	314	3

Replicate	Type	Protein 1	Protein 2	Residue 1	Residue 2	Spectrum Count
B	inter	CRM1	SPN1	594	323	4
B	inter	CRM1	SPN1	594	343	5
B	inter	CRM1	SPN1	674	223	6
B	inter	CRM1	SPN1	674	228	4
B	inter	CRM1	SPN1	680	223	28
B	inter	CRM1	SPN1	680	228	1
B	inter	CRM1	SPN1	686	223	12
B	inter	CRM1	SPN1	700	211	1
B	inter	CRM1	SPN1	700	223	1
B	inter	CRM1	SPN1	741	223	7
B	inter	CRM1	SPN1	1049	32	1
B	inter	CRM1	SPN1	1049	34	1
B	inter	CRM1	SPN1	1049	323	1
B	inter	CRM1	Ran	1	1	1
B	inter	CRM1	Ran	2	2	8
B	inter	CRM1	Ran	2	28	1
B	inter	CRM1	Ran	2	60	3
B	inter	CRM1	Ran	122	2	7
B	inter	CRM1	Ran	190	152	1
B	inter	CRM1	Ran	331	134	6
B	inter	CRM1	Ran	426	159	5
B	inter	CRM1	Ran	446	123	1
B	inter	CRM1	Ran	446	127	2
B	inter	CRM1	Ran	446	134	1
B	inter	CRM1	Ran	455	127	1
B	inter	CRM1	Ran	455	132	2
B	inter	CRM1	Ran	455	134	1
B	inter	CRM1	Ran	492	159	3
B	inter	CRM1	Ran	674	167	3
B	inter	CRM1	Ran	686	1	1
B	inter	CRM1	Ran	700	60	1
B	inter	CRM1	Ran	700	127	30
B	inter	CRM1	Ran	700	134	1
B	inter	CRM1	Ran	741	28	1
B	inter	CRM1	Ran	741	37	4
B	inter	CRM1	Ran	757	37	12
B	inter	CRM1	Ran	757	127	25
B	inter	CRM1	Ran	757	152	19
B	inter	CRM1	Ran	1012	99	11
B	inter	CRM1	Ran	1049	99	1
B	inter	CRM1	Ran	1049	134	1
B	inter	SPN1	Ran	92	1	1
B	inter	SPN1	Ran	93	159	2
B	inter	SPN1	Ran	96	12	1
B	inter	SPN1	Ran	167	152	1
B	inter	SPN1	Ran	211	2	1
B	inter	SPN1	Ran	223	2	2
B	inter	SPN1	Ran	223	142	1
B	inter	SPN1	Ran	223	159	3
B	inter	SPN1	Ran	223	167	6
B	inter	SPN1	Ran	343	1	2

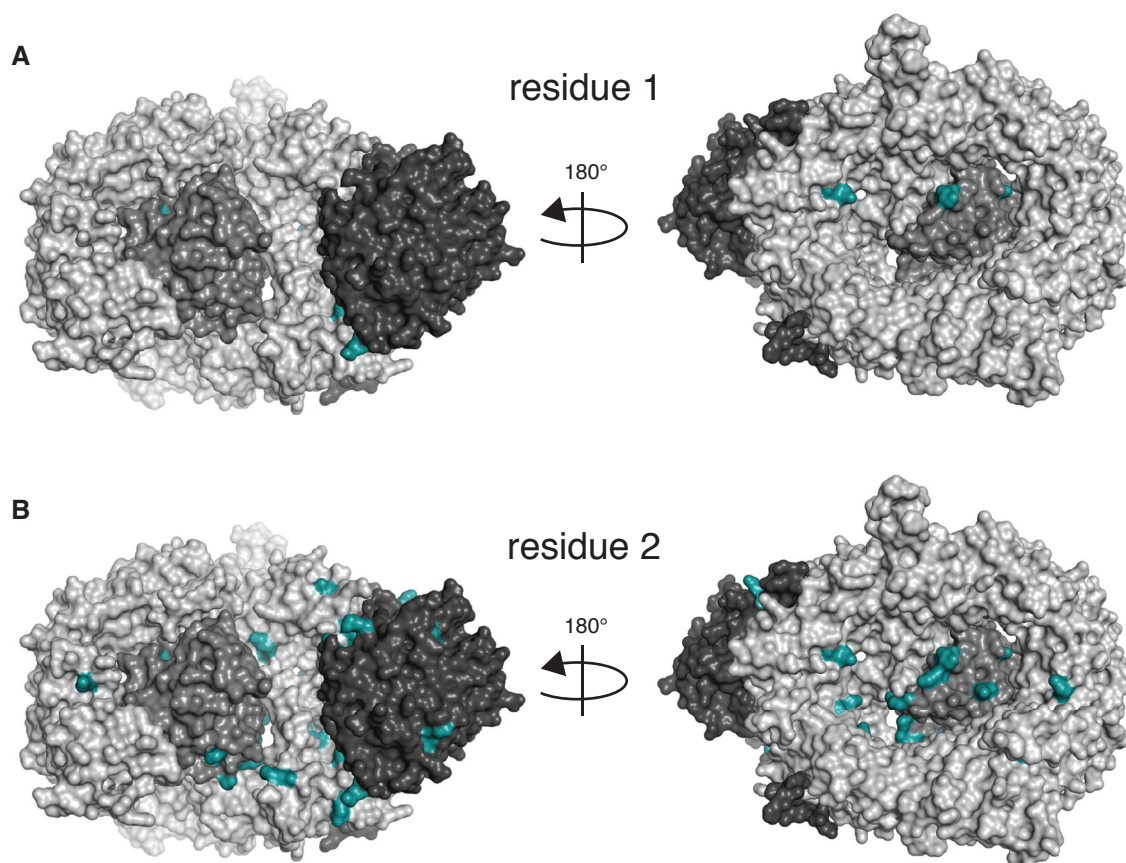


Figure S2: The N-terminus of His-Nup214(1916-2033)-His unspecifically cross-links residues across the surface of the export complex. The structure shows CRM1 (light gray), Ran (medium gray) and SPN1 (dark gray) (PDB ID: 3GJX, [127]). The cross-links of the residues (A) 1 and (B) 2 of His-Nup214(1916-2033)-His mapped onto the export complex are highlighted in green.

Table S3: Cross-linking of His-Nup214(K1916-2033)-His complex with BS³.

Replicate	Type	Protein 1	Protein 2	Residue 1	Residue 2	Spectrum Count
A	intra	Nup214mut	Nup214mut	1	1	20
A	intra	Nup214mut	Nup214mut	1	22	6
A	intra	Nup214mut	Nup214mut	2	22	14
A	intra	Nup214mut	Nup214mut	2	35	3
A	intra	Nup214mut	Nup214mut	2	49	19
A	intra	Nup214mut	Nup214mut	22	1	6
A	intra	Nup214mut	Nup214mut	22	2	14
A	intra	Nup214mut	Nup214mut	22	49	3
A	intra	Ran	Ran	1	2	9
A	intra	Ran	Ran	1	159	1
A	intra	Ran	Ran	2	28	4
A	intra	Ran	Ran	2	37	2
A	intra	Ran	Ran	2	38	4
A	intra	Ran	Ran	2	142	1
A	intra	Ran	Ran	2	159	1
A	intra	Ran	Ran	2	167	2
A	intra	Ran	Ran	12	37	1
A	intra	Ran	Ran	12	38	3
A	intra	Ran	Ran	23	37	14
A	intra	Ran	Ran	23	38	2
A	intra	Ran	Ran	23	159	1
A	intra	Ran	Ran	28	37	3
A	intra	Ran	Ran	28	38	6
A	intra	Ran	Ran	28	99	1
A	intra	Ran	Ran	37	127	2
A	intra	Ran	Ran	37	152	16
A	intra	Ran	Ran	99	123	1
A	intra	Ran	Ran	99	130	3
A	intra	Ran	Ran	99	132	17
A	intra	Ran	Ran	99	134	31
A	intra	Ran	Ran	99	141	5
A	intra	Ran	Ran	99	142	10
A	intra	Ran	Ran	99	159	1
A	intra	Ran	Ran	123	130	5
A	intra	Ran	Ran	123	134	3
A	intra	Ran	Ran	127	130	9
A	intra	Ran	Ran	127	132	24
A	intra	Ran	Ran	127	152	15
A	intra	Ran	Ran	134	142	6
A	intra	Ran	Ran	134	159	4
A	intra	Ran	Ran	142	142	4
A	intra	Ran	Ran	142	159	6
A	intra	SPN1	SPN1	2	2	4
A	intra	SPN1	SPN1	32	52	1
A	intra	SPN1	SPN1	32	93	3
A	intra	SPN1	SPN1	32	144	7
A	intra	SPN1	SPN1	32	223	1
A	intra	SPN1	SPN1	32	233	1
A	intra	SPN1	SPN1	32	314	10
A	intra	SPN1	SPN1	32	317	7
A	intra	SPN1	SPN1	32	321	5
A	intra	SPN1	SPN1	32	323	11
A	intra	SPN1	SPN1	32	327	6
A	intra	SPN1	SPN1	32	343	5
A	intra	SPN1	SPN1	34	52	3
A	intra	SPN1	SPN1	34	93	3
A	intra	SPN1	SPN1	34	144	6
A	intra	SPN1	SPN1	34	314	2
A	intra	SPN1	SPN1	34	317	1
A	intra	SPN1	SPN1	34	323	9
A	intra	SPN1	SPN1	34	327	1
A	intra	SPN1	SPN1	34	343	1
A	intra	SPN1	SPN1	52	93	3
A	intra	SPN1	SPN1	52	314	4
A	intra	SPN1	SPN1	52	323	5
A	intra	SPN1	SPN1	52	327	2
A	intra	SPN1	SPN1	52	345	1
A	intra	SPN1	SPN1	54	323	1
A	intra	SPN1	SPN1	80	80	4
A	intra	SPN1	SPN1	80	81	1
A	intra	SPN1	SPN1	80	92	10
A	intra	SPN1	SPN1	80	93	7
A	intra	SPN1	SPN1	81	93	2
A	intra	SPN1	SPN1	81	223	1
A	intra	SPN1	SPN1	93	144	6
A	intra	SPN1	SPN1	128	144	2
A	intra	SPN1	SPN1	144	314	5

Replicate	Type	Protein 1	Protein 2	Residue 1	Residue 2	Spectrum Count
A	intra	SPN1	SPN1	144	317	2
A	intra	SPN1	SPN1	144	323	6
A	intra	SPN1	SPN1	167	211	5
A	intra	SPN1	SPN1	211	211	2
A	intra	SPN1	SPN1	211	223	2
A	intra	SPN1	SPN1	211	327	1
A	intra	SPN1	SPN1	211	343	1
A	intra	SPN1	SPN1	221	228	3
A	intra	SPN1	SPN1	223	223	4
A	intra	SPN1	SPN1	223	314	2
A	intra	SPN1	SPN1	223	317	2
A	intra	SPN1	SPN1	223	321	1
A	intra	SPN1	SPN1	223	323	3
A	intra	SPN1	SPN1	223	327	7
A	intra	SPN1	SPN1	223	343	10
A	intra	SPN1	SPN1	298	314	3
A	intra	SPN1	SPN1	298	317	3
A	intra	SPN1	SPN1	314	323	10
A	intra	SPN1	SPN1	314	327	20
A	intra	SPN1	SPN1	314	343	7
A	intra	SPN1	SPN1	314	345	5
A	intra	SPN1	SPN1	317	323	3
A	intra	SPN1	SPN1	317	327	5
A	intra	SPN1	SPN1	317	343	1
A	intra	SPN1	SPN1	321	323	2
A	intra	SPN1	SPN1	321	327	6
A	intra	SPN1	SPN1	323	343	14
A	intra	SPN1	SPN1	323	345	5
A	intra	SPN1	SPN1	327	345	1
A	intra	CRM1	CRM1	1	1	2
A	intra	CRM1	CRM1	1	2	1
A	intra	CRM1	CRM1	1	144	1
A	intra	CRM1	CRM1	1	537	1
A	intra	CRM1	CRM1	2	103	1
A	intra	CRM1	CRM1	2	122	3
A	intra	CRM1	CRM1	2	686	2
A	intra	CRM1	CRM1	2	700	1
A	intra	CRM1	CRM1	54	88	16
A	intra	CRM1	CRM1	54	129	6
A	intra	CRM1	CRM1	76	122	3
A	intra	CRM1	CRM1	88	92	7
A	intra	CRM1	CRM1	92	144	24
A	intra	CRM1	CRM1	92	190	9
A	intra	CRM1	CRM1	92	192	7
A	intra	CRM1	CRM1	92	1049	1
A	intra	CRM1	CRM1	103	112	2
A	intra	CRM1	CRM1	103	144	5
A	intra	CRM1	CRM1	103	192	1
A	intra	CRM1	CRM1	103	1049	1
A	intra	CRM1	CRM1	104	144	1
A	intra	CRM1	CRM1	104	1049	1
A	intra	CRM1	CRM1	124	172	1
A	intra	CRM1	CRM1	144	190	7
A	intra	CRM1	CRM1	144	192	5
A	intra	CRM1	CRM1	144	312	2
A	intra	CRM1	CRM1	144	492	2
A	intra	CRM1	CRM1	144	693	1
A	intra	CRM1	CRM1	190	1049	3
A	intra	CRM1	CRM1	192	1049	10
A	intra	CRM1	CRM1	312	590	1
A	intra	CRM1	CRM1	415	426	2
A	intra	CRM1	CRM1	415	479	6
A	intra	CRM1	CRM1	415	537	1
A	intra	CRM1	CRM1	426	492	2
A	intra	CRM1	CRM1	426	700	1
A	intra	CRM1	CRM1	446	568	1
A	intra	CRM1	CRM1	446	594	8
A	intra	CRM1	CRM1	446	700	9
A	intra	CRM1	CRM1	446	757	2
A	intra	CRM1	CRM1	455	594	5
A	intra	CRM1	CRM1	455	1049	5
A	intra	CRM1	CRM1	492	522	7
A	intra	CRM1	CRM1	514	522	5
A	intra	CRM1	CRM1	514	560	10
A	intra	CRM1	CRM1	522	534	3
A	intra	CRM1	CRM1	522	560	44
A	intra	CRM1	CRM1	522	563	3
A	intra	CRM1	CRM1	531	534	13
A	intra	CRM1	CRM1	531	537	1
A	intra	CRM1	CRM1	531	680	1
A	intra	CRM1	CRM1	537	568	2

Replicate	Type	Protein 1	Protein 2	Residue 1	Residue 2	Spectrum Count
A	intra	CRM1	CRM1	560	568	5
A	intra	CRM1	CRM1	560	594	1
A	intra	CRM1	CRM1	594	700	20
A	intra	CRM1	CRM1	594	1049	9
A	intra	CRM1	CRM1	680	693	3
A	intra	CRM1	CRM1	680	741	6
A	intra	CRM1	CRM1	686	700	2
A	intra	CRM1	CRM1	686	983	1
A	intra	CRM1	CRM1	693	700	12
A	intra	CRM1	CRM1	693	741	16
A	intra	CRM1	CRM1	693	757	15
A	intra	CRM1	CRM1	700	757	25
A	inter	Nup214mut	Ran	1	142	3
A	inter	Nup214mut	Ran	2	1	1
A	inter	Nup214mut	Ran	2	2	18
A	inter	Nup214mut	Ran	2	28	3
A	inter	Nup214mut	Ran	2	37	11
A	inter	Nup214mut	Ran	2	38	1
A	inter	Nup214mut	Ran	2	99	5
A	inter	Nup214mut	Ran	2	127	2
A	inter	Nup214mut	Ran	2	134	3
A	inter	Nup214mut	Ran	2	152	2
A	inter	Nup214mut	Ran	2	159	1
A	inter	Nup214mut	Ran	22	1	1
A	inter	Nup214mut	Ran	22	134	1
A	inter	Nup214mut	Ran	49	2	1
A	inter	Nup214mut	SPN1	1	32	1
A	inter	Nup214mut	SPN1	1	93	1
A	inter	Nup214mut	SPN1	1	223	4
A	inter	Nup214mut	SPN1	1	314	2
A	inter	Nup214mut	SPN1	1	323	1
A	inter	Nup214mut	SPN1	2	32	2
A	inter	Nup214mut	SPN1	2	34	2
A	inter	Nup214mut	SPN1	2	52	4
A	inter	Nup214mut	SPN1	2	80	2
A	inter	Nup214mut	SPN1	2	93	12
A	inter	Nup214mut	SPN1	2	144	2
A	inter	Nup214mut	SPN1	2	211	3
A	inter	Nup214mut	SPN1	2	223	22
A	inter	Nup214mut	SPN1	2	228	2
A	inter	Nup214mut	SPN1	2	314	6
A	inter	Nup214mut	SPN1	2	317	1
A	inter	Nup214mut	SPN1	2	323	8
A	inter	Nup214mut	SPN1	2	327	5
A	inter	Nup214mut	SPN1	2	343	2
A	inter	Nup214mut	SPN1	22	34	2
A	inter	Nup214mut	SPN1	22	80	3
A	inter	Nup214mut	SPN1	22	211	2
A	inter	Nup214mut	SPN1	22	223	14
A	inter	Nup214mut	SPN1	22	317	1
A	inter	Nup214mut	SPN1	22	327	1
A	inter	Nup214mut	SPN1	35	1	1
A	inter	Nup214mut	SPN1	35	223	7
A	inter	Nup214mut	SPN1	35	314	1
A	inter	Nup214mut	SPN1	49	1	1
A	inter	Nup214mut	SPN1	49	2	1
A	inter	Nup214mut	SPN1	49	223	2
A	inter	Nup214mut	CRM1	1	560	1
A	inter	Nup214mut	CRM1	1	686	1
A	inter	Nup214mut	CRM1	2	192	2
A	inter	Nup214mut	CRM1	2	426	1
A	inter	Nup214mut	CRM1	2	534	5
A	inter	Nup214mut	CRM1	2	594	2
A	inter	Nup214mut	CRM1	2	680	3
A	inter	Nup214mut	CRM1	2	686	4
A	inter	Nup214mut	CRM1	2	700	1
A	inter	Nup214mut	CRM1	2	741	1
A	inter	Nup214mut	CRM1	2	757	1
A	inter	Nup214mut	CRM1	2	1049	2
A	inter	Nup214mut	CRM1	22	104	1
A	inter	Nup214mut	CRM1	22	415	2
A	inter	Nup214mut	CRM1	22	531	1
A	inter	Nup214mut	CRM1	22	686	1
A	inter	Nup214mut	CRM1	22	700	2
A	inter	Nup214mut	CRM1	35	680	2
A	inter	Nup214mut	CRM1	49	446	1
A	inter	Nup214mut	CRM1	73	426	2
A	inter	Nup214mut	CRM1	117	22	3
A	inter	CRM1	SPN1	1	313	1
A	inter	CRM1	SPN1	1	314	1
A	inter	CRM1	SPN1	104	1	2

Replicate	Type	Protein 1	Protein 2	Residue 1	Residue 2	Spectrum Count
A	inter	CRM1	SPN1	144	211	1
A	inter	CRM1	SPN1	331	228	1
A	inter	CRM1	SPN1	415	32	3
A	inter	CRM1	SPN1	426	93	2
A	inter	CRM1	SPN1	446	144	1
A	inter	CRM1	SPN1	446	314	1
A	inter	CRM1	SPN1	492	93	1
A	inter	CRM1	SPN1	522	32	7
A	inter	CRM1	SPN1	522	34	9
A	inter	CRM1	SPN1	522	80	1
A	inter	CRM1	SPN1	531	80	1
A	inter	CRM1	SPN1	531	93	1
A	inter	CRM1	SPN1	534	32	1
A	inter	CRM1	SPN1	534	34	1
A	inter	CRM1	SPN1	534	93	6
A	inter	CRM1	SPN1	534	144	1
A	inter	CRM1	SPN1	534	323	1
A	inter	CRM1	SPN1	537	34	6
A	inter	CRM1	SPN1	560	32	11
A	inter	CRM1	SPN1	560	314	1
A	inter	CRM1	SPN1	560	317	1
A	inter	CRM1	SPN1	563	32	4
A	inter	CRM1	SPN1	568	34	1
A	inter	CRM1	SPN1	594	314	1
A	inter	CRM1	SPN1	594	323	4
A	inter	CRM1	SPN1	594	343	1
A	inter	CRM1	SPN1	674	221	1
A	inter	CRM1	SPN1	674	223	8
A	inter	CRM1	SPN1	674	228	6
A	inter	CRM1	SPN1	674	314	1
A	inter	CRM1	SPN1	680	223	25
A	inter	CRM1	SPN1	680	345	1
A	inter	CRM1	SPN1	686	1	1
A	inter	CRM1	SPN1	686	223	9
A	inter	CRM1	SPN1	700	223	2
A	inter	CRM1	SPN1	741	223	9
A	inter	CRM1	SPN1	757	323	1
A	inter	CRM1	SPN1	1049	34	1
A	inter	CRM1	Ran	1	1	2
A	inter	CRM1	Ran	1	123	1
A	inter	CRM1	Ran	2	2	10
A	inter	CRM1	Ran	2	28	1
A	inter	CRM1	Ran	2	60	6
A	inter	CRM1	Ran	92	123	2
A	inter	CRM1	Ran	92	141	1
A	inter	CRM1	Ran	122	2	5
A	inter	CRM1	Ran	124	2	1
A	inter	CRM1	Ran	312	2	1
A	inter	CRM1	Ran	331	134	6
A	inter	CRM1	Ran	426	159	5
A	inter	CRM1	Ran	446	127	4
A	inter	CRM1	Ran	446	132	1
A	inter	CRM1	Ran	446	134	1
A	inter	CRM1	Ran	446	152	1
A	inter	CRM1	Ran	455	123	1
A	inter	CRM1	Ran	455	127	1
A	inter	CRM1	Ran	455	132	7
A	inter	CRM1	Ran	455	134	7
A	inter	CRM1	Ran	492	159	6
A	inter	CRM1	Ran	560	37	1
A	inter	CRM1	Ran	568	159	1
A	inter	CRM1	Ran	674	167	2
A	inter	CRM1	Ran	680	2	1
A	inter	CRM1	Ran	700	123	1
A	inter	CRM1	Ran	700	127	29
A	inter	CRM1	Ran	741	28	2
A	inter	CRM1	Ran	741	37	4
A	inter	CRM1	Ran	757	37	13
A	inter	CRM1	Ran	757	60	1
A	inter	CRM1	Ran	757	127	20
A	inter	CRM1	Ran	757	152	20
A	inter	CRM1	Ran	1012	99	13
A	inter	CRM1	Ran	1049	99	2
A	inter	CRM1	Ran	1049	134	1
A	inter	SPN1	Ran	34	1	1
A	inter	SPN1	Ran	34	159	1
A	inter	SPN1	Ran	80	2	1
A	inter	SPN1	Ran	93	1	2
A	inter	SPN1	Ran	93	2	2
A	inter	SPN1	Ran	93	159	2
A	inter	SPN1	Ran	167	152	1

Replicate	Type	Protein 1	Protein 2	Residue 1	Residue 2	Spectrum Count
A	inter	SPN1	Ran	211	2	1
A	inter	SPN1	Ran	223	2	2
A	inter	SPN1	Ran	223	134	1
A	inter	SPN1	Ran	223	159	4
A	inter	SPN1	Ran	223	167	3
A	inter	SPN1	Ran	314	123	1
A	inter	SPN1	Ran	343	134	2
A	inter	SPN1	Ran	345	134	1
B	intra	Nup214mut	Nup214mut	1	1	4
B	intra	Nup214mut	Nup214mut	1	2	1
B	intra	Nup214mut	Nup214mut	1	22	2
B	intra	Nup214mut	Nup214mut	2	2	2
B	intra	Nup214mut	Nup214mut	2	22	18
B	intra	Nup214mut	Nup214mut	2	35	5
B	intra	Nup214mut	Nup214mut	2	49	16
B	intra	Nup214mut	Nup214mut	22	49	3
B	intra	Nup214mut	Nup214mut	49	117	1
B	intra	Ran	Ran	1	2	5
B	intra	Ran	Ran	1	28	1
B	intra	Ran	Ran	2	23	1
B	intra	Ran	Ran	2	28	4
B	intra	Ran	Ran	2	37	1
B	intra	Ran	Ran	2	38	6
B	intra	Ran	Ran	2	99	1
B	intra	Ran	Ran	2	142	1
B	intra	Ran	Ran	2	159	1
B	intra	Ran	Ran	2	167	2
B	intra	Ran	Ran	12	37	1
B	intra	Ran	Ran	12	38	1
B	intra	Ran	Ran	12	99	1
B	intra	Ran	Ran	23	37	12
B	intra	Ran	Ran	23	38	1
B	intra	Ran	Ran	23	159	1
B	intra	Ran	Ran	28	37	2
B	intra	Ran	Ran	28	38	6
B	intra	Ran	Ran	28	99	2
B	intra	Ran	Ran	28	159	1
B	intra	Ran	Ran	37	127	3
B	intra	Ran	Ran	37	132	1
B	intra	Ran	Ran	37	152	12
B	intra	Ran	Ran	38	99	1
B	intra	Ran	Ran	99	123	2
B	intra	Ran	Ran	99	130	2
B	intra	Ran	Ran	99	132	17
B	intra	Ran	Ran	99	134	28
B	intra	Ran	Ran	99	141	3
B	intra	Ran	Ran	99	142	10
B	intra	Ran	Ran	99	159	1
B	intra	Ran	Ran	123	130	6
B	intra	Ran	Ran	123	134	1
B	intra	Ran	Ran	123	159	1
B	intra	Ran	Ran	127	130	7
B	intra	Ran	Ran	127	132	29
B	intra	Ran	Ran	127	152	20
B	intra	Ran	Ran	134	141	3
B	intra	Ran	Ran	134	142	2
B	intra	Ran	Ran	134	152	1
B	intra	Ran	Ran	134	159	3
B	intra	Ran	Ran	142	142	4
B	intra	Ran	Ran	142	159	3
B	intra	SPN1	SPN1	32	52	1
B	intra	SPN1	SPN1	32	93	3
B	intra	SPN1	SPN1	32	144	5
B	intra	SPN1	SPN1	32	223	1
B	intra	SPN1	SPN1	32	314	9
B	intra	SPN1	SPN1	32	317	10
B	intra	SPN1	SPN1	32	321	5
B	intra	SPN1	SPN1	32	323	14
B	intra	SPN1	SPN1	32	327	2
B	intra	SPN1	SPN1	32	343	3
B	intra	SPN1	SPN1	34	52	2
B	intra	SPN1	SPN1	34	93	3
B	intra	SPN1	SPN1	34	144	8
B	intra	SPN1	SPN1	34	314	4
B	intra	SPN1	SPN1	34	317	1
B	intra	SPN1	SPN1	34	323	8
B	intra	SPN1	SPN1	34	327	2
B	intra	SPN1	SPN1	52	93	1
B	intra	SPN1	SPN1	52	314	3
B	intra	SPN1	SPN1	52	323	3
B	intra	SPN1	SPN1	52	327	1

Replicate	Type	Protein 1	Protein 2	Residue 1	Residue 2	Spectrum Count
B	intra	SPN1	SPN1	52	343	1
B	intra	SPN1	SPN1	80	81	2
B	intra	SPN1	SPN1	80	92	9
B	intra	SPN1	SPN1	80	93	6
B	intra	SPN1	SPN1	80	144	2
B	intra	SPN1	SPN1	81	93	5
B	intra	SPN1	SPN1	93	144	5
B	intra	SPN1	SPN1	128	144	4
B	intra	SPN1	SPN1	144	314	4
B	intra	SPN1	SPN1	144	317	2
B	intra	SPN1	SPN1	144	321	1
B	intra	SPN1	SPN1	144	323	4
B	intra	SPN1	SPN1	167	211	7
B	intra	SPN1	SPN1	211	211	2
B	intra	SPN1	SPN1	211	223	2
B	intra	SPN1	SPN1	211	314	2
B	intra	SPN1	SPN1	211	323	1
B	intra	SPN1	SPN1	211	343	2
B	intra	SPN1	SPN1	221	228	5
B	intra	SPN1	SPN1	223	223	4
B	intra	SPN1	SPN1	223	314	2
B	intra	SPN1	SPN1	223	317	1
B	intra	SPN1	SPN1	223	321	2
B	intra	SPN1	SPN1	223	323	5
B	intra	SPN1	SPN1	223	327	7
B	intra	SPN1	SPN1	223	343	6
B	intra	SPN1	SPN1	223	345	1
B	intra	SPN1	SPN1	298	314	4
B	intra	SPN1	SPN1	298	317	2
B	intra	SPN1	SPN1	314	321	1
B	intra	SPN1	SPN1	314	323	10
B	intra	SPN1	SPN1	314	327	12
B	intra	SPN1	SPN1	314	343	9
B	intra	SPN1	SPN1	314	345	5
B	intra	SPN1	SPN1	317	323	3
B	intra	SPN1	SPN1	317	327	7
B	intra	SPN1	SPN1	317	343	1
B	intra	SPN1	SPN1	321	323	1
B	intra	SPN1	SPN1	321	327	3
B	intra	SPN1	SPN1	323	343	12
B	intra	SPN1	SPN1	323	345	6
B	intra	SPN1	SPN1	327	345	3
B	intra	CRM1	CRM1	1	2	1
B	intra	CRM1	CRM1	1	537	1
B	intra	CRM1	CRM1	2	112	1
B	intra	CRM1	CRM1	2	122	9
B	intra	CRM1	CRM1	2	312	1
B	intra	CRM1	CRM1	54	88	23
B	intra	CRM1	CRM1	54	129	7
B	intra	CRM1	CRM1	76	122	2
B	intra	CRM1	CRM1	88	92	9
B	intra	CRM1	CRM1	92	144	25
B	intra	CRM1	CRM1	92	190	11
B	intra	CRM1	CRM1	92	192	6
B	intra	CRM1	CRM1	92	700	1
B	intra	CRM1	CRM1	92	1049	1
B	intra	CRM1	CRM1	103	112	2
B	intra	CRM1	CRM1	103	144	7
B	intra	CRM1	CRM1	103	192	1
B	intra	CRM1	CRM1	103	1049	1
B	intra	CRM1	CRM1	104	1049	2
B	intra	CRM1	CRM1	122	129	2
B	intra	CRM1	CRM1	124	172	1
B	intra	CRM1	CRM1	144	190	4
B	intra	CRM1	CRM1	144	192	6
B	intra	CRM1	CRM1	144	492	1
B	intra	CRM1	CRM1	190	1049	2
B	intra	CRM1	CRM1	192	1049	9
B	intra	CRM1	CRM1	312	594	1
B	intra	CRM1	CRM1	339	1049	1
B	intra	CRM1	CRM1	415	479	4
B	intra	CRM1	CRM1	426	492	1
B	intra	CRM1	CRM1	446	568	1
B	intra	CRM1	CRM1	446	594	9
B	intra	CRM1	CRM1	446	700	9
B	intra	CRM1	CRM1	446	757	2
B	intra	CRM1	CRM1	455	594	7
B	intra	CRM1	CRM1	455	1049	3
B	intra	CRM1	CRM1	492	522	9
B	intra	CRM1	CRM1	514	522	5
B	intra	CRM1	CRM1	514	560	15

Replicate	Type	Protein 1	Protein 2	Residue 1	Residue 2	Spectrum Count
B	intra	CRM1	CRM1	522	534	1
B	intra	CRM1	CRM1	522	560	38
B	intra	CRM1	CRM1	522	563	3
B	intra	CRM1	CRM1	522	741	1
B	intra	CRM1	CRM1	531	534	13
B	intra	CRM1	CRM1	531	537	1
B	intra	CRM1	CRM1	531	680	2
B	intra	CRM1	CRM1	534	594	2
B	intra	CRM1	CRM1	537	568	1
B	intra	CRM1	CRM1	560	568	9
B	intra	CRM1	CRM1	560	594	2
B	intra	CRM1	CRM1	560	700	1
B	intra	CRM1	CRM1	563	522	3
B	intra	CRM1	CRM1	563	594	2
B	intra	CRM1	CRM1	594	700	19
B	intra	CRM1	CRM1	594	1049	5
B	intra	CRM1	CRM1	680	693	6
B	intra	CRM1	CRM1	680	741	4
B	intra	CRM1	CRM1	686	700	2
B	intra	CRM1	CRM1	686	741	2
B	intra	CRM1	CRM1	686	983	1
B	intra	CRM1	CRM1	693	700	11
B	intra	CRM1	CRM1	693	741	18
B	intra	CRM1	CRM1	693	757	13
B	intra	CRM1	CRM1	700	741	1
B	intra	CRM1	CRM1	700	757	22
B	intra	CRM1	CRM1	752	757	1
B	inter	Nup214mut	Ran	2	2	22
B	inter	Nup214mut	Ran	2	28	2
B	inter	Nup214mut	Ran	2	37	10
B	inter	Nup214mut	Ran	2	99	7
B	inter	Nup214mut	Ran	2	127	2
B	inter	Nup214mut	Ran	2	134	2
B	inter	Nup214mut	Ran	2	142	1
B	inter	Nup214mut	Ran	2	152	1
B	inter	Nup214mut	Ran	2	159	4
B	inter	Nup214mut	Ran	22	132	1
B	inter	Nup214mut	Ran	22	134	1
B	inter	Nup214mut	Ran	22	159	1
B	inter	Nup214mut	SPN1	1	34	1
B	inter	Nup214mut	SPN1	1	223	1
B	inter	Nup214mut	SPN1	1	321	1
B	inter	Nup214mut	SPN1	2	32	4
B	inter	Nup214mut	SPN1	2	34	1
B	inter	Nup214mut	SPN1	2	52	2
B	inter	Nup214mut	SPN1	2	80	1
B	inter	Nup214mut	SPN1	2	93	11
B	inter	Nup214mut	SPN1	2	144	2
B	inter	Nup214mut	SPN1	2	211	1
B	inter	Nup214mut	SPN1	2	223	22
B	inter	Nup214mut	SPN1	2	228	1
B	inter	Nup214mut	SPN1	2	314	4
B	inter	Nup214mut	SPN1	2	317	1
B	inter	Nup214mut	SPN1	2	323	8
B	inter	Nup214mut	SPN1	2	327	5
B	inter	Nup214mut	SPN1	2	343	1
B	inter	Nup214mut	SPN1	22	34	1
B	inter	Nup214mut	SPN1	22	223	17
B	inter	Nup214mut	SPN1	22	314	1
B	inter	Nup214mut	SPN1	22	321	1
B	inter	Nup214mut	SPN1	35	223	8
B	inter	Nup214mut	SPN1	35	314	1
B	inter	Nup214mut	SPN1	49	1	1
B	inter	Nup214mut	SPN1	49	223	2
B	inter	Nup214mut	SPN1	49	327	1
B	inter	Nup214mut	CRM1	2	426	1
B	inter	Nup214mut	CRM1	2	534	9
B	inter	Nup214mut	CRM1	2	594	1
B	inter	Nup214mut	CRM1	2	680	3
B	inter	Nup214mut	CRM1	2	686	5
B	inter	Nup214mut	CRM1	2	693	1
B	inter	Nup214mut	CRM1	2	741	1
B	inter	Nup214mut	CRM1	2	1049	2
B	inter	Nup214mut	CRM1	22	415	1
B	inter	Nup214mut	CRM1	22	686	1
B	inter	Nup214mut	CRM1	22	693	1
B	inter	Nup214mut	CRM1	22	700	1
B	inter	Nup214mut	CRM1	22	741	2
B	inter	Nup214mut	CRM1	35	680	1
B	inter	Nup214mut	CRM1	49	426	1
B	inter	Nup214mut	CRM1	49	446	1

Replicate	Type	Protein 1	Protein 2	Residue 1	Residue 2	Spectrum Count
B	inter	Nup214mut	CRM1	49	680	2
B	inter	Nup214mut	CRM1	117	22	2
B	inter	CRM1	SPN1	1	223	1
B	inter	CRM1	SPN1	2	211	1
B	inter	CRM1	SPN1	92	228	1
B	inter	CRM1	SPN1	104	1	1
B	inter	CRM1	SPN1	122	81	1
B	inter	CRM1	SPN1	144	314	1
B	inter	CRM1	SPN1	331	228	1
B	inter	CRM1	SPN1	415	32	4
B	inter	CRM1	SPN1	426	93	3
B	inter	CRM1	SPN1	446	221	1
B	inter	CRM1	SPN1	446	321	1
B	inter	CRM1	SPN1	492	93	1
B	inter	CRM1	SPN1	522	32	6
B	inter	CRM1	SPN1	522	34	13
B	inter	CRM1	SPN1	531	80	1
B	inter	CRM1	SPN1	531	93	2
B	inter	CRM1	SPN1	534	93	7
B	inter	CRM1	SPN1	534	96	1
B	inter	CRM1	SPN1	534	144	2
B	inter	CRM1	SPN1	534	223	1
B	inter	CRM1	SPN1	537	2	2
B	inter	CRM1	SPN1	537	34	4
B	inter	CRM1	SPN1	560	32	8
B	inter	CRM1	SPN1	560	323	1
B	inter	CRM1	SPN1	563	32	3
B	inter	CRM1	SPN1	563	314	1
B	inter	CRM1	SPN1	594	314	3
B	inter	CRM1	SPN1	594	323	4
B	inter	CRM1	SPN1	594	343	4
B	inter	CRM1	SPN1	674	223	9
B	inter	CRM1	SPN1	674	228	5
B	inter	CRM1	SPN1	674	314	1
B	inter	CRM1	SPN1	674	323	1
B	inter	CRM1	SPN1	680	223	29
B	inter	CRM1	SPN1	680	345	2
B	inter	CRM1	SPN1	686	93	1
B	inter	CRM1	SPN1	686	223	12
B	inter	CRM1	SPN1	700	2	1
B	inter	CRM1	SPN1	700	223	1
B	inter	CRM1	SPN1	700	317	1
B	inter	CRM1	SPN1	741	223	11
B	inter	CRM1	SPN1	1049	32	1
B	inter	CRM1	SPN1	1049	34	1
B	inter	CRM1	SPN1	1049	323	2
B	inter	CRM1	Ran	1	1	3
B	inter	CRM1	Ran	2	2	11
B	inter	CRM1	Ran	2	28	1
B	inter	CRM1	Ran	2	60	5
B	inter	CRM1	Ran	92	123	2
B	inter	CRM1	Ran	92	142	1
B	inter	CRM1	Ran	122	2	4
B	inter	CRM1	Ran	124	134	1
B	inter	CRM1	Ran	331	123	1
B	inter	CRM1	Ran	331	134	7
B	inter	CRM1	Ran	426	159	5
B	inter	CRM1	Ran	446	127	4
B	inter	CRM1	Ran	446	132	1
B	inter	CRM1	Ran	446	152	1
B	inter	CRM1	Ran	455	123	1
B	inter	CRM1	Ran	455	127	2
B	inter	CRM1	Ran	455	132	7
B	inter	CRM1	Ran	455	134	5
B	inter	CRM1	Ran	492	159	6
B	inter	CRM1	Ran	560	152	1
B	inter	CRM1	Ran	674	167	2
B	inter	CRM1	Ran	700	127	27
B	inter	CRM1	Ran	700	159	1
B	inter	CRM1	Ran	741	28	4
B	inter	CRM1	Ran	741	37	6
B	inter	CRM1	Ran	757	37	11
B	inter	CRM1	Ran	757	127	19
B	inter	CRM1	Ran	757	152	16
B	inter	CRM1	Ran	1012	99	11
B	inter	CRM1	Ran	1049	99	2
B	inter	CRM1	Ran	1049	134	2
B	inter	SPN1	Ran	92	1	2
B	inter	SPN1	Ran	93	159	2
B	inter	SPN1	Ran	128	2	1
B	inter	SPN1	Ran	167	152	1

Replicate	Type	Protein 1	Protein 2	Residue 1	Residue 2	Spectrum Count
B	inter	SPN1	Ran	223	2	3
B	inter	SPN1	Ran	223	159	2
B	inter	SPN1	Ran	223	167	3
B	inter	SPN1	Ran	314	123	1
B	inter	SPN1	Ran	323	99	1
B	inter	SPN1	Ran	323	132	1
B	inter	SPN1	Ran	323	152	1
B	inter	SPN1	Ran	343	134	2
B	inter	SPN1	Ran	343	152	1
B	inter	SPN1	Ran	345	132	1

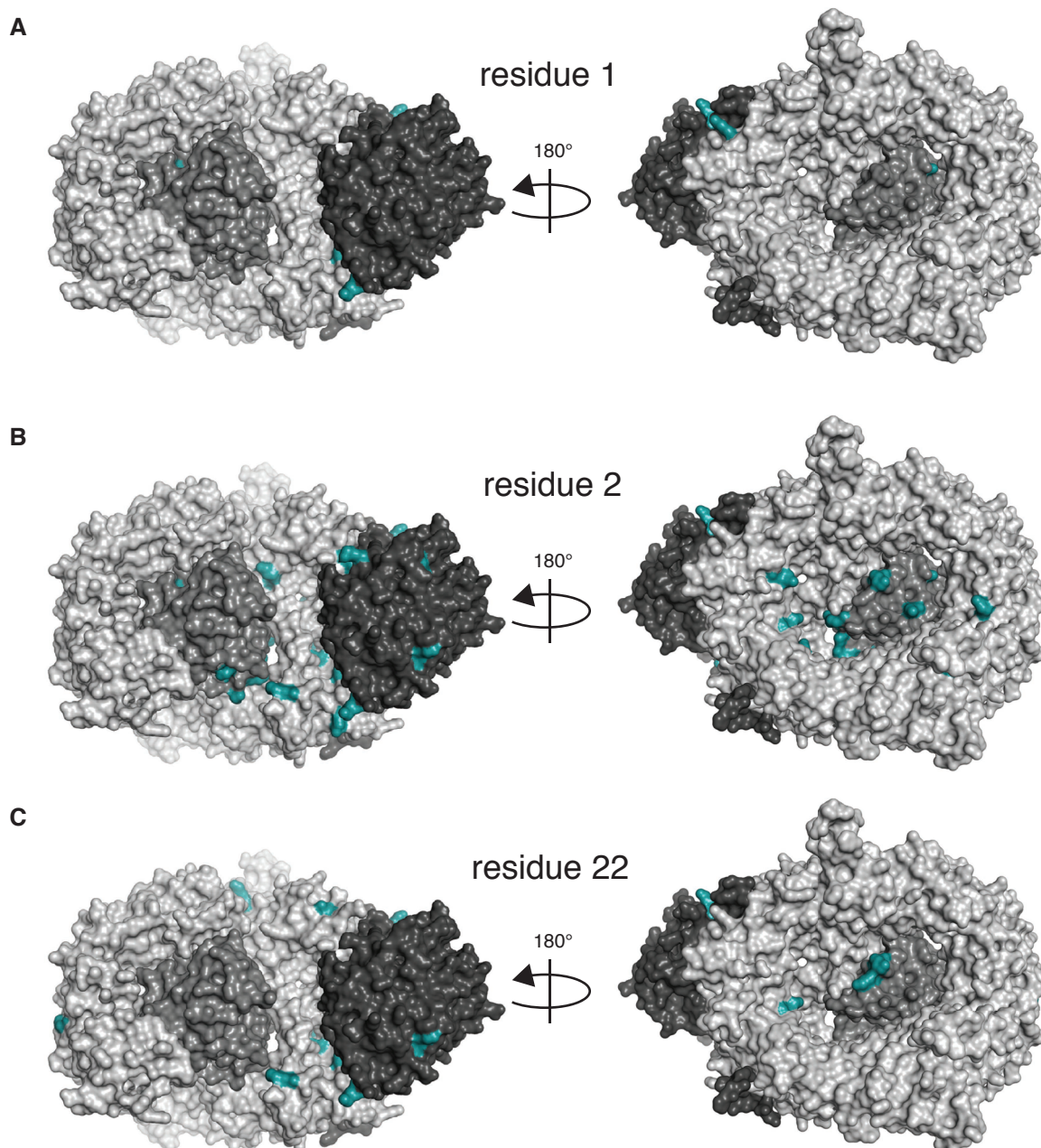


Figure S3: The N-terminus of His-Nup214(K1916-2033)-His unspecifically cross-links residues across the surface of the export complex. The structure shows CRM1 (light gray), Ran (medium gray) and SPN1 (dark gray) (PDB ID: 3GJX, [127]). The cross-links of the residues (A) 1, (B) 2 and (C) 22 of His-Nup214(K1916-2033)-His mapped onto the export complex are highlighted in green.

C.3 Cross-linking of the MBP-Nup214(1916-2033)-His complex with BS³ and EDC

Table S4: Cross-linking of the MBP-Nup214(1916-2033)-His complex with BS³.

Linker	Type	Protein 1	Protein 2	Residue 1	Residue 2	Spectrum Count
BS ³	intra	MBP-Nup214	MBP-Nup214	1	296	1
BS ³	intra	MBP-Nup214	MBP-Nup214	16	27	1
BS ³	intra	MBP-Nup214	MBP-Nup214	16	43	3
BS ³	intra	MBP-Nup214	MBP-Nup214	16	298	23
BS ³	intra	MBP-Nup214	MBP-Nup214	16	306	1
BS ³	intra	MBP-Nup214	MBP-Nup214	26	30	26
BS ³	intra	MBP-Nup214	MBP-Nup214	26	35	19
BS ³	intra	MBP-Nup214	MBP-Nup214	26	43	5
BS ³	intra	MBP-Nup214	MBP-Nup214	27	35	1
BS ³	intra	MBP-Nup214	MBP-Nup214	27	43	2
BS ³	intra	MBP-Nup214	MBP-Nup214	30	43	1
BS ³	intra	MBP-Nup214	MBP-Nup214	30	120	2
BS ³	intra	MBP-Nup214	MBP-Nup214	35	47	11
BS ³	intra	MBP-Nup214	MBP-Nup214	47	400	2
BS ³	intra	MBP-Nup214	MBP-Nup214	84	103	13
BS ³	intra	MBP-Nup214	MBP-Nup214	84	120	1
BS ³	intra	MBP-Nup214	MBP-Nup214	84	176	2
BS ³	intra	MBP-Nup214	MBP-Nup214	84	306	10
BS ³	intra	MBP-Nup214	MBP-Nup214	84	314	3
BS ³	intra	MBP-Nup214	MBP-Nup214	89	103	1
BS ³	intra	MBP-Nup214	MBP-Nup214	89	306	5
BS ³	intra	MBP-Nup214	MBP-Nup214	89	314	3
BS ³	intra	MBP-Nup214	MBP-Nup214	103	128	1
BS ³	intra	MBP-Nup214	MBP-Nup214	103	176	34
BS ³	intra	MBP-Nup214	MBP-Nup214	103	274	20
BS ³	intra	MBP-Nup214	MBP-Nup214	103	400	1
BS ³	intra	MBP-Nup214	MBP-Nup214	120	138	23
BS ³	intra	MBP-Nup214	MBP-Nup214	120	314	22
BS ³	intra	MBP-Nup214	MBP-Nup214	128	143	2
BS ³	intra	MBP-Nup214	MBP-Nup214	138	180	1
BS ³	intra	MBP-Nup214	MBP-Nup214	138	201	9
BS ³	intra	MBP-Nup214	MBP-Nup214	138	203	1
BS ³	intra	MBP-Nup214	MBP-Nup214	141	201	3
BS ³	intra	MBP-Nup214	MBP-Nup214	143	128	2
BS ³	intra	MBP-Nup214	MBP-Nup214	143	176	1
BS ³	intra	MBP-Nup214	MBP-Nup214	145	180	2
BS ³	intra	MBP-Nup214	MBP-Nup214	171	180	12
BS ³	intra	MBP-Nup214	MBP-Nup214	171	468	1
BS ³	intra	MBP-Nup214	MBP-Nup214	176	176	4
BS ³	intra	MBP-Nup214	MBP-Nup214	176	190	5
BS ³	intra	MBP-Nup214	MBP-Nup214	176	201	1
BS ³	intra	MBP-Nup214	MBP-Nup214	176	257	4
BS ³	intra	MBP-Nup214	MBP-Nup214	180	201	3
BS ³	intra	MBP-Nup214	MBP-Nup214	180	400	1
BS ³	intra	MBP-Nup214	MBP-Nup214	190	190	2
BS ³	intra	MBP-Nup214	MBP-Nup214	190	252	7
BS ³	intra	MBP-Nup214	MBP-Nup214	201	220	19
BS ³	intra	MBP-Nup214	MBP-Nup214	201	298	1
BS ³	intra	MBP-Nup214	MBP-Nup214	252	274	4
BS ³	intra	MBP-Nup214	MBP-Nup214	257	298	1
BS ³	intra	MBP-Nup214	MBP-Nup214	274	278	5
BS ³	intra	MBP-Nup214	MBP-Nup214	278	306	1
BS ³	intra	MBP-Nup214	MBP-Nup214	296	306	1
BS ³	intra	MBP-Nup214	MBP-Nup214	298	314	5
BS ³	intra	MBP-Nup214	MBP-Nup214	314	314	6
BS ³	intra	Ran	Ran	1	38	1
BS ³	intra	Ran	Ran	23	37	1
BS ³	intra	Ran	Ran	28	37	4
BS ³	intra	Ran	Ran	28	38	10
BS ³	intra	Ran	Ran	37	123	1
BS ³	intra	Ran	Ran	37	127	3
BS ³	intra	Ran	Ran	37	152	16
BS ³	intra	Ran	Ran	99	127	1
BS ³	intra	Ran	Ran	99	130	1
BS ³	intra	Ran	Ran	99	132	8
BS ³	intra	Ran	Ran	99	134	22
BS ³	intra	Ran	Ran	99	141	1
BS ³	intra	Ran	Ran	99	142	9
BS ³	intra	Ran	Ran	123	130	7
BS ³	intra	Ran	Ran	127	130	3
BS ³	intra	Ran	Ran	127	132	27
BS ³	intra	Ran	Ran	127	152	26
BS ³	intra	Ran	Ran	127	159	1

Linker	Type	Protein 1	Protein 2	Residue 1	Residue 2	Spectrum Count
BS ³	intra	Ran	Ran	134	141	1
BS ³	intra	Ran	Ran	134	159	2
BS ³	intra	Ran	Ran	142	159	1
BS ³	intra	SPN1	SPN1	2	2	2
BS ³	intra	SPN1	SPN1	2	262	1
BS ³	intra	SPN1	SPN1	32	32	2
BS ³	intra	SPN1	SPN1	32	52	1
BS ³	intra	SPN1	SPN1	32	93	2
BS ³	intra	SPN1	SPN1	32	144	4
BS ³	intra	SPN1	SPN1	32	314	6
BS ³	intra	SPN1	SPN1	32	323	6
BS ³	intra	SPN1	SPN1	32	327	2
BS ³	intra	SPN1	SPN1	32	343	2
BS ³	intra	SPN1	SPN1	34	52	3
BS ³	intra	SPN1	SPN1	34	93	1
BS ³	intra	SPN1	SPN1	34	144	3
BS ³	intra	SPN1	SPN1	34	314	1
BS ³	intra	SPN1	SPN1	34	323	1
BS ³	intra	SPN1	SPN1	52	81	1
BS ³	intra	SPN1	SPN1	52	93	4
BS ³	intra	SPN1	SPN1	52	314	4
BS ³	intra	SPN1	SPN1	52	323	6
BS ³	intra	SPN1	SPN1	52	327	2
BS ³	intra	SPN1	SPN1	52	343	3
BS ³	intra	SPN1	SPN1	80	80	2
BS ³	intra	SPN1	SPN1	80	81	1
BS ³	intra	SPN1	SPN1	80	92	1
BS ³	intra	SPN1	SPN1	80	93	2
BS ³	intra	SPN1	SPN1	93	144	2
BS ³	intra	SPN1	SPN1	128	233	1
BS ³	intra	SPN1	SPN1	144	314	2
BS ³	intra	SPN1	SPN1	144	323	1
BS ³	intra	SPN1	SPN1	167	211	6
BS ³	intra	SPN1	SPN1	211	223	2
BS ³	intra	SPN1	SPN1	221	228	1
BS ³	intra	SPN1	SPN1	223	314	4
BS ³	intra	SPN1	SPN1	223	323	3
BS ³	intra	SPN1	SPN1	223	327	3
BS ³	intra	SPN1	SPN1	223	343	4
BS ³	intra	SPN1	SPN1	298	314	2
BS ³	intra	SPN1	SPN1	314	327	1
BS ³	intra	SPN1	SPN1	317	323	1
BS ³	intra	SPN1	SPN1	321	323	2
BS ³	intra	SPN1	SPN1	323	343	2
BS ³	intra	CRM1	CRM1	1	22	3
BS ³	intra	CRM1	CRM1	1	537	1
BS ³	intra	CRM1	CRM1	2	22	2
BS ³	intra	CRM1	CRM1	54	88	5
BS ³	intra	CRM1	CRM1	76	122	2
BS ³	intra	CRM1	CRM1	76	560	1
BS ³	intra	CRM1	CRM1	88	54	5
BS ³	intra	CRM1	CRM1	88	92	5
BS ³	intra	CRM1	CRM1	92	103	1
BS ³	intra	CRM1	CRM1	92	124	1
BS ³	intra	CRM1	CRM1	92	144	6
BS ³	intra	CRM1	CRM1	92	190	3
BS ³	intra	CRM1	CRM1	92	192	2
BS ³	intra	CRM1	CRM1	92	1012	1
BS ³	intra	CRM1	CRM1	144	172	1
BS ³	intra	CRM1	CRM1	144	190	4
BS ³	intra	CRM1	CRM1	192	1049	3
BS ³	intra	CRM1	CRM1	415	479	1
BS ³	intra	CRM1	CRM1	415	674	2
BS ³	intra	CRM1	CRM1	426	492	1
BS ³	intra	CRM1	CRM1	446	594	5
BS ³	intra	CRM1	CRM1	446	700	5
BS ³	intra	CRM1	CRM1	455	594	3
BS ³	intra	CRM1	CRM1	492	522	4
BS ³	intra	CRM1	CRM1	514	522	1
BS ³	intra	CRM1	CRM1	514	560	5
BS ³	intra	CRM1	CRM1	522	514	1
BS ³	intra	CRM1	CRM1	522	534	4
BS ³	intra	CRM1	CRM1	522	560	6
BS ³	intra	CRM1	CRM1	531	534	2
BS ³	intra	CRM1	CRM1	560	594	1
BS ³	intra	CRM1	CRM1	594	700	19
BS ³	intra	CRM1	CRM1	594	1049	2
BS ³	intra	CRM1	CRM1	680	693	2
BS ³	intra	CRM1	CRM1	693	700	7

Linker	Type	Protein 1	Protein 2	Residue 1	Residue 2	Spectrum Count
BS ³	intra	CRM1	CRM1	693	757	4
BS ³	intra	CRM1	CRM1	700	757	24
BS ³	intra	CRM1	CRM1	752	757	4
BS ³	intra	CRM1	CRM1	1049	1049	2
BS ³	inter	MBP-Nup214	Ran	143	134	1
BS ³	inter	MBP-Nup214	Ran	176	37	1
BS ³	inter	MBP-Nup214	Ran	176	123	1
BS ³	inter	MBP-Nup214	Ran	180	123	1
BS ³	inter	MBP-Nup214	Ran	201	28	2
BS ³	inter	MBP-Nup214	Ran	298	37	1
BS ³	inter	MBP-Nup214	SPN1	26	223	2
BS ³	inter	MBP-Nup214	SPN1	27	223	1
BS ³	inter	MBP-Nup214	SPN1	30	223	3
BS ³	inter	MBP-Nup214	SPN1	30	228	1
BS ³	inter	MBP-Nup214	SPN1	35	223	1
BS ³	inter	MBP-Nup214	SPN1	43	223	19
BS ³	inter	MBP-Nup214	SPN1	47	223	27
BS ³	inter	MBP-Nup214	SPN1	84	223	3
BS ³	inter	MBP-Nup214	SPN1	89	223	2
BS ³	inter	MBP-Nup214	SPN1	103	223	30
BS ³	inter	MBP-Nup214	SPN1	120	223	3
BS ³	inter	MBP-Nup214	SPN1	138	223	4
BS ³	inter	MBP-Nup214	SPN1	141	54	2
BS ³	inter	MBP-Nup214	SPN1	145	262	1
BS ³	inter	MBP-Nup214	SPN1	176	223	18
BS ³	inter	MBP-Nup214	SPN1	180	223	38
BS ³	inter	MBP-Nup214	SPN1	190	223	7
BS ³	inter	MBP-Nup214	SPN1	201	223	5
BS ³	inter	MBP-Nup214	SPN1	274	223	8
BS ³	inter	MBP-Nup214	SPN1	298	223	1
BS ³	inter	MBP-Nup214	SPN1	314	223	2
BS ³	inter	MBP-Nup214	SPN1	386	167	1
BS ³	inter	MBP-Nup214	SPN1	386	223	11
BS ³	inter	MBP-Nup214	SPN1	400	223	1
BS ³	inter	MBP-Nup214	CRM1	16	144	3
BS ³	inter	MBP-Nup214	CRM1	30	339	1
BS ³	inter	MBP-Nup214	CRM1	43	22	1
BS ³	inter	MBP-Nup214	CRM1	84	312	1
BS ³	inter	MBP-Nup214	CRM1	120	531	10
BS ³	inter	MBP-Nup214	CRM1	176	531	1
BS ³	inter	MBP-Nup214	CRM1	203	92	2
BS ³	inter	MBP-Nup214	CRM1	203	693	1
BS ³	inter	MBP-Nup214	CRM1	220	560	1
BS ³	inter	MBP-Nup214	CRM1	257	92	1
BS ³	inter	MBP-Nup214	CRM1	278	534	3
BS ³	inter	MBP-Nup214	CRM1	314	144	1
BS ³	inter	MBP-Nup214	CRM1	468	22	2
BS ³	inter	CRM1	SPN1	2	128	1
BS ³	inter	CRM1	SPN1	331	52	1
BS ³	inter	CRM1	SPN1	415	32	2
BS ³	inter	CRM1	SPN1	415	54	1
BS ³	inter	CRM1	SPN1	492	93	3
BS ³	inter	CRM1	SPN1	522	32	12
BS ³	inter	CRM1	SPN1	522	34	13
BS ³	inter	CRM1	SPN1	531	80	1
BS ³	inter	CRM1	SPN1	531	81	2
BS ³	inter	CRM1	SPN1	531	93	2
BS ³	inter	CRM1	SPN1	534	34	1
BS ³	inter	CRM1	SPN1	534	93	6
BS ³	inter	CRM1	SPN1	560	32	8
BS ³	inter	CRM1	SPN1	560	34	1
BS ³	inter	CRM1	SPN1	560	314	1
BS ³	inter	CRM1	SPN1	563	32	4
BS ³	inter	CRM1	SPN1	674	223	6
BS ³	inter	CRM1	SPN1	680	223	27
BS ³	inter	CRM1	SPN1	686	223	10
BS ³	inter	CRM1	SPN1	741	223	7
BS ³	inter	CRM1	SPN1	1049	323	1
BS ³	inter	CRM1	Ran	2	60	1
BS ³	inter	CRM1	Ran	331	134	15
BS ³	inter	CRM1	Ran	426	159	3
BS ³	inter	CRM1	Ran	446	127	1
BS ³	inter	CRM1	Ran	446	132	1
BS ³	inter	CRM1	Ran	492	159	6
BS ³	inter	CRM1	Ran	700	123	1
BS ³	inter	CRM1	Ran	700	127	35
BS ³	inter	CRM1	Ran	741	37	2
BS ³	inter	CRM1	Ran	757	37	12
BS ³	inter	CRM1	Ran	757	127	16

Linker	Type	Protein 1	Protein 2	Residue 1	Residue 2	Spectrum Count
BS ³	inter	CRM1	Ran	757	152	20
BS ³	inter	CRM1	Ran	1012	99	11
BS ³	inter	CRM1	Ran	1049	99	3
BS ³	inter	CRM1	Ran	1049	134	1
BS ³	inter	SPN1	Ran	80	71	1
BS ³	inter	SPN1	Ran	93	159	1
BS ³	inter	SPN1	Ran	167	152	1
BS ³	inter	SPN1	Ran	221	159	2

Table S5: Cross-linking of the MBP-Nup214(1916-2033)-His complex with EDC.

Linker	Type	Protein 1	Protein 2	Residue 1	Residue 2	Spectrum Count
EDC	intra	MBP-Nup214	MBP-Nup214	23	27	6
EDC	intra	MBP-Nup214	MBP-Nup214	26	29	2
EDC	intra	MBP-Nup214	MBP-Nup214	27	31	1
EDC	intra	MBP-Nup214	MBP-Nup214	30	39	3
EDC	intra	MBP-Nup214	MBP-Nup214	31	43	4
EDC	intra	MBP-Nup214	MBP-Nup214	31	47	2
EDC	intra	MBP-Nup214	MBP-Nup214	35	45	3
EDC	intra	MBP-Nup214	MBP-Nup214	35	46	3
EDC	intra	MBP-Nup214	MBP-Nup214	39	47	4
EDC	intra	MBP-Nup214	MBP-Nup214	42	47	30
EDC	intra	MBP-Nup214	MBP-Nup214	47	79	2
EDC	intra	MBP-Nup214	MBP-Nup214	56	84	1
EDC	intra	MBP-Nup214	MBP-Nup214	56	400	1
EDC	intra	MBP-Nup214	MBP-Nup214	79	103	10
EDC	intra	MBP-Nup214	MBP-Nup214	83	89	6
EDC	intra	MBP-Nup214	MBP-Nup214	84	288	2
EDC	intra	MBP-Nup214	MBP-Nup214	84	372	1
EDC	intra	MBP-Nup214	MBP-Nup214	88	103	1
EDC	intra	MBP-Nup214	MBP-Nup214	96	103	4
EDC	intra	MBP-Nup214	MBP-Nup214	112	128	12
EDC	intra	MBP-Nup214	MBP-Nup214	120	131	34
EDC	intra	MBP-Nup214	MBP-Nup214	120	132	7
EDC	intra	MBP-Nup214	MBP-Nup214	180	372	9
EDC	intra	MBP-Nup214	MBP-Nup214	190	359	7
EDC	intra	MBP-Nup214	MBP-Nup214	190	372	1
EDC	intra	MBP-Nup214	MBP-Nup214	278	372	2
EDC	intra	MBP-Nup214	MBP-Nup214	288	306	1
EDC	intra	MBP-Nup214	MBP-Nup214	398	400	1
EDC	intra	Ran	Ran	28	34	1
EDC	intra	Ran	Ran	28	36	7
EDC	intra	Ran	Ran	36	38	6
EDC	intra	Ran	Ran	91	99	1
EDC	intra	Ran	Ran	99	107	1
EDC	intra	Ran	Ran	148	159	1
EDC	intra	SPN1	SPN1	1	110	1
EDC	intra	SPN1	SPN1	2	110	1
EDC	intra	SPN1	SPN1	32	39	12
EDC	intra	SPN1	SPN1	32	42	2
EDC	intra	SPN1	SPN1	34	202	1
EDC	intra	SPN1	SPN1	39	314	2
EDC	intra	SPN1	SPN1	42	52	1
EDC	intra	SPN1	SPN1	52	42	1
EDC	intra	SPN1	SPN1	52	57	14
EDC	intra	SPN1	SPN1	54	57	14
EDC	intra	SPN1	SPN1	77	81	1
EDC	intra	SPN1	SPN1	78	81	3
EDC	intra	SPN1	SPN1	80	82	1
EDC	intra	SPN1	SPN1	144	202	1
EDC	intra	SPN1	SPN1	215	228	1
EDC	intra	SPN1	SPN1	220	223	3
EDC	intra	SPN1	SPN1	220	314	1
EDC	intra	CRM1	CRM1	22	24	2
EDC	intra	CRM1	CRM1	84	92	1
EDC	intra	CRM1	CRM1	88	1039	2
EDC	intra	CRM1	CRM1	92	468	1
EDC	intra	CRM1	CRM1	190	1039	1
EDC	intra	CRM1	CRM1	312	332	2
EDC	intra	CRM1	CRM1	434	693	1
EDC	intra	CRM1	CRM1	439	700	1
EDC	intra	CRM1	CRM1	443	446	2
EDC	intra	CRM1	CRM1	529	534	1
EDC	intra	CRM1	CRM1	683	693	5
EDC	intra	CRM1	CRM1	693	683	5
EDC	intra	CRM1	CRM1	693	754	1
EDC	intra	CRM1	CRM1	700	754	2

Linker	Type	Protein 1	Protein 2	Residue 1	Residue 2	Spectrum Count
EDC	intra	CRM1	CRM1	752	754	2
EDC	intra	CRM1	CRM1	1012	1017	1
EDC	intra	CRM1	CRM1	1039	1049	2
EDC	inter	MBP-Nup214	Ran	15	2	2
EDC	inter	MBP-Nup214	Ran	15	28	1
EDC	inter	MBP-Nup214	Ran	29	38	1
EDC	inter	MBP-Nup214	Ran	30	107	1
EDC	inter	MBP-Nup214	Ran	372	159	4
EDC	inter	MBP-Nup214	SPN1	29	2	1
EDC	inter	MBP-Nup214	SPN1	35	3	1
EDC	inter	MBP-Nup214	SPN1	35	74	1
EDC	inter	MBP-Nup214	SPN1	39	2	1
EDC	inter	MBP-Nup214	SPN1	315	228	1
EDC	inter	MBP-Nup214	CRM1	56	446	1
EDC	inter	MBP-Nup214	CRM1	59	446	1
EDC	inter	MBP-Nup214	CRM1	103	575	1
EDC	inter	MBP-Nup214	CRM1	176	443	1
EDC	inter	MBP-Nup214	CRM1	289	22	1
EDC	inter	MBP-Nup214	CRM1	359	522	1
EDC	inter	MBP-Nup214	CRM1	400	677	1
EDC	inter	MBP-Nup214	CRM1	400	1013	2
EDC	inter	CRM1	SPN1	334	54	1
EDC	inter	CRM1	SPN1	436	313	1
EDC	inter	CRM1	SPN1	529	34	4
EDC	inter	CRM1	SPN1	757	318	1
EDC	inter	CRM1	SPN1	1032	93	1
EDC	inter	CRM1	Ran	426	2	1
EDC	inter	CRM1	Ran	459	123	1
EDC	inter	CRM1	Ran	797	99	1
EDC	inter	CRM1	Ran	840	134	1
EDC	inter	SPN1	Ran	298	36	1

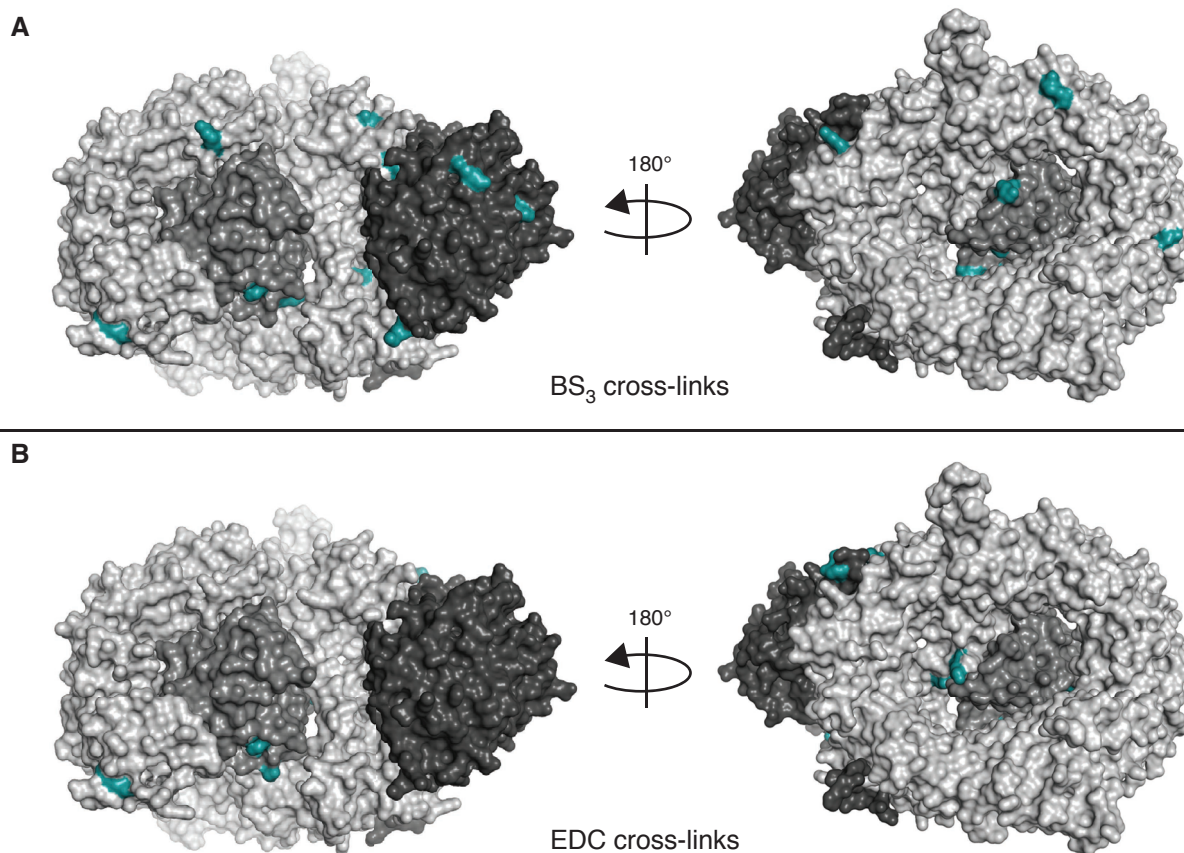


Figure S4: The MBP-tag of Nup214(1916-2033) cross-links indiscriminately to the surface of the export complex and was therefore excluded from further analysis. The structure shows CRM1 (light gray), Ran (medium gray) and SPN1 (dark gray) (PDB ID: 3GJX, [127]). The cross-links by (A) BS³ and (B) EDC of MBP-tag onto the export complex are highlighted in green.

D Protein alignments

D.1 Alignment of *H. sapiens* CRM1 and *S. cerevisiae* Xpo1p

Conservation									
CRM1 (<i>H. sapiens</i>)	1	M P A I M T M L A D	H A A R Q L L D F S	Q K L D I N L L D N	V V N C L Y H G E G	A Q Q R M A Q E V L	50		
Xpo1 (<i>S. cerevisiae</i>)	1	M E G - - - - -	- - - - - I L D F S	N D L D I A L L D Q	V V S T F Y Q G S G	V Q Q K Q A Q E I L	38		
Conservation									
CRM1 (<i>H. sapiens</i>)	51	T H L K E H P D A W	T R V D T I L E F S	Q N M N T K Y Y G L	Q I L E N V I K T R	W K I L P R N Q C E	100		
Xpo1 (<i>S. cerevisiae</i>)	39	T K F Q D N P D A W	Q K A D Q I L Q F S	T N P Q S K F I A L	S I L D K L I T R K	W K L L P N D H R I	88		
Conservation									
CRM1 (<i>H. sapiens</i>)	101	G I K K Y V V G L I	I K T S S D P T C V	E K E K V Y I G K L	N M I L V Q I L K Q	E W P K H W P T F I	150		
Xpo1 (<i>S. cerevisiae</i>)	89	G I R N F V V G M I	I S M C Q D D E V F	K T Q K N L I N K S	D L T L V Q I L K Q	E W P Q N W P E F I	138		
Conservation									
CRM1 (<i>H. sapiens</i>)	151	S D I V G A S R T S	E S L C Q N N M V I	L K L L S E E V F D	F S S G Q I T Q V K	S K H L K D S M C N	200		
Xpo1 (<i>S. cerevisiae</i>)	139	P E L I G S S S S S	V N V C E N N M I V	L K L L S E E V F D	F S A E Q M T Q A K	A L H L K N S M S K	188		
Conservation									
CRM1 (<i>H. sapiens</i>)	201	E F S Q I F Q L C Q	F V M E N S Q N A P	L V H A T L E T L L	R F L N W I P L G Y	I F E T K L I S T L	250		
Xpo1 (<i>S. cerevisiae</i>)	189	E F E Q I F K L C F	Q V L E Q G S S S S	L I V A T L E S L L	R Y L H W I P Y R Y	I Y E T N I L E L L	238		
Conservation									
CRM1 (<i>H. sapiens</i>)	251	I Y K F L N V P M F	R N V S L K C L T E	I A G V S V S Q - -	- - Y E E Q F V T L	F T L T M M Q L K -	295		
Xpo1 (<i>S. cerevisiae</i>)	239	S T K F M T S P D T	R A I T L K C L T E	V S N L K I P Q D N	D L I K R Q T V L F	F Q N T L Q Q I A T	288		
Conservation									
CRM1 (<i>H. sapiens</i>)	296	Q M L P L N T N I R	L A Y S N G K D D E	Q N F I Q N L S L F	L C T F L K E H D Q	L I E K R L N L R E	345		
Xpo1 (<i>S. cerevisiae</i>)	289	S V M P V T A D L K	A T Y A N A N G N D	Q S F L Q D L A M F	L T T Y L A R N R A	L L E S D E S L R E	338		
Conservation									
CRM1 (<i>H. sapiens</i>)	346	T L M E A L H Y M L	L V S E V E E T E I	F K I C L E Y W N H	L A A E L Y R E S P	F - - S T S A S P L	393		
Xpo1 (<i>S. cerevisiae</i>)	339	L L L N A H Q Y L I	Q L S K I E E R E L	F K T T L D Y W H N	L V A D L F Y E V Q	R L P A T E M S P L	388		
Conservation									
CRM1 (<i>H. sapiens</i>)	394	L S - - - G S Q H F	D V - - - - -	- - - - - P P R R Q	L Y L P M L F K V R	L L M V S R M A K P	427		
Xpo1 (<i>S. cerevisiae</i>)	389	I Q L S V G S Q A I	S T G S G A L N P E	Y M K R F P L K K H	I Y E E I C S Q L R	L V I I E N M V R P	438		
Conservation									
CRM1 (<i>H. sapiens</i>)	428	E E V L V V E N D Q	G E V V R E F M K D	T D S I N L Y K N M	R E T L V Y L T H L	D Y V D T E R I M T	477		
Xpo1 (<i>S. cerevisiae</i>)	439	E E V L V V E N D E	G E I V R E F V K E	S D T I Q L Y K S E	R E V L V Y L T H L	N V I D T E E I M I	488		
Conservation									
CRM1 (<i>H. sapiens</i>)	478	E K L H N Q V N G T	E W S W K N L N T L	C W A I G S I S G A	M H E E D E K R F L	V T V I K D L L G L	527		
Xpo1 (<i>S. cerevisiae</i>)	489	S K L A R Q I D G S	E W S W H N I N T L	S W A I G S I S G T	M S E D T E K R F V	V T V I K D L L D L	538		
Conservation									
CRM1 (<i>H. sapiens</i>)	528	C E Q K R G K D N K	A I I A S N I M Y I	V G Q Y P R F L R A	H W K F L K T V V N	K L F E F M H E T H	577		
Xpo1 (<i>S. cerevisiae</i>)	539	T V K K R G K D N K	A V V A S D I M Y V	V G Q Y P R F L K A	H W N F L R T V I L	K L F E F M H E T H	588		
Conservation									
CRM1 (<i>H. sapiens</i>)	578	D G V Q D M A C D T	F I K I A Q K C R R	H F V Q V Q V G E V	M P F I D E I L N N	I N T I I C D L Q P	627		
Xpo1 (<i>S. cerevisiae</i>)	589	E G V Q D M A C D T	F I K I V Q K C K Y	H F V I Q Q P R E S	E P F I Q T I I R D	I Q K T T A D L Q P	638		
Conservation									
CRM1 (<i>H. sapiens</i>)	628	Q Q V H T F Y E A V	G Y M I G A Q T D Q	T V Q E H L I E K Y	M L L P N Q V W D S	I I Q Q A T K N V D	677		
Xpo1 (<i>S. cerevisiae</i>)	639	Q Q V H T F Y K A C	G I I I S E E R S V	A E R N R L L S D L	M Q L P N M A W D T	I V E Q S T A N P T	688		
Conservation									
CRM1 (<i>H. sapiens</i>)	678	I L K D P E T V K Q	L G S I L K T N V R	A C K A V G H P F V	I Q L G R I Y L D M	L N V Y K C L S E N	727		
Xpo1 (<i>S. cerevisiae</i>)	689	L L L D S E T V K I	I A N I I K T N V A	V C T S M G A D F Y	P Q L G H I Y Y N M	L Q L Y R A V S S M	738		
Conservation									
CRM1 (<i>H. sapiens</i>)	728	I S A A I Q A N G E	M V T K Q P L I R S	M R T V K R E T L K	L I S G W V S R S N	D P Q M V A E N F V	777		
Xpo1 (<i>S. cerevisiae</i>)	739	I S A Q V A A E G L	I A T K T P K V R G	L R T I K K E I L K	L V E T Y I S K A R	N L D D V V K V L V	788		
Conservation									
CRM1 (<i>H. sapiens</i>)	778	P P L L D A V L I D	Y Q R N V P A A R E	P E V L S T M A I I	V N K L G G H I T A	E I P Q I F D A V F	827		
Xpo1 (<i>S. cerevisiae</i>)	789	E P L L N A V L E D	Y M N N V P D A R D	A E V L N C M T T V	V E K V G H M I P Q	G V I L I L Q S V F	838		
Conservation									
CRM1 (<i>H. sapiens</i>)	828	E C T L N M I N K D	F E E Y P E H R T N	F F L L L Q A V N S	H C F P A F L A I P	P T Q F K L V L D S	877		
Xpo1 (<i>S. cerevisiae</i>)	839	E C T L D M I N K D	F T E Y P E H R V E	F Y K L L K V I N E	K S F A A F L E L P	P A A F K L F V D A	888		
Conservation									
CRM1 (<i>H. sapiens</i>)	878	I I W A F K H T M R	N V A D T G L Q I L	F T L L Q N V A Q -	- E E A A A Q S F Y	Q T Y F C D I L Q H	925		
Xpo1 (<i>S. cerevisiae</i>)	889	I C W A F K H N N R	D V E V N G L Q I A	L D L V K N I E R M	G N V P F A N E F H	K N Y F F I F V S E	938		
Conservation									
CRM1 (<i>H. sapiens</i>)	926	I F S V V T D T S H	T A G L T M H A S I	L A Y M F N L V E E	G K I S T S L - - -	- N P G N P V N N Q	971		
Xpo1 (<i>S. cerevisiae</i>)	939	T F F V L T D S D H	K S G F S K Q A L L	L M K L I S L V Y D	N K I S V P L Y Q E	A E V P Q G T S N Q	988		
Conservation									
CRM1 (<i>H. sapiens</i>)	972	I F L Q E Y V A N L	L K S A F P H L Q D	A Q V K L F V T G L	F S L N Q D I P A F	K E H L R D F L V Q	1021		
Xpo1 (<i>S. cerevisiae</i>)	989	V Y L S Q Y L A N M	L S N A F P H L T S	E Q I A S F L S A L	T K Q Y K D L V V F	K G T L R D F L V Q	1038		
Conservation									
CRM1 (<i>H. sapiens</i>)	1022	I K E F A G E D T S	D L F L E E R E I A	L R O A D E E K H K	R O M S V P G I F N	P H E I P E E M C D	1071		
Xpo1 (<i>S. cerevisiae</i>)	1039	I K E V G G D P T D	Y L F A E D K E N A	L M E Q N R L E R E	K A A K I G G L L K	P S E L D D - - - -	1084		

Figure S5: Alignment of *H. sapiens* CRM1 (gi 68052989/ sp O14980.1) and *S. cerevisiae* Xpo1p (gi 399300/ sp P30822.1)

D.2 Alignment of *H. sapiens* Nup214 and *S. cerevisiae* Nup159

Conservation												
Nup214 (<i>H. sapiens</i>)	1	MGDEM	DAMIP	EREMKDFQFR	ALKKVRI	FDS -PEELPKERS	SLLAVSNKYG	49				
Nup159 (<i>S. cerevisiae</i>)	1	MSSLKDE	-VP	TETSEDFGFK	FLGQKQILPS	FNEKLPFASL	QNLDISNSKS	49				
Conservation												
Nup214 (<i>H. sapiens</i>)	50	LVFAGG	ASGL	QIFPTKNLLI	QNKPGDDPNK	IVDKVQGLLV	PMKFFPIHHLA	99				
Nup159 (<i>S. cerevisiae</i>)	50	LFVA	--ASGS	KAVVGELQLL	RDHITS DSTP	LTFKWEKEIP	DVIFVCFH	--95				
Conservation												
Nup214 (<i>H. sapiens</i>)	100	LSCDNL	TLISA	--CMMSS	SEYGSII	AFFDVRT	FSNEAKQQR	PFAYHKLKLD	147			
Nup159 (<i>S. cerevisiae</i>)	96	--GDQV	LVST	RNALYS	LDLE	ELSEFRTVTS	FEKPVFQLKN	VNNTLVILNS	143			
Conservation												
Nup214 (<i>H. sapiens</i>)	148	AGGM	-VIDMK	WNPT	--VPS	MVAVCLADGS	I AVLQVTETV	KVCATLPSTV	193			
Nup159 (<i>S. cerevisiae</i>)	144	VNDLSA	LDLR	TKSTK	QLAQN	VTSFDV TNSQ	LAVLLKDRSF	Q-----	184			
Conservation												
Nup214 (<i>H. sapiens</i>)	194	AVT	SVCWSPK	GKQLAVG	KQNG	GTVVQYLPTL	QEKKVI	PCPP	FYEDHPVRV	243		
Nup159 (<i>S. cerevisiae</i>)	185	--SFAW	---	-----RN		GEME KQFEFS	LPSELE	ELPV	EEYSPLSVTI	220		
Conservation												
Nup214 (<i>H. sapiens</i>)	244	L--DVL	WIG	TYVFA	IVYAA	ADGTL	ETSPD	VVMALLPKKE	EKHPEIFVNF	290		
Nup159 (<i>S. cerevisiae</i>)	221	LSPQDFL	---	AVFGN	VI SE	TDD--EVSYD		QKMYII	---EKHIDGSASF	259		
Conservation												
Nup214 (<i>H. sapiens</i>)	291	ME	---PCY	GSCTER	QH HY	Y--LSY	IEEW	D--LVLAASA	ASTEVSILAR	331		
Nup159 (<i>S. cerevisiae</i>)	260	QETFD	ITPPF	GQIVR	FPYMY	KVTL	SLG LIEP	DANVNV	LASS	CSSEVSIW	--307	
Conservation												
Nup214 (<i>H. sapiens</i>)	332	QSDQ	INWESW	LLEDSS	RAEL	PVTDKSD	-DS	LPMGVVVDYT	NQVEIT	--IS	378	
Nup159 (<i>S. cerevisiae</i>)	308	DSKQV	IEPS-	--QD	SERAVL	PISEET	DKDT	NPIGVA	VDVV	TSGTILEPCS	354	
Conservation												
Nup214 (<i>H. sapiens</i>)	379	DEK	TLPPAPV	LMLL	STDGV	-----	--CPFY	MINQ	NP--GV	KSLI	414	
Nup159 (<i>S. cerevisiae</i>)	355	GVDT	IERLPL	VYIL	LNNEGSL	QIVGL	FHVAA	IKSGHYS	INL	ESLEHEKSL	404	
Conservation												
Nup214 (<i>H. sapiens</i>)	415	KTP	ERLSLEG	ERQPK	SPGST	PTTPT	SSQAP	QKLDASA	AAAA	PASLPPSSPA	464	
Nup159 (<i>S. cerevisiae</i>)	405	PTSEK	IP IAG	QEQE	EKKKNN	ESSKAL	SEN	F--TS	ANTS	GFTFLKTQPA	451	
Conservation												
Nup214 (<i>H. sapiens</i>)	465	API	ATFSLLP	AG	-GAPT	VFS	FGSSSLKS	--SAT	VTGE	PPSYSSGSDS	508	
Nup159 (<i>S. cerevisiae</i>)	452	AANSL	QSQSS	STFG	A--S	FGSSAF	KIDL	PSV	SSTSTGV	ASSEQDATDP	498	
Conservation												
Nup214 (<i>H. sapiens</i>)	509	SKAA	PGPGPS	TFSF	VPPSKA	SLAPT	PAASP	VA--PSAAS		FSFGSSGFKP	555	
Nup159 (<i>S. cerevisiae</i>)	499	ASAKP	-----	--VFG	KPAFG	AIAKE	PSTSE	YAFG	KPSFGA	PSFGSG--KS	539	
Conservation												
Nup214 (<i>H. sapiens</i>)	556	TLEST	PVPSV	SAPN	IAMKPS	FPPST	SAVKV	NLS	-EKFTA	ATSTPVSSSQ	604	
Nup159 (<i>S. cerevisiae</i>)	540	SVES	PASGSA	FGKPS	FGTSPS	FGSGN	SSVEP	PASGS	AFGK	SFGTSPFSGG	589	
Conservation												
Nup214 (<i>H. sapiens</i>)	605	SAPP	MSPFSS	ASKPA	ASGPL	SHPT	PLSAPP	SSVPL	KSSVL	PSPSGRSAQG	654	
Nup159 (<i>S. cerevisiae</i>)	590	N-----	SS	AEP	PASGSAF	GKPS	FGTSAF	GTASS	NETNS	GSIFGKA	AFG632	
Conservation												
Nup214 (<i>H. sapiens</i>)	655	SSSP	VPSMVQ	KSPR	ITPPAA	KPGS	PQAKSL	QPAVA	EAKQGH	QWKDSDPVMA	704	
Nup159 (<i>S. cerevisiae</i>)	633	SSSF	AP A--	-----		-----		-----		-----	639	
Conservation												
Nup214 (<i>H. sapiens</i>)	705	GIGEE	IAHFQ	KELE	E LKART	SKAC	FQVGTS	EEMK	MLRTES	DDLHTFLLEI	754	
Nup159 (<i>S. cerevisiae</i>)	640	-----		-----		-----		-----		-----	639	
Conservation												
Nup214 (<i>H. sapiens</i>)	755	KETTES	LHGD	ISSL	KTTLLE	GFAG	VEEARE	QNER	NRDSGY	LHLLYKRPLD	804	
Nup159 (<i>S. cerevisiae</i>)	640	-----		-----		-----		--NNEL	FGS	NFTISKPTVD	656	
Conservation												
Nup214 (<i>H. sapiens</i>)	805	PKSE	AQLQEI	RRLH	QYVKFA	VQDV	NDVLDL	EWDQ	HLEQKK	KQRHLLVPER	854	
Nup159 (<i>S. cerevisiae</i>)	657	SPKE	-----	-----		-----		-----		-----	660	
Conservation												
Nup214 (<i>H. sapiens</i>)	855	ETL	FNTLANN	REI	INQQRKR	LNHL	VDSLQ	LRLY	KQTS	SLSSAVPSQS	904	
Nup159 (<i>S. cerevisiae</i>)	661	-----		-----		-----VDS		-----		--TSPFPSSG	671	
Conservation												
Nup214 (<i>H. sapiens</i>)	905	SIH	SFSDLE	SLCN	ALLKTT	IESHT	KSLPK	VPAKL	SMPMKQ	AQLRNFLAKR	954	
Nup159 (<i>S. cerevisiae</i>)	672	D-----		-----		-QSE	DESKSD	VDSS	STPFG-	-----	690	
Conservation												
Nup214 (<i>H. sapiens</i>)	955	KTP	VRSTAP	ASLS	RS AFLS	QRY	YEDL	SST	SSVSQSL	ESEDARTSCK	1004	
Nup159 (<i>S. cerevisiae</i>)	691	-TK	PNTSTK	KT	---NAF	---DFG	SS	SFG	S	GFSKAL	ESVSDTTFK	729
Conservation												
Nup214 (<i>H. sapiens</i>)	1005	DDEA	VVQAPR	HAP	VVRTPSI	QPSLL	PHAAP	FAK	SHLVHGS	SPGVMGT	SVA1054	
Nup159 (<i>S. cerevisiae</i>)	730	FGT	-----	-----		-----QASP		FSSQ	--LGNK	SPFSSFTKDD	754	

Conservation									
Nup214 (<i>H. sapiens</i>)	1055	TSASKIIPQG	ADSTMLATKT	VKHGAPSPSH	PISAPQAAAA	AALRRQMASQ			1104
Nup159 (<i>S. cerevisiae</i>)	755	TE-----	-NGSLSKGST	SEINDDNEEH	ESNGPNVSG-	-----			784
Conservation									
Nup214 (<i>H. sapiens</i>)	1105	APAVNTLTES	TLKNVPQVVN	VQELKNNPAT	PSTAMGSSVP	YSTAKTTPHV			1154
Nup159 (<i>S. cerevisiae</i>)	785	-----NDLTD	TVEQTSST--	-----RLPET	PSDEDGEVVE	EEAQKSPI--			821
Conservation									
Nup214 (<i>H. sapiens</i>)	1155	LTPVAANQAK	QGSLINSLKP	SGPTPASGQL	SSGDKASGTA	KIETAVTSTP			1204
Nup159 (<i>S. cerevisiae</i>)	822	-----	-GKLTETIKK	SANIDMAGLK	NPVFGNHVKA	KSESPFSAFA			860
Conservation									
Nup214 (<i>H. sapiens</i>)	1205	SASGQFSKPF	SFSPSGTGFN	FGIITPTPSS	NFTAAGGATP	STKESSQPPA			1254
Nup159 (<i>S. cerevisiae</i>)	861	T---NITKPS	STTPA---FS	FGNSTMNKSN	TSTVSPMEEA	DTKETSEKGP			904
Conservation									
Nup214 (<i>H. sapiens</i>)	1255	FSSGGGSKPS	YEAIPSSPP	SGITSASNTT	PGEPAASSSR	PVAPSGTALS			1304
Nup159 (<i>S. cerevisiae</i>)	905	ITLKSVENPF	LPAKEERTGE	SSKKDHNDPP	KDGYVSGSEI	SVRTSESAFD			954
Conservation									
Nup214 (<i>H. sapiens</i>)	1305	TTSSKLETTP	SKLGEELLFPS	SLAGETLGSF	SGLRVGQADD	STKPTNKASS			1354
Nup159 (<i>S. cerevisiae</i>)	955	TTANE-EIIPK	SQDVN----N	HEKSETDPKY	SQHAVVDHDN	KSKEMNETSK			999
Conservation									
Nup214 (<i>H. sapiens</i>)	1355	TSLTSTQPT-	--KTSGVP--	---SGFNFTA	PPVLGKHTEP	PVT-----			1389
Nup159 (<i>S. cerevisiae</i>)	1000	NNERSGQPNH	GVQGDGIALK	KDNEKENFDS	NMAIKQFEDH	QSSEEDASEK			1049
Conservation									
Nup214 (<i>H. sapiens</i>)	1390	---SSATTT	SVAPPAATST	SSTAVFGSLP	VTSAGSSGVI	SFGGTSLSAG			1435
Nup159 (<i>S. cerevisiae</i>)	1050	DSRQSSEVKE	SDDNMSLNSD	RDESISESYD	KLEDINTDEL	PHGGAEAFKAR			1099
Conservation									
Nup214 (<i>H. sapiens</i>)	1436	KTSFSFGSQ	TNSTVPPSAP	PPTTAATPLP	TSFPTLSFGS	LLSSATTPSL			1485
Nup159 (<i>S. cerevisiae</i>)	1100	EVSASADFV	QTSL-----	EDNYAESGIQ	TD---LSESS	KENEVQTDAI			1140
Conservation									
Nup214 (<i>H. sapiens</i>)	1486	PM---SAGRS	TEEATSSALP	EKPGDSEVSA	SAASLLEEQQ	SAQLPQAPPQ			1532
Nup159 (<i>S. cerevisiae</i>)	1141	PVKHNSTQTV	KKEAVDNLQ	TEP--VETCN	FVQTFEGDE	NYLAEQCKPK			1188
Conservation									
Nup214 (<i>H. sapiens</i>)	1533	---TSDS	VKKEPVLAQP	AVSNSGTAAS	STSLVALSAE	ATPATTGVPD			1576
Nup159 (<i>S. cerevisiae</i>)	1189	QLKEYYTSK	VSNIPFVSQ-	---NSTLRLI	ESTFQTVEAE	FTVLMENIRN			1234
Conservation									
Nup214 (<i>H. sapiens</i>)	1577	ARTEAVPPAS	SFSVPGQTAV	TAAAISSAGP	VAVETSSTPI	ASSTTSIVAP			1626
Nup159 (<i>S. cerevisiae</i>)	1235	MDTFFTDQSS	IPLVKR----	TVRSINNLYT	WRIPEAEI-L	LNIQNNIKCE			1279
Conservation									
Nup214 (<i>H. sapiens</i>)	1627	GPSAEAAAFG	TVTSGSSVFA	QPPAASSSSA	FNQLTNNTAT	APSATPV---			1673
Nup159 (<i>S. cerevisiae</i>)	1280	QMQUITNANIQ	DLKEKVTDYV	RKDIA-----	-QITEDVAN	AKEEYLFLMH			1322
Conservation									
Nup214 (<i>H. sapiens</i>)	1674	FGQVAASTAP	SLFGQQTGST	ASTAAATPQV	SSSGFSSPAF	GTTAPGVFGQ			1723
Nup159 (<i>S. cerevisiae</i>)	1323	FDDASSGYVK	DLSTHQFRMQ	KTLRQKLFDV	SAKINHTEEL	----LNILKL			1368
Conservation									
Nup214 (<i>H. sapiens</i>)	1724	TTFGQASVFG	QSASSAASVF	SFSQPGF-SS	VPAFGQPASS	TPTSTSGSVF			1772
Nup159 (<i>S. cerevisiae</i>)	1369	FTVKNKRLLD	NPLVAKLAKE	SLARDGLLKE	IKLLREQVSR	LQLEEKGKKA			1418
Conservation									
Nup214 (<i>H. sapiens</i>)	1773	GAASSTSSSS	SFSFGQSSPN	TGGGLFGQSN	APAFGQSPGF	GQGGSVFGGT			1822
Nup159 (<i>S. cerevisiae</i>)	1419	SSFDASSSIT	KDMKGFKVVE	VGLAMNTKKQ	IGDFFKNLNM	AK-----			1460
Conservation									
Nup214 (<i>H. sapiens</i>)	1823	SAATTTAATS	GFSFCQASGF	GSSNTGSVFG	QAASTGGIVF	GQQSSSSSSGS			1872
Nup159 (<i>S. cerevisiae</i>)	1460	-----	-----	-----	-----	-----			1460
Conservation									
Nup214 (<i>H. sapiens</i>)	1873	VFGSGNTGRG	GGFFSGLGGK	PSQDAANKNP	FSSASGGFGS	TATSNTSNLF			1922
Nup159 (<i>S. cerevisiae</i>)	1460	-----	-----	-----	-----	-----			1460
Conservation									
Nup214 (<i>H. sapiens</i>)	1923	GNSGAKTFGG	FASSSFGEQK	PTGTTFSSGGG	SVASQGFQFS	SPNKTGGFGA			1972
Nup159 (<i>S. cerevisiae</i>)	1460	-----	-----	-----	-----	-----			1460
Conservation									
Nup214 (<i>H. sapiens</i>)	1973	APVFGSPPTF	GGSPGFGGVP	AFGSAPAFTS	PLGSTGGKVF	GEGTAAASAG			2022
Nup159 (<i>S. cerevisiae</i>)	1460	-----	-----	-----	-----	-----			1460
Conservation									
Nup214 (<i>H. sapiens</i>)	2023	GFGFGSSSNT	TSFGTLASQN	APTFGSLSQQ	TSGFGTQSSG	FSGFGSGTGG			2072
Nup159 (<i>S. cerevisiae</i>)	1460	-----	-----	-----	-----	-----			1460
Conservation									
Nup214 (<i>H. sapiens</i>)	2073	F S F G S N N S S V	Q G F G G W R S						2090
Nup159 (<i>S. cerevisiae</i>)	1460	-----	-----						1460

Figure S6: Alignment of *H. sapiens* Nup214 (gi 205831380/ sp P35658.2) and *S. cerevisiae* Nup159 (gi 731862/ sp P40477.1).

D.3 Alignment of *H. sapiens* RanBP3 and *S. cerevisiae* Yrb2p

Conservation									
RanBP3 (<i>H. sapiens</i>)	1	MADLANEEKP	AIAPPVVFVQ	KDKGQKSPA E	QKNLSDSGEE	PRGEAEAPHH	50		
Yrb2 (<i>S. cerevisiae</i>)	1	-----	-----	-----	-----	-----	0		
Conservation									
RanBP3 (<i>H. sapiens</i>)	51	GTGHPESAGE	HALEPPAPAG	ASASTPPPPA	PEAQLPPFPR	ELAGRSAGGS	100		
Yrb2 (<i>S. cerevisiae</i>)	1	-----	-----	-----	-----	-----	0		
Conservation									
RanBP3 (<i>H. sapiens</i>)	101	SPEGGEDSDR	EDGNYCPPVK	RERTSSLTQF	PPSQSEERSS	GFRLKPPTLI	150		
Yrb2 (<i>S. cerevisiae</i>)	1	-----	-----	-----	-----	-----	0		
Conservation									
RanBP3 (<i>H. sapiens</i>)	151	HGQAPSAGLP	SQKPKEQQRS	VLRPAVLQAP	QPKALSQTVP	SSGTNGVSLP	200		
Yrb2 (<i>S. cerevisiae</i>)	1	-----	-----	-----	-----	MSETNGGNA	10		
Conservation									
RanBP3 (<i>H. sapiens</i>)	201	ADCTGAVPAA	-----	SPDTAAWRSP	SEAADEVCAL	EEKEPQKNES	240		
Yrb2 (<i>S. cerevisiae</i>)	11	RENSEVKQTA	VENPIDKLDG	TPKRPREKQD	DEQAEET---	SDKSEAPNKN	57		
Conservation									
RanBP3 (<i>H. sapiens</i>)	241	SNASEEEACE	KKDPATQQA F	VFGQNLDRV	KLINESVDEA	DM-ENAGHPS	289		
Yrb2 (<i>S. cerevisiae</i>)	58	DEEKKEEGKK	DQEPSHKKIK	V-----DDG	KTVESGIVED	DKKEDKFVFG	101		
Conservation									
RanBP3 (<i>H. sapiens</i>)	290	ADTPTATNYF	LQYISSS---	LENSTNSADA	SSNK-----FV	FGQNMSEVL	332		
Yrb2 (<i>S. cerevisiae</i>)	102	AASKFGTGFG	VAKKDTKDGD	ATTSTESLPA	SDSKTKKPPFA	FGSGLS----	147		
Conservation									
RanBP3 (<i>H. sapiens</i>)	333	SPPKLNEVSS	DANRENAAAE	SGSESSSQEA	TPEKESLAE-	-----SAAAY	376		
Yrb2 (<i>S. cerevisiae</i>)	148	-----FGS	GFNILKNKTE	NNSESEKKAT	DVDKDKVHSG	SEQLANASED	190		
Conservation									
RanBP3 (<i>H. sapiens</i>)	377	TKATARKCLL	EKVEVITGEE	AESNVLQMQC	KLFVFDKTSQ	SWVERGRGLL	426		
Yrb2 (<i>S. cerevisiae</i>)	191	TKDKPKPLKL	QKQEVKSGEE	SEECIYQVNA	KLYQLSNIKE	GWKERGVGII	240		
Conservation									
RanBP3 (<i>H. sapiens</i>)	427	RLNDMASTDD	GTLQSRLVMR	TQGSRLRILN	TKLWAQMqid	KA-----SE	470		
Yrb2 (<i>S. cerevisiae</i>)	241	KINKSK----	DVEKTRIVMR	SRGILKVILN	IQLVKGFTVQ	KGFTGSLQSE	287		
Conservation									
RanBP3 (<i>H. sapiens</i>)	471	KSIRITAMDT	EDQGVKVFLI	SASSKDTGQL	YAALHHRILA	LRSRVEQEQE	520		
Yrb2 (<i>S. cerevisiae</i>)	288	KFIRLLAVD-	DNGDPAQYAI	KTGKKETTD-	--ELYNIIVK	SVPK-----	327		
Conservation									
RanBP3 (<i>H. sapiens</i>)	521	AKMPAPEPGA	APSNEEDDSD	DDDVLAPSGA	TAAGAGDEGD	GQTTGST	567		
Yrb2 (<i>S. cerevisiae</i>)	327	-----	-----	-----	-----	-----	327		

Figure S7: Alignment of *H. sapiens* RanBP3 (gi 51316528/ sp Q9H6Z4.1) and *S. cerevisiae* Yrb2p (gi 731821/ sp P40517.1)

E Interactions of Nup214 to CRM1 in the crystal structure of the Nup214 complex

Table S6: Interactions of Nup214 to CRM1 in the crystal structure.

FG-site	Nup214 residues	CRM1 residue	HEAT repeat	interaction type	
1	Thr1918	Asn727	15A	polar	
		Ala730	15A	hydrophobic/ vdW	
	Ser1919	Glu726	15A	hydrophobic/ vdW	
		Asn727	15A	polar	
		Val676	14A	hydrophobic/ vdW	
	Leu1921	Val676	14A	hydrophobic/ vdW	
	Phe1922 [I]	Ile669	14A	hydrophobic/ vdW	
		Asn719	15A	polar	
		Val720	15A	hydrophobic/ vdW	
		Cys723	15A	hydrophobic/ vdW	
		Ser1925	His11 (*)	N-term (*)	hydrophobic/ vdW
		Lys1928	Asp782	16A	polar
	Phe1930	Val31 (*)	1A (*)	hydrophobic/ vdW	
		Cys34 (*)	1A (*)	hydrophobic/ vdW	
		Ala46 (*)	1B (*)	hydrophobic/ vdW	
		Val49 (*)	1B (*)	hydrophobic/ vdW	
		Gln1931	Gln42 (*)	1B (*)	polar
		Ser1936	Asp824	17A	polar
	Ser1937	Asp824	17A	polar	
		Phe1938 [II]	Phe823	17A	hydrophobic/ vdW
			Phe827	17A	hydrophobic/ vdW
			Glu828	17A	hydrophobic/ vdW
	Gln1941	Pro867	18A	hydrophobic/ vdW	
	Pro1943	Leu864	18A	hydrophobic/ vdW	
		Ala865	18A	hydrophobic/ vdW	
		Ile866	18A	hydrophobic/ vdW	
		Pro868	18A	hydrophobic/ vdW	
	Thr1944	Pro868	18A	hydrophobic/ vdW	
	Phe1947 [III]	Pro868	18A	hydrophobic/ vdW	
		Phe871	18A	hydrophobic/ vdW	
		Ala910	19A	hydrophobic/ vdW	
		Ser913	19A	hydrophobic/ vdW	
		Phe914	19A	hydrophobic/ vdW	
Tyr918		19A	hydrophobic/ vdW		
Thr917		19A	hydrophobic/ vdW		
Ser1948		Thr917	19A	hydrophobic/ vdW	
2	Phe1982 [IV]	Leu831	17A	hydrophobic/ vdW	
		Leu873	18A	hydrophobic/ vdW	
		Asp876	18A	hydrophobic/ vdW	
		Ser877	18A	hydrophobic/ vdW	
		Trp880	18A	hydrophobic/ vdW	
	Gly1983	Asp876	18A	polar	
	Gly1984	His925	19A	polar	
	Ser1985	His925	19A	hydrophobic/ vdW	

FG-site	Nup214 residues	CRM1 residue	HEAT repeat	interaction type
	Pro1986	Gln924	19A	hydrophobic/ vdW
		His925	19A	hydrophobic/ vdW
		Ser928	19A	hydrophobic/ vdW
	Phe1988 [V]	Leu873	18A	hydrophobic/ vdW
		Asp876	18A	hydrophobic/ vdW
		Phe927	19A	hydrophobic/ vdW
		Ser928	19A	hydrophobic/ vdW
		Thr931	19A	hydrophobic/ vdW
3	Lys2010	Gln98	3A	polar
	Val2011	Gly101	3A	hydrophobic/ vdW
	Phe2012 [VI]	Val63	2A	hydrophobic/ vdW
		Asp64	2A	polar
		Gln98	3A	polar
		Gly101	3A	hydrophobic/ vdW
		Ile102	3A	hydrophobic/ vdW
		Leu83	3B	hydrophobic/ vdW
	Glu2014	Glu68	2A	polar
	Ala2017	Tyr105	3A	hydrophobic/ vdW
	Ser2020	Gly108	3A	hydrophobic/ vdW
	Ala2021	Gly108	3A	hydrophobic/ vdW
		Lys104	3A	hydrophobic/ vdW
		Val107	3A	hydrophobic/ vdW
	Phe2024 [VII]	Ile111	3A	hydrophobic/ vdW
		Asp152	4A	hydrophobic/ vdW
		Ile153	4A	hydrophobic/ vdW
	Gly2025	4A	polar	

Polar interactions (e.g. hydrogen bonds) are ≤ 3.5 Å while hydrophobic and van-der-Waals (vdW) interactions are ≤ 4 Å. The asterisk indicates interactions to the symmetry-related CRM1 molecule. Numbers in square brackets indicate the respective binding pockets on CRM1 that the phenylalanine residues bind to.

F Comparison of the CRM1-RanGTP-SPN1 architecture in the crystal structure of the Nup214 complex and the export complex

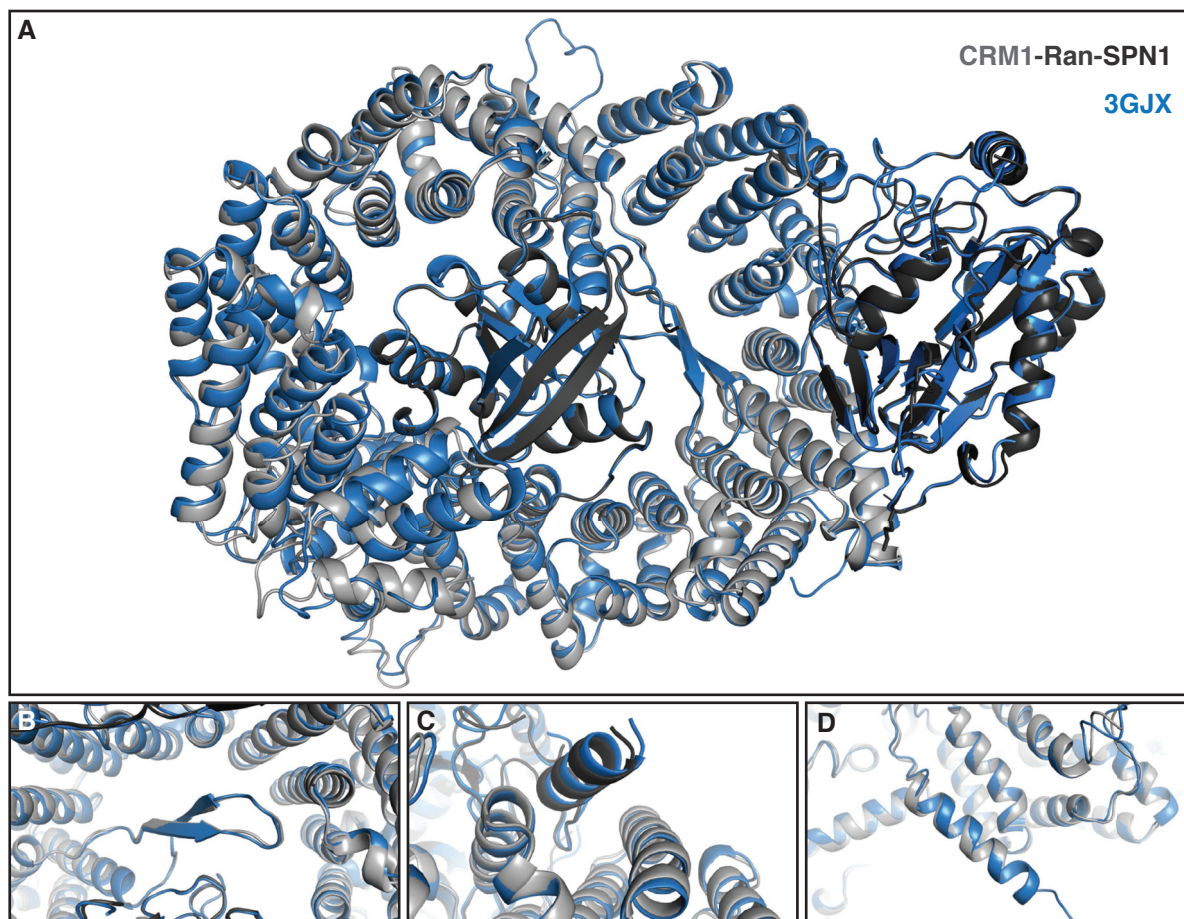


Figure S8: Comparison of the CRM1-RanGTP-SPN1 architecture in the crystal structure of the Nup214 complex and the export complex. (A) The export complex (PDB ID: 3GJX, blue) was aligned with CRM1 (light gray), RanGTP (medium gray) and SPN1 (dark gray) from the Nup214 complex. (B) The Acidic loop is in a closed conformation in both structures. (C) The NES binding cleft is in an open conformation in both structures. Binding of the NES in the binding cleft is unaltered. (D) The C-terminal helix is located in a stack with the other HEAT repeats in both structures.

G Nup214 fragments and mutants

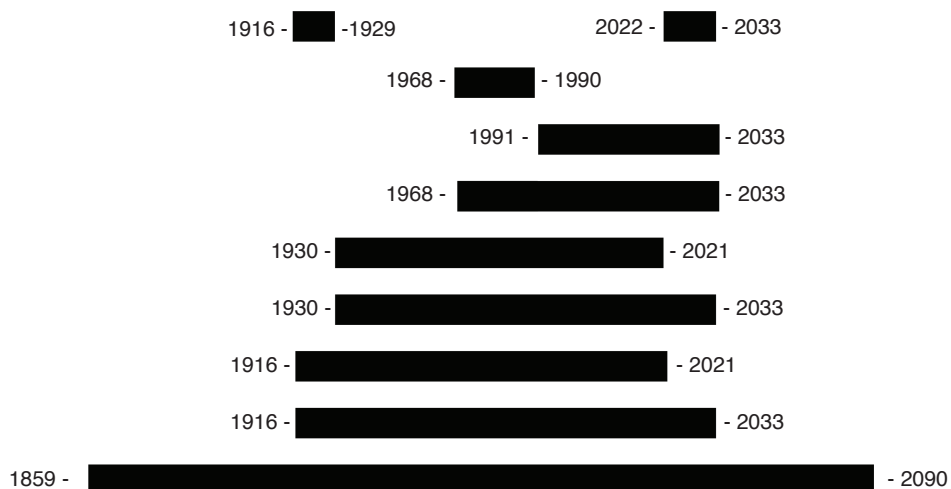


Figure S9: Nup214 fragments of different lengths used in this study.

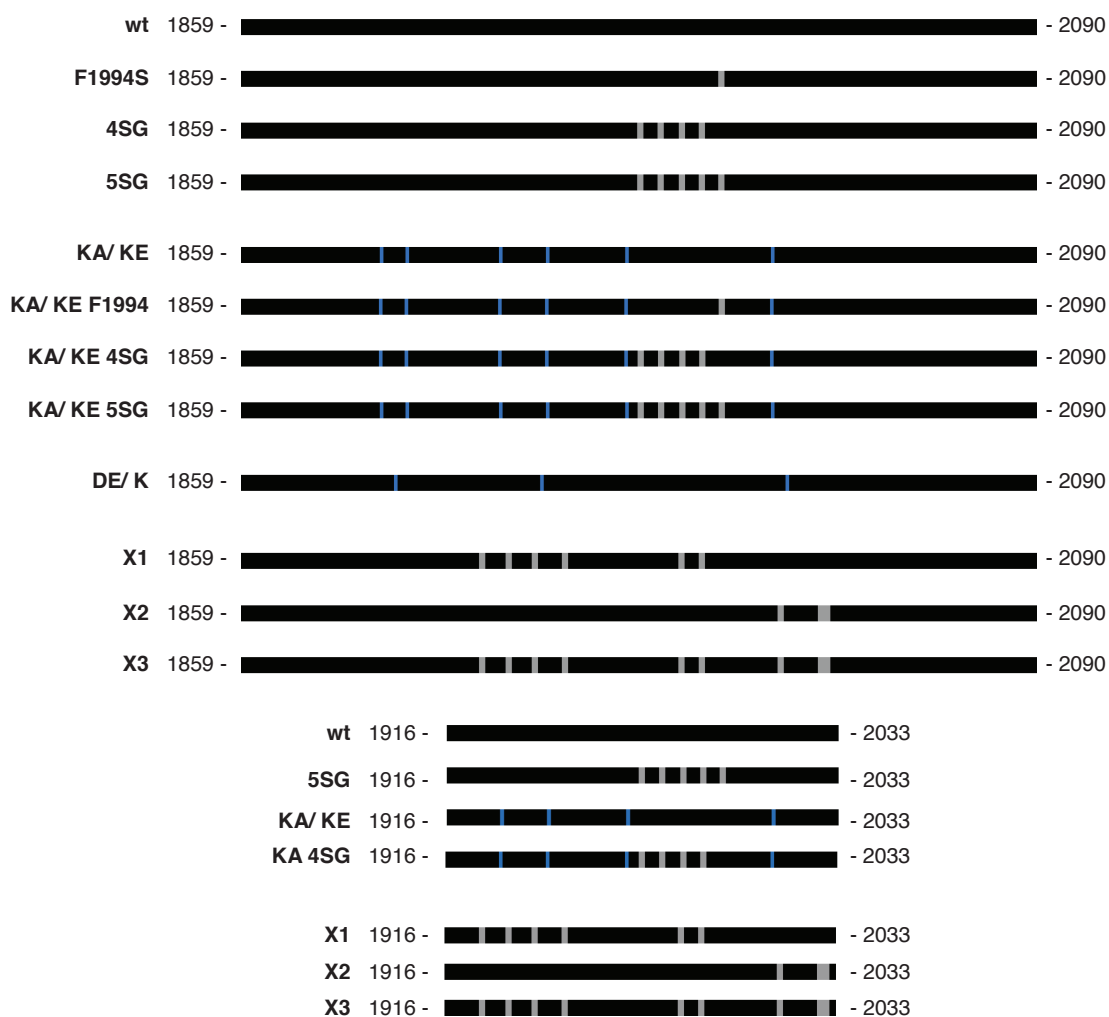


Figure S10: Nup214 mutants used in this study. Mutated phenylalanines are colored in gray, mutated charged amino acids are colored in blue.

H CRM1 mutants

Table S7: CRM1 mutants designed to impair binding to Nup214.

Mutated residues	Pockets	Expression tested	Protein
K680Q	L	no	
K680R	L	no	
A731Q	L	no	
L744W	L	yes	soluble
M748R	L	no	
K680Q A731Q	L	yes	soluble
L679R	I	no	
L679W	I	no	
C723M	I	no	
F823A	II	yes	soluble
D824K	II	yes	soluble
T917E	III	yes	soluble
Y918W	III	yes	soluble
W880A	IV	yes	soluble
H925W	V	yes	soluble
S928K	V	yes	soluble
L83F	VI	yes	insoluble
L83R	VI	no	
I102Q	VI	yes	insoluble
I102W	VI	yes	insoluble
L134F	VII	yes	insoluble
F149W	VII	yes	soluble
D152W	VII	no	
A156F	VII	yes	soluble
N167R	VII	no	
L679W K680R	L+I	yes	soluble
K680Q A731Q L679R	L+I	yes	soluble
K680Q A731Q C723M	L+I	yes	soluble
L679R L744W	L+I	yes	soluble
L679W L744W	L+I	no	
C723M L744W	L+I	yes	soluble
L83F L744W	L+VI	yes	insoluble
L83F C723M	i+VI	yes	insoluble
D824K S928K	III+V	yes	soluble
I102W F149W	VI+VII	no	
I102W N167R	VI+VII	no	
I102W D152F	VI+VII	no	
L83F F149W	VI+VII	yes	insoluble
L83R F149W	VI+VII	no	
I102Q F149W	VI+VII	no	
L83F D152W	VI+VII	yes	insoluble
L83R D152W	VI+VII	no	

Mutated residues	Pockets	Expression tested	Protein
I102Q D152W	VI+VII	no	
L83F A156F	VI+VII	yes	soluble
L83R A156F	VI+VII	no	
I102Q A156F	VI+VII	no	
K680Q A731Q L679R D824K	L+I+II	yes	soluble
K680Q A731Q L679R S928K	L+I+V	yes	soluble
L83F K680Q A731Q L679R	L+I+VI	yes	insoluble
K680Q A731Q L679R F149W	L+I+VII	yes	insoluble
I102Q F149W L744W	L+VI+VII	no	
I102Q F149W C723M	L+VI+VII	yes	insoluble
L83F D152W K680Q A731Q C723M	L+I+VI+VII	yes	insoluble
L83F D152W L679W L744W	L+I+VI+VII	yes	insoluble
L83F D152W C723M L744W	L+I+VI+VII	yes	insoluble
L83F A156F K680Q A731Q C723M	L+I+VI+VII	yes	insoluble
L83F A156F L679W L744W	L+I+VI+VII	yes	insoluble
L83F A156F C723M L744W	L+I+VI+VII	yes	insoluble
I102Q F149W K680Q A731Q C723M	L+I+VI+VII	yes	insoluble
I102Q F149W L679W L744W	L+I+VI+VII	no	
I102Q F149W C723M L744W	L+I+VI+VII	no	

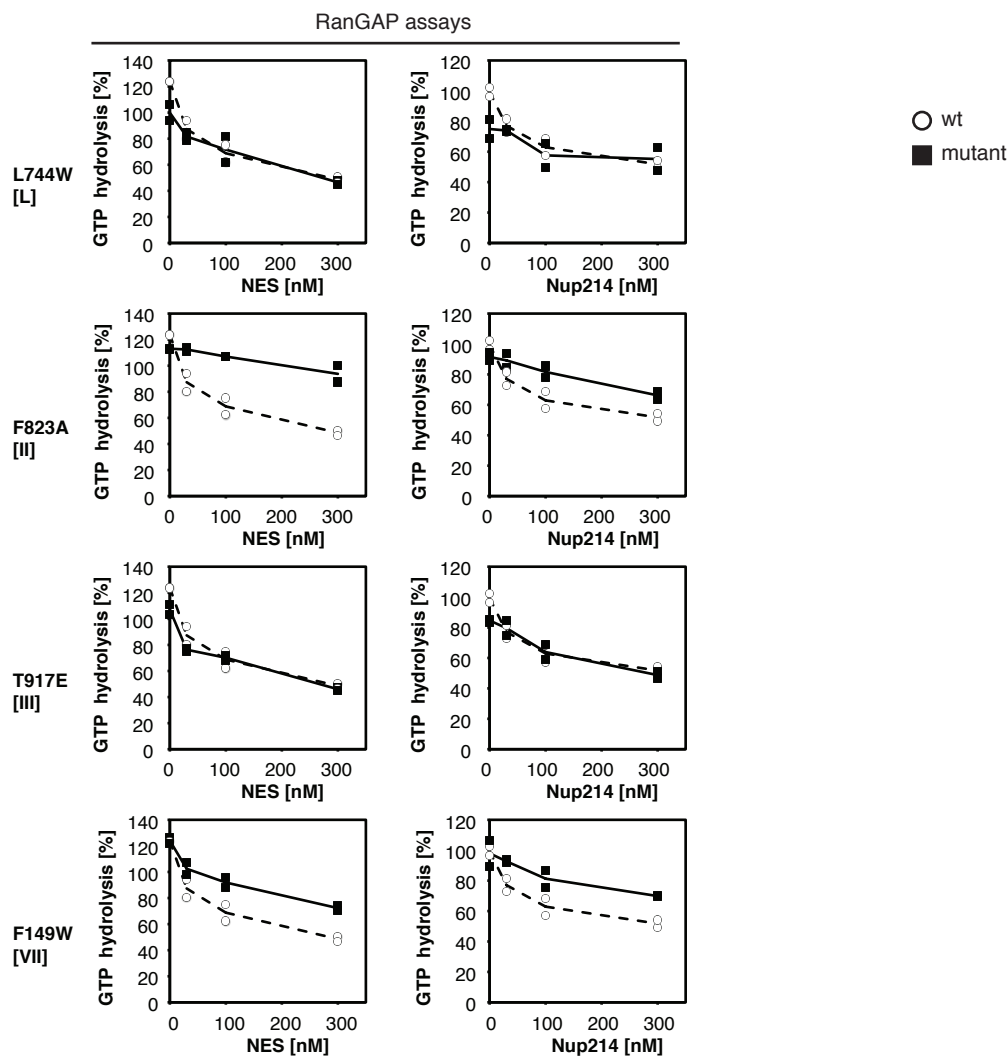


Figure S11: CRM1 single mutants showed diverse binding to NES and Nup214. CRM1 mutants showed diverse binding to NES/ RanGTP and Nup214. The CRM1 mutants were plotted (black square) individually in comparison to the wildtype CRM1 (white circle). The average of the values is indicated by the black line for the CRM1 mutants and the dashed line for the CRM1 wildtype. The individual values and averages of two independent experiments were plotted. Square brackets indicate the altered FG-binding pocket of the CRM1 mutant. (left panel) NES peptide or (middle panel) MBP-Nup214(1916-2033)-His was titrated to 100 nM of the CRM1 mutants and Ran loaded with ^{32}P - γ -GTP in RanGAP assays. (right panel) Permeabilized GFP-NFAT cells were incubated with 30 nM of the respective CRM1 mutants. Residual nuclear fluorescence was analyzed by flow cytometry. Values were normalized to fluorescence intensities at 0 minutes and plotted in relation to a kinetic without added CRM1 (gray).

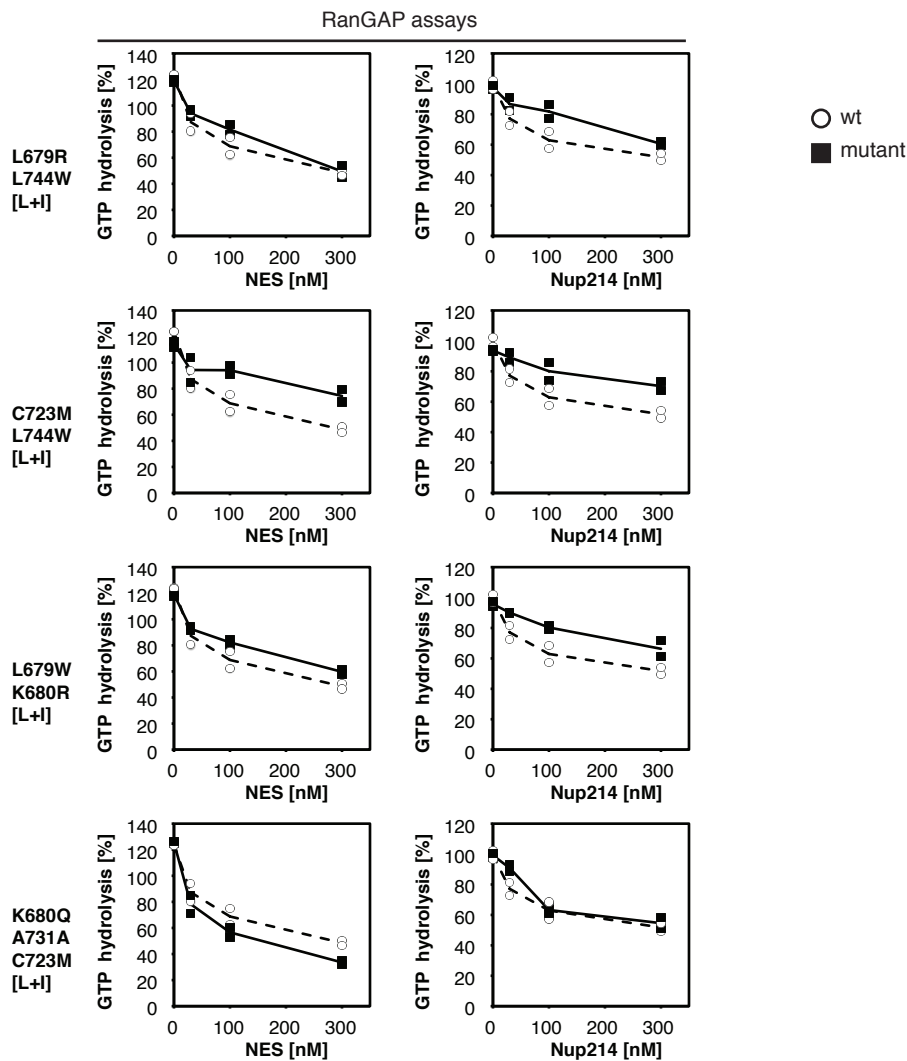


Figure S12: CRM1 double and triple mutants showed diverse binding to NES and Nup214. CRM1 mutants showed diverse binding to NES/ RanGTP and Nup214. The CRM1 mutants were plotted (black square) individually in comparison to the wildtype CRM1 (white circle). The average of the values is indicated by the black line for the CRM1 mutants and the dashed line for the CRM1 wildtype. The individual values and averages of two independent experiments were plotted. Square brackets indicate the altered FG-binding pocket of the CRM1 mutant. (left panel) NES peptide or (middle panel) MBP-Nup214(1916-2033)-His was titrated to 100 nM of the CRM1 mutants and Ran loaded with ^{32}P - γ -GTP in RanGAP assays. (right panel) Permeabilized GFP-NFAT cells were incubated with 30 nM of the respective CRM1 mutants. Residual nuclear fluorescence was analyzed by flow cytometry. Values were normalized to fluorescence intensities at 0 minutes and plotted in relation to a kinetic without added CRM1 (gray).

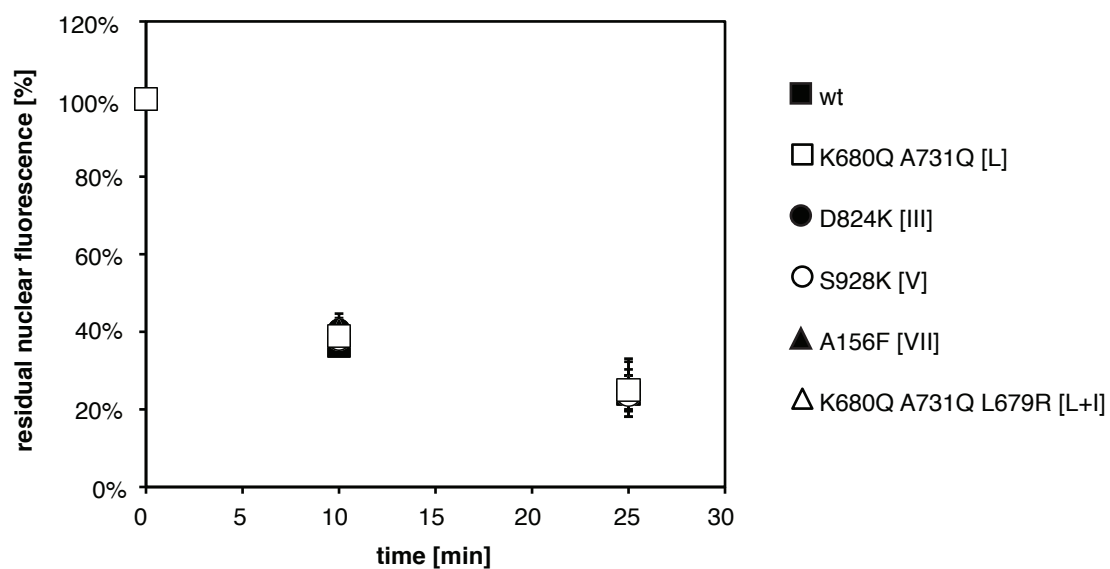


Figure S13: Export kinetics. 100 nM CRM1 mutants were titrated to permeabilized GFP-NFAT cells together with Ran and an ATP-regenerating system. Residual nuclear fluorescence was analyzed by flow cytometry. The average and standard deviation of two independent experiments were plotted. Some of the error bars are too small to be seen.

I Comparison of CRM1 from the Nup214 complex crystal structure to Xpo1p from the Yrb2 complex

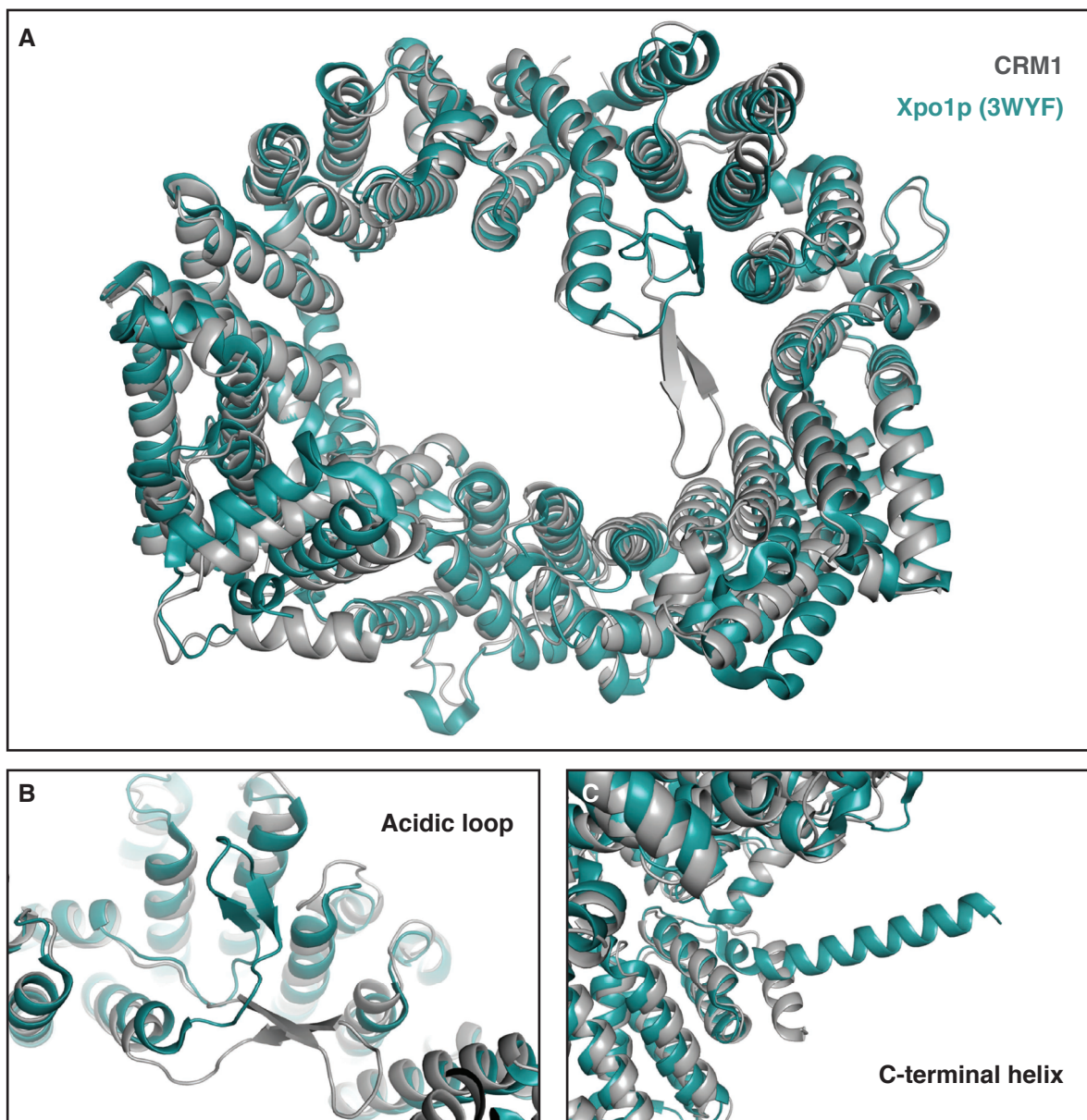


Figure S14: Comparison of CRM1 from the Nup214 complex crystal structure to Xpo1p from the Yrb2 complex (PDB ID: 3WYF). (A) The overall structure of CRM1 (gray) and Xpo1 (green) is similar, but (B) the acidic loop and (C) the C-terminal helix show distinctly different conformations.

J Abbreviations

Table S8: Abbreviations.

aa	amino acid
APS	Ammonium Persulfate
ATP	adenosine-5-triphosphate
bp	base pair
BSA	bovine serum albumin
CRM1	chromosome region maintenance 1
DMEM	Dulbecco's modified eagles medium
DMSO	dimethyl sulfoxide
dNTPs	2'-desoxynucleoside-5'-triphosphate
DTT	dithiothreitol
<i>E. coli</i>	<i>Escherichia coli</i>
EDTA	ethylenediaminetetraacetic acid
EtOH	ethanol
FG-repeat	phenylalanine glycine repeat
GAP	GTPase-activating protein
GDP	guanosine-5'-diphosphate
GST	glutathione-S-transferase
GTP	guanosine-5'-triphosphate
<i>H. sapiens/ Hs</i>	<i>Homo sapiens</i>
HCl	hydrochloric acid
HEAT	Huntingtin Elongation Factor A Subunit Tor
HEPES	2-[4-(2-hydroxyethyl)piperazin-1-yl]ethanesulfonic acid
HIV	human immunodeficiency virus
IPTG	isopropyl-beta-D-thiogalactopyranoside
kDa	kilo dalton
LB	Luria-Bertani
LMB	Leptomycin B
MBP	Maltose binding protein
MCS	multiple cloning site
MPIbpc	Max Planck Institute for Biophysical Chemistry
<i>M. musculus/ Mm</i>	<i>Mus musculus</i>
NES	nuclear export signal
NFAT	nuclear factor of activated T-cells
NLS	nuclear localization signal
NPC	nuclear pore complex
Nup	nucleoporin
PAGE	polyacrylamide gel electrophoresis
PCR	polymerase chain reaction
PDB	Protein Data Base
PMSF	phenylmethylsulphonyl fluoride
Ran	Ras-related nuclear protein
RCC1	Regulator of chromatin condensation 1
RFP	red fluorescent protein
rpm	rotations per minute

<i>S. cerevisiae/ Sc</i>	<i>Saccharomyces cerevisiae</i>
SDS	sodium dodecyl sulphate
siRNA	small interfering RNA
SPN1	snurportin 1
SV40	Simian virus 40
TAE	Tris/ Acetate/ EDTA
Triton X-100	4-octylphenol polyethoxylate
Tween 20	polyoxyethylene (20) sorbitan monolaurate
UV	ultraviolet
v/v	volume per volume
w/o	without
w/v	weight per volume
WGA	wheat germ agglutinin
wt	wildtype

K Amino acid codes

Table S9: Amino acid codes.

Amino acid	3-letter code	1-letter code
Alanine	Ala	A
Arginine	Arg	R
Asparagine	Asn	N
Aspartic Acid	Asp	D
Cystein	Cys	C
Glutamine	Gln	Q
Glutamic Acid	Glu	E
Glycine	Gly	G
Histidine	His	H
Isoleucine	Ile	I
Leucine	Leu	L
Lysine	Lys	K
Methionine	Met	M
Phenylalanine	Phe	F
Proline	Pro	P
Serine	Ser	S
Threonine	Thr	T
Tryptophan	Trp	W
Tyrosine	Tyr	Y
Valine	Val	V

Curriculum vitae

Personal Data

Name	Sarah Alexandra Port
Date of Birth	September 9th, 1985
Place of Birth	Dachau
Nationality	German

Education

06/2011-04/2015	PhD Thesis at Georg-August-Universität Göttingen GGNB Program "Biomolecules: Structure-Function-Dynamics" Doctoral studies in the laboratory of Prof. Ralph H. Kehlenbach
01/2010-03/2010	Research Project at the Protein & Proteomics Centre, National University of Singapore Group of Prof. Lin Qingsong: "Functional assays and validation of differentially expressed proteins in human leukemia cell lines with and without Genistein treatment"
10/2008-12/2010	Master of Science in Molecular Biotechnology at Technische Universität München Modules: Protein biochemistry and -engineering, Molecular Medicine, Plant Biochemistry, Human Resource Management Exchange semester at the National University of Singapore (8/2009-12/2009) Master Thesis at the Chair of Plant Systems Biology: "Determination of the substrate specificity of the D6 protein kinase of <i>Arabidopsis thaliana</i> by proteomic methods"
08/2007-10/2007	SiROP Excellence Project at the Institute of Cell Biology at ETH Zurich (Switzerland) , Group of Prof. Theo Wallimann: "AMPK-related kinases"
10/2005-09/2008	Bachelor of Science in Molecular Biotechnology at Technische Universität München Bachelor Thesis at the Institute of Cell Biology at ETH Zurich (Switzerland): "Polycistronic Expression of an Eukaryotic Chaperone System in Bacteria"
09/1995 -07/2004	Abitur at Josef-Hofmiller-Gymnasium Freising

Publications

Ketan Thakar, Samir Karaca, Sarah A. Port, Henning Urlaub and Ralph H. Kehlenbach (2013) Identification of CRM1-dependent Nuclear Export Cargos Using Quantitative Mass Spectrometry. *Molecular & Cellular Proteomics*, 12, 664-678

Melina Zourelidou, Birgit Absmanner, Benjamin Weller, Inês C.R. Barbosa, Björn C. Willige, Astrid Fastner, Verena Streit, Sarah A. Port, Jean Colcombet, Sergio de la Fuente van Bentem, Heribert Hirt, Bernhard Kuster, Waltraud X. Schulze, Ulrich Z. Hammes, Claus Schwechheimer (2014) Auxin efflux by PIN-FORMED proteins is activated by two different protein kinases, D6 PROTEIN KINASE and PINOID. *eLIFE*.02860

Karthik Narasimhan, Yew Mun Lee and Teck Kwang Lim, Sarah A. Port, Jin-Hua Han, Chien-Shing Chen and Qingsong Lin (2015) Genistein exerts anti-leukemic effects on genetically different acute myeloid leukemia cell lines by inhibiting protein synthesis and cell proliferation while inducing apoptosis - molecular insights from an iTRAQ™ quantitative proteomics study. *Oncoscience*, 2(2), 111-124